



Universidad de Oviedo

Universidá d'Uviéu

University of Oviedo

Programa de Doctorado en Materiales

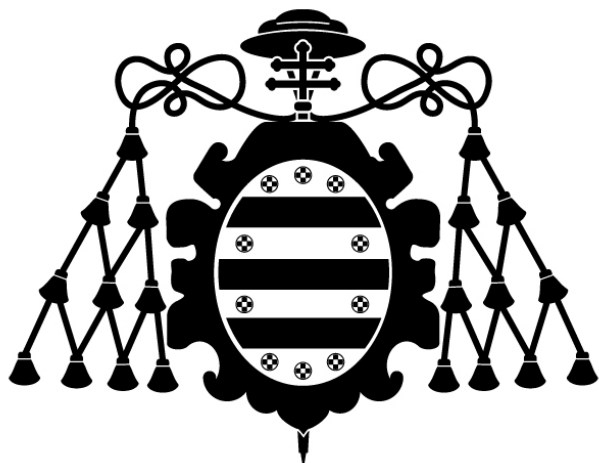
TUNING THE PROPERTIES OF TITANIA AND POLYMERIC
CARBON NITRIDE PHOTOCATALYSTS FOR TOTAL AND
SELECTIVE OXIDATION REACTIONS

FOTOCATALIZADORES BASADOS EN DIÓXIDO DE
TITANIO Y NITRURO DE CARBONO POLIMÉRICO EN
REACCIONES DE OXIDACIÓN TOTAL Y SELECTIVA

TESIS DOCTORAL

Marina Ilkaeva

2018



Universidad de Oviedo
Universidá d'Uviéu
University of Oviedo

Programa de Doctorado en Materiales

TUNING THE PROPERTIES OF TITANIA AND POLYMERIC
CARBON NITRIDE PHOTOCATALYSTS FOR TOTAL AND
SELECTIVE OXIDATION REACTIONS

FOTOCATALIZADORES BASADOS EN DIÓXIDO DE
TITANIO Y NITRURO DE CARBONO POLIMÉRICO EN
REACCIONES DE OXIDACIÓN TOTAL Y SELECTIVA

TESIS DOCTORAL

Directores: Prof. José Rubén García Menéndez

Dr. Eva Díaz Fernandez

Acknowledgements

On the first place, I would like to thank my supervisors. I am very grateful to Prof. Rubén García Menéndez for his immense support and patience, for being always here when he was needed, for words of encouragement, for believing in me, for offering me to start this Ph. D. I would like to express my gratitude to Dr. Eva Díaz for directing my work, for giving me possibilities to develop professionally and for her moral support.

I am thankful to Prof. Salvador Ordóñez, for his optimism, for letting me be a part of the group, for always finding the right solutions.

Many thanks to Prof. Santiago García Granda and to his group: to Laura, Rafa and Mohammed, for all the help I received from you. To my colleagues Igor, Alla, Alex, Arancha, Camino, Bea and Zakariae. To Elena y Sergei for their support and hospitality. To the CRC group: Laura, Jenny, Raquel, Jorge and Diego. Special acknowledgement I would like to give to Yolanda who helped me a lot in the beginning of my Ph. D. I would like to acknowledge all the technical and scientific assistance I received from the SCTs staff Alfonso, David, Emilio, Azucena and Óscar.

I give my gratitude to the group of the University of Palermo, to Prof. Leonardo Palmisano, Dr. Elisa García-López, Dr. Giuseppe Marci, Dr. Marianna Bellardita, Rita Pomilla and Dr. Francesco Parrino. I had there a great research experience as well as a lot of inspiration from you.

I feel very grateful to the scientific group of South Ural State University led by Prof. Viacheslav Avdin who helped me in the beginning of my career.

I give my gratitude to the group of Plataforma Solar de Almeria, to Dr. Sixto Malato, Dr. Ignacio Maldonado, Elisa Ramos, Isabel Fernandez Calderero and Agustín Carrión.

Finally, I would like to thank my family, in spite of being so far away, for all the support I had from you.

Abstract

The use of solar light irradiation as energy source along with molecular oxygen from air and water as oxidants in photocatalysis are the prerequisites for the development of a green, sustainable, non-hazardous, and economically viable chemical technology. Under the light irradiation a transfer of an electron from the valence band to the conduction band of the photocatalyst occurs triggering different kind of radical species formation. The formed radicals are capable of total as well as of partial oxidation of organic molecules, hence the photocatalysis finds its application in two types of catalytic chemical reactions, e.g. mineralization and selective partial oxidation. Despite the extensive study of this phenomenon in the recent years, the practical implementation of these processes remains hindered for various reasons. The application of photocatalysis for water decontamination requires a catalyst, which, apart from being active, is also a stable, easily recoverable and reusable. The presently existing synthetic approaches do not usually provide sufficient control over the mentioned qualities of the photocatalysts or their implementation is expensive or non-environmentally friendly. From the perspective of partial photocatalytic oxidation, the principal challenge related to the control of the reaction selectivity, especially in green solvents such as water, persists and calls for the development of new methods for photocatalysts synthesis and modification. In this Thesis the reactions of total and partial oxidation of organic molecules in the presence of titania and polymeric carbon nitride (PCN) photocatalysts have been studied. Titanium dioxide, owing to the easiness of $\bullet\text{OH}$ radicals formation, has successfully been used for the water decontamination from emerging pollutants. Whereas, PCN utilising mildly oxidative $\bullet\text{O}_2^-$ species has been applied for the partial photo-oxidation of organic compounds to the corresponding aldehydes. The main focus of the present work is on the tuning of the properties of these two photocatalysts for their effective performance in the abovementioned fields.

The problem of a growing number of emerging pollutants usually present in water in small concentrations complicating their complete elimination has recently arisen to a frightening level. One of such compounds proceeding from cosmetic and pharmaceutical products, hence usually found in wastewater, is 2-(4-methylphenoxy)ethanol (MPET), a chemical whose stability and degradation mechanism are largely unknown. In order to tackle this issue, titania-based photocatalysts for UV-driven decomposition of MPET have been applied. The method for the effective titania photocatalysts synthesis included the solvent exchange approach utilising a water-soluble titania peroxo complex as a precursor. It has been found that by varying the carbon chain length of the applied solvent (aliphatic alcohol) it is possible to control the average size of the forming TiO₂ spherical particles (in the range from 50 to 260 nm). The procedure of converting the prepared material from non-porous spheres to the mesoporous ones has been developed. The prepared titania spheres have demonstrated a degree of activity close to that of the commercial titania Aeroxide P25. However, the reusability test has shown that the activity of Aeroxide P25 decreases significantly after the third reaction cycle because of its small particle size of about 20 nm and hence a poor recoverability, while the synthesised titania spheres owing to its particle shape and size can be repeatedly used for at least four cycles without any significant loss of their photocatalytic activity. As a rule, photo-oxidation processes do not directly lead to the complete mineralisation of organic matter to CO₂ and H₂O, but certain intermediates, sometimes even more toxic than the starting pollutant might be produced. Therefore, the identification of the reaction by-products is of key importance. The mechanism of the photo-decomposition of MPET has been proposed and several partially oxidised products of it have been identified. It was found that in the course of MPET photo-oxidation in the presence of TiO₂ a toxic *p*-cresol is formed. However, the prepared mesoporous titania spheres have proved to be efficient not only for MPET, but also for *p*-cresol degradation. The study concludes with the toxicity estimation of the treated water confirming that the desired effect of its detoxification by the TiO₂ photocatalysis has been achieved.

In another part of the work, the reaction of the photocatalytic partial oxidation of MPET in the presence of pristine and modified PCN photocatalyst has been studied. Among the all utilised materials in photocatalysis, PCN is one of the best candidates to promote the partial oxidation of organic molecules under UV-vis irradiation. It has unique electronic properties prohibiting the direct formation of notoriously unselective •OH radicals by water oxidation.

The oxidative activation of relatively inert benzylic C-H bonds is a challenge for synthetic organic chemistry. The task becomes even more complicated if other easily oxidised substituents are also present on the phenyl ring. Unlike TiO₂, which by oxidising MPET produces *p*-cresol and eventually CO₂ and H₂O, PCN oxidises the MPET benzylic carbon forming 4-(2-hydroxyethoxy)benzaldehyde (HEB) with the selectivity of 57%. It has been shown that the H₂O₂ treatment of PCN results in the enhanced selectivity to this product reaching the values in the range of 82-87% in water medium. It has been proposed on the bases of experimental evidence and theoretical calculations that the performed treatment gives the PCN-H₂O₂ material, which contains H₂O₂ bonded to the non-condensed NH₂-species of carbon nitride in a similar way as in the molecular melamine-H₂O₂ adduct. The presence of the PCN-H₂O₂ surface complex creates a steric hindrance for the direct interaction between the oxyethanol group of MPET and the amino-groups of carbon nitride, thus promoting the selectivity towards HEB formation.

Biomass, originated from the agriculture sector and wood industry, is an immense source of valuable chemicals and the interest towards its valorisation is not surprising. There are some typical compounds that are obtained from the abundant biomass feedstock such as a platform 5-hydroxymethyl-2-furaldehyde (HMF). HMF itself has few applications, while the products of its oxidation 2,5-furandicarboxaldehyde (FDC) and 2,5-furandicarboxylic acid (FDCA) are the monomers for polymer synthesis. It is known from the literature that the photo-oxidation of HMF in organic solvents can produce FDC with selectivity values of about 80%, whereas in water medium TiO₂ and PCN-assisted HMF photo-conversion was only able to reach 30% and 40-50%, respectively. In this Thesis the synthesis of the PCN-H₂O₂ adduct with the improved selectivity in the HMF to FDC photocatalytic transformation has been proposed. PCN-H₂O₂ has shown selectivity of 80% to FDC under UV irradiation and up to 89% under natural sunlight. It has been revealed that the synthesised photocatalyst having hydrogen peroxide coordinated to its NH₂ surface species is stable up to 200 °C if heated in air, and it does not release H₂O₂ under irradiation or heating in water suspensions. It has been proposed that the non-condensed carbon nitride species are responsible for the generation of •OH radicals leading to the decrease of the reaction selectivity, but in the PCN-H₂O₂ adduct these sites are blocked by the coordinated hydrogen peroxide, thus allowing to avoid the unselective substrate conversion.

A scaling up of the photocatalyst synthesis and its subsequent use in a pilot-plant scale reactor without losing its efficiency with respect to that achieved in laboratory experiments is always a difficult task. The PCN-H₂O₂ adduct has been tested for partial selective oxidation of HMF, 4-methoxybenzyl alcohol (MBA), benzyl alcohol (BA) molecules to the corresponding aldehydes at the Almeria Solar Platform in a 15.5 L volume Compound Parabolic Collector (CPC) photo-reactor under natural solar irradiation and in water medium. The selectivity of HMF to FDC photo-oxidation in CPC has been found in the range 70-90%, which is comparable with the laboratory tests. Moreover, the varied concentrations of the photocatalysts, as well as the substrates, have proved the viability of the partial photocatalytic oxidation of aromatic alcohols under real-life conditions. The kinetic model built on the basis of the obtained experimental data suggests that the reaction is satisfactorily described by the Langmuir-Hinshelwood mechanism.

Resumen

El uso de la luz solar como fuente de energía, junto con la aplicación del oxígeno molecular del aire y el agua como oxidante en fotocátalisis, son prerequisites necesarios para el desarrollo de tecnologías de química "verde", sostenibles, inocuas, y económicamente viables. Bajo irradiación ultravioleta (UV) o luz solar, en un fotocatalizador, electrones de la banda de valencia pasan a la de conducción, provocando en su retorno la formación de diferentes tipos de radicales capaces de promover reacciones de oxidación total o parcial, que hacen que la fotocátalisis encuentre aplicación en procesos de mineralización y oxidación parcial selectiva. A pesar de los numerosos estudios realizados en los últimos años, la implementación práctica de estos procesos continúa siendo escasa. La aplicación de la fotocátalisis a la descontaminación de agua requiere un catalizador que posea, además de alta actividad, estabilidad, facilidad de recuperación, y capacidad de regeneración. Los métodos sintéticos actuales no siempre proveen el control suficiente sobre el comportamiento del fotocatalizador, al tiempo que su implementación puede ser cara e, incluso, medioambientalmente no recomendable. En procesos de oxidación fotocatalítica parcial, actualmente, el reto principal se relaciona con el control sobre la selectividad de la reacción y, especialmente, en disolventes "verdes" como el agua, se centra en el desarrollo de nuevos métodos de síntesis y modificación de los materiales fotocatalizadores. En esta Tesis Doctoral se han estudiado reacciones de oxidación total y parcial de moléculas orgánicas, usando dióxido de titanio y nitruro de carbono polimérico como fotocatalizadores, prediseñados para este fin. El dióxido de titanio, debido a la facilidad de formación de radicales $\bullet\text{OH}$, se ha aplicado con éxito en la descontaminación de aguas, mientras que el nitruro de carbono polimérico, que genera radicales $\bullet\text{O}_2^-$ moderadamente oxidantes, se ha utilizado en la foto-oxidación parcial de compuestos orgánicos a sus aldehídos.

Los contaminantes emergentes suelen presentarse en aguas en concentraciones bajas, lo que dificulta su eliminación efectiva. Uno de estos compuestos, el 2-(4-metilfenoxi)etanol

(MPET), cuya fuente principal son productos cosméticos y farmacéuticos, presenta en agua una estabilidad y unos mecanismos de descomposición que, en su mayor parte, son desconocidos. En esta Tesis Doctoral, se ha abordado este problema utilizando fotocatalizadores basados en dióxido de titanio para la descomposición de MPET bajo irradiación UV, que han sido sintetizados por métodos basados en el intercambio de disolventes, incluyendo el uso de un peroxocomplejo de titanio como precursor en medio acuoso. Se ha encontrado que la longitud de la cadena alifática de los alcoholes utilizados como disolvente permite modular el tamaño medio de las partículas esféricas de TiO₂ entre 50 y 260 nm, habiéndose desarrollado un procedimiento de transformación de las esferas de titania no porosas a mesoporosas. Los nuevos materiales han mostrado un nivel de actividad próximo al de la titania comercial, Aeroxide P25. En ensayos de reutilización, la actividad del Aeroxide P25 disminuye significativamente después de tres ciclos de reacción debido a que el pequeño tamaño de las partículas (~20 nm) hace difícil su recuperación, mientras que las esferas de titania sintetizadas en este trabajo, a consecuencia de su tamaño y forma, pueden ser utilizadas al menos en cuatro ciclos sin pérdida significativa de su actividad fotocatalítica. Usualmente, los procesos de foto-oxidación no conducen directamente a la mineralización completa del sustrato orgánico hasta CO₂ y H₂O, siendo posible la aparición de compuestos intermedios, incluso más tóxicos que los contaminantes iniciales, por lo que su identificación es una cuestión clave. En este trabajo, se ha propuesto un mecanismo de foto-descomposición de MPET y se han identificado varios productos parcialmente oxidados, entre los que se encuentra el *p*-cresol, previamente a su foto-degradación. Medidas de toxicidad del agua tratada demostraron la eficacia de los nuevos materiales en procesos de foto-descontaminación.

Entre los posibles materiales fotocatalíticos, el nitruro de carbono es uno de los mejores candidatos a promover la oxidación parcial de moléculas orgánicas bajo irradiación UV. Este material posee propiedades únicas, que impiden la formación en agua de radicales •OH, escasamente selectivos. La activación oxidativa de enlaces bencílicos C-H relativamente inertes es un reto actual de la química orgánica sintética, cuya consecución se complica en presencia de sustituyentes fácilmente oxidables en el anillo fenólico. En esta Tesis Doctoral, se ha abordado la foto-oxidación parcial de MPET en presencia de nitruro de carbono prístino y modificado. A diferencia del TiO₂, donde la oxidación de MPET produce *p*-cresol y eventualmente CO₂ y H₂O, el nitruro de carbono prístino conduce a 4-(2-

hidroxietoxi)benzaldehído (HEB) con una selectividad del 57%, que aumenta hasta el 82-87% cuando el nitruro de carbono se activa con H_2O_2 , probablemente como consecuencia de la presencia de H_2O_2 enlazada a grupos NH_2 no condensados del nitruro de carbono, de forma semejante al aducto molecular melamina- H_2O_2 . La presencia del complejo superficial nitruro de carbono-agua oxigenada, por motivos estéricos, impedirá la interacción directa entre el grupo oxietanol del MPET y los grupos amino del nitruro de carbono, siendo responsable del aumento de selectividad en la formación de HEB.

La biomasa procedente de los sectores agrícola y forestal es una enorme fuente de productos químicos valiosos, siendo de gran interés su valorización. Entre los compuestos que se pueden obtener de la biomasa, se encuentra el 5-hidroximetil-2-furaldehído (HMF). Aunque las aplicaciones del HMF son escasas, los monómeros producto de su oxidación, 2,5-furandicarboxaldehído (FDC) y el ácido 2,5-furandicarboxílico (FDCA), se utilizan en síntesis polimérica. La literatura describe que la foto-oxidación de HMF en medio orgánico conduce a la formación de FDC con elevada selectividad (~80%), mientras que en medio acuoso, utilizando TiO_2 o nitruro de carbono, sólo se alcanzan foto-conversiones del 30% y 40-50%, respectivamente. En esta Tesis Doctoral se propone el uso del aducto nitruro de carbono-agua oxigenada en la transformación fotocatalítica de HMF a FDC en medio acuoso, alcanzándose una selectividad del 89% bajo irradiación solar, con la ventaja adicional de que el material es estable en aire hasta 200 °C, sin liberación de H_2O_2 bajo irradiación y/o calentamiento en suspensiones acuosas. Se ha propuesto que las especies no condensadas de nitruro de carbono son las responsables de la generación de radicales $\bullet OH$ que provocan un descenso en la selectividad en la reacción, mientras que en el aducto nitruro de carbono-agua oxigenada estos sitios están bloqueados por H_2O_2 coordinada, evitando la conversión no selectiva del sustrato.

El proceso de escalado en la síntesis de un fotocatalizador y su posterior uso en una planta piloto, sin pérdida de eficiencia con respecto a los experimentos a escala laboratorio, es siempre una tarea difícil. En esta Tesis Doctoral, el aducto nitruro de carbono-agua oxigenada se utilizó en la oxidación parcial de HMF, alcohol 4-metoxibencílico (MBA) y alcohol bencílico (BA) a sus aldehídos correspondientes en la Plataforma Solar de Almería en un foto-reactor CPC (*Compound Parabolic Collector*), con un volumen de 15.5 L, en medio acuoso y bajo luz solar. La selectividad en la foto-oxidación de HMF a FDC fue del 70-90%, comparable con la obtenida previamente en experimentos de laboratorio. Además, estudios

realizados variando la concentración de los fotocatalizadores, junto al uso de sustratos de diferentes tipos, han demostrado la viabilidad de la oxidación fotocatalítica parcial en condiciones reales. Finalmente, resaltar que el modelo cinético obtenido de los datos experimentales hace que la reacción pueda ser descrita satisfactoriamente mediante un mecanismo Langmuir-Hinshelwood.

Contents

CONTENTS	XIV
LIST OF FIGURES	XVI
NOMENCLATURE.....	XVII
ÍNDICES DE CALIDAD.....	XIX
COMUNICACIONES A CONGRESOS.....	XX
CHAPTER 1 INTRODUCTION.....	1
1.1 PRINCIPLES OF HETEROGENEOUS PHOTOCATALYSIS.....	1
1.1.1 <i>Quantum, photonic yields and efficiencies</i>	5
1.1.2 <i>Parameters influencing the photocatalytic reactions rates</i>	8
1.1.2.1 <i>Photocatalytic processes occurring in the bulk</i>	8
1.1.2.2 <i>Photocatalytic processes occurring at the interface: Mass transfer and adsorption</i>	11
1.2 PHOTOCATALYSIS FOR TOTAL OXIDATION REACTIONS.....	13
1.2.1 <i>Aqueous phase photo-oxidation of organic pollutants in the presence of TiO₂</i>	14
1.2.2 <i>Methods for controlling titanium dioxide crystal phase</i>	18
1.2.3 <i>Titanium dioxide synthesis using H₂O₂-assisted methods</i>	19
1.2.4 <i>Tuning titanium dioxide morphology</i>	21
1.2.5 <i>Photocatalyst recyclability</i>	23
1.3 PHOTOCATALYSIS FOR PARTIAL PHOTO-OXIDATION.....	24
1.3.1 <i>Polymeric carbon nitride application in partial selective photocatalytic oxidation</i>	25
1.3.2 <i>Methods for polymeric carbon nitride synthesis</i>	28
1.3.3 <i>Control of textural properties of polymeric carbon nitride</i>	32
1.3.3.1 <i>Polymeric carbon nitride exfoliation strategies</i>	32
1.3.3.2 <i>Template-assisted methods for polymeric carbon nitride synthesis</i>	34
1.3.4 <i>Modification of melon structural units of polymeric carbon nitride</i>	35
1.3.5 <i>Carbon nitride doping and functionalisation</i>	35
1.4 PHOTOREACTORS.....	39
CHAPTER 2 OBJECTIVES.....	45

CHAPTER 3	MATERIALS AND METHODS	49
3.1	MATERIALS	49
3.2	SYNTHESIS	50
3.2.1	<i>Titanium dioxide spherical particles preparation.....</i>	<i>50</i>
3.2.2	<i>Preparation of H₂O₂-treated PCN for MPET partial photo-oxidation</i>	<i>51</i>
3.2.3	<i>Preparation of PCN-H₂O₂ adduct for HMF photo-conversion.....</i>	<i>52</i>
3.2.4	<i>Synthesis of H₂O₂-treated PCN for HMF photo-conversion in a solar pilot plant</i>	<i>53</i>
3.3	CHARACTERIZATION.....	53
3.4	PHOTOCATALYTIC REACTIONS	56
3.4.1	<i>Photocatalytic degradation of organic pollutant in the presence of TiO₂.....</i>	<i>56</i>
3.4.2	<i>Photocatalytic conversion of MPET and HMF in the presence of PCN-H₂O₂ adduct..</i>	<i>58</i>
CHAPTER 4	RESULTS AND DISCUSSION	63
4.1	TITANIA SPHERICAL PARTICLES FOR PHOTOCATALYTIC DEGRADATION OF ORGANIC POLLUTANTS.....	63
4.2	MODIFIED POLYMERIC CARBON NITRIDE FOR ORGANIC MOLECULES SELECTIVE PHOTO-OXIDATION	106
4.2.1	<i>PCN-H₂O₂ adduct for C-H bond chemoselective photo-oxidation of alkylphenolethoxylates</i>	<i>106</i>
4.2.2	<i>PCN-H₂O₂ adduct for selective photo-oxidation of 5-hydroxymethylfurfural to 2,5-furandicarboxaldehyde</i>	<i>143</i>
4.2.3	<i>PCN-H₂O₂ adduct for selective photo-oxidation of 5-hydroxymethylfurfural and aromatic alcohols in solar pilot plant.....</i>	<i>188</i>
CHAPTER 5	CONCLUSIONS.....	223
	REFERENCES.....	229

List of Figures

Figure 1.1 – Potentials for various redox couples in water (pH 7) and the band-edge positions of semiconductor photocatalysts.

Figure 1.2 – Schematic illustration of the electronic structure of the pristine and doped TiO₂.

Figure 1.3 – Dependence of the photocatalyst concentration on the reaction rate.

Figure 1.4 – Elementary reactions in TiO₂ photocatalysis with corresponding timescales.

Figure 1.5 – Proposed degradation pathway of phenol over titania.

Figure 1.6 – Proposed mechanism for the formation of the observed products during the photo-degradation of phenoxyacetic acid.

Figure 1.7 – Representation of the titania natural polymorphs crystalline cells: anatase, rutile, brookite.

Figure 1.8 – Proposed oxidation mechanism of alcohols on PCN.

Figure 1.9 – Schematic representation of carbon nitride condensation from different precursors.

Figure 1.10 – (a) Atomic structure model of a perfect graphitic C₃N₄ sheet consisting of melem units, and two melem units with a nitrogen atom substituted at different periodic sites by a sulfur atom and (b) the proposed oxygen functionalization of carbon nitride.

Figure 1.11 – Main types of photoreactors for various applications.

Figure 1.12 – Example of parabolic-trough reactor.

Figure 1.13 – Example of non-concentrating photoreactor solar collector at the Almeria Solar Platform (Spain).

Figure 1.14 – Example of a compound parabolic concentrator.

Figure 2.1 – UV-lamp equipped photocatalytic reactor for MPET photo-oxidation.

Figure 2.2 – UV-lamps equipped photocatalytic reactor for alkylphenoxyethoxylates and HMF photo-conversion.

Figure 2.3 – Photocatalytic setup for the natural solar light promoted oxidation of HMF.

Figure 2.4 – Pilot plant scale CPC solar photoreactor located at the Almeria Solar Platform (Spain).

Nomenclature

BA – benzyl alcohol

BAL – benzaldehyde

BG – Band Gap

CB – Conduction Band

DRS – Diffusive-Reflectance Spectra

DR UV-vis – Diffusive-Reflectance Ultraviolet-Visible

DTA – Differential Thermal Analysis

EELS – Electron Energy-Loss Spectroscopy

FDC – 2,5-furandicarboxaldehyde

FFA – 5-formyl-2-furoic acid

FTIR – Fourier-Transform Infrared

g-C₃N₄ – Graphitic Carbon Nitride

GC-MS – Gas Chromatography Mass-Spectrometry

HEB – 4-(2-hydroxyethoxy)benzaldehyde

HMF – 5-hydroxymethyl-2-furfural

HRTEM –High-Resolution Transmission Electron Microscopy

HPLC – High Performance Liquid Chromatography

IUPAC – International Union of Pure and Applied Chemistry

MAS NMR – Magic-Angle Spinning Nuclear Magnetic Resonance

MBA – 4-methoxybenzyl alcohol

MBAL – 4-methoxybenzaldehyde

MOF – Metal Organic Framework

MPET – 2-(4-methylphenoxy)ethanol

P25 – Titanium Dioxide Photocatalyst (Aeroxide P25, Evonik P25, Degussa P25)

PL – Photoluminescence

PXRD – Powder X-ray Diffraction

SEM – Scanning Electron Microscopy

SC – Semiconductor

SE – Solvent-Exchange

SSA – Specific Surface Area

TEM – Transmission Electron Microscopy

TG – Thermogravimetry

TOC – Total Organic Carbon

TOF – Turnover Frequency

TON – Turnover Number

UV – Ultraviolet

VB – Valence Band

VIS – Visible

XPS – X-ray Photoelectron Spectroscopy

Índices de calidad

De acuerdo con el Reglamento de los Estudios de Doctorado aprobado por el Consejo de Gobierno de la Universidad de Oviedo el 17 de Junio de 2013 (Boletín Oficial del Principado de Asturias N° 146, de 25-06-2013), para presentar la Tesis Doctoral como Compendio de Publicaciones es necesario incluir en la presente Memoria un informe con el factor de impacto de las publicaciones presentadas, junto con un detalle informativo sobre la calidad de las mismas, basado en el índice de impacto y en la posición que ocupa la revista científica dentro de una determinada categoría. El informe correspondiente a los índices de impacto de las revistas en las que se han publicado, o están en trámite de publicación, los artículos que forman parte de la presente Memoria de Tesis Doctoral se resume en la siguiente Tabla.

Relación de las publicaciones derivadas de la presente Tesis Doctoral
(datos obtenidos de Journal Citations Reports® del año 2016).

Revista	Año	Índice de Impacto	Área	Nº de orden / nº total	Cuartil
Journal of Hazardous Materials	2017	6.065	Engineering, Civil	1/125	Q1
			Engineering, Environmental	5/49	Q1
			Environmental Sciences	13/229	Q1
Green Chemistry	2017	9.125	Chemistry, Multidisciplinary	15/166	Q1
			Green & Sustainable Science & Technology	1/31	Q1
Journal of Catalysis	2018	6.844	Chemistry, Physical	20/146	Q1
			Engineering, Chemical	5/135	Q1
Catalysis Today	2018	4.636	Chemistry, Applied	6/72	Q1
			Chemistry, Physical	30/146	Q1
			Engineering, Chemical	12/135	Q1

Comunicaciones a Congresos

1. M. Ilkaeva, I. Krivtsov, Z. Amghouz, S. Khainakov, J.R. García, E. Díaz, S. Ordóñez. *Peroxo method for the preparation of photocatalytically active titania spheres for emerging micropollutant degradation*. XIV Congreso Nacional de Materiales, Gijón, Spain, 8-10 June 2016. Oral.
2. M. Ilkaeva, I. Krivtsov, Z. Amghouz, S. Khainakov, J.R. García, E. Díaz, S. Ordóñez. *Application of recyclable TiO₂ spheres for photocatalytic degradation of emerging pollutants*. 9th European Meeting on Solar Chemistry and Photocatalysis: Environmental Applications (SPEA), Strasbourg, France, 13–16 June 2016. Poster and Flash Oral.
3. M. Ilkaeva, I. Krivtsov, S. Khainakov, J.R. García, E. Díaz, S. Ordóñez. *Peroxo method for TiO₂ nanoparticles preparation and their application in photodegradation of emerging pollutants*. 16th International Congress on Catalysis (ICC 16), Beijing, China, 3-8 June 2016. Poster.
4. M. Ilkaeva, I. Krivtsov, Z. Amghouz, S. Khainakov, J.R. García, E. Díaz, S. Ordóñez. *Application of the peroxo method for synthesis of photoactive mesoporous TiO₂ spheres*. 40th Meeting of Iberian Adsorption Society (40 RIA), Évora, Portugal, 5-7 September 2016. Poster.
5. M. Ilkaeva, I. Krivtsov, E. Salas-Colera, J.R. García, E. Díaz, S. Ordóñez. *XAS study of anatase TiO₂ doping with interstitial nitrogen and oxygen species*. 30th European Crystallography Meeting, Basel, Suiza, 28 August – 1 September 2016. Poster.
6. M. Ilkaeva, I. Krivtsov, S. Khainakov, J.R. García, E. Díaz, S. Ordóñez. *g-C₃N₄ assisted chemoselective C-H bond photooxidation of 2-(4-methylphenoxy)ethanol in water with O₂*. Reunión de la Sociedad Española de Catálisis (SECAT17), Oviedo, Spain, 26-28 June 2017. Poster.

Chapter 1 Introduction

1.1 Principles of Heterogeneous Photocatalysis

According to the IUPAC (International Union of Pure and Applied Chemistry), *photocatalysis* is defined as “change in the rate of a chemical reaction or its initiation under the action of light in the presence of a substance – the photocatalyst – that absorbs light and is involved in the chemical transformation of the reaction partners” [1]. If the reaction meets all this requirement it is called photocatalytic.

Similar to heterogeneous catalysis, in photocatalysis, in order to increase the reaction rate, the activation energy barrier needs to be overcome. Another similarity is that the catalyst and photocatalyst are not consumed during the reaction they promote and can be used repeatedly in consecutive cycles. If conventional catalysis is initiated by an increment of temperature in photocatalysis UV- or visible-light photons supplies the energy for the catalytic transformations to take place. As to the differences, in catalysis the catalyst's efficiency is often expressed in terms of turnover number (TON) or turnover frequency (TOF), the same parameters can hardly be defined for heterogeneous photocatalysis since an actual number of photocatalytically active centres is usually unknown. Although these parameters can be determined with high precision for homogeneous photocatalysis [1]. Palmisano *et al.* assigned the principal difference between the catalytic and photocatalytic processes to the appearance in the latter of such steps as absorption of a photon by the material, subsequent generation of electron/hole pair able to recombine or induce oxidation or reduction reactions, formation of charge carriers and their trapping on the surface of the semiconductor (SC) [2].

Generally, in photocatalysis the reagents are physisorbed, whereas in catalysis the nature of the adsorption of reaction participants is chemical [2].

When it comes to the history of photocatalysis, usually the researchers make a reference to the remarkable progress achieved by Fujishima and Honda in the photoelectrochemical water splitting in 1972 [3], which had resulted in the extensive use of TiO₂ nanomaterials for environmental purification and energy storage/conversion applications. Nonetheless, before 1972 a lot of photocatalytic experiments had been performed. In an exhaustive summary of the history of semiconductor photocatalysis Serpone *et al.* [4] indicated that such phenomena as photocorrosion, photoadsorption of oxygen, and sensitization of photoconductivity were reported for the first time in the early twentieth century. At the very beginning, the term photocatalysis ("photokatalyse") appeared in a book by Plotnikow in 1910 [5] and later it was introduced by Landau in France in 1913. One of the first photocatalytic experiments were carried out by Eibner in 1911, where discoloration of Prussian blue dye by ZnO under irradiation was studied, and by Tammann who observed photocorrosion of ZnO under the sunlight in 1920. It should also be mentioned that the group of Terenin published several papers on photocatalysis in early 1930s [4]. Clearly, the past century had evidenced a significant number of works in the field of photocatalysis or related to it, which are seldom mentioned by the present day researchers. Nowadays, photocatalysis is still a very promising area for investigation, as it opens the possibilities of using a free solar light as an energy source and environmentally-friendly oxidants, namely, O₂ from air and H₂O. It is especially important today in a view of the running out fossil fuels and environmental pollution.

Photocatalysis taking place at the interfacial boundary between two phases (solid/liquid, solid/gas, liquid/gas) is heterogeneous photocatalysis, contrary to homogenous one, where, such as in the case of the photo-Fenton, the photocatalyst is present in the molecular form. In heterogeneous photocatalysis, when a photon of energy higher than or equal to the band gap (BG) energy is absorbed by a semiconductor, an electron e⁻ from the valence band (VB) is promoted to the conduction band (CB) with simultaneous generation of a hole h⁺ on the VB. Thus, the charge carriers are generated upon illumination and they can get trapped in the semiconductor bulk, recombine or they can take part in various redox reactions. Titania is one of the most common photocatalysts for its nontoxicity, high reactivity, chemical stability and

low cost. Apart from titania, there is a variety of semiconductor materials such as CeO₂, ZnO, ZnS, CdS, MoO₃, WO₃, Bi₂WO₆, NiO [6], C₃N₄ [7] and metal-organic frameworks (MOFs) [8] also demonstrating photocatalytic properties. Each semiconductor material possesses different electronic structure resulting in varying energies of the VB and the CB as presented in Fig.1.1 [9].

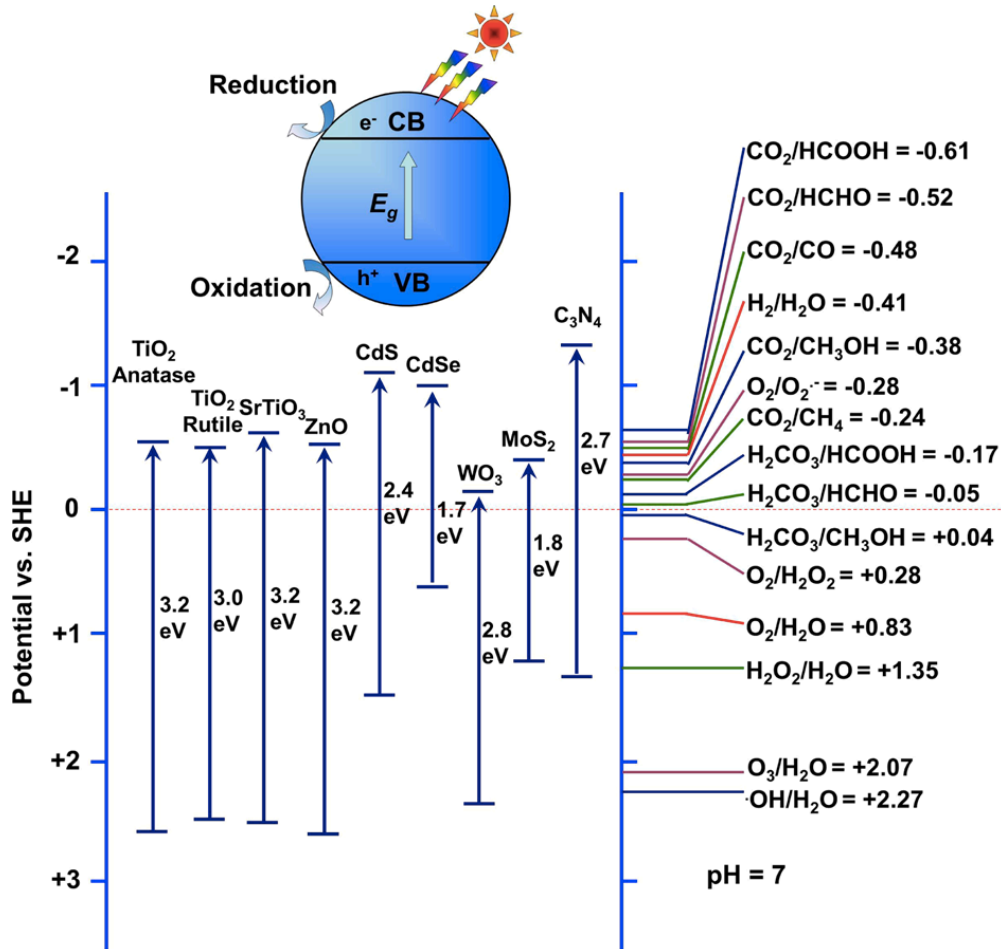
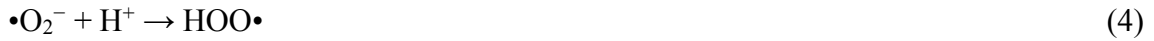


Figure 1.1 – Potentials for various redox couples in water (pH 7) and the band-edge positions of semiconductor photocatalysts [9].

The heterogeneous photocatalytic process is a complex sequence of reactions (Fig 1.2) that can be expressed by the following set of simplified equations [10]:





A lot of efforts have been applied to tune the properties of the photocatalytic materials aiming to decrease the recombination of excited charge carriers (Eq. 7) and back-electron recombination between the two primal products, to attain better absorption of light in the visible range and to control produced radicals. Thus, the basic problem of chemical solar energy harvesting is how to inhibit the primary and secondary charge recombination. Many techniques are known to be efficient for achieving these purposes; among them are found metal and non-metal doping, control of crystalline phase, surface modification, heterojunction creation, etc.

Many studies are devoted to the extension of the absorption range of SC to visible-light by doping the materials with anions or cations [11-14]. Along with the absorption onset change, as to say the BG displacement, one can deduce that the doping would also lead to the modification of the VB or CB potentials or mid-gap states might be created instead (Fig. 1.2), implying that the ability of the photocatalyst to oxidise or reduce organic or water molecules can become poorer. On the other hand, creating heterojunctions, z-scheme photocatalytic systems or sensitising photocatalysts by the use of dyes lead to the activation under visible light, while retaining optimal oxidative (reductive) properties of the pristine photocatalyst intact. In addition, ligand-to-metal charge transfer (LMCT) oxidation also helps to reduce the unsuitable effect in selective photo-oxidation reactions related to the generation of certain undesirable photogenerated species. Thus, while designing efficient photocatalytic material it is important to consider that the extension of the activation range to the visible light might

eventually lead to a poorer performance, hence the balance between these parameters has to be found.

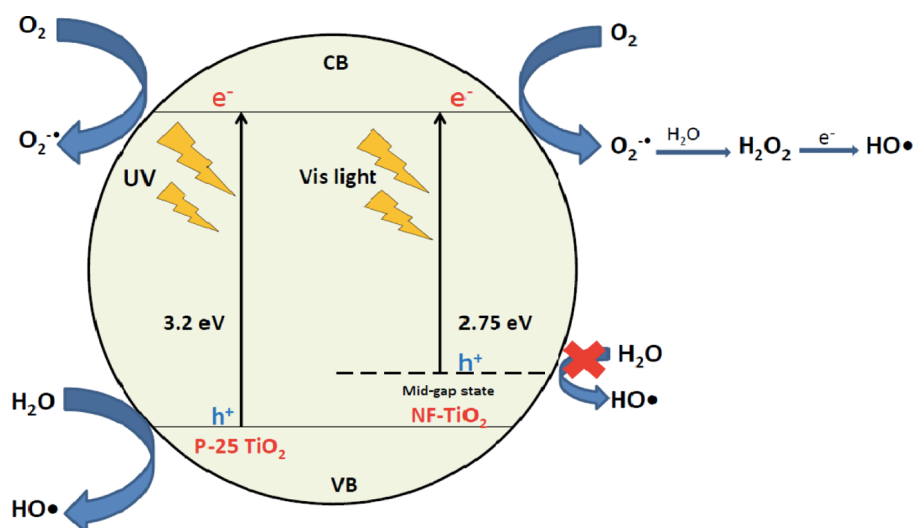


Figure 1.2 – Schematic illustration of the electronic structure of the pristine and doped TiO₂ [13].

Summarising, heterogeneous photocatalysis is a powerful and versatile process, which allows carrying out a great number of oxidative and reductive reactions using light as an energy source (Fig. 1.1). The main challenge in this area is related to gaining control over the properties of the photo-active materials and conditions of the reaction in order to reach the desired photocatalytic activity.

1.1.1 Quantum, photonic yields and efficiencies

In order to understand the effectiveness of the photocatalyst for light-assisted organic substrate conversion, its performance is expressed in terms of *quantum* or *photonic yield* and *quantum* or *photonic efficiency*. According to IUPAC, *quantum yield* (Φ) is "a number of defined events, occurring per photon absorbed by the system at a specified wavelength" [1]. It must be mentioned that in homogeneous photochemistry quantum yield can be measured very precisely, while in heterogeneous photocatalysis there are some difficulties related to the scattering phenomena, which reduce the number of absorbed photons and which are hard to account for. Also it is important to consider that in the suspensions of powdered

nanostructured material shadowing effects take place and that up to 13-76% of the light arriving at the powder surface may be lost [15,16]. Only for non-porous materials or transparent nanoparticles quantum yield can be measured with sufficient accuracy. To overcome the problems related to the comparison of photoreactivity, the use of incident photon flux (*photonic*) is proposed. Hence, *photonic yield* refers to the "ratio of the rate of the photoreaction measured for a specified time interval (usually the initial conditions) to the rate of incident photons of monochromatic light inside the irradiation window of the reactor". It implies that the main difference between these two terms is that "*photonic*" refers to the number of photons arriving on a surface of the reactor, while "*quantum*" means a number of photons absorbed by the system.

Another parameter that could help the effectiveness evaluation of the photocatalytic processes is *photonic efficiency*. *Efficiency* implies that the irradiation used in the photo-reactions is polychromatic, which is true for the majority of the experiments in heterogeneous photocatalysis, besides it seems more suitable in terms of the real-life applications, e.g. photocatalytic reactions under the natural solar light. *Photonic efficiency* (ζ) is "a ratio of the rate of the photoreaction measured for a specified time interval (usually the initial conditions) to the rate of incident photons within a defined wavelength interval inside the irradiation window of the reactor" [1], which is, unfortunately, usually found to be rather small. In fact, time-resolved spectroscopic studies reveal that most of the photogenerated e^-/h^+ pairs (up to 90%) recombine rapidly after the excitation. This is assumed to be a reason for the relatively low ζ -values (<10%) of most semiconductor-promoted photocatalytic reactions [15]. There is no surprise that a great effort has been undertaken towards the synthesis of the semiconductor materials, where good charge carrier separation after material excitation would allow to suppress the high rate of recombination, but still it remains a challenge. Nevertheless, we should bear in mind that the solar energy is a cost-free and photocatalytic reactions usually are carried out under ambient conditions, without heating or pressurising the reaction vessel and applying green solvents, normally water, thus the time consumed for such processes is compensated by the low expenses.

Although many studies report the determination of the photonic and quantum efficiencies for heterogeneous photocatalytic systems, the approaches and the parameters considered for

the quantifications differ [17-22]. The detailed analysis of apparent quantum efficiency, as well as careful examination of the influence of physical and chemical parameters, have been described [19]. It appears that for the calculation of apparent quantum efficiency the most influential physical parameter is morphology of the photocatalyst. In case of chemical variables, both activity and usually omitted selectivity of the reaction are found to be of significance.

A simple and more practicable procedure allowing the comparison of the rates of reactions performed in the same photoreactor has been proposed. It deals with the measuring of the reaction rate as a function of increasing photocatalyst concentration [16, 23-25]. The reaction rate initially increases linearly with the increase of the photocatalyst concentration (Fig. 1.3, curve A-B), because of the growing quantity of the absorbed photons, and then, it remains constant in a region B-C, the range of the catalyst loading representing the optimal light absorption. The resulting optimum rate shows a pseudo-photon efficiency that enables a comparison of “photocatalytic activities”. In some cases, a rate decrease is observed (Fig. 1.3, curve B-D), owing to a reduced penetration depth and an increased scattering of the incident light beam [26,27].

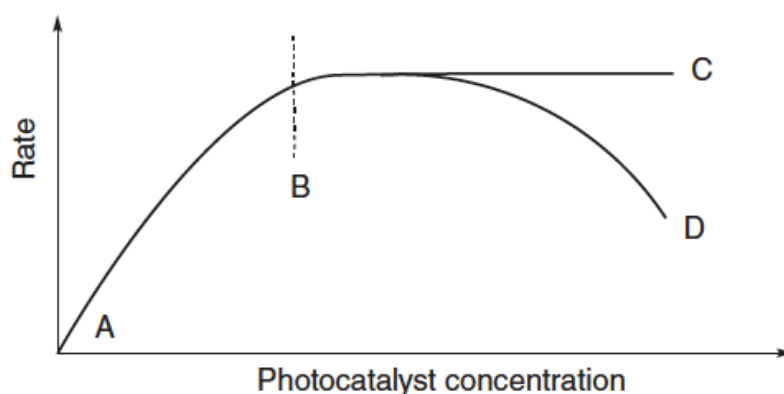


Figure 1.3 – Dependence of the photocatalyst concentration on the reaction rate [25].

Thus, in order to reach the maximum photon absorption by the photocatalyst, the importance of the experiment conditions optimisation must be accounted for. Also, to properly compare the experimental data such parameters as optimal catalyst loading, light

intensity and radiation wavelength, and using a benchmark photocatalyst (e.g. P25, Hombikat) as reference are to be considered.

1.1.2 Parameters influencing the photocatalytic reactions rates

For the successful performance of the photocatalyst, it is important to control various parameters. The variables influencing the photocatalytic reaction rates can be subdivided into intrinsic, where the properties of photocatalytic material affect the performance and extrinsic, those referring to the environment and experimental conditions, in which the semiconductor is meant to be used. Intrinsic parameters include crystal phase, crystallite size, exposed crystal face, dopants, vacancies, other types of bulk defects and the surface state. While the extrinsic ones imply the type of solvent, structure of a substrate, pH, concentrations of photocatalyst and substrate, impurities and photon flux. The boundary between the intrinsic and extrinsic parameters lies on the surface of the photocatalyst and surrounding environment (liquid, gas). All the mentioned parameters influence interfacial reactions and their rates.

Some intrinsic and extrinsic parameters are strongly coupled. For example, while the degree of aggregation could be inherent to a given material, it is also simultaneously influenced by pH. The inclination of the particles to aggregation can subsequently influence adsorption of molecules, light scattering, photon absorption, charge carrier dynamics, etc. Perhaps, for the properties such as the exposed surface area and mesoporosity of a photocatalyst, such classification for intrinsic and extrinsic parameters does not capture their real nature [28].

1.1.2.1 Photocatalytic processes occurring in the bulk

As was described in the previous chapters, in SC materials under the action of light irradiation electron/hole pair is created, which later can undergo recombination, can be trapped in the bulk of the material or take part in various redox reactions (Eq. 1-7).

Ultrafast processes such as the generation, trapping and recombination of the CB electrons and the VB holes occur on femto, pico and nano time scales, while the interfacial surface reactions take place on the ms and second scale as it was established for titania [28] (Fig.

1.4). In general, the charge trapping can be favourable if (i) it helps charge separation; (ii) it permits charge storage; and (iii) the trap sites are close to the sites enabling their transfer to adsorbates [29].

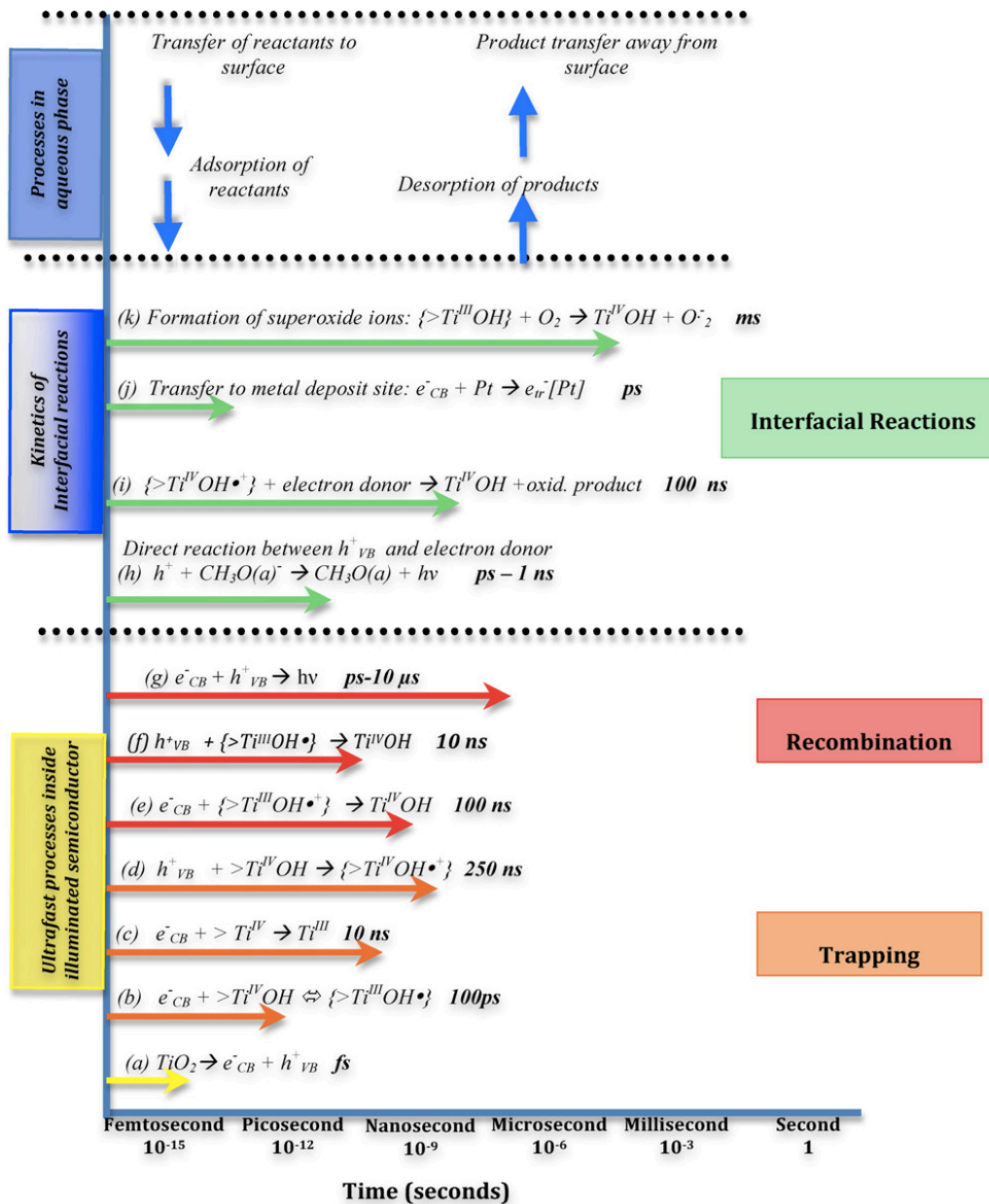


Figure 1.4 – Elementary reactions in TiO_2 photocatalysis with corresponding timescales [28].

It is supposed that, after the SC excitation and charge carriers generation, holes are forced to move to the surface and electrons to the bulk of the material. However, other studies

suggest that the electrons can also be trapped on the surface of SC. In case of titania, Ti^{4+} cations in the bulk or Ti^{4+} -OH at the surface are expected to play a role of the electron traps, giving rise to Ti^{3+} cations [30,31], while holes are getting trapped either at a bridging O^{2-} or transferred to the surface-bound OH^- anions resulting in the formation $\bullet O^-$ or/and $\bullet OH$ centres, respectively [32]. In the absence of electron scavenger such as O_2 , the lifetime of the trapped electron can last for a very long period. Bahnemann *et al.* [33] were the first to reveal that there are at least two different types of hole traps in excited TiO_2 particles; deeply trapped holes, which are long-lived and unreactive, and shallowly trapped holes, which exhibit a high oxidation potential.

If considering the suspension of a semiconductor as a 3D network, it is important to mention the so-called "antenna effect", where the charge transfer can occur from one particle to another. It is supposed that in this 3D network atomic planes of the particles are aligned in a precise way allowing the transfer of electrons or holes without the interference of interfacial trapping processes [34].

The key factors of slowing down the transport of charges to the surface are structural disorders, barriers at grain boundaries, the succession of trapping and detrapping events, and electrostatics depending on the charge concentration per particle [35]. Therefore, in that case, the doping by ions or other impurities sometimes causes not only desired visible light activation but also it decreases the activity of the material, as it creates defects in the semiconductor crystalline structure, which are potential centres for charge carriers recombination.

It is clear from Figure 1.4 that the metal addition such as Au, Pt, Pd can increase the rate of electron transfer to the substrate and this process takes ps to perform, while in case of the recombination it takes place from ps to ms. There is no surprise that this method was widely used to produce more efficient photocatalysts [36,37].

Photo-generated holes are either transferred to the adsorbed pollutant, causing its immediate oxidation, or they are first transferred to the adsorbed water molecules, generating hydroxyl radicals ($\bullet OH$). The dynamic of the hole transfer to substrate was studied for several substrates anions, e.g. SCN^- [38-40], various alcohols [41,42], carbohydrates [43] and it was

found to be in the range of ~ 100 fs - 1 ns. While transfer dynamic studies for electron to substrate, for example, O_2 , from Figure 1.4 is about milliseconds [28].

1.1.2.2 Photocatalytic processes occurring at the interface: Mass transfer and adsorption

The mass transport to the proximity of active sites of a semiconductor as well as the adsorption of a substrate can promote the interaction with the photo-generated active species or with the holes directly, hereby governing the rate of the photocatalytic process.

In heterogeneous photocatalysis usually dispersed and/or porous particles are used and the actual operating surface is not known since some parts of the material are not illuminated as a consequence of internal shading. For this reason, SSA is commonly used to characterise the specific activity of the catalyst active centres. Increasing of SSA can play a twofold role: it can negatively affect the photocatalytic performance as the increase of SSA causes a rise of the number of the defects in the material surface layer acting as recombination centres. On the other hand, a positive role of a large SSA is that it favours an increase of the number of potential adsorption sites for the preconcentration of a substrate in the proximity of the material's active sites leading to a more efficient electron transfer process.

When talking about photocatalysts it is important to consider the presence of adsorbed water molecules on its surface as usually all such reactions deal with water purification or the synthesis of organic compounds in water as a green solvent. Moreover, even in case of the use of photocatalysts in gas phase, there always will be at list several layers of adsorbed water molecules on the semiconductor surface. Let us consider a benchmark photocatalyst titanium dioxide. According to [44], the TiO_2 surface is covered with three water layers containing distinct water species: (i) the innermost layer with highly immobilized water, (ii) the intermediate layer consisting of relatively mobile water, and (iii) the outermost layer with mobilized water under the chemical exchange with water. From there, to elucidate the proper photocatalytic kinetics the process of diffusion and incorporation of the substrate should be taken into account. As was reported by Nosaka *et al.* [45], according to the solid state NMR studies at room temperature ethanol molecule was incorporated into the outmost layer of

water molecules and stabilized by hydrogen bonding. Heating at 150 °C resulted in the evaporation of water molecules and reaction of ethanol with titanol groups. Cooling down to room temperature revealed that this process was reversible. It was also suggested that water molecules allow the movement of protons from site to site on the surface and also the displacement of O atoms along and across the bridging O rows [46-48].

The dependence between the dynamics of water molecules on the surface of TiO₂ and the activation energy of the oxidation of three model substrates was addressed in [49]. By means of Fast Field Cycling (FFC) NMR Relaxometry it was possible to determine the activation energy values associated with the mobility of water on the solid surface. Interestingly, the competition on the surface between water molecules and target substrate molecules was proved experimentally.

The important role of the oxygen adsorption should also be discussed. In the case of titania, which is more frequently used for pollutants degradation because of the ability to oxidise water molecules resulting in highly oxidative •OH radicals generation, oxygen adsorption on the surface in its turn leads to •O₂⁻ superoxide that, apart from being active in the substrate oxidation, helps electron/hole pair separation and recombination suppression [50,51]. In the work of Berger *et al.* by combining EPR and FTIR studies it was found that the efficient electron scavenging by adsorbed O₂ at 140 K produces two long-lived O₂⁻ surface species associated with different titanium cation surface sites [52]. For C₃N₄ it was confirmed that •O₂⁻ radicals play the major role in the selective oxidation of the organic molecules [53,54]. Thus, oxygen adsorption kinetics determine photo-oxidation capability of semiconductors to a large extent.

In the review by Palmisano *et al.* [55], it was demonstrated that during the photo-oxidation of aromatic alcohols two parallel oxidative processes on the photocatalyst surface participate: The first one is the partial oxidation, giving rise to the corresponding aldehyde; and the second one is a complete oxidation eventually producing CO₂. It is commonly considered that photocatalysis takes place on a surface or near it, for the primer assumption, it is obvious that a good adsorption should favour a reaction kinetic. To describe the kinetics of the photocatalytic reactions zero-, first-order and most commonly applied Langmuir-

Hinshelwood (LH) models are used. The rationale that controlling adsorption may be used to obtain specificity is based on the pre-assumption that the degradation rates obey the LH kinetics, which, for single-sites adsorption (Eq. 8), is:

$$r = -\frac{dC_A}{dt} = k_r \vartheta_A = k_r \frac{K_A C_A}{1 + \sum K_i C_i} \quad (8)$$

where C_i is the concentration of species A or i in the bulk, k_r is the reaction rate constant, and K_i is the equilibrium constant of adsorption for species A or i [56]. From this model, the increase in the coverage of the solid catalyst leads to the higher reaction rates, where the influence of the saturation conditions is to be considered.

1.2 Photocatalysis for Total Oxidation Reactions

Photocatalysis is a suitable method for tackling organic pollutants in water and air media. It is especially important that this approach is capable of providing total oxidation of organic matter to a range of harmless products such as CO₂, H₂O and depending on the nature of the contaminant NO₂ or sulfur oxides. However, not all of the semiconductor photocatalysts meet the requirements of environmental applications either because of their insufficient oxidative power, low stability or high cost. The extensive investigation of various types of materials with photocatalytic activity carried out in the last decades has concluded that TiO₂ stands out of the range of the tested substances for photochemical applications and up to now it is most likely to be the best choice for light-driven total oxidation of organic compounds reactions.

Titania is one of the most studied photocatalysts due to its excellent properties such as photo, chemical and thermal stability, non-toxicity and low cost. Titanium dioxide is widely used as an inorganic pigment in paints, plastics, paper, leather, textile, food, cosmetics, etc. Other known applications are chromatographic separation, lithium-ion batteries, gas sensors, drug delivery vehicles and photocatalysis. Its use in the area of the photocatalysis usually lies in the fields of water treatment, air purification, self-cleaning surfaces production, generation of energy and alternative fuels, green chemistry and green engineering medical and biomedical applications [57]. Such extensive use of TiO₂ resulted in the commercialisation of

the two famous titania powders Aeroxide P25 and Hombikat, which are composed of anatase and rutile mixture and pure anatase nanoparticles, respectively. These commercial materials are the references in the world of photocatalysis, whose extraordinary properties challenge the scientist to develop more efficient semiconductors. In the present Chapter numerous factors determining the titania activity such as crystalline phase, morphology and doping will be addressed.

1.2.1 Aqueous phase photo-oxidation of organic pollutants in the presence of TiO₂

The industrial impact on the environment is getting more prominent with each year as the number of pollutants produced as wastes during industrial processes or coming with domestic wastewater is growing and its accumulation in the environment is inevitable. Various chemicals have been detected in the treated effluents from municipal wastewater treatment plants [58-60]. They include pesticides, dyes, pharmaceuticals, hormones, drugs, antibiotics, personal care products, disinfection by-products, surfactants, chelating agents, flame retardants, perfluorinated chemicals, etc. These compounds constitute a group of unregulated chemicals present in water and considered to be very harmful both for the human health and for the environment defined as emerging pollutants [61]. According to the recent works, the presence of these compounds was found even in the treated drinking water [62,63], since the implemented treatments both in the Wastewater Treatments Plants and the Drinking Water Treatment Plants are not capable of the removal of these pollutants. That is why the demand for eco-friendly and effective methods for water contaminants removal has become an imperative task. The main obstacle in the path of their removal is the low concentrations (from ppm to ppb) at which these emerging pollutants appear in aqueous medium. One of the promising solutions to this problem can be found in the utilisation of advanced oxidation processes (AOPs). They usually deal with water purification or wastewater treatment aiming for the degradation of toxic and undesirable compounds by means of H₂O₂, O₃, UV irradiation and photocatalysts triggering the generation of active free radical species. Among all, photocatalysis is known as an efficient oxidation process for degrading organic pollutants

at low concentrations by transforming them into H₂O and CO₂. Furthermore, these transformations are conducted under conditions avoiding heating, high pressure, toxic chemicals or other additives, apart from harmless semiconductors.

To the free radicals produced by means of semiconductor exposed to UV light one usually attribute hydroxyl radical ($\bullet\text{OH}$), superoxide anion radical ($\bullet\text{O}_2^-$), hydroperoxyl radical ($\bullet\text{OOH}$) and singlet oxygen ($^1\text{O}_2$) [64,13]. Certainly, direct interaction of the hole h^+ with the substrate or direct electron transfer to it cannot be excluded. Among them, a hydroxyl radical is known to be a non-selective species with the strong oxidative potential of +2.8 V. It rapidly reacts with the most of organic molecules degrading them eventually to CO₂ and H₂O. Hydroxyl radicals generally interact with organic compounds via three pathways: electrophilic addition (Eq. 9), hydrogen atom abstraction (Eq. 10) and electron transfer (Eq. 11) [65].



In a variety of studies on photo-degradation of aromatic compounds the addition of $\bullet\text{OH}$ radical creating phenol derivatives was established as the first reaction stage [66]. From Figure 1.5 one can see that in a typical reaction of phenol photo-oxidation the $\bullet\text{OH}$ radical attacks the phenyl ring (a), yielding catechol (b), resorcinol (c), benzene-1,2,3-triol (d) and hydroquinone (e), then the subsequent oxidation leads to the ring opening products such as maleic acid (f) following by the formation of short-chain organic acids, e.g. 3-hydroxy propyl carboxylic acid (g), 2-hydroxy propanal (i), glycolic acid (j) and finally to CO₂ and H₂O [67,68].

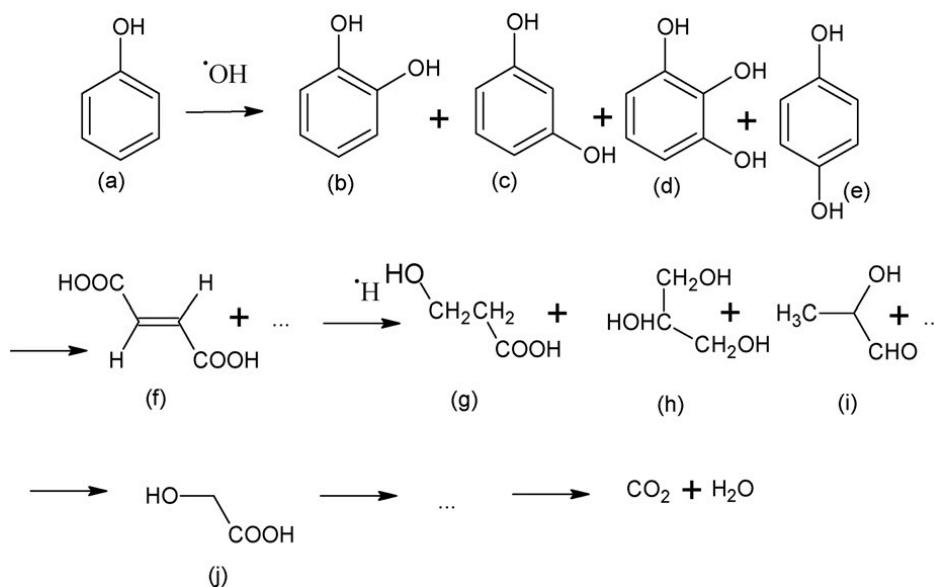


Figure 1.5 – Proposed degradation pathway of phenol over titania [68].

Along with the degradation of starting pollutants, it is also important to monitor the formation and decay of the intermediates formed in the course of the photo-reaction, as to control all the transformation steps the substrate undergoes and to identify possible hazardous by-products. Occasionally, even more toxic substances than a substrate can be created during a degradation process [69,70], this fact stresses the necessity of total mineralization of organic pollutants, which is the main goal of wastewater treatment.

The group of Bahnemann published a great number of works devoted to the study of the mechanisms of degradation of various aromatic compounds and detecting the reaction intermediates [71-74]. It was found that the irradiation of phenoxyacetic acid in the presence of titania led to the formation of two intermediate products, namely, phenol (4) and 1,2-diphenoxyethane (6). Plausible mechanisms for the formation of these two products are shown in Figure 1.6, where at the first stage the compound undergoes the $\cdot\text{OH}$ radical attack, its subsequent addition and loss of the ($-\text{OCH}_2\text{COOH}$) group to give phenol (4). Alternatively, the model compound 1 on addition of hydroxyl radical followed by loss of CO_2 may lead to the formation of the 1,2-diphenoxyethane (6) as the result [71]. Similar mechanisms including the transfer of an electron forming the radical anion, which further may undergo addition of a hydroxyl radical, followed by a loss of functional group were

proposed. Though, in some cases, the cyclisation products were also detected as intermediates [72-74].

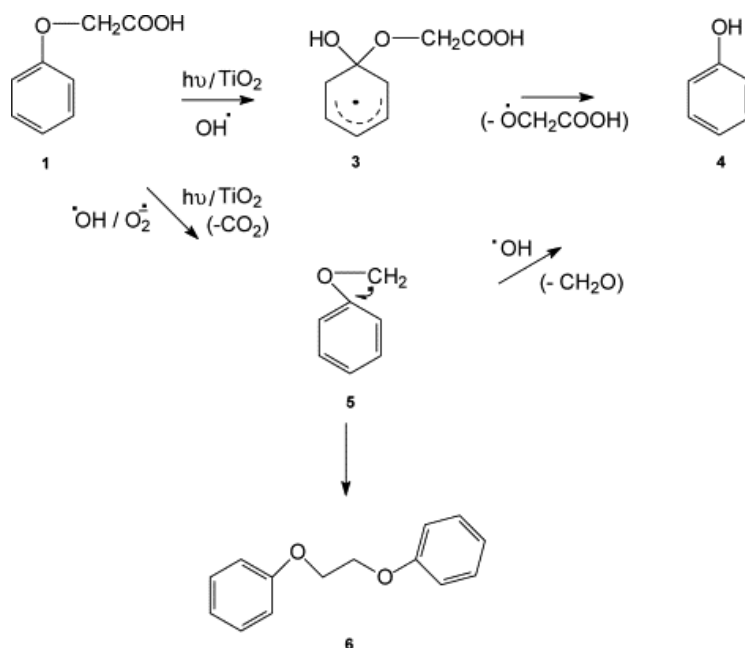


Figure 1.6 – Proposed mechanism for the formation of the observed products during the photo-degradation of phenoxyacetic acid [71].

The possible synergetic or antagonistic effects of the pollutants produced during the photocatalytic reactions is often neglected, however, it may have a great influence on the toxicity of the treated water streams [75]. A standard method frequently used to determine ecotoxicity in the aqueous medium is based on the *Vibrio fischeri* bioassay [76]. Not only the organic part of the photocatalytic suspension is to be considered while speaking about the toxicity of the treated water. The disaggregation of the titania particles under UV light might take place leading to the release of nanoparticles into the solution, which can eventually enhance the toxicity of the system [77,78]. Consequently, the photocatalytic wastewater treatment is a rather complex process requiring that all of the abovementioned aspects to be assessed for ensuring the acceptable quality of the purified water.

1.2.2 Methods for controlling titanium dioxide crystal phase

There are three natural polymorphs of titania: anatase, rutile and brookite (Fig. 1.7). They differ by the crystalline structure and electronic properties. For example, their BG values are 3.2, 3.0 and ~ 3.2 eV, respectively. Anatase phase is unanimously considered to be the most photocatalytically efficient, that is why it is used in a variety of applications as the preferred titania polymorph. Some authors suggested that this superior activity can be explained by the fact that the CB of anatase is about 0.3 eV more positive than the CB of rutile and the excess of electrons in the CB of anatase has more driving force for the reduction of the reactants [79]. Moreover, according to the experimental data obtained by Kakuma *et al.*, the rate of the $\bullet\text{OH}$ radicals formation on anatase phase is higher than the one for rutile [80]. The differences in the surface hydroxylation may also contribute to the contrast of photoactivity of the material. Additionally, the lower activity of rutile is also attributed to its lower capacity to adsorb O_2 , which is necessary to prevent electron-hole recombination [79].

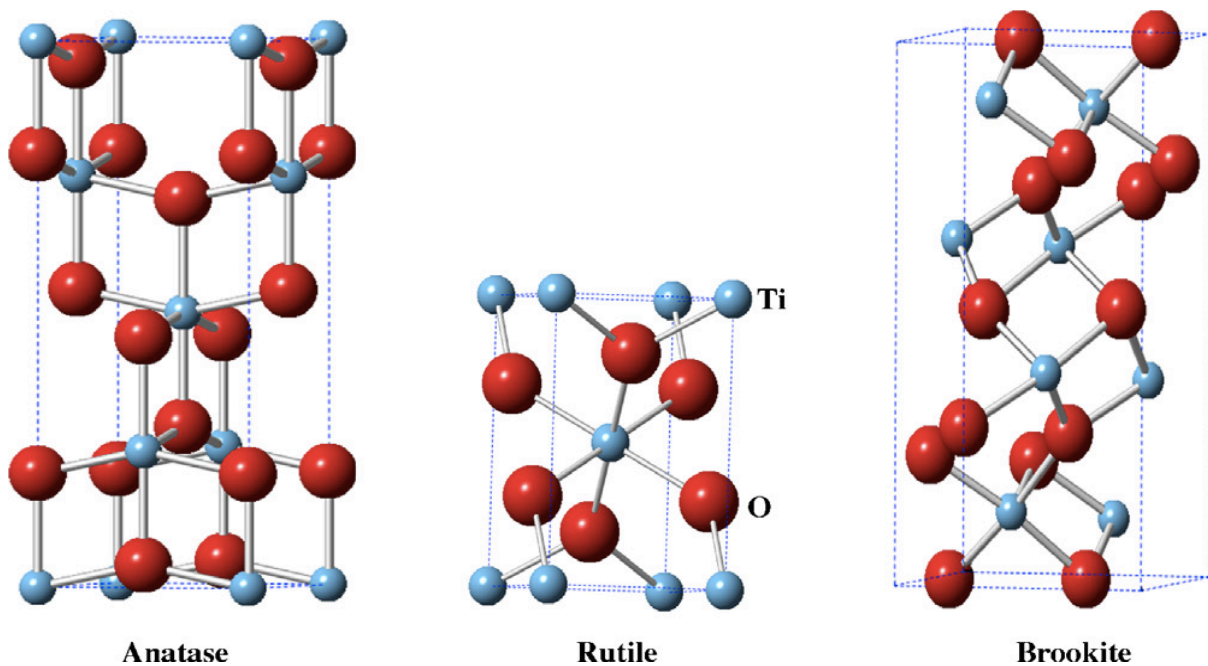


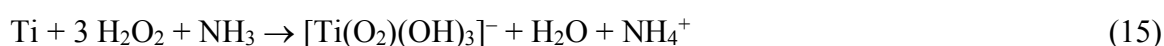
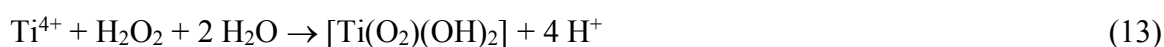
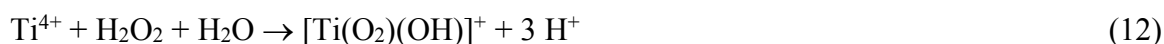
Figure 1.7 – Representation of the titania natural polymorphs crystalline cells: anatase, rutile, brookite [81].

Unfortunately, anatase, unlike rutile, is a metastable phase. Pure anatase is only stable if its particle size does not exceed a critical size, whose upper limit is 15 nm [82], which was also supported by theoretical calculations [83]. Alternatively, the stability of this polymorph can be achieved by various approaches such as preparing mixed $\text{TiO}_2\text{-M}_x\text{O}_y$ type oxides, for example $\text{TiO}_2\text{-SiO}_2$ [84-86], $\text{TiO}_2\text{-ZrO}_2$ [87], $\text{TiO}_2\text{-WO}_3$ [88], $\text{TiO}_2\text{-Cr}_2\text{O}_3$ [89], by ion doping [90-93] or by creating the defect sites of different nature in anatase crystalline cell, for instance by generation of oxygen vacancies or Ti^{3+} containing sites [94]. It is important to mention that the defects discussed above indeed stabilise anatase phase, but on the other hand, they also decrease the crystallinity of the photocatalyst creating disordered regions and hence the potential recombination centres for e^-/h^+ [95]. Thermal treatment is widely applied, in order to improve the crystallinity of anatase, but in this case, the average particle size grows making anatase polymorph less stable. Thus, the balance between the phase stability, high crystallinity and crystal size are the crucial factors to be considered while designing the TiO_2 photocatalysts.

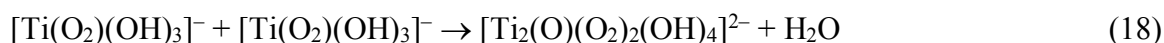
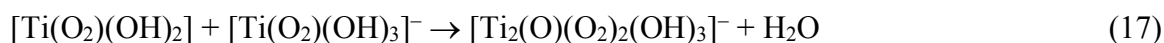
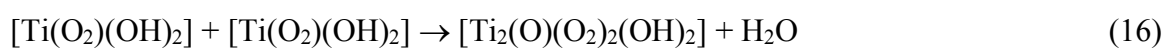
1.2.3 Titanium dioxide synthesis using H_2O_2 -assisted methods

Liquid-phase synthetic approaches for titania preparation are more effective and versatile than the vapour-phase ones since better control of structure and morphology of the final products are generally achieved [96]. These methods usually include solvothermal, microwave-assisted, reflux, sol-gel or sonochemical procedures. In these techniques, the control of the nucleation processes and growth usually is carried out by the use of organic ligands requiring their elimination after the synthesis, which is frequently complicated and incomplete. The tendency towards the green synthesis of photocatalysts has resulted in a search for new precursors for titanium dioxide, which would help to avoid the use of toxic and unstable compounds like titanium alkoxides and structure directing agents. An alternative way to solve this problem could be found in the utilization of water-soluble titanium peroxo complexes, where H_2O_2 coordinates Ti atom and subsequently, while forming titania, leaves only water as a by-product.

Usually the synthesis of peroxy-hydroxy complexes of titanium, e.g. $[\text{Ti}(\text{O}_2)(\text{OH})_3]^-$ or $[\text{Ti}(\text{O}_2)(\text{OH})_2]$, includes direct reaction between titanium tetrachloride and hydrogen peroxide in acid media (Eqs. 12-14) or the reaction between metallic Ti and H_2O_2 in the presence of ammonia (Eq. 15). Also, the reaction of freshly prepared precipitates of titanic acid with H_2O_2 leads to the formation of bright-orange or yellow coloured, depending on the pH, solutions [97].



Here are some examples of the dimer complexes formation (Eqs. 16-18):



Dimer complexes presented above can undergo further self-condensation or can react with other dimers or monomers forming oligomeric fragments. As the result of this prolonged condensation the precipitate of hydroxy peroxy titanium $[\text{Ti}(\text{O})(\text{O}_2)_2(\text{OH})_2]_n$ is produced. The excess of hydrogen peroxide helps to keep the $[\text{Ti}(\text{O}_2)(\text{OH})_3]^-$ from precipitation, thus no organic ligands are needed to ensure the complex stability. Varying the pH value provides the control of mono-, di- and oligomeric complexes formation and allowing eventually to tailor the properties of the resulted oxide. However, in some studies, titanium peroxy complexes were further stabilized with organic ligands, e.g. lactic acid [98], citric acid [99] or tartaric acid [100] what resulted in better control of the crystalline phase or the morphology of the oxide material produced from these precursors.

Furthermore, the approaches implying the use of metal peroxo complexes are also effective for the mixed oxide synthesis such as the case of TiO₂-WO₃ heterojunction with satisfied WO₃ distribution and high photocatalytic activity [101] and for the low temperature peroxo-assisted hydrothermal synthesis of N-doped TiO₂ [102,103]. As was revealed by Etacheri *et al.* [93] titania synthesized from titanium peroxo complex possessed high thermal stability of anatase phase up to 900 °C. Later, Krivtsov *et al.* [104] scrutinised the local structure of such exceptionally stable titania anatase by EXAFS and XPS study reaching the conclusion that the initially produced N-doped titania lose N atoms at high temperatures, which is accompanied by the occupation of the created vacant sites by the atmospheric oxygen. Eventually, it results that the coordination number of the titanium surrounded by interstitial oxygens increases, and owing to the defects produced the thermal stability becomes higher. High thermal stability of titania also was reached by using the solvent-exchange (SE) method, where titania peroxo complex was precipitated using several organic solvents, however, one might suggest that the mechanism underlying its stability is very similar to the cases reported by Etacheri *et al.* [93] and Krivtsov *et al.* [94].

1.2.4 Tuning titanium dioxide morphology

The control of the shape of titania crystals and the morphology of their agglomerates is also an important challenge since they affect the photocatalyst's performance to a significant extent by influencing the electrical conductivity, optical, magnetic and photocatalytic properties.

The morphology of solid materials can be divided into several sub-groups: zero-dimensional (0D), such as molecular metal clusters and complexes, one-dimensional (1D) (wires, rods, nanotubes), two-dimensional (2D) (films, sheets), and three-dimensional structures (3D) of bulk solids. It is worth mentioning that the morphology could be defined by the crystal shape itself (for example rods, wires, nanotubes) or by the aggregates of crystals or particles (films, spherical particles).

Starting from 1D materials, there is a wide range of methods allowing control over the morphology of the photocatalysts based on titania. Among them are nonhydrolytic solution approach [105] and hot filament method for the titania nanowires production for gas sensing [106]. The application of more sophisticated approaches for governing the morphology such as biomineralisation assisted with enzymes is less frequent. In the work of Nonoyama *et al.* [107] the low-temperature synthesis of rutile phase nanofibres was achieved. Moreover, nitrogen that was in the peptide structure was successfully introduced into the TiO₂ during the sintering as a doping element leading to the shift of the absorption edge of the material to the visible light range.

For the preparation of 2D materials, such as films, several approaches were applied among them were dip coating [108], sol-gel [109,110], solvothermal synthesis with the following drop-casting deposition of a mesoporous thin layer [111], block copolymer-assisted sol-gel route with spray coating for titania.

In the field of TiO₂ 3D structures, the synthesis of titania spherical particles is of particular interest [112]. Spherical shape provides the material with such properties as uniformity and close packing, thus facilitating its sedimentation and reuse in batch catalytic processes or making it applicable as a chromatographic stationary phase. A wide range of methods allowing synthesis of titania spherical particles is known, which includes hard templating, utilizing organic as well as silica materials [113,114], soft template-assisted alkoxide based sol-gel syntheses [115-117] or less common template-free methods, where titanium organometallic source is used [118,119], synthesis in emulsions [120-122], or by aerosol formation [123]. The tunability of the porosity of titania spheres is very important as it is the parameter which determines the accessibility of the reactants to the surface sites of the catalyst. Caruso *et al.*, by varying the amount of structure-directing agent involved in the sol-gel synthesis, made possible to control the porosity in the range of 14-23 nm [115]. The easier and more straightforward procedure for the preparation of titania hierarchical spherical structures with tunable porosity was achieved by the application of hydrothermal procedure in the presence of ammonia ensuring the porosity of the TiO₂ spheres [124].

Titania spheres can also have a hollow structure, which provides some advantages over their bulk counterparts in certain industrial applications, e.g., fillers, pigments, and coatings, because of a lower density of the hollow particles. This type of spheres with enhanced photocatalytic activity was synthesized by sol-gel method with the subsequent thermal treatment for the carbon-containing template removal or NaF etching for silica elimination [125-127].

1.2.5 Photocatalyst recyclability

Recyclability is an important and desirable property of the photocatalyst, since it allows the utilisation of the photo-active material repeatedly in the consecutive reaction cycles. Achieving easy recoverability is an attractive goal, which would promote the application of photocatalysis for water purification on an industrial scale.

Titania Aeroxide P25, due to its high photocatalytic activity, is considered as "golden standard" among the all variety of the commercially available titanium dioxide materials. In spite of being an effective photocatalyst, it possesses a significant drawback as it is composed of small particles of around 20 nm, which are difficult to separate from the suspension after the reaction and, as a consequence, high amount of the photocatalyst gets finally lost [128]. Charbonneau *et al.* in order to overcome this problem, proposed an easy and effective method in which small Aeroxide P25 particles were aggregated by introducing di-carboxylate linkers following the fast and low-temperature infra-red drying for the linkers elimination [129]. The resultant material possessed developed porous structure and had high SSA values, although, the change in photo-activity before and after the aggregation was not studied. Bahamonde *et al.* [130] studied three commercial photocatalysts (P25 Aeroxide, P25/20 VP Aeroperl and P90 Aeroxide) with similar structural and electronic properties but different morphology and aggregate sizes. P25/20 VP Aeroperl is a granulated version of P25 photocatalyst and P90 Aeroxide consists of even smaller particles of 14 nm. Interestingly, it was found that the phenol photocatalytic oxidation followed $P25 > P90 > P25/20$ order that implies that granulated material was less active.

Magnetic-TiO₂ composite materials were also suggested for achieving separation of photocatalyst from the reaction medium [131-135], as well were thin films [136,137], membranes [138], and sub-micron or micron-size spherical particles. Microspheres find their application in many fields, but most importantly, spherical particles provide a desirable form for a solid catalyst facilitating its reuse [139-141].

In the book [142] Kisch stressed the necessity of proving a true catalytic nature of heterogeneous photo-assisted reactions. Similar to the case of conventional catalysis, in photocatalysis the material must not be consumed during the reaction and provide its repetitive use. Often the reported reaction is only claimed to be photocatalytic, although the repetitive use of the photocatalysts is not demonstrated.

1.3 Photocatalysis for Partial Photo-Oxidation

Contrary to the case discussed in the preceding chapter, partial photocatalytic oxidation requires another type of semiconductors to efficiently perform selective organic compounds transformations to desirable products. The positions of the VB of TiO₂ is clearly inappropriate to promote this kind of reactions and especially in water medium, apart from that one may consider that the material with lower hydroxylation degree and higher affinity to organic molecules would demonstrate better performance. Although there is a wide selection of inorganic and metal-organic photocatalysts capable of partial oxidation driven by light irradiation, the economic and environmental reasoning call for less expensive and non-toxic catalyst whose preparation procedure would be scalable to meet the needs of industry. Polymeric carbon nitride is a promising non-metallic photocatalyst, which has recently evoked an interest of the research community, due to its facile synthesis, high chemical stability, attractive electronic structure and the fact that it consists of earth-abundant elements, carbon and nitrogen. Interestingly, carbon nitride is one of the oldest synthetic polymers [7], whereas its utilization in the heterogeneous catalysis arena started only recently in 2006 [143], and thank to the discovery of Wang *et al.*, a metal-free conjugated semiconductor photocatalyst, g-C₃N₄, was reported to possess a significant activity for photocatalytic H₂ evolution [144].

There are seven known phases of C_3N_4 , which include α - C_3N_4 , β - C_3N_4 , cubic C_3N_4 , pseudocubic C_3N_4 , g-h-triazine, g-o-triazine, and g-h-heptazine with BGs of around 5.49, 4.85, 4.30, 4.13, 2.97, 0.93, and 2.88 eV, respectively [145]. However, the most stable one at ambient conditions is considered to be tri-s-triazine-based C_3N_4 [146]. Besides, this particular phase, unlike TiO_2 photocatalysts, possesses BG allowing absorbance of a visible light portion of irradiance in the range of 450-460 nm, thus increasing even more the utilization of this material for the solar-light promoted photocatalysis. Recently, a great number of comprehensive and inspiring reviews has been published underlying the interest of researchers towards the investigation of polymeric carbon nitride (PCN) materials [7,147-151].

1.3.1 Polymeric carbon nitride application in partial selective photocatalytic oxidation

Polymeric carbon nitride finds its application for contaminants degradation in water [152], in the reactions of selective photo-oxidation [53,54,153], H_2 production via water splitting [150] and CO_2 reduction [149]. This chapter will be focused on the partial photo-oxidation of organic molecules using PCN-based materials.

Carbon nitride, in addition to its high ability to reduce water protons to molecular hydrogen, possesses a valence band potential which does not permit direct water oxidation to $\bullet OH$ radicals [144], hence reducing the presence of notoriously unselective oxidative species in water suspensions of photocatalyst with organic compounds. It is generally supposed that the main oxidative species in partial oxidation reactions under UV irradiation are $\bullet O_2^-$ radicals. The proposed scheme of organic alcohols photo-oxidation to subsequent aldehydes with help of $\bullet O_2^-$ is shown in Figure 1.8 [154].

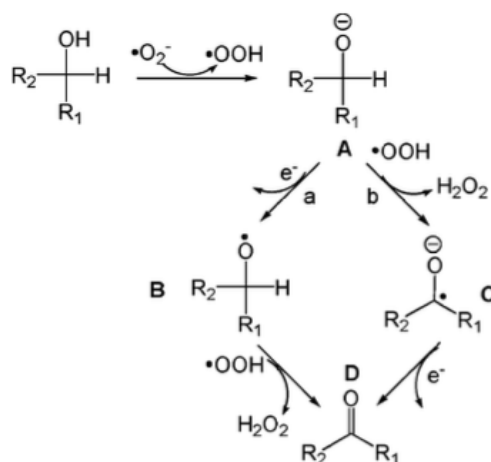


Figure 1.8 – Proposed oxidation mechanism of alcohols on PCN [154].

The selective oxidation of the methyl group substituent of aromatic compounds to the corresponding carbonyl and carboxyl functionalities is a process of an immense importance for the activation of raw materials in organic synthesis [155]. The C–H bond oxidation of alkyl side-chains in aromatic hydrocarbons is well-developed, and many catalytic approaches are successfully applied for this purpose [156-159]. The presence of competitive easily oxidised substituents in a benzyl ring such as electron donating –C–OH, C=O, –O–C, or –NH₂ groups complicates achieving activation of a more inert C–H bond. Thus, a variety of methods utilizing homogeneous oxidation [160-162], photoactive complexes [163], metal oxide-supported noble metal nanoparticles [164], enzymes [165,166] and electrochemical oxidation in ionic liquids [167] have been developed to overcome this obstacle. Many of the existing oxidation protocols are complicated and expensive, they often demand the presence of toxic oxidants and/or organic solvents, also external heat must be supplied for the reaction to take place. Thus, they are energy consuming and not environmentally benign. The use of molecular oxygen as a green oxidant and UV or visible-light irradiation as an energy source for the partial oxidation of organic molecules along with the application of inexpensive, non-toxic, easily recoverable and zero-waste semiconductor photocatalysts such as TiO₂ or g-C₃N₄ have recently attracted attention [168,169]. So far, the published data on photo-conversion of organic molecules in the presence of semiconductor photocatalysts have been limited to the oxidation of the hydroxyl group of aromatic and aliphatic alcohols to the

carbonyl group [154,170], sulfides to sulfoxides [171], amines to imenes [172,173], and to the oxidation of benzene or the alkyl group of hydrocarbon compounds [174-176]. Although Verma *et al.* reported the carbon nitride promoted photo-oxidation of C–H groups of substituted toluenes, they stated that g-C₃N₄ was not active in the absence of vanadium oxide and H₂O₂ [174]. It implies that the quest for the greener and the easier ways to selectively photo-activate C–H bonds is still on and the optimal photocatalysts and reaction conditions for such transformations to take place are to be found.

Wood industry and agricultural sector release a large amount of by-products and wastes, which if processed appropriately, can be converted into a range of valuable chemicals or fuels. Cellulose, an abundant biomass compound, can be upgraded by undergoing hydrolysis producing hexose sugars, which after being subsequently dehydrated give the biomass platform molecule 5-hydroxymethyl furfural (HMF) [177,178]. While HMF itself has few applications, the products of its oxidation 2,5-furandicarboxylic acid (FDCA) and 2,5-diformylfuran, also known as 2,5-furandicarboxaldehyde (FDC), possess properties making them valuable for polymer production [179-183]. Many catalytic procedures have been developed for obtaining both FDCA [184,185] and FDC [186-190] by oxidising HMF, but photocatalysis is among the most economic and greener alternatives as it benefits from a nearly free energy source, which is solar radiation, and does not require toxic oxidants. Light-initiated transformation of biomass aiming to produce fuel has recently been reported by Wakerley *et al.* [191], while the approaches for its chemical upgrading has been reviewed in [192]. HMF itself was subjected to the electrophotocatalytic [193] and photocatalytic conversion in aqueous phase using TiO₂ as the photocatalyst, and FDC was found to be the main oxidation product of this reaction [104,194]. Although TiO₂ and especially N-doped TiO₂ promoted the formation of FDC from HMF, the selectivity of this process was low reaching 30% for the best photocatalysts, owing to the formation on the TiO₂ surface of highly oxidative hydroxyl radicals inducing the substrate mineralisation [104]. Despite this attractive property, this material has mostly been used for conversion of aromatic alcohols [154,174,195,196] and hydrocarbons [175,197-199] in organic solvents [200], while reports on its performance in aqueous phase are scarce [201,54]. Recently, the enhanced selectivity of PCN for aqueous phase HMF to FDC photo-oxidation with respect to that previously

achieved in the presence of TiO₂ [194] has been reported [53,54]. A detrimental effect of the presence of non-polymerised carbon nitride species on the selectivity of photo-oxidation has also been observed [53]. Thermal etching applied to bulk PCN, principally with the purpose of increasing its SSA, also eliminated excessive NH and NH₂ moieties from the PCN surface resulting in the growth of selectivity toward the FDC production from 30% to 50% under solar irradiation [53].

Replacing organic solvents with water as a medium for partial oxidation is an important challenge since it makes the process cost-effective and environmentally benign. Although, the difficulties of carrying out selective oxidation in aqueous phase are well-known for titanium dioxide, e.g. complications in interactions of the substrate with reactive species on the surface of TiO₂ and favouring the production of unselective •OH radicals. However, the literature survey shows that this question is barely addressed for the carbon nitride photocatalysis. HMF photo-oxidation in the organic solvent catalysed by thermally exfoliated PCN resulted in the selectivity to FDC of up to 75%, which is significantly higher than the corresponding value obtained in aqueous medium [53]. Obviously, the presence of water has a detrimental effect on the reaction selectivity. As was discussed above it is commonly accepted that PCN cannot form •OH radicals by directly oxidising water with photo-generated holes, whilst it is possible by the action of photo-generated electrons mediating H₂O₂ formation [202]. The reaction of an aromatic compound with hydroxyl radical leads to the ring opening and the formation of aliphatic intermediates thus reducing the selectivity of the photo-oxidation reaction. However, the question of the generation of hydroxyl radicals on carbon nitride remains controversial and it is not completely clear the role of the non-polymerised and partially polymerised carbon nitride species in selective oxidation. There is a demand for a research which would shed some light on these aspects of PCN-driven photo-reactions and to find the means of controlling the PCN selectivity in aqueous phase.

1.3.2 Methods for polymeric carbon nitride synthesis

Satisfactory thermal stability of g-C₃N₄ material approaching 600 °C in air allows diversification of the methods that can be applied for its production. Among them are thermal

condensation that can be carried out either in inert atmosphere, or under a self-produced atmosphere containing ammonia vapours, which is created when precursor is heated in a closed crucible [144], solvothermal and microwave-assisted approaches [203-205], supramolecular pre-assembly [206,207], molten salt technique [208-210], chemical vapour deposition (CVD) [211] and plasma sputtering deposition strategies [212]. There is a variety of different carbon nitride precursors, but economic reasoning makes urea, thiourea, melamine, dicyandiamide, cyanamide the most widely used.

After the first prediction of β - C_3N_4 as new superhard material [213,214] a lot of attempts using plasma or hot-filament-assisted CVD technique were done in order to deposit carbon nitride films on Ni, Fe and Si substrates applying a mixture of N_2 and CO, C_2H_2 , CH_4 , $C_2(CN)_4$ and fullerene as carbon and nitrogen sources [211,215-217]. Also sputtering [218-221] and laser ablation methods [222,223] were used. Nonetheless, the desired stoichiometric C_3N_4 has never been produced. The most common method for carbon nitride synthesis for catalytic applications has become a simple thermal condensation in air or under inert gas flow. It was found that the temperature increase causes a sequence of transformations of C_3N_4 precursors, which are accompanied by the deammonification processes giving rise to such molecules as melamine, melam, melem, melon and finally polymeric carbon nitride (Fig. 1.9) [224]. If the starting compound is melamine, it initially forms a dimer called melam ($[(H_2N)_2(C_3N_3)]_2NH$) that rapidly reacts above 360-390 °C to form a heptazine-based molecule called melem (triamino-tri-s-triazine, triamino-heptazine, $C_6N_7(NH_2)_3$). Several routes for its formation were proposed starting from the direct formation of melem from melamine or through the stage of melam formation [225]. In [226] several adducts of melem and melamine, which potentially can be the intermediate products to melon, were obtained by heating the precursor in sealed glass ampules. At higher temperatures melem condenses to form oligomers, which after being heated up to 500 °C transform to melon consisting of 1D chains of amine-linked heptazine fragments with the formula $[C_6N_7(NH_2)(NH)]_n$, also known under the name of Liebig's melon [227]. At 520 °C polymeric carbon nitride is finally produced [224]. The general formula of carbon nitrides written as C_3N_4 can be a cause of confusion, as it does not contain H atoms, however, in practice it is impossible to reach total deammonification of the material as $-NH$ and $-NH_2$ groups will always be present at the

borders of the non-polymerized fragments and H content is usually of 1.5 wt% or higher. Although layered carbon nitride structure is somewhat similar to the graphene one, the term "graphitic carbon nitride", "graphitic CN" or "g-C₃N₄" frequently encountered in literature appear to be not entirely correct and the use of an alternative term, polymeric carbon nitride (PCN), is encouraged instead [228].

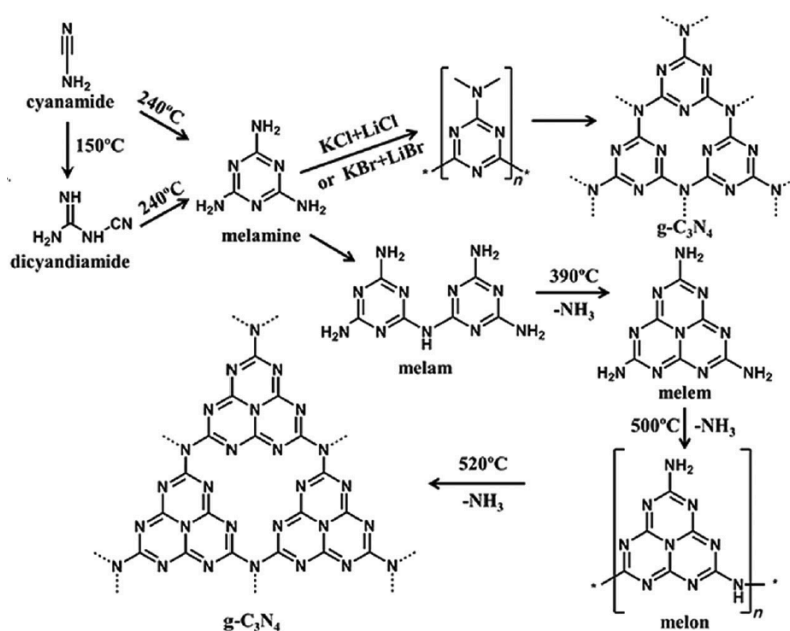


Figure 1.9 – Schematic representation of carbon nitride condensation from different precursors [224].

Another strategy for carbon nitride preparation is molecular pre-assembly, where precursor's molecules are arranged in aggregates by noncovalent bonding under equilibrium conditions due to the specificity of this kind of interactions. This method has certain advantages before the conventional thermal condensation of PCN precursors, as it allows to control the material polymerization utilizing well-organized supramolecular structures avoiding the use of templates and inhibiting the sublimation occurring for low-molecular weight precursor. Indeed, supramolecular pre-assembly of triazine molecules has become an interesting method to improve photocatalytic properties of this material. For example, melamine can form supramolecular aggregates with the cyanuric acid of different types depending on the used solvent [229-231], complexes of melamine-trithiocyanuric acid [232],

or with its derivatives were also reported [233]. This strategy was applied in the work of Antonietti *et al.* where melamine-cyanuric acid building blocks were used for the synthesis of C_3N_4 with tuned morphologies (spheres, flowers, rods, and tubes) [207].

The formation of poly(heptazine imide) demonstrates that thermal treatment of carbon- and nitrogen-containing monomers and oligomers stops short of full condensation and deamination once melon aggregates of a certain size are formed. This is believed to be a kinetic problem that can be addressed by adding solvent that provides more mobility for reactants [228]. For this reason, salt melt method is widely applied. As it was discussed above, the condensation of polymeric carbon nitride takes place at 500-520 °C in inert atmosphere, and it is obvious that not all of the common solvents are suitable. Apart from the use of salts as a solvent for the carbon nitride condensation they can also serve as templates for tailoring the material porosity and morphology. Through this strategy, it is possible to obtain a polymeric structure based on triazine units instead of the heptazine ones [224,234] (Fig. 1.9). In a pioneering work on carbon nitride synthesis utilizing above mentioned technique [208], Bojdys *et al.* in attempt to reach highly crystalline carbon nitride material used the eutectic LiCl-KCl mixture possessing high-temperature stability, non-corrosive properties and its melting point was below the polycondensation point of s-heptazine. However, the intercalation of Li and Cl into PCN is unavoidable in this case, thus compromising the purity of the obtained products [234]. Also, for the ionothermal synthesis different cations were known to be used such as Co, Sn, Zn, Cs and Na [235-237].

Microwave-assisted methods for carbon nitride production have some notable advantages before the conventional solvothermal or ionothermal approaches, as it makes the process time-saving through the achievement of the high heating rates of the precursor. Hu and co-workers, synthesized the PCN microspheres with enhanced photocatalytic activity by subjecting the precursor to a temperature of only 180 °C for 60-120 min [205]. Another example of successful polycondensation is a microwave heating of N-rich precursor in a crucible, where the whole process took several minutes to accomplish [204]. In the work of Liu [203] a novel route combining the hydrothermal pre-treatment of dicyandiamide followed by microwave heating resulted in a holey C_3N_4 material with extended light absorption range.

C₃N₄ nanorod networks were fabricated by solvothermal synthesis through the polycondensation of cyanuric chloride and melamine in acetonitrile at 180 °C for 96 h. [238].

1.3.3 Control of textural properties of polymeric carbon nitride

The described above methods for the carbon nitride condensation are attractive because of their simplicity, but they have a considerable drawback, which is a low SSA of the resulting material, usually only about 10 m² g⁻¹. This is attributed to the stacking of polymerized heptazine layers. Within the C₃N₄ layer, the C and N atoms are covalently bonded, whereas van der Waals forces inherent in the hydrogen bonding between the partially-polymerized and non-polymerized carbon nitride species hold the layers together. In order to break these strong hydrogen bonds and consequently increase SSA, improve optical, electrical and mechanic properties, one can delaminate the as-prepared PCN by top-down strategies such as thermal or chemical exfoliation. Alternatively, bottom-up strategies can be applied implying the use of hard or soft templates to direct the condensation pathway of PCN sources.

1.3.3.1 Polymeric carbon nitride exfoliation strategies

One of the attractive and frequently used methods for the exfoliation of bulk carbon nitride is the thermal etching. Liu *et al.* [239] proposed a simple top-down technique consisted in thermal treatment of bulk PCN in air producing the material, which retained the PCN structure but at the same time possessed SSA of 306 m²·g⁻¹. This approach was later successfully applied by García-López and co-workers [53], where delaminated carbon nitride showed higher selectivity in the photo-oxidation reaction of HMF to FDC in water medium. The improved selectivity was assigned to the elimination of the low-condensed carbon nitride fragments in the course of thermal oxidation. However, to the downsides of this method one can attribute the low yield of the exfoliated material, as the largest part of it is oxidized in air, and the difficulties of controlling the reproducibility. Carrying out the same thermal exfoliation procedure in inert atmosphere does not lead to the same results and the SSA

barely changes, while applying H₂ flow causes hydrogenation of carbon nitride and, possibly, its partial gasification, thus favouring the increased SSA [240,241]. The results obtained in the discussed studies suggest that the enhancement of SSA occurring while treating carbon nitride at high temperatures is hardly can be attributed to the weakening of the hydrogen bonding between the melon layers leading to the exfoliation, but it is most possibly the consequence of the partial gasification of the material.

Liquid-phase exfoliation, due to its simplicity, has become a widely applied technique for improving textural properties of bulk PCN. Ultrasonic-assisted liquid exfoliation of PCN was carried out in various organic solvents [242-244] and in water [245] as the dispersion medium. Yang *et al.* [242] found that the sonication of PCN in iso-propanol provided the formation of the material with remarkable SSA values reaching 384 m²·g⁻¹. Another method consisted in a sonication of the carbon nitride powder in mixed solvents, ethanol (isopropanol, dimethyl formamide) and water, was proposed [246], however, the SSA values reported for C₃N₄ exfoliated via this method were only about 60 m²·g⁻¹. Although the results obtained applying liquid-phase exfoliation of PCN seem promising, this method is not exempt from downsides. The principal obstacles complicating its wider implementations are prolonged sonication time, need for the separation of the bulk and exfoliated parts of the material and relatively small yields seldom exceeding 15%. Solvothermal approach for PCN delamination was also developed. The atomically thin mesoporous nanomesh of graphitic carbon nitride having the SSA of 331 m²·g⁻¹ was prepared by solvothermal treatment of its bulk counterpart [247].

Chemical exfoliation strategies imply the use of acids or bases, sometimes coupled with the sonication or solvothermal treatment. NaOH etching followed by sonication [248] or subjection to solvothermal conditions [249] were successfully applied for the PCN delamination. As for the acid chemical exfoliation, H₂SO₄ [250,251], HNO₃ [252], HCl [253,254] were utilized. The comparative analysis of the effect of different exfoliation techniques such as chemical, ultrasonic irradiation, hydrothermal, ball milling on the PCN properties reported in [255] clearly demonstrated that only the thermal etching is capable of

enhancing SSA of carbon nitride significantly (up to $161 \text{ m}^2\cdot\text{g}^{-1}$), while the same parameter obtained using other approaches did not exceed $14 \text{ m}^2\cdot\text{g}^{-1}$.

1.3.3.2 Template-assisted methods for polymeric carbon nitride synthesis

Another approach allowing the tuning of the photocatalysts textural properties by introducing the porosity and controlling the morphology is the bottom-up techniques based on the use of templates. These methods promote the formation of PCN with larger SSA, a higher quantity of active sites and more efficient charge separation, which are all supposed to enhance photocatalytic activity [228]. Usually, templating is divided into hard and soft. Hard templating implies the use of rigid solid materials with known and well-ordered structure and morphology during the PCN condensation followed by their posterior removal commonly using appropriate solvents. By this process the solids with different pore geometries and architectures from nanometres to macroscale are produced. Typical structure directing agent used as a hard template for PCN synthesis is silica having a range of various morphologies or porous structure including micro-, meso- and macroporosity [256-260]. For the template synthesis silica carcass was mixed with the PCN precursor and subjected to the thermal treatment to initiate their interaction, filling the template's pores and carbon nitride condensation. The second step usually involves the removal of silica by dissolving it with HF or NH_4F . Mesoporous silica matrices allowed to vary SSA values of the produced carbon nitrides from 8 to $373 \text{ m}^2\cdot\text{g}^{-1}$ [256]. Widely known commercial silicas MCM-41 [258] and SBA-15 [261] were used to render mesoporosity to PCN. In another example, silica nanoparticles induced the formation of mesopores in carbon nitride with the mean size of 12 nm and produced the material with $439 \text{ m}^2\cdot\text{g}^{-1}$ of SSA [259]. The morphology control of PCN via the hard templating is also possible such as the preparation of this photocatalyst in the forms of nanorods [262] and nanospheres [263] were reported.

Soft templating is considered as a green procedure for the improving the PCN textural properties, since it offers application of non-toxic organic templates such as surfactants, ionic

liquids, block polymers etc., which after the synthesis are removed from the obtained material by extraction or thermal oxidation. Nonionic surfactants and amphiphilic block polymers such as Triton X100 [264-266], P123 [267], F127, Brij30, Brij58 and Brij76 [268] etc. were successfully acted as soft-template directing agents for introducing porosity into polymeric carbon nitride photocatalysts. Ionic liquids can play a twofold role by acting as the reaction medium possessing high chemical and thermal stability, as well as the structure directing agents. The viability of this approach was demonstrated using 1-butyl-3-methylimidazolium tetrafluoroborate [269,270], 1-butyl-3-methylimidazolium hexafluorophosphate [271,272] for PCN preparation.

1.3.4 Modification of melon structural units of polymeric carbon nitride

In order to reduce the charge carriers recombination, improve photocatalytic efficiency and electrical conductivity different means of modification of carbon nitride such as doping and copolymerization, which will be discussed in the present chapter, have been proposed.

To modify the electronic properties of the PCN material aiming to achieve its more efficient use under visible light or tune its redox potential and charge-carrier mobility various types of doping are widely applied. Carbon nitride doping approaches are usually divided into nonmetal, metal and simultaneous nonmetal and metal doping. The modification can proceed in-situ during the course of carbon nitride polymerization (usually a source containing doping element is added before or during carbon nitride polymerization) and ex-situ approaches where doping is carried out after C_3N_4 is produced.

1.3.5 Carbon nitride doping and functionalisation

A great number of works have been devoted to the nonmetal atoms incorporation into the PCN structure using in-situ or ex-situ approaches. Among the common doping elements are

found S [273], P [54,272,274], B [275], F [276], O [277-284], and even simultaneous doping by several non-metals (B/P/S) has been reported [285].

For the introduction of the dopant atom into the structure of polymeric carbon nitride, usually accompanied with the substitution of N atoms in the matrix, in-situ doping techniques are preferred [272,274-276], while ex-situ approaches are less common [273,278,281] due to the complexity of the experimental setups and the difficulty of substitution of C or N atoms in the rigid structure of the conjugated polymer. For instance, it is possible to introduce P atom in the PCN matrix by in-situ doping utilizing P containing ionic liquid [273] or by simple thermolysis of melamine and hexachlorotriphosphazene or sodium hypophosphite monohydrate [274]. Other examples of nonmetal doping include carbon nitride doped with boron prepared from a mixture of melamine and boron oxide in the semiclosed system [275], C₃N₄ fluorination by ammonium fluoride [276] or O-doping by means of the precursor pre-treatment with hydrogen peroxide [282].

To the ex-situ doping one can attribute the sulphur incorporation into the PCN structure carried out by Liu *et al.* [273], where the C₃N₄ powder treatment at 450 °C in the gaseous H₂S atmosphere led to the homogeneous substitution of lattice nitrogen for sulphur atoms (Fig. 1.10 (a)). Although the reported method allowed to achieve the desired substitution of N atoms, the use of a highly toxic and corrosive gas for S-doping at high temperature should be discouraged, especially in a view of the possibility to produce S-doped PCN from thiourea source. Ex-situ O-doping of PCN was accomplished by the solvothermal synthesis in the presence of H₂O₂ [278,281]. However, it is still not clear whether O replaces C or N atoms in the PCN network or it is present in the oxygenated species attached to the carbon nitride surface functional groups. The views of the researchers on this account contradict, since no direct experimental evidence for the either of the two possible suggestions has been presented up to now. There are several works where carbon nitride self-doping was performed, in which substitution of nitrogen by carbon atoms was observed [283,284]. Such type of doping is primarily responsible for the extended absorption of visible-light for the more efficient use of the doped material for its application under real-life conditions.

Interestingly, sometimes the functionalisation of the PCN borders or non-polymerised units, instead of the substitution of N atoms in the structure occurs. In [54] the in-situ doping approach resulted in the functionalization of PCN with PO_4 groups. The use of phosphates for the preparation of P-PCN does not allow to produce the material having a part of its N-atoms replaced by phosphorous instead the PO_4 tetrahedra coordinate the melamine-derived molecules by attaching to its NH_2 -groups. This type of interaction eventually leads to the PCN, where non-polymerised carbon nitride species are bonded to the phosphate moieties, thus the photocatalytic properties of such material become significantly modified with respect to those of the pristine one. The treatment of PCN with a mixture of inorganic acids led to the formation of electrophilic functional groups as C–O, C=O and COOH [279] whose formation after the mild hydrothermal treatment of C_3N_4 was also proposed in [280]. In case of the hydrothermal carbon nitride oxidation in the presence of H_2O_2 , the formation of –OH and –NO groups was suggested such as it is shown in Figure 1.10 (b) [278]. The functionalisation of PCN by the creation of N–C–O bonds on its surface was achieved by the photo-Fenton oxidation of pristine carbon nitride [277].

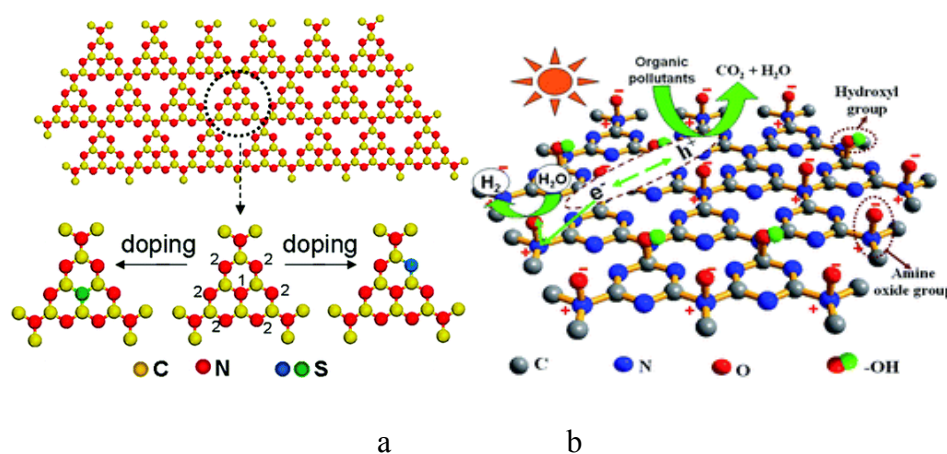


Figure 1.10 – (a) Atomic structure model of a perfect graphitic C_3N_4 sheet consisting of melem units, and two melem units with a nitrogen atom substituted at different periodic sites by a sulfur atom [273] and (b) the proposed oxygen functionalization of carbon nitride [278].

The nonmetal doped carbon nitrides demonstrate higher photocatalytic activity towards the hydrogen production, water pollutants degradation and selective partial photo-oxidation reactions than their pristine counterparts [54,272,273,275,276]. The remarkable performance

of the doped photocatalysts is usually attributed to the improvement of the light absorption, especially in the visible part of the spectra, better separation of the photo-induced charge carriers and enhanced adsorption characteristics.

Apart from the non-metal, metal doping has also been broadly applied for the promotion of the photocatalysts properties for certain applications. Antonietti *et al.* [175,286] in-situ prepared a series of Fe, Co, Ni, Mn and Cu-doped PCN that provided the material with additional new functionalities mimicking metalloenzymes for H₂O₂ activation or for the epoxidation of styrene with O₂. It is unlike the case of the transition metal-doping of titania, where the principal goal is to achieve the improved charge separation by trapping the photo-generated electrons on metal centres and promoting the holes reactivity. In carbon nitrides the holes have lesser potential and the oxidation usually takes place via the action of CB electrons, which produce superoxide radical species. Hence, the enhancement of the photocatalytic performance of the metal-doped PCNs is primarily due to the transfer of the charge to the metal centres, which then participate in photocatalytic oxidation. Simultaneous in-situ doping by non-metal and metal can also be beneficial for the photocatalyst's performance. The improved activity, in this case, is due to the synergistic effect of both heteroelements, such as the case of Fe and P co-doping, which inhibits the crystal growth of polymeric carbon nitride, enhances the SSA and decreases the band gap energy [287]. In [288] the PCN co-doping with Fe and C led to a narrowed band gap, a more positive VB potential, and improved electronic conductivity.

One can single out the alkaline metal doping as the mechanism of the dopants interaction with the PCN differ significantly from the above discussed cases. Lithium, sodium and potassium atoms are capable of intercalation into the layered PCN causing a dramatic effect on the C₃N₄ structure. In-situ potassium-doping resulted in the enhanced photocatalytic activity of K-C₃N₄, this improvement was assigned to the decreased VB position of g-C₃N₄ via potassium incorporation and better separation of generated charge carriers [289]. Na-doping [290] led to a smaller grain size, larger SSA, narrower band gap energy and better separation rate of the photogenerated electrons and holes.

Co-polymerization is a form of a molecular doping where different organic molecules can be introduced in the carbon nitride pattern for the improvement of its electrical, optical and photocatalytic properties. In the review [228] suitable organic comonomers for anchoring into the carbon nitride matrix were divided into three groups: (i) including π -conjugated aromatic molecules, such as benzene and its derivatives, (ii) π -rich aromatic molecules, such as thiophene and its derivatives, and (iii) π -deficient aromatic molecules, for example, pyridine-based motifs. The fact that the majority of the precursors for the PCN synthesis bear cyano or amino groups gave an idea to the researchers to use them as comonomer molecules. By the co-polymerization of dicyandiamide with barbituric acid Wang *et al.* first demonstrated extension of light absorption for the resulted C_3N_4 [291]. After that Wang's research group continued the investigation in this area introducing in PCN thiophene motif [292,293] or such molecules as 2-aminobenzonitrile and diaminomaleonitrile [294]. Other researchers were focused on anchoring pyridine rings as π -deficient aromatic molecules [295,296] or series of aromatic aldehydes [297].

1.4 Photoreactors

Not only the physicochemical properties of the material or the substrate nature affect the photocatalytic performance, but the external experimental conditions have also a great influence on it. For example, the shape of the reactor and the material from which it is made of are responsible for the light penetration into the suspension, which is one of the principal parameters determining photocatalysis. Stirring is also important, it provides the uniform distribution of the solid inside the reactor favouring its interaction with light and the dissolved substances. It is different for photocatalytic films, where instead of stirring the flow of reactants is applied. In this chapter, different types of photoreactors used for liquid phase reactions will be discussed.

The key parameters in the photoreactor design determining its geometry and configuration usually are: (i) the choice of phase (liquid or gas); (ii) type and particle size of the photocatalyst; (iii) distribution of the photocatalyst (fixed or suspended); (iv) type, content, and distribution of reactants; (v) mass transfer; (vi) fluid dynamics (laminar or turbulent

flow); (vii) temperature control; (viii) reaction mechanism; and (ix) reaction kinetics as well as the purpose of application and (x) irradiation source (Fig. 1.5) [298].

Theoretically, initial rates of photocatalytic reactions are directly proportional to the amount of catalyst as they depend on the number of active sites. However, above a certain amount of the catalyst the rates level off as was shown in Figure 1.3. An optimum catalyst loading depends on the reactor geometry. The type of the reactor can be flat-plate, batch reactor, flow reactor without and with recirculation, membrane reactor or annular reactor etc. Photoreactors are made for UV, UV-visible light, UV polychromatic lamps, or solar radiation and such aspects as spectrum, intensity, direction of the irradiance used in the photocatalytic reaction should be taken into consideration while designing the photocatalytic system [299]. Photoreactors can be non- and light-concentrating allowing for the latter all the solar radiation arriving at the aperture plane to be reflected and concentrated on the absorber tube. The position of the irradiance source can be immersed light source, external light source, and distributed light sources such as reflectors or optical fibres [298]. In the laboratory-scale set up immersed light source is frequently applied as it gives the possibility to evaluate such parameters as quantum or photonic yield of the reaction, but at the same time, this type of reactors is expensive. Photoreactors according to the purpose of the use are subdivided into those for biomass or CO₂ conversion, wastewater, air treatment or disinfection and water splitting are presented in Figure 1.11 [298].

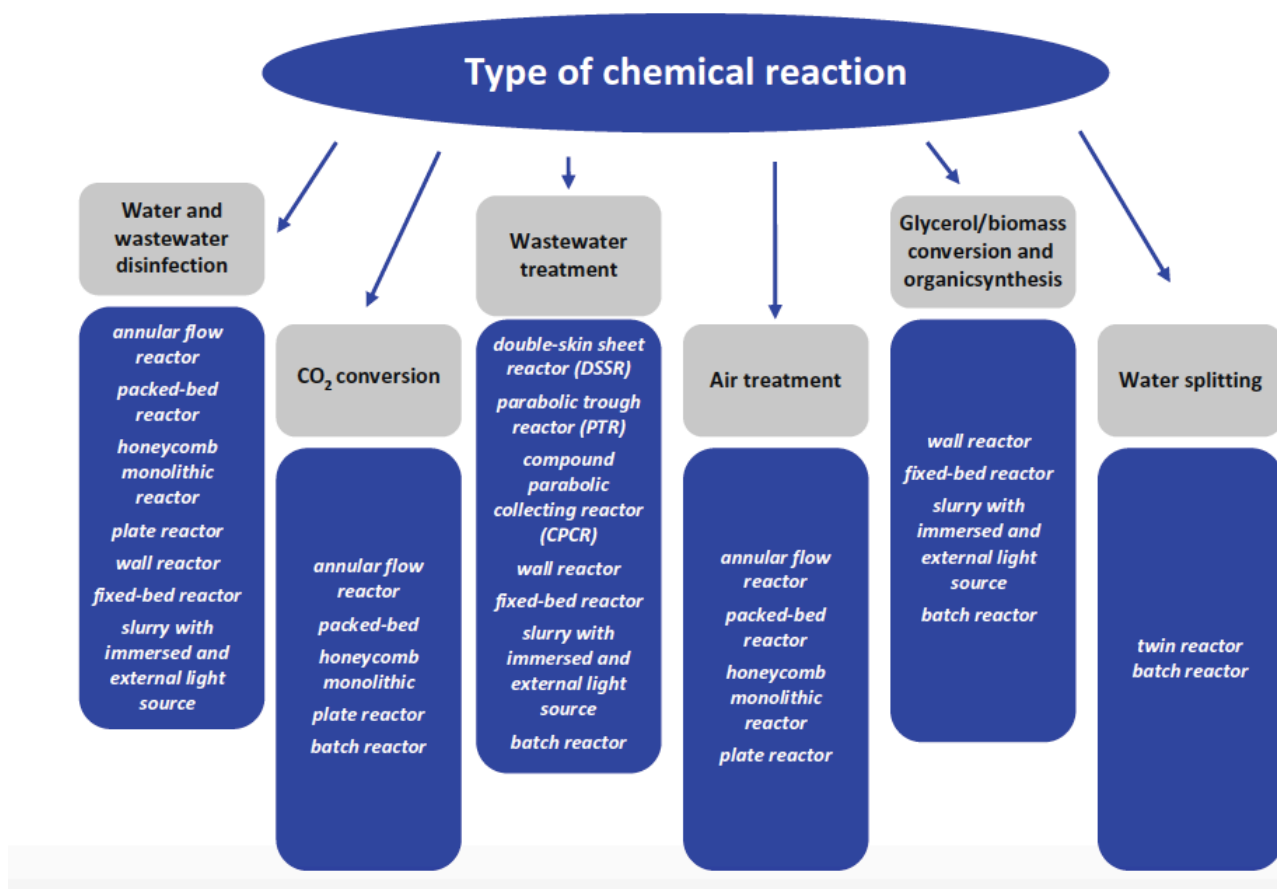


Figure 1.11 – Main types of photoreactors for various applications [298].

There are various reactor configurations applied for liquid phase reactions but usually slurry type reactors are used, where photocatalyst is suspended in a solvent providing high total surface area per unit volume. On the other hand, the immobilized photocatalyst reactor, in which photocatalyst is fixed to the support, is less common. The advantages of the slurry reactor system are simplicity of construction, excellent heat transfer performance, using a lower amount of the catalyst than in the case of immobilized catalyst reactor, well-mixed catalyst suspension, online removal and addition of the catalyst and the mass transfer limitations are typically negligible. Thus the photocatalytic reaction mechanisms in this case are usually dominated by adsorption kinetics [300]. The main disadvantage while utilizing a slurry reactor is a difficulty related to the separation of the photocatalyst from the reaction media. To the advantages of immobilized reactors one can attribute the absence of the

necessity for the photocatalyst recovery, continuous operation, while the downsides to it are the low surface area-to-volume ratio and inefficient use of irradiation.

In case of solar photoreactor systems, usually there are two major design issues to be addressed: (i) whether to use a suspended or a supported photocatalyst and (ii) whether to use concentrated or non-concentrated sunlight [298]. The most common reactors are (i) parabolic-trough reactors (PTRs), (ii) non-concentrating flat-plate reactors and (iii) compound parabolic collecting reactors (CPCRs). In the concentrating design, solar radiation is collected in a photocatalytic reactor by a reflecting surface, and because of this, for the same light-harvesting area, the reactor volume is smaller than in the case of the non-concentrating system. PTRs consist of a platform that has one or two motors controlled by a solar tracking system that maintains the collector aperture plane perpendicular to the incoming solar radiation. The suspension-containing absorber tube is located at the geometric focal line of the parabolic trough, the inner part of which is an aluminium or silver mirror (Fig. 1.12) [142].

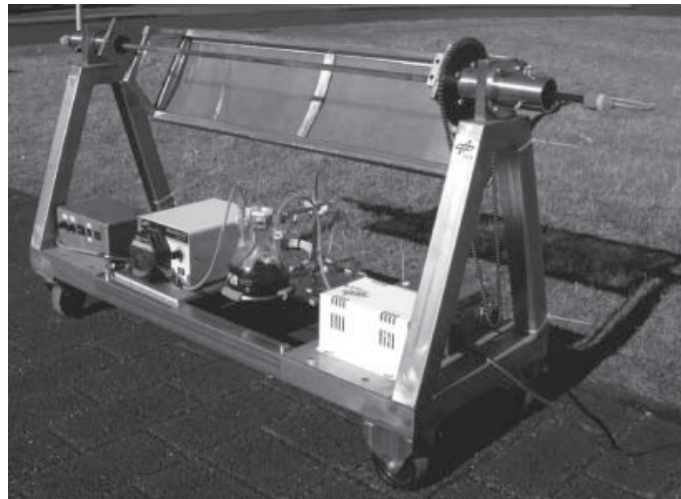


Figure 1.12 – Example of parabolic-trough reactor [142].

Non-concentrating photoreactors have no moving parts or solar tracking devices. This kind of reactor does not concentrate radiation, and because of this, efficiency is not limited by factors connected with reflection, concentration, or solar tracking (Fig. 1.13) [301]. In this system, optical efficiency is higher as compared to the concentrating reactors. Moreover, the

non-concentrating system can utilize the diffuse and direct portion of the solar UVA. One-sun collectors are usually cheaper than PTRs because their elements are simpler, and the surface required for their installation is smaller.

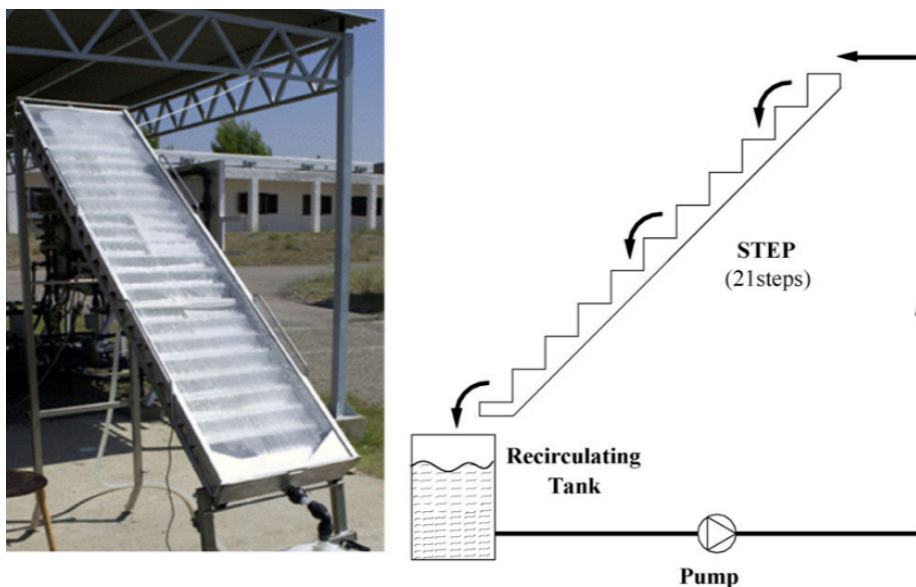


Figure 1.13 – Example of non-concentrating photoreactor solar collector at the Almeria Solar Platform (Spain) [301].

Compound parabolic collectors belong to the most promising photocatalytic solar reactors combining the advantages of parabolic-trough concentrator and non-concentrating system. CPCs are low-concentration static collectors with a reflective surface and can be designed for any given reactor shape. Water flows through the tubes to a tank by a centrifugal pump, allowing a turbulent regime inside them (Fig. 1.14) [302].

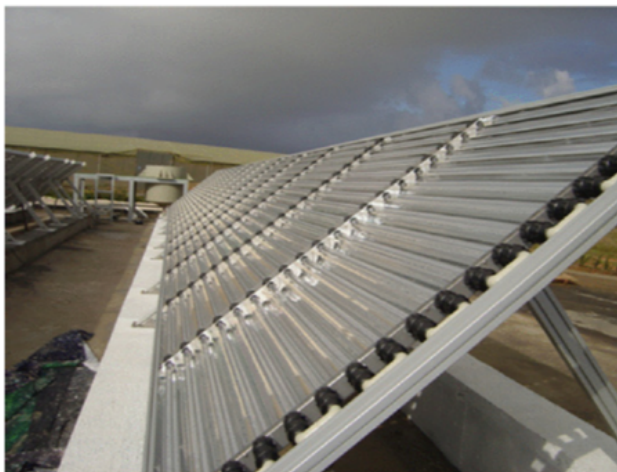


Figure 1.14 – Example of a compound parabolic concentrator [302].

In conclusion, it is of great importance to choose the right type of the reactor for the certain process, in order to obtain the desired results. As for UV lamps for laboratory test setup, slurry type reactors seem to be the best choice, while for the photo-oxidation under natural solar light for the pilot scale reactors CPC reactors are presently the most promising.

Chapter 2 Objectives

The literature survey has revealed that for the practical application of photocatalytic methods for water decontamination from emerging pollutants the materials currently in use lack such indispensable properties as efficiency and recoverability. Therefore, the main goal of the present Thesis in what concerns the total oxidation reactions is to develop methods for synthetic and post-synthetic modification of titanium dioxide (TiO₂), which would permit tailoring its properties in such a way as to achieve high efficiency and recoverability in photocatalytic decontamination of emerging organic pollutants in water medium. To comply with the stated goal, the following objective is formulated:

- Synthesis of efficient mesoporous photocatalysts based on titania anatase with particle shape and size facilitating their effective reusing in consecutive photocatalytic cycles of pollutants degradation in water under UV irradiation. Once the material with the desired properties is obtained, its photocatalytic performance to be tested in photo-oxidation of an emerging pollutant, 2-(4-methylphenoxy)ethanol, peruse its degradation mechanism identifying the possible reactions intermediates and ensuring the efficiency of TiO₂ assisted photocatalytic water decontamination.

The use of partial photo-oxidation for chemicals production is hampered by a difficult control of the reaction selectivity, especially in water medium. It is true even for PCN, which, although having all the prerequisites necessary to be a promising mildly oxidative catalyst for C–H and C–OH bonds oxidation of aromatic compounds, also promotes some undesirable side-reaction leading to the decrease of the product yield. Synthetic and post-synthetic approaches for PCN photocatalysts preparation are necessary to maximize the selectivity of

OBJECTIVES

partial photo-oxidation reactions destined to produce high added value chemicals. In order to reach the established goals, the following specific objectives are proposed:

- Development of a simple and environmentally benign method for the chemoselective C–H bond photo-oxidation of alkylphenoethoxylates using PCN as photocatalyst, O₂ as a green oxidant and UV light as an energy source.
- Synthesis of a new PCN–H₂O₂ adduct photocatalyst with high selectivity for partial oxidation of organic compounds followed by the determination of structural and physicochemical properties of the prepared photo-active material. The evaluation of the performance of the PCN–H₂O₂ adduct in the selective organic transformation of biomass-derived molecule 5-hydroxymethylfurfural (HMF) to the compound of high-added value 2,5-furandicarboxaldehyde (FDC) under UV and natural solar light irradiation. Establishing the mechanism of the selective HMF to FDC transformation on PCN–H₂O₂.
- Test of the PCN–H₂O₂ adduct in the selective partial photo-oxidation of HMF to FDC in water medium under the real conditions on the pilot scale photo-reactor under natural solar irradiation.

Objetivos

Una prospección bibliográfica previa al inicio de este trabajo reveló que, para la aplicación práctica de métodos fotocatalíticos a la eliminación en agua de contaminantes emergentes, los materiales disponibles presentaban graves carencias tanto en eficiencia como en recuperabilidad. Por tanto, respecto a las reacciones de oxidación total, el objetivo principal de esta Tesis Doctoral es el desarrollo de métodos sintéticos y post-sintéticos para la modificación del dióxido de titanio (TiO_2) con el fin de alcanzar eficiencias y recuperabilidades satisfactorias en reacciones de eliminación de contaminantes orgánicos en agua. Con este objetivo general, se establecen los siguientes objetivos específicos:

- Sintetizar un fotocatalizador mesoporoso eficiente, basado en anatasa, cuyas partículas, además de propiciar la degradación fotocatalítica de los contaminantes en agua bajo irradiación UV, presenten la forma y el tamaño adecuado para su reutilización en varios ciclos consecutivos. El comportamiento fotocatalítico de los nuevos materiales se ensayará en la foto-oxidación del contaminante emergente 2-(4-metilfenoxi)etanol, determinándose su mecanismo de degradación e identificando los intermedios de reacción posibles, al tiempo que se asegura la eficiencia en la descontaminación fotocatalítica del agua en presencia de TiO_2 .

El uso de la foto-oxidación parcial para la producción de productos químicos valiosos está obstaculizado por la dificultad de controlar la selectividad de la reacción, especialmente en agua. Esto sucede incluso en el caso de nitruro de carbono ya que, a pesar de que este material posee los prerrequisitos necesarios para ser un catalizador moderadamente oxidativo de enlaces C–H y C–OH de compuestos aromáticos, también promueve algunas reacciones secundarias no deseadas que resultan en un descenso en el rendimiento del producto. Por

tanto, es imprescindible el uso de técnicas sintéticas y post-sintéticas para la preparación de fotocatalizadores basados en nitruro de carbono para maximizar la selectividad de reacciones de foto-oxidación parcial destinadas a la síntesis de productos químicos de alto valor añadido. Con este objetivo general se establecen los siguientes objetivos específicos:

- Desarrollar un método simple y ambientalmente benigno para la foto-oxidación quimioselectiva de enlaces C–H en alquifenoletoxilatos usando nitruro de carbono como fotocatalizador, O₂ como el oxidante "verde" y UV como la fuente de energía.
- Sintetizar un nuevo fotocatalizador basado en el aducto nitruro de carbono-agua oxigenada con elevada selectividad en la oxidación parcial de compuestos orgánicos, incluyendo la determinación estructural y las propiedades físico-químicas del material foto-activo. Evaluar el comportamiento del aducto nitruro de carbono-agua oxigenada en la transformación selectiva del 5-hidroximetilfurfural (HMF), una molécula derivada de biomasa, al compuesto de alto valor añadido 2,5-furandicarboxaldehído (FDC), bajo luz UV e irradiación solar. Establecer el mecanismo de transformación selectiva de HMF a FDC en la presencia del aducto nitruro de carbono-agua oxigenada.
- Investigar el comportamiento del aducto nitruro de carbono-agua oxigenada en la foto-oxidación selectiva de HMF a FDC en agua en condiciones reales en un foto-reactor piloto bajo la irradiación solar.

Chapter 3 Materials and Methods

3.1 Materials

For the synthesis of TiO₂ a non-volatile and stable under ambient conditions titanium oxysulfate hydrate (Aldrich), TiOSO₄·H₂O, precursor, containing 17 wt% of sulfuric acid, was used. Ammonia 20 wt% water solution (VWR Chemicals) was applied as precipitation agent and for the pH correction, as well as hydrochloric acid 37-38 wt% water solution (J.T. Baker). Hydrogen peroxide 30 wt% water solution was obtained from Aldrich. Apart from water, methanol, ethanol and *n*-propanol were used as solvents (all VWR Chemicals). To compare the properties of the synthesized photocatalysts with the commercial products Aeroxide P25 was purchased from Aldrich.

The starting materials for graphitic carbon nitride syntheses were melamine (99% purity) and 30 wt% hydrogen peroxide water solution. All the chemicals were of analytical grade and used as received from Aldrich without additional purification. Sodium hydroxide, potassium hydroxide and potassium chloride were purchased from VWR Chemicals.

Several substrates were used in order to assess the photocatalytic performance of the prepared materials. For the photocatalytic tests, MPET of 98% purity was obtained from TCI Europe as well as 4-(2-hydroxyethoxy)-benzaldehyde (HEB) (98%). *p*-Cresol of 99% purity were purchased from Aldrich. 3-(2-methylphenoxy)ethanol (98%), and 3-(2-hydroxyethoxy)benzaldehyde (95%) were obtained from TCI Europe. 4-methylbenzyl alcohol, 2-(4-methylphenyl)ethanol, (4-methylphenoxy)acetic acid and 4-formylphenoxyacetic acid were purchased from Alfa Aesar. Methanol, *t*-butyl alcohol, *p*-benzoquinone (all of 99% purity), were purchased from Aldrich and used as a set of

scavengers for photo-generated holes, $\bullet\text{OH}$ and $\bullet\text{O}_2^-$, respectively. Acetonitrile (Aldrich, HPLC grade, 99.9 %) was used as solvent for the selected experiments. Chloroform (99% purity) and ethyl acetate (HPLC grade, 99.9%) were used as an extracting agents. 5-hydroxymethylfurfural (HMF) (Aldrich, 98% purity), benzyl alcohol (BA) and 4-methoxybenzyl alcohol (4MBA) were the substrates chosen for the study of their partial photocatalytic oxidation to 2,5-furandicarboxaldehyde (FDC), benzaldehyde (BAL) and 4-methoxybenzaldehyde (4MBAL), respectively. BA, BAL, 4MBA, 4MBAL, FDC 5-formyl-2-furoic acid (FFA) (all Aldrich, 99% purity) were used to calibrate HPLC system. TiOSO_4 1.5 wt% water solution (Aldrich) was applied for monitoring the evolution of H_2O_2 during the reaction.

3.2 Synthesis

3.2.1 Titanium dioxide spherical particles preparation

Adjusting the previously reported method [94] by decreasing titania precursor concentration and increasing Ti: NH_3 ratio in the solvent-exchange preparation procedure the formation of titania spherical particles was achieved. Firstly, titanium hydroxide was precipitated from 25 mL of 0.1 M titanium oxysulfate solution by adding 2 mL of 20 wt% $\text{NH}_3 \cdot \text{H}_2\text{O}$ aqueous solution. The precipitate was centrifuged, washed and dissolved by adding 2.5 mL of 30 wt% hydrogen peroxide. The reaction mixture volume was adjusted to 25 mL by distilled water and pH value was set to 9.5 by adding ammonia. Then, the ice-cooled solution of peroxo complex was mixed with the equal volume of methanol, ethanol or *n*-propanol and the suspension was formed. The obtained suspension was aged, isolated by centrifugation and washed with deionized water. The post-synthetic treatment of the titania spheres prepared in the presence of *n*-propanol was carried out in the following way: The amorphous precipitate, formed after *n*-propanol addition and aged for 24 h, was suspended in 50 mL of water-ethanol mixture (1:1 ratio by volume) at pH 4, which was adjusted by addition of HCl (1 M). The suspension was refluxed for 21 h and then the solid phase was separated by centrifugation at 3000 rpm and washed with deionized water. All precipitates were dried at 70 °C for 24 h before being subjected to investigation. Later, the samples were

thermally treated in a muffle furnace at 500, 650 and 800 °C at a heating rate of 3 °C min⁻¹ and calcination time of 30 min. The samples prepared by isolation of titania particles from the solutions containing methanol, ethanol, *n*-propanol and after the post-synthetic treatment were designated as TiMex, TiEtx, TiPrx, and TiPrRx, respectively, where “x” indicates the calcination temperature (in °C). The choice of the calcination temperature range was based on the previous study [94], where maximum photocatalytic activity was reached for the samples calcined at 800 °C.

3.2.2 Preparation of H₂O₂-treated PCN for MPET partial photo-oxidation

Bulk polymeric carbon nitride (PCN) samples were prepared via the thermal condensation method from melamine following the procedure reported in [303]. 10 g of melamine was placed in a ceramic crucible covered with a lid and heated in a muffle furnace at 2 °C min⁻¹ up to 520 °C, then left for 2 h at the reached temperature and slowly cooled down. The C₃N₄ sample derived from melamine was labelled as MCN. The bulk carbon nitride prepared from melamine (MCN) was used as the precursor for the thermally exfoliated C₃N₄ [53,239,304]. To this purpose, 6 g of MCN was powdered in a mortar, evenly spread on the bottom of a ceramic bowl with a diameter of 14 cm, calcined in a static air atmosphere at 500 °C by using a temperature ramp of 2 °C min⁻¹ and maintained for 4 h. The thermally exfoliated carbon nitride was coded as TE. The MCN and TE samples were treated with hydrogen peroxide by the following way. To 1 g of the MCN or TE samples 20 mL of H₂O₂ (30%) was added, then the suspension was mildly heated (70 °C) while stirring until the complete evaporation of the liquid, and finally the solid samples were thoroughly washed with deionized water and dried at 70 °C in an oven. The H₂O₂-treated MCN and TE samples were designated as MCN_O and TE_O, respectively.

Also, the carbon nitride samples were treated with NaOH, HCl and KOH/KCl using the procedures reported in refs. [249,253,305], respectively; they were designated as MCN_Na, MCN_W and MCN_K, respectively. For the MCN_Na preparation, 1 g of MCN and 2 M solution of NaOH was placed in an autoclave and treated under autogenous pressure for 24 h at 180 °C; for the MCN_W synthesis, 1 g of MCN was placed in 37% solution of HCl and

stirred for 4 h; MCN_K was prepared by the thermal condensation of 10 g of melamine in presence of 7.5 g of KCl and 0.28 g of KOH at 520 °C for 2 h. All the samples were washed with distilled water and dried at 70 °C for 24 h before using them in the reactions.

3.2.3 Preparation of PCN-H₂O₂ adduct for HMF photo-conversion

Bulk PCN was prepared via the thermal condensation method described above [303]. Briefly, 10 g of melamine was placed in a ceramic crucible, which was covered with a lid and heated in a muffle furnace at 2 °C min⁻¹ up to 520 °C, once the temperature was reached it was left for 2 h and slowly cooled down afterwards. In a view of low SSA, the bulk PCN was then subjected to thermal etching as was previously reported in [53,239,304] in order to produce high surface area PCN. For this purpose, 6 g of bulk carbon nitride was powdered in a mortar, evenly spread on the bottom of a ceramic bowl with a diameter of 12 cm, heated in a static air atmosphere at 500 °C by using a temperature ramp of 3 °C min⁻¹ and maintained for 4 h at the reached temperature before being cooled down. This procedure yielded 2.8 g of the thermally etched PCN sample, designated as TE. Finally, the TE sample was treated with H₂O₂ following the formulation proposed above. For this, 2.8 g of TE was stirred in 50 mL of H₂O₂ aqueous solution (30%) in an open beaker while heating at 70 °C until complete evaporation of the liquid was achieved. The obtained solid was washed thoroughly with deionized water, until H₂O₂ was no longer detected in the washing liquid, filtered and finally dried at 80 °C for 24 h giving the PCN-H₂O₂ adduct (TEO). After that, a part of the TEO sample, 0.87 g in each case, was treated at 200, 300, and 400 °C in air for 2 h, the obtained samples were designated as TEO_x, where “x” states for the treatment temperature. For the sake of comparison, H₂O₂ modification of TE was also carried out using reflux treatment at 70 °C (TEO_R). Melamine-hydrogen peroxide complex (MHP) was synthesized, for the aim of using it as a reference for the assignment of carbon nitride surface species formed after the reaction with hydrogen peroxide. For this purpose, 10 g of melamine was mixed with 50 mL of 30 wt% H₂O₂ and let stirring while heated at 70 °C until the solvent was evaporated. The obtained solid was dried at 70 °C for 24 h.

3.2.4 Synthesis of H₂O₂-treated PCN for HMF photo-conversion in a solar pilot plant

Bulk PCN was prepared via the same thermal condensation method mentioned above [303] using melamine as a precursor. The scaled-up preparation of bulk PCN proceeded by placing 60 g of melamine in a covered ceramic crucible and by heating it in an oven up to 520 °C at 2 °C min⁻¹. The temperature was maintained for 6 h, and after that the system was slowly cooled down giving about 36 g of carbon nitride. The obtained PCN consisting of a yellow powder underwent a successive heating in air atmosphere, to obtain thermally etched PCN (TE) with improved physicochemical features [53,239,304]. It was prepared starting from 20 g of the powdered PCN, which was evenly spread on an aluminium sheet with dimensions 15 x 22 cm², then heated in air up to 520 °C at 3 °C min⁻¹ and kept (7 h) at this temperature before being cooled down. The thermal etching produced *ca.* 9 g of TE. The procedure was repeated until 200 g of the thermally etched PCN (TE) was obtained, and then TE was powdered and thoroughly mechanically mixed. After that, the pale yellow TE powder was divided into two aliquots, one of them was left as it was, while the other one was treated with H₂O₂ according to the procedure reported mentioned above. Briefly, 500 mL of aqueous H₂O₂ solution (30 wt%) containing 100 g of TE was stirred in an open beaker under heating at 70 °C to evaporate the liquid. Once dry, the powder was washed with water until the complete absence of H₂O₂ in the washing liquid, filtered and dried at 80 °C for 24 h. The finally the obtained dark yellow-to-orange powder was labelled as TEO. The SSAs of the TE and TEO samples resulted to be 129 and 59 m²·g⁻¹, respectively.

3.3 Characterization

Powder X-ray diffraction (PXRD) patterns were recorded in an X'pert PANalytical diffractometer, using Ni-filtered Cu-K α ($\lambda = 0.15418$ nm) radiation source and PixCell1D (tm) detector or Rigaku Ultima IV with the similar characteristics. The mean crystal size of the TiO₂ samples was estimated by the Scherrer equation from the (101) reflection of anatase and (110) reflection for the rutile phases (Eq. 19).

$$D = \frac{K\lambda}{\beta \cos\theta} \quad (19)$$

where D is the mean crystal size, K is a dimensionless shape factor, λ is the X-ray wavelength, β is the broadening at half the maximum intensity, and θ is the Bragg angle.

Infrared spectra of the samples were recorded with 4 cm^{-1} resolution using an ATR module of a Varian 620-IR spectrometer. Diffuse reflectance spectra (DRS) were obtained in air at room temperature in the 250–800 nm wavelengths range by means of a Shimadzu UV-2700 or Shimadzu UV-2401 PC spectrophotometer, with BaSO_4 as the reference material considering titania or carbon nitride as indirect semiconductors.

SEM images were obtained by using a JEOL 6610LV scanning electron microscope (the samples were coated with gold prior to observation).

Micromeritics ASAP 2020 was used to obtain adsorption-desorption isotherms of N_2 at 77 K. The surface area, pore volume and pore-size distribution were calculated from the low-temperature nitrogen adsorption data using BET and BJH approaches. Prior to the experiment the samples were degassed under vacuum at 200, 250 or 350 °C for 4 h.

Mettler Toledo TGA/SDTA851 was used to investigate the thermal decomposition of the prepared samples under an O_2 flow of 50 mL min^{-1} with the heating rate 10 °C min^{-1} in the temperature range 25-1000 °C.

The surface elemental composition of the PCN samples and binding energies of C, N and O were measured by X-ray Photoelectron Spectroscopy (XPS) on a SPECS system equipped with a Hemispherical Phoibos analyser operating in a constant pass energy, using $\text{MgK}\alpha$ radiation ($h\nu = 1253.6 \text{ eV}$). Surface elemental composition of the studied materials was estimated using CasaXPS software. The deconvolution of the XPS peaks were carried in accordance with the NIST binding energies database, using Shirley function to create a baseline and Gaussians function to make spectra fit.

The solid state ^1H , ^{13}C MAS NMR, and ^1H - ^{13}C CPMAS NMR spectra were registered at the spinning rates of 8, 5 or 12 kHz using a Bruker Avance III 400WB spectrometer.

The concentration of H₂O₂ released into water suspension from the PCN–H₂O₂ adduct was estimated photocolorimetrically using the titanium oxysulfate based method.

The mass-spectroscopic (MS) thermal desorption analysis was carried out using a Micromeritics Autochem II 2920 system coupled with a ThermoStar mass spectrometer. For the analysis, 100 mg of a powdered PCN was put onto a fiberglass support inside a quartz U-tube, purged for 60 min with argon gas flowing through the sample at a rate of 10 mL min⁻¹ at 35 °C and then heated at 10 °C min⁻¹ up to 400 °C.

Point of zero charge (PZC) was measured using Zetasizer Nano ZS90.

Transmission electron microscopy (TEM), high resolution transmission electron microscopy (HRTEM), selected area electron diffraction (SAED) and nanobeam electron diffraction (NBD) studies were performed on a JEOL JEM-2100F transmission electron microscope operated at an accelerating voltage of 200 kV, equipped with a field emission gun (FEG) and an ultra-high resolution pole-piece that provided a point-resolution better than 0.19 nm. The samples for TEM were dispersed in ethanol, sonicated and sprayed on a holey carbon film coated copper grid and then allowed to air-dry, finally, Gatan SOLARUS 950 was used before observation.

RT emission spectra were measured using a standard spectrofluorometer Edinburgh Instruments FLSP920 (Edinburgh, Scotland, UK), equipped with a 450W Xe lamp excitation source, at an excitation wavelength of 365 nm.

Geometry optimization of dimelem, MPET molecules and their molecular complexes with and without hydrogen peroxide was carried out by Kohn-Sham method in B3LYP/6-311+G (d, p) approximation in the Firefly 8.0.1 program [306] with visualization in Chemcraft [307] package. The absence of imaginary vibration frequencies controlled in all cases. The resulting wave functions were used for QTAIM [308] analysis. The summarizing energy of interacted fragments was estimated with EML approach [309,310] as a sum of corresponding hydrogen bond energies between considered compounds in complexes. For that the potential energy density, $v(\text{rb})$, at the bond critical points rb , of the electron density were calculated. The

electron density (ED) and molecular electrostatic potential [311] (MEP) distributions were performed using Multiwfn [312] and MoleCoolQT [313] programs.

3.4 Photocatalytic Reactions

3.4.1 Photocatalytic degradation of organic pollutant in the presence of TiO₂

Photocatalytic properties of the prepared titania samples and the commercial Aeroxide P25 were investigated in the decomposition of MPET in aqueous-phase under UV-light. Since the as-prepared materials were amorphous, their photocatalytic tests were not performed. The UV-light source was a Helios Italquartz GR.E 500 W high-pressure mercury lamp (maximum radiation at 365 nm and impinging radiation was estimated to be 2.7 W·m⁻²) equipped with a Pyrex water-cooling jacket cutting-off the radiation wavelengths below 300 nm. In all experiments, 100 mg of sample was placed in a 250 mL Duran Glass reactor containing 200 mL of MPET solution in deionized water (20 mg L⁻¹). The reactor was set at 25 cm from the light source and the suspension was magnetically stirred. Firstly, adsorption of MPET on the titania samples was measured in dark. After this, the suspension was exposed to UV-light and the aliquots of 3 mL were taken at appropriate intervals during the total irradiation time of 6 h if not stated otherwise. Then, the solution was filtered from the photocatalyst with 0.2 μm PTFE filter, extracted with chloroform (at volume ratio 1:1), and the concentrations of MPET and the reaction intermediate (*p*-cresol) were determined by GC–MS technique. A Shimadzu GC/MS QP2010 Plus system, equipped with 30 m long Teknokroma TRB-5MS capillary column, was previously calibrated by using standard solutions of the studied compounds. Photolysis of the MPET solution was carried out under the same experimental conditions, but in the absence of photocatalyst. The total organic carbon (TOC) was measured using a Shimadzu TOC-V CSH Analyzer for the initial MPET solution, as well as after 360, 600, and 840 min of the photocatalytic reaction. Recyclability of the most active photocatalysts was tested in consecutive MPET photodecomposition cycles. For this purpose, the photocatalysts were separated from the reaction medium after 6 h of the reaction, by centrifugation at 3000

MATERIALS AND METHODS

rpm for 3 min, then washed three times with deionized water, and dried at 70 °C for 48 h. The remaining amount of the photocatalyst was determined and reused in the following photo-degradation runs.

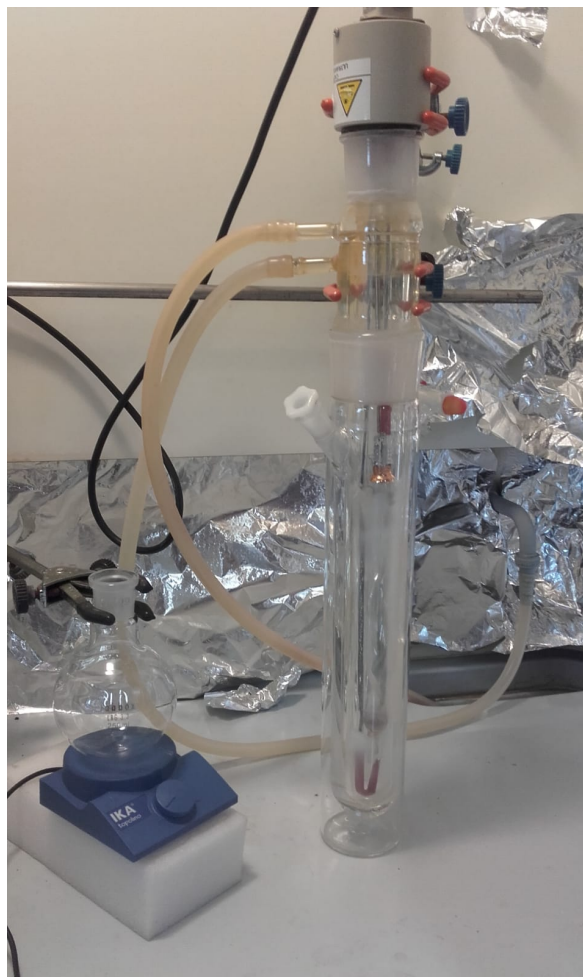


Figure 2.1 – UV-lamp equipped photocatalytic reactor for MPET photo-oxidation.

The toxicity of the reaction solutions at different irradiation times was estimated according to the standard Microtox suggested protocol using a Microtox Model 500 Toxicity Analyzer [76]. The samples were placed in a 2% NaCl medium with an aliquot of marine bacterium *Vibrio fischeri* and the luminescence was measured after 5 and 15 min of incubation. The toxicity of water suspensions of Aeroxide P25 and TiPrR800 priory filtered through 0.2 μM PTFE filter was measured after 8 h of irradiation. Phenol and $\text{ZnSO}_4 \cdot 7\text{H}_2\text{O}$ were used as positive controls.

3.4.2 Photocatalytic conversion of MPET and HMF in the presence of PCN–H₂O₂ adduct

The partial photocatalytic oxidation of MPET to HEB in the presence of carbon nitride was carried out in a Pyrex cylindrical photoreactor (internal diameter: 32 mm, height: 188 mm) containing 150 mL of aqueous suspension, irradiated by six external Actinic BL TL MINI 15 W/10 Philips fluorescent lamps emitting in the 340–420 nm wavelength range with the main emission peak at 365 nm (Fig. 2.2). The reaction was carried out at about 25 °C and the reactor was provided by a thimble where water was allowed to circulate. Selected experiments were carried out in absence of O₂ by continuously bubbling N₂ throughout the runs to estimate the influence of O₂ on the reaction. The initial MPET concentration was 0.5 mM at the natural pH. The amount of a solid photocatalyst used for the experiments was 40 mg (80 mg for the recyclability study), except for the pristine carbon nitride MCN and MCN_O, for which 75 mg was used, due to their poorer light absorbance compared to the other samples. In this way, all the entering photons were virtually absorbed by the suspension. Some experiments were performed by reusing one of the best materials (TE_O) in order to verify its performance in a series of the consecutive reaction runs. Selected scavengers were used, in order to establish the reactive species responsible for MPET conversion and the selectivity to HEB. Methanol (MeOH) was used as a hole scavenger, *t*-butyl alcohol (*t*-BuOH) as an •OH radical scavenger and *p*-benzoquinone to scavenge •O₂⁻ radicals. The concentration of methanol, *p*-benzoquinone and *tert*-butyl alcohol scavengers was 2 mM. Samples of the irradiated solution were withdrawn at fixed time intervals. Then, the solution was filtered from the photocatalyst with 0.25 μm PTFE filter, extracted with ethyl acetate (at volume ratio 1:1). Liquid aliquots were analyzed by a GC–MS technique, using a Shimadzu 2100 Ultra GC–MS equipped with a Teknokroma TRB-5MS (95%) dimethyl (5%) diphenyl polysiloxane copolymer column to identify and to determine the concentration of MPET, HEB and *p*-cresol. Standards purchased from Sigma-Aldrich and TCI with a purity >98% were used to identify the products formed during the reaction and to obtain the calibration curves. HPLC analysis of (4-methylphenoxy)acetic acid photo-oxidation products was carried out using an Agilent 1200 Series instrument equipped with

MATERIALS AND METHODS

Agilent Eclipse CDB-C18 column. The determination was done in the flow of acetonitrile (20 %) and 13mM trifluoroacetic acid (80 %) at 40 °C.



Figure 2.2 – UV-lamps equipped photocatalytic reactor for alkylphenoethoxylates and HMF photo-conversion.

Partial photocatalytic oxidation of HMF to FDC with carbon nitride was carried out in a Pyrex cylindrical photo-reactor (internal diameter: 32 mm, height: 188 mm) containing 150 mL of aqueous suspension, irradiated by six external Actinic BL TL MINI 15 W/10 Philips fluorescent lamps emitting in the 340-420 nm wavelength range with the main emission peak at 365 nm (Fig. 2.2). The reactions were carried out at about 25 °C as the reactor open to the atmosphere was provided with a thimble, where water was allowed to circulate. The initial HMF concentration was 0.5 mM at the natural pH. The amount of solid photocatalyst used for the experiments was 100 mg. In this way, all the entering photons were virtually absorbed by the suspension. The impinging radiation energy in the range 315-400 nm was measured by

MATERIALS AND METHODS

a radiometer Delta Ohm DO9721 with an UVA probe and its average value was 3.9 W m^{-2} . Some experiments were performed by reusing one of the most efficient materials (TEO), in order to verify its performance in a series of three consecutive reaction runs. For this experiment after the photocatalytic reaction the suspension of TEO was left for 24 h to separate the photocatalyst from the solution. Then, the solution was decanted, and 150 mL of HMF 0.5 mM was introduced into the reactor and the photocatalytic reaction was repeated. Samples of the irradiated solution were withdrawn at fixed time intervals and immediately filtered through $0.25 \mu\text{m}$ membranes (Polypropylene, VWR) to separate the photocatalyst particles. Liquid aliquots were analysed by a Thermo Scientific Dionex UltiMate 3000 HPLC equipped with a Diode Array detector to identify and to determine the concentration of HMF, FDC and FFA. A REZEK ROA Organic acid H^+ column was applied with a mobile phase of aqueous 2.5 mM H_2SO_4 solution at a flow rate of 0.6 mL min^{-1} . Standards purchased from Sigma-Aldrich with a purity $>99\%$ were used to identify the products formed during the reaction and to obtain the calibration curves.

The photocatalytic reactions under natural solar irradiation were carried out on clear sunny days in Palermo (Italy) from 9:30 to 13:30. Typically, 75 mL of 0.5 mM HMF solution and 50 mg of the PCN samples were introduced into a round-shaped Pyrex batch reactor having a total volume of 125 mL and a diameter of 10 cm (Fig. 2.3). Additionally, the TEO sample was tested at varying initial HMF concentrations of 1 and 2 mM. The reactor was closed and no gases were fed during the tests as preliminary experiments had proved that the quantity of atmospheric O_2 present in the system was sufficient to induce the oxidation. The suspensions of the PCN samples in HMF solution were continuously magnetically stirred and approximately 2.5 mL were withdrawn every 30 min and analysed by using the previously described analytical procedure. The photon flux was measured every 10 min throughout the photocatalytic runs.



Figure 2.3 – Photocatalytic setup for the natural solar light promoted oxidation of HMF.

The pilot-plant photocatalytic experiments were carried out in a CPC solar photoreactor located at the Plataforma Solar de Almería (Spain). The CPC was not a concentrating one, i.e. the ratio between the sun-exposed surface and that of the reactor was approximately equal to 1.1. The set-up consisted of a plug flow photoreactor (PFP) in a total recycle loop with a not-reacting stirred tank whose function was providing aeration and sample withdrawing for analyses. The plug flow photoreactor (PFP) was equipped with a CPC having five UV-transparent glass tubes (inner diameter 45 mm, outer diameter 50 mm, irradiated length 1460 mm) connected in series and placed on a fixed support inclined 37° (latitude of the PSA) with respect to the horizontal plane and facing South to maximize the daily incidence of solar radiation (Fig. 2.4). The aqueous suspension was continuously fed to the PFP upwards from the not-reacting tank by means of a centrifugal pump. The suspension flow rate, maintained constant for all the runs, was 12 L min^{-1} . The Reynolds number value was equal to *ca.* 5700, indicating a turbulent regime of the flow inside the tubes. The total volume of suspension (V_t) charged in the whole system was 15.5 L, whereas the irradiated volume, i.e. the volume of suspension contained in the glass tubes, was 11.6 L. The irradiated volume was 75% of the total one (dead volume was accounted for to 25%). The total irradiated area in the photoreactor was 1.055 m^2 and the suspension slightly heated throughout the experiments, reaching temperatures of *ca.* 42-45 °C at the end of the run.



Figure 2.4 – Pilot plant scale CPC solar photoreactor located at the Almeria Solar Platform (Spain).

Chapter 4 Results and discussion

4.1 Titania Spherical Particles for Photocatalytic Degradation of Organic Pollutants

Synthesis of photocatalytically active titania spherical particles is an attractive task since this material possess certain important properties for its successful reuse in the photocatalytic reactions. Likewise, the tuning material porous characteristics is another important challenge as it determines substrate accessibility to the photocatalysts surface and affects the material photocatalytic activity.

A wide range of methods allowing synthesis of titania spherical particles is known, which includes hard templating, utilizing organic as well as silica materials [113,114], soft template-assisted alkoxide based sol-gel syntheses [115-117] or less common template-free methods, where titanium organometallic source is used [118,119], synthesis in emulsions [120-122], or by aerosol formation [123]. Usually, for the titania synthesis titanium alkoxides are used as precursors. This type of Ti source has several downsides such as toxicity, high cost and instability of the precursor implying the special conditions of its storage and utilization. On the other hand, the use of the inorganic titanium containing salts is tangled with the difficulties to control the synthesis pathway. The fact that Ti atom (Ti^{4+}), present in organic and inorganic precursors, has a significantly large positive partial charge derived from its higher electrophilic character that imparts higher reactivity with water and as the consequence the control over the nucleation processes and growth is complicated [314].

RESULTS AND DISCUSSION

Titanium peroxo complexes were found to be a suitable alternative to the titanium alkoxides and inorganic salts. This precursor is water soluble, non-toxic, cost-effective, leaves only water as a by-product during the formation of the oxide phase. The control of the synthesis is realized by the complexation of Ti atom by hydrogen peroxide, thus no organic ligands are needed to ensure the complex stability [97]. Varying the pH value directs the complexes formation eventually allowing to define the properties of the resulted oxide.

The problem of growing number of water contaminants creates the necessity of studying of contaminant degradation pathway as sometimes more toxic substances can be created during a degradation process [69,70]. Along with the degradation of starting pollutants, it is also important to monitor the formation and decay of the intermediates formed in the course of the photo-reaction, as to control all the transformation steps the substrate undergoes and to identify possible hazardous intermediates. The possible synergetic or antagonistic effects of the pollutants produced during the photocatalytic reactions is often neglected, however, it may have a great influence on the toxicity of the treated water streams [75].

The following research paper is devoted to the synthesis of the photocatalysts based on titanium dioxide spherical particles and their application for 2-(4-methylphenoxy)ethanol (MPET) degradation in water. On the first stage of the titania synthesis, aqueous titanium peroxo complex was prepared. The second stage included utilization of solvent-exchange method inducing titania amorphous spheres formation followed by the reflux post-treatment procedure for creation of mesoporosity within the TiO₂ spheres. On the last stage, titania was subjected to thermal treatment to obtain highly crystalline anatase phase. The thorough study of the properties of the prepared materials using XRD, low-temperature N₂ adsorption, SEM and TEM microscopy revealed the influence of the used synthetic conditions as well as the post-synthetic treatment on the titania spherical particles formation. Successful application of the prepared photocatalyst in the reaction of MPET photo-oxidation was performed. The mechanism of the MPET degradation included toxic *p*-cresol formation as an intermediate, which decomposition was tracked as well. The prepared mesoporous titania spheres proved efficiency not only for the initial compound photo-degradation but also for the toxic intermediate, *p*-cresol. The satisfactory recyclability of the synthesized TiO₂ spheres was

RESULTS AND DISCUSSION

confirmed by their utilization in four consecutive photo-oxidation cycles while commercial titania lost its activity after the third one.

Article I

“Photocatalytic degradation of 2-(4-methylphenoxy)ethanol over TiO₂
spheres”

Journal of Hazardous Materials

332 (59–69)

Year 2017

DOI: 10.1016/j.jhazmat.2017.02.055

Impact Index: 6.065

Photocatalytic degradation of 2-(4-methylphenoxy)ethanol over TiO₂ spheres

Marina Ilkaeva^{a,b}, Igor Krivtsov^{a,b,*}, Eva Díaz^c, Zakariae Amghouz^d, Yolanda Patiño^c, Sergei Khainakov^d, José R. García^a and Salvador Ordóñez^c

^a Department of Organic and Inorganic Chemistry, University of Oviedo-CINN, 33006, Oviedo, Spain

^b Nanotechnology Education and Research Center, South Ural State University, 454080, Chelyabinsk, Russia

^c Department of Chemical and Environmental Engineering, University of Oviedo, 33006, Oviedo, Spain

^d Scientific Technical Services, University of Oviedo, 33006, Oviedo, Spain

* Corresponding author.

E-mail address: uo247495@uniovi.es; zapasoul@gmail.com (I. Krivtsov)

Abstract

The photocatalytic TiO₂-assisted decomposition of 2-(4-methylphenoxy)ethanol (MPET) in aqueous solution has been studied for the first time. The intermediate compounds of MPET photodegradation have been also determined. A toxic p-cresol is formed in significant quantities during the photocatalytic reaction. A solvent-exchange approach for a template-free preparation of spherical TiO₂ particles has been described, which is based solely on precipitation of hydrous titania from aqueous titanium peroxo complex by using organic solvents. The proposed method favours the formation of spherical titania particles with a mean size varying from 50 to 260 nm depending on the choice of solvent. The procedure for converting nonporous titania spheres into mesoporous material maintaining the same spherical morphology has been developed. The synthesized TiO₂ spheres demonstrate a degree of MPET photo-degradation close to that of the commercial titania Aeroxide P25, besides being successfully recovered and reused for four reaction cycles without loss of catalytic activity. The effectiveness of the commercial Aeroxide P25 in MPET photodegradation, on the other hand, suffers 10-time drop during the third reaction cycle, which is attributed to its poor recoverability because the photocatalyst is composed of small particle size of 20 nm.

Keywords: emerging pollutants; micropollutants; titanium peroxo complex; anatase-based photocatalysts

1. Introduction

Recent times have witnessed a fast development of industry promoted by invested capital, market growth and increased demands for new products. Thus, it is not surprising that a large and worrying number of emerging substances and pollutants is frequently encountered in waste waters, and so new measures must be taken for their removal. In particular, emerging pollutants, proceeding from cosmetic and chemical industries and usually encountered in water media, are undesirable compounds and considered harmful for the environment and human health. There are many ways suggested for their elimination, such as adsorption, advanced oxidation, photolysis, electrocatalysis, etc [1-5]. The main obstacle in the path of their removal is the low concentrations at which these emerging pollutants appear in aqueous solutions. One of these undesirable compounds is 2-(4-methylphenoxy)ethanol (MPET), and it is usually found in decorative cosmetics, fine fragrances, shampoos, toilet soaps, and other toiletries, as well as in non-cosmetic products, such as household cleaners and detergents. The worldwide consumption of MPET is close to 0.01–0.1 metric tons per year [6], so the interest in its removal from the environment is not surprising. Photocatalysis is known as an efficient oxidation process for degrading organic pollutants at low concentration by transforming them into H₂O and CO₂. These transformations are conducted under conditions avoiding heating, high pressure, toxic chemicals or additives. Unfortunately, the decomposition process usually does not lead directly to the mineralization, but some oxidation by-products are also formed. Sometimes, intermediate compounds formed during the photooxidation processes can be even more hazardous than the initial pollutant, which makes their determination of key importance [7-9]. There is a considerable number of papers dealing with the selective photocatalytic oxidation of aromatic alcohols and ethers to the corresponding aldehydes [10-17]. However, to the best of our knowledge, this is the first study of photocatalytic decomposition of MPET focused on the total mineralization, revealing the formation of intermediates with their consecutive degradation pathway.

RESULTS AND DISCUSSION

Titanium dioxide is the most widespread photocatalyst, which is due to its low-cost, non-toxicity and chemical stability, being attracted much attention recently [18-20]. Photocatalytic degradation of organic pollutant has become an extensive practice and special success has been achieved by Aeroxide P25 (Degussa P25) photocatalyst, which is due to the presence of anatase-rutile interface, its high crystallinity and relatively high surface area. However, the small particle size of Aeroxide P25 (around 20 nm) causes certain complications regarding the photocatalyst recovery and reuse. Unquestionably, the reusability of photocatalytic materials in the reaction cycles is required for the practical implementation of this technique. Several ways are proposed to achieve this aim, such as preparation of magnetic composite materials [21-25], thin film [26,27], and synthesis of sub-micron or micron-size spheres, which find their applications in many fields [28-35], but most importantly, spherical particles provide a desirable form for a solid catalyst facilitating its reuse [31,36,37]. The preparation of spherical titania particles demands special experimental setups or expensive (and occasionally volatile and toxic) organic structure-directing agents. The general procedures for the synthesis of TiO₂ spheres include the impregnation of hard template such as organic or silica spheres [38,39], soft template-assisted alkoxide-based sol-gel synthesis [40-42], or template-free approaches [43,44], using organometallic titanium sources, especially glycolate. While, only few preparation methods utilizing inorganic titania sources are known [45], peroxy method is a good alternative to alkoxide-based or template-assisted procedures, since no toxic organic solvents or inert atmosphere are required. Titanium peroxy complexes are utilised for preparation of Na-titanates spherical particles [46] and TiO₂:Nb spheres via ultrasonic spray pyrolysis [47]. In the present study, we apply peroxy-mediated procedure for preparing TiO₂ spheres with controlled particle size and porosity, and this was achieved by a choice of solvent used for the synthesis or by post-synthetic treatment.

2. Experimental

2.1. Materials

Titanium oxysulfate hydrate ($\text{TiOSO}_4 \cdot n\text{H}_2\text{O}$) and 30 wt% hydrogen peroxide were purchased from Aldrich. Hydrochloric acid 37-38 wt% water solution was obtained from J.T. Baker. Chloroform (99% purity), ammonium hydroxide 20 wt% water solution, methanol, ethanol and n-propanol (all VWR Chemicals) were of analytical grade and used as received without further purification. For the photocatalytic test, MPET of 98% purity was obtained from TCI Europe NV as well as 4-(2-hydroxy-ethoxy)-benzaldehyde (HEB). p-Cresol of 99% purity was purchased from Aldrich.

2.2. Synthesis

In this work we found that adjusting our previously reported method [48], by decreasing titania precursor concentration and increasing Ti: NH_3 ratio in the solvent-exchange preparation procedure, promotes formation of titania spherical particles.

Firstly, titanium hydroxide was precipitated from 25 mL of 0.1 M titanium oxysulfate solution by adding 2 mL of 20 wt% $\text{NH}_3 \cdot \text{H}_2\text{O}$ aqueous solution. The precipitate was centrifuged, washed and dissolved by adding 2.5 mL of 30 wt% hydrogen peroxide. The reaction mixture volume was adjusted to 25 mL by distilled water and pH value was set to 9.5 by adding ammonia. Then, the ice-cooled solution of peroxo complex was mixed with the equal volume of methanol, ethanol or n-propanol and then the suspension was formed. The obtained suspension was aged, isolated by centrifugation and washed with deionized water. The post-synthetic treatment of the titania spheres prepared in the presence of n-propanol was carried out in the following way: the amorphous precipitate, formed after n-propanol addition and aging for 24 h, was suspended in the 50 mL of water-ethanol mixture (1:1 ratio by volume) at pH 4, which was adjusted by addition of HCl (1 M). The suspension was refluxed for 21 h and then the solid phase was separated by centrifugation at 3000 rpm and washed with deionized water. All precipitates were dried at 70 °C for 24 h before being subjected to

investigation. Later, the samples were thermally treated in a muffle furnace at 500, 650 and 800 °C at a heating rate of 3 °C·min⁻¹ and calcination time of 30 min. The samples prepared by isolation of titania particles from the solutions containing methanol, ethanol, n-propanol and after the post-synthetic treatment were designated as TiMex, TiEtx, TiPrx, and TiPrRx, respectively, where “x” indicates the calcination temperature (in °C). The choice of the calcination temperature range was based on the previous study [48], where maximum photocatalytic activity was reached for the samples calcined at 800 °C.

2.3. Characterization

Powder XRD patterns were recorded in an X’pert PANanalytical diffractometer, using Ni-filtered Cu-K α radiation source. The mean crystal sizes were calculated by Scherrer equation for anatase (101) reflection. A Shimadzu UV-2700 spectrophotometer with integrated sphere attachment was used to obtain diffusive reflectance spectra from the prepared oxides supported on the barium sulfate pellets. Band gap energy was estimated by applying Kubelka-Munk function to the DR UV spectra. SEM images were obtained by using a JEOL 6610LV scanning electron microscope; the samples were coated with gold prior to observation. Micromeritic ASAP 2020 was used to obtain adsorption-desorption isotherms of N₂ at 77 K. Specific surface area (SSA) and pore size distribution were calculated from the low-temperature nitrogen adsorption data using BET and BJH approaches, respectively. Prior to the experiment the samples were outgassed under vacuum at 200 °C (for TiPrR) or 250 °C (for all other samples). TEM studies were performed on a JEOL JEM-2100F transmission electron microscope operated at accelerating voltage of 200 kV, equipped with a field emission gun (FEG) and with an ultra-high resolution pole-piece that provided point-resolution better than 0.19 nm. The samples for TEM were dispersed in ethanol, sonified and sprayed on a holey carbon film-coated copper grid and then allowed to air-dry; finally, Gatan SOLARUS 950 was used before observation. Point of zero charge (PZC) was measured using Zetasizer Nano ZS90.

2.4. Photocatalytic test

Photocatalytic properties of the prepared materials and the commercial Aeroxide P25 were investigated for the decomposition of MPET in aqueous-phase under UV light. Since the as-prepared materials were amorphous, their photocatalytic tests were not performed. The UV-light source was a Helios Italquartz GR.E 500 W high-pressure mercury lamp (maximum radiation at 365 nm and impinging radiation was estimated to be $2.7 \text{ W}\cdot\text{m}^{-2}$) equipped with a Pyrex water-cooling jacket cutting-off the radiation wavelengths below 300 nm. In all experiments, 100 mg of samples was placed in a 250 mL Duran Glass reactor having 200 mL of MPET solution in deionized water ($20 \text{ mg}\cdot\text{L}^{-1}$). The reactor was set at 25 cm from the light source and the suspension was magnetically stirred. Firstly, adsorption of MPET on the titania samples was measured in the dark. After this, the suspension was exposed to UV-light and the aliquots of 3 mL were taken at appropriate intervals during the total irradiation time of 6 h if not stated otherwise. Then, the solution was filtered from the photocatalyst with $0.25 \mu\text{m}$ PTFE filter, extracted with chloroform (at volume ratio 1:1), and the concentration of MPET and the reaction intermediate (p-cresol) were determined by GC-MS technique. The Shimadzu GC/MS QP2010 Plus system, equipped with 30 m long Teknokroma TRB-5MS capillary column, was previously calibrated by using standard solutions of the studied compounds. Photolysis of the MPET solution was carried out under the same experimental conditions, but in the absence of a photocatalyst. The total organic carbon (TOC) was measured using a Shimadzu TOC-V CSH Analyzer for the initial MPET solution, as well as after 360, 600, and 840 min of the photocatalytic reaction. Recyclability of the most active photocatalysts was tested in consecutive MPET photodecomposition cycles. For this purpose, the photocatalysts were separated from the reaction medium after 6 h of the reaction, by centrifugation at 3000 rpm for 3 min, then washed three times with deionized water, and dried at $70 \text{ }^\circ\text{C}$ for 48 h. The remaining amount of the photocatalyst was determined and reused in the following photodegradation runs.

The toxicity of the reaction solutions at different irradiation times was estimated according to the standard Microtox suggested protocol using a Microtox Model 500 Toxicity Analyzer [49]. The samples were placed in a 2% NaCl medium with an aliquot of marine bacterium

Vibrio fischeri and the luminescence was measured after 5 and 15 min of incubation. The toxicity of water suspensions of Aeroxide P25 and TiPrR800 priory filtered through 0.2 μM PTFE filter were measured after 8h of irradiation. Phenol and $\text{ZnSO}_4 \cdot 7\text{H}_2\text{O}$ were used as positive controls.

3. Results and Discussion

3.1. Morphology and N_2 physisorption

The SEM images (Fig. 1) show that the particle size largely depends on the organic solvent used for the preparation. The samples prepared by adding methanol (TiMe) or ethanol (TiEt) to the peroxotitanium complex (PTC) solution have an average particle size of 50 nm (Fig. 1a, b), while this average is close to 200-300 nm (Fig. 1c) when n-propanol is used. The decrease in the overall particle diameter, as well as minor shape deformations were observed for the samples calcined at the higher temperatures, as expected considering the sintetering and crystal growth (Fig. S1). It is worth mentioning that all prepared samples retain the spherical morphology up to 800 $^\circ\text{C}$ (Fig. S1). A similar effect of the solvent on the size of the spherical aggregates were observed for silica-titania spheres prepared via the peroxo method [50]. However, the formation of pure TiO_2 particles of the same shape in the absence of any silica source indicates that the assemblage of the spheres runs independently and it is not governed by Stöber process [51]. The particle size is an important property of any photocatalyst defining its reusability in consecutive reactions. For this reason, the TiPr sample has been chosen for the reflux treatment, due to its largest sphere size. It should be mentioned that no significant difference has been observed between particle size of TiPr and TiPrR (Fig. 1c and Fig. 1d). According to SEM images, the spherical particles of TiMe, TiEt and TiPr possess smooth surface, whereas particles of TiPrR demonstrate remarkable roughness (Fig. 1). The samples calcined at 500 $^\circ\text{C}$, which did not undergo the post-synthetic treatment, show comparatively low SSA values (16-35 m^2/g) without suffering significant changes up to 800 $^\circ\text{C}$ (11-21 m^2/g) (Table 1). Unsurprisingly, the lowest SSA has been found for the samples of TiPr series, which have the largest particle size (Table 1).

RESULTS AND DISCUSSION

Table 1 – Properties of the prepared photocatalysts.

sample	T (°C)	SSA (m ² /g)				Crystal size (nm)				Band gap (eV)	
		As prepared	500	650	800	As prepared	500	650	800	500	800
		TiMe	-	29	31	21	-	26	28	44	3.28
TiEt	-	35	18	21	-	19	30	41	3.24	3.23	
TiPr	-	16	13	11	-	23	25	41	3.31	3.24	
TiPrR	210	125	84	33	6	11	15	37	3.40	3.24	

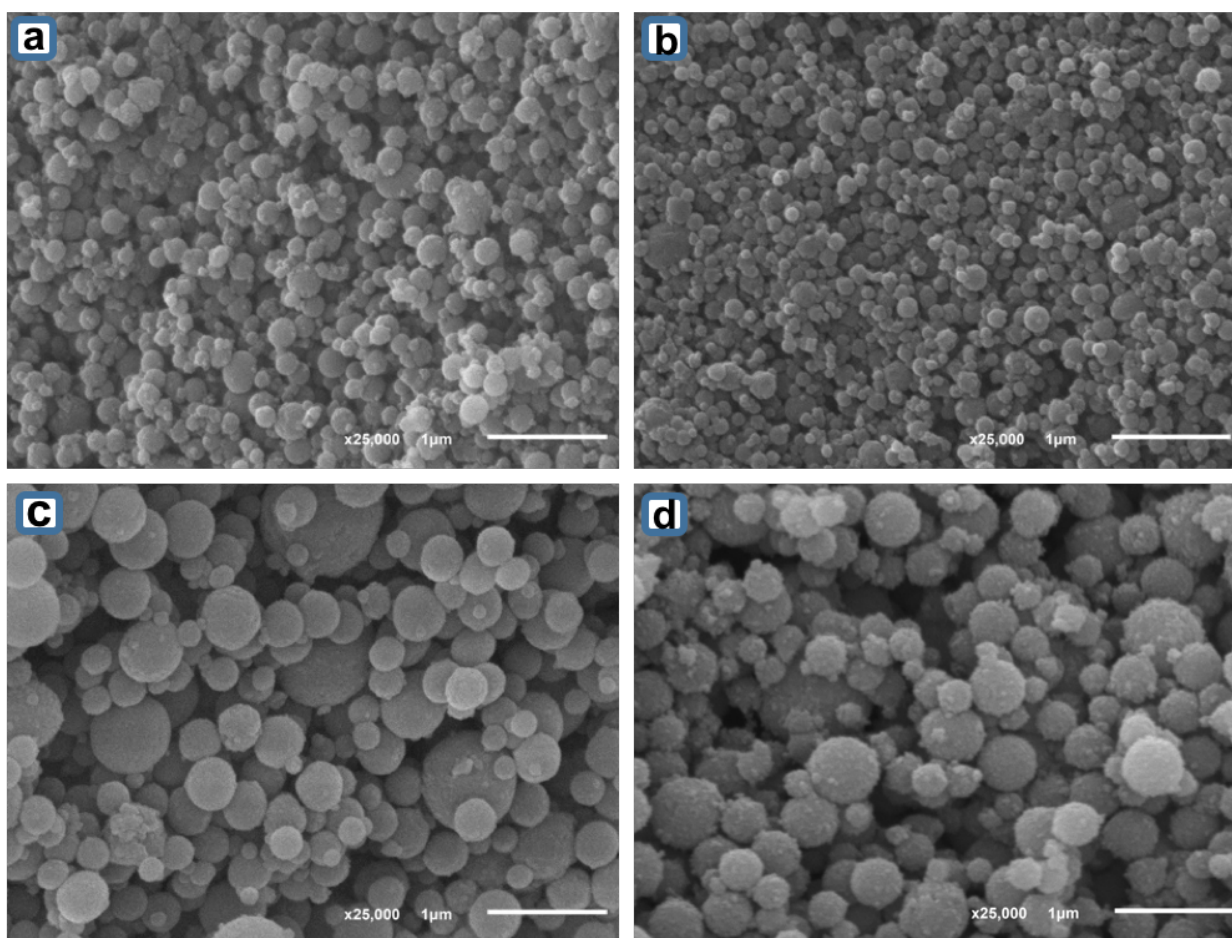


Figure 1 – SEM images of as-synthesized samples: TiMe (a), TiEt (b), TiPr (c), TiPrR (d).

RESULTS AND DISCUSSION

The effect of the post-synthetic treatment on the porosity of TiO₂ spheres is obvious, as SSA values reach 210 and 125 m²/g for samples TiPrR and TiPrR500, respectively. Further increase in the calcination temperature up to 800 °C leads to crystal growth and pore shrinkage resulting in a substantial decrease of SSA down to 33 m²/g. The samples calcined without undergoing the post-synthetic treatment exhibit type-IV or type-III isotherm, according to IUPAC classification, with a barely distinguishable hysteresis loop in the range of P/P₀ 0.90-0.99, which is an indication of the interparticle porosity (Fig. 2a, Fig. S2). The heat treatment temperature has a little influence on the porosity of TiPr samples, while the reflux treatment (TiPrR) reveals a drastic effect on the porosity (Fig. 2). SSA of TiPr and TiPrR samples calcined at 500 °C (Table 1) differ by up to one order of magnitude. Moreover, the N₂ adsorption-desorption isotherm of the sample that underwent post-synthetic treatment shows featured prominent hysteresis loop of H1-type at P/P₀ 0.65-0.90, indicating the presence of the mesopores most likely to be attributed to the internal particle porosity. The pore size distribution analysis clearly demonstrates that TiPrR500 sample has a large mesopore volume (1.5 cm³/g) with a mean size of 10 nm, while this value is negligible for TiPr500 (Fig. 2a). Further heat treatment up to 800 °C for TiPrR800 has resulted in a significant reduction of SSA (Table 1) and pore volume (Fig. 2b); however, the SSA value for this sample is still higher than for others samples treated under the same conditions. Also, despite the obvious deterioration of the textural properties, TiPrR800 retains the mesopores with an average pore size of 15 nm. From the N₂ physisorption analysis, it is clear that the proposed reflux treatment of the amorphous precursor results in enhancement of such desirable photocatalytic properties as mesoporosity and specific surface area.

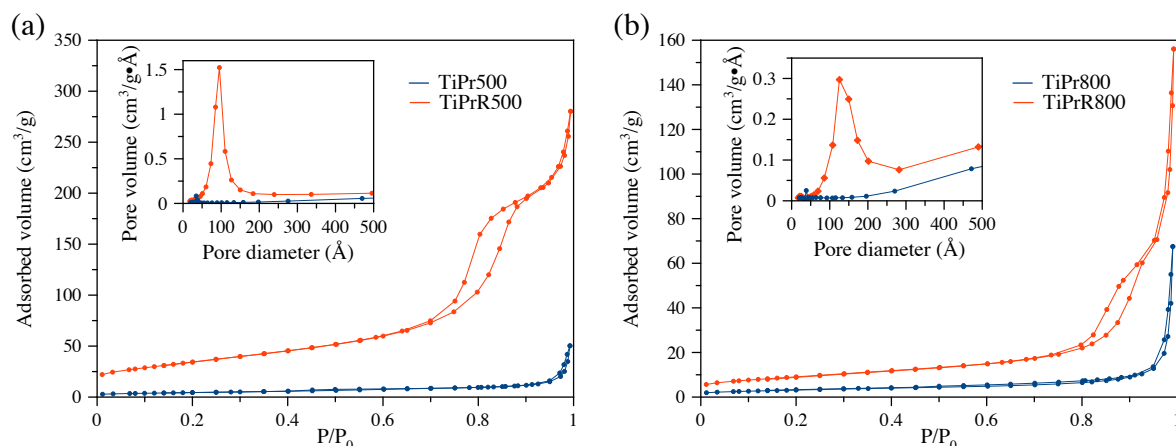


Figure 2 – N_2 adsorption-desorption isotherms and average pore size distribution of TiPrR and TiPr samples calcined at 500 °C (a) and 800 °C (b).

3.2. XRD studies

In our previous work [48], we successfully synthesized nanoparticles of TiO_2 anatase stable up to 1000 °C by using a similar solvent-exchange method. In this present study, we have chosen lower calcination temperatures, because the TiO_2 nanoparticles treated at higher temperatures are less photocatalytically active [48]. Considering the previously obtained results, it is unsurprising that all prepared samples show only the presence of anatase phase stable up to 800 °C (Fig. 3). The crystal sizes of TiMe, TiEt, and TiPr samples, calculated from the PXRD data by means of Scherrer equation, vary from 20 nm for the samples calcined at 500 °C up to 40 nm for those treated at 800 °C (Table 1). The sample that underwent the post-synthetic treatment (TiPrR) appears to have slightly different features. It is already crystalline after the reflux treatment and consequently its crystal growth under calcination follows a different mechanism, resulting in somewhat smaller crystal sizes (Table 1).

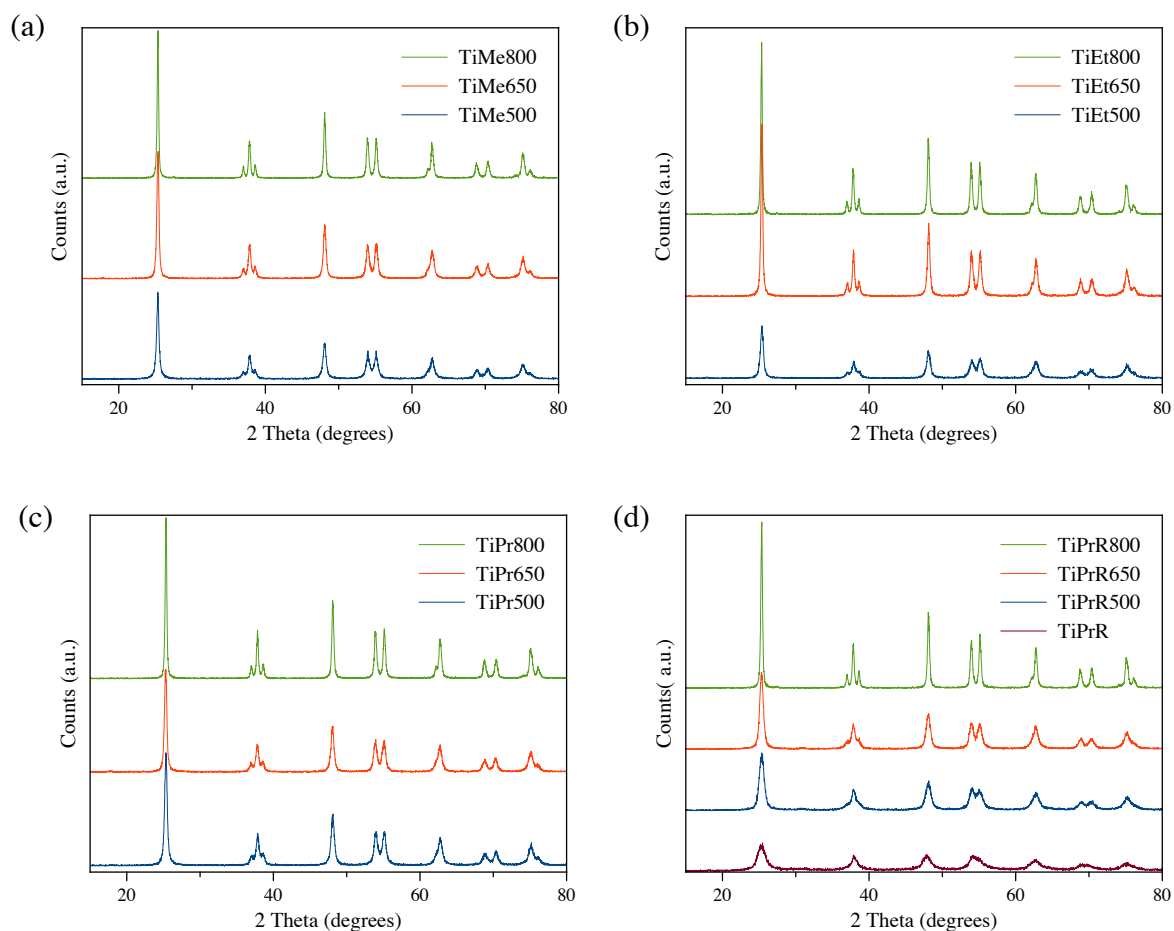


Figure 3 – PXR D patterns of TiMe (a), TiEt (b), TiPr (c), and TiPrR (d) samples at different calcination temperatures.

Normally the band gap energy of TiO_2 anatase is 3.2 eV, however, this parameter for the samples treated at 500 °C exceeds this value, and the presence of the defects in the crystal structure caused by the nitrogen incorporation, coming from ammonia used for the synthesis, is a possible reason for that [48]. Further heating to 800 °C promotes the narrowing of the band gap value by eliminating the crystal defects (Table 1).

3.3. TEM studies

As it has been discussed in the subsections 3.1 and 3.2, the spherical particles prepared by the proposed technique demonstrate very similar structural and morphological features,

RESULTS AND DISCUSSION

which are only modified by the post-synthetic treatment. In the same way, similar materials in a nanoparticulate form have the highest photocatalytic activity when they are calcined at 800 °C [48]. Therefore, TiPr, TiPr800, TiPrR and TiPrR800 samples were selected to be studied in more detail using TEM. For instances, Figure S3 represents the particle-size histograms of samples TiPr (a), TiPr800 (b), TiPrR (c), and TiPrR800 (d) determined by counting more than 180 particles. The solid blue line corresponds to the Log-normal distribution function fit with a mean size of 0.17(1), 0.21(3), 0.263(7) and 0.262(3) μm , respectively (Table S1). As it was expected, the spherical particles of TiPr sample are totally amorphous according to selected area electron diffraction (SAED) patterns and HRTEM images (Fig. 4a). While in the case of TiPr800 sample, we can clearly observe aggregates made up of densely packed TiO_2 nanocrystals, forming spherical particles (Fig. 4b). Both particle and crystal sizes are in good agreement with SEM and XRD data, respectively. SAED pattern (Fig. 4b) shows the polycrystalline nature of the spherical particles and all the observed diffraction rings have been unambiguously assigned to the anatase phase ($a = 3.776 \text{ \AA}$, $b = 9.486 \text{ \AA}$, space group $I4_1/amd$; ICSD PDF4: 002-0406) in agreement with its simulated pattern, being Miller indices depicted. Similarly, HRTEM images (for instances Fig. 4b) prove the highly crystalline nature of these TiO_2 nanoparticles with an interplanar spacing of 3.51 \AA characterizing the anatase TiO_2 {101} facet. Furthermore, the spheres formed after the post-synthetic treatment (TiPrR) are already crystalline as confirmed by SAED pattern (Fig. 5a). The HRTEM images (Fig. 5a) show the presence of small TiO_2 nanocrystals measure approximately 10 nm, which are loosely assembled in these spherical aggregates, whereas thermal treatment at 800 °C (TiPrR800) provokes the crystal growth of the nanocrystallites up to 50 nm, but maintaining the average size of the spheres (see Fig. S3), and hence reducing the internal porosity of the spherical particles (Fig. 5b); however, more loose assembly of TiO_2 nanocrystals is still obviously manifesting compared to that of TiPr800.

RESULTS AND DISCUSSION

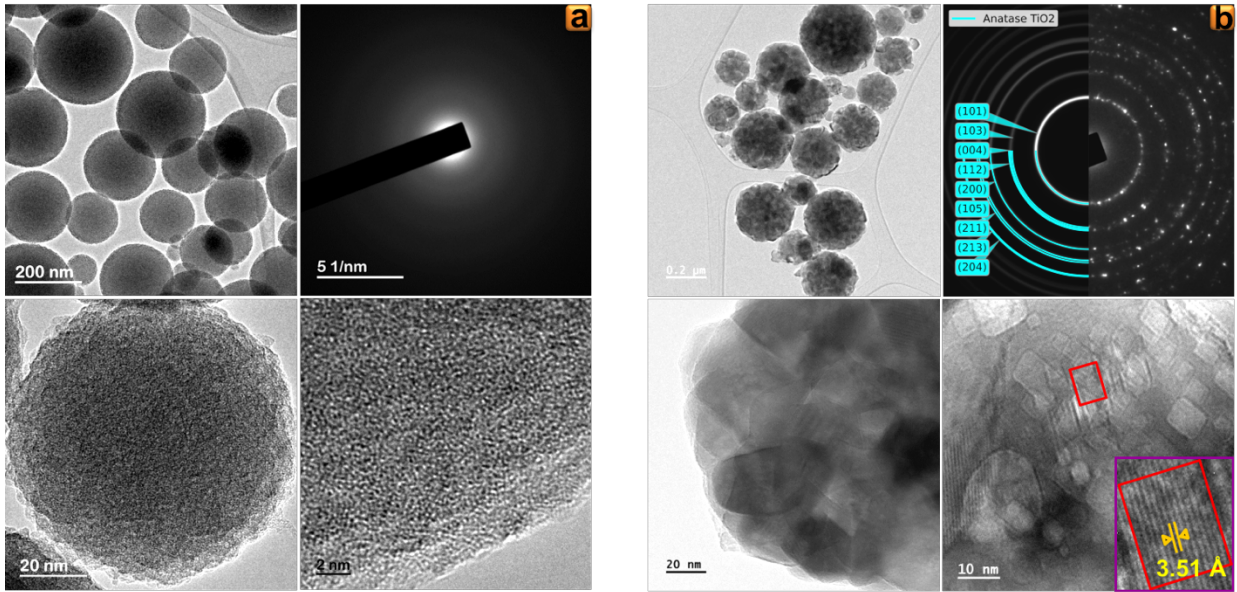


Figure 4 – TEM images and SAED patterns (experimental and simulated) of TiPr (a) and TiPr800 (b) samples.

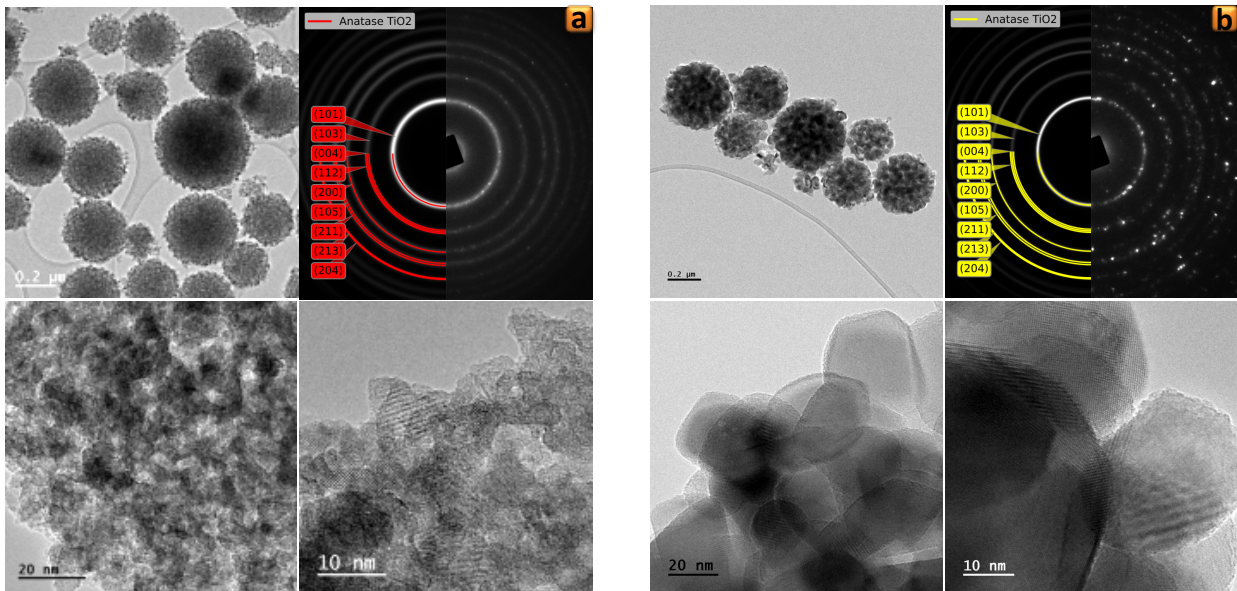


Figure 5 – TEM images and SAED patterns (experimental and simulated) of TiPrR (a) and TiPr800 (b) samples.

RESULTS AND DISCUSSION

Table 2 – First-order kinetic constant (min^{-1}) of MPET degradation and correlation coefficient R.

	TiMe		TiEt		TiPr		TiPrR		Aeroxide P25	
	k1	R	k1	R	k1	R	k1	R	k1	R
As-prepared	-	-	-	-	-	-	0.0046	-	0.0263	0.96
500 °C	0.0015	0.94	0.0012	0.98	0.0011	0.99	0.0074	0.94	-	-
650 °C	0.0040	0.98	0.0038	0.99	0.0034	0.99	0.0093	0.99	-	-
800 °C	0.0053	0.99	0.0059	0.99	0.0060	0.99	0.0139	0.96	-	-

Summarizing the data obtained using the characterization method described in the subsections 3.1–3.3 above, one can conclude that the prepared samples are composed solely of the anatase phase and they have insignificant differences in many structural features, such as unit cell parameters (Table S2) or band gap values (Table 1). Though the titania samples might be structurally identical, the dissimilarity of their particle sizes, SSA and pore sizes can affect the photocatalytic properties to a large extent.

3.4. Photocatalytic degradation of MPET

Before starting to study the photocatalytic properties of the prepared titania materials, the photolysis of MPET in aqueous solution and its adsorption were measured. The photolysis was found to be responsible for the decrease of only 2.5 % of MPET initial concentration, while its adsorption on all investigated samples did not exceed 1 %. The TiO_2 spheres, calcined at the same temperatures and which have not undergone the post-synthetic treatment, show similar performance in the UV-assisted degradation of MPET (Fig. 6, Table 2). The highest values of MPET removal (ca. 80 %) are reached for this type of the samples thermally treated at 800 °C, and the same effect of calcination temperature was observed earlier for TiO_2 nanoparticles [48].

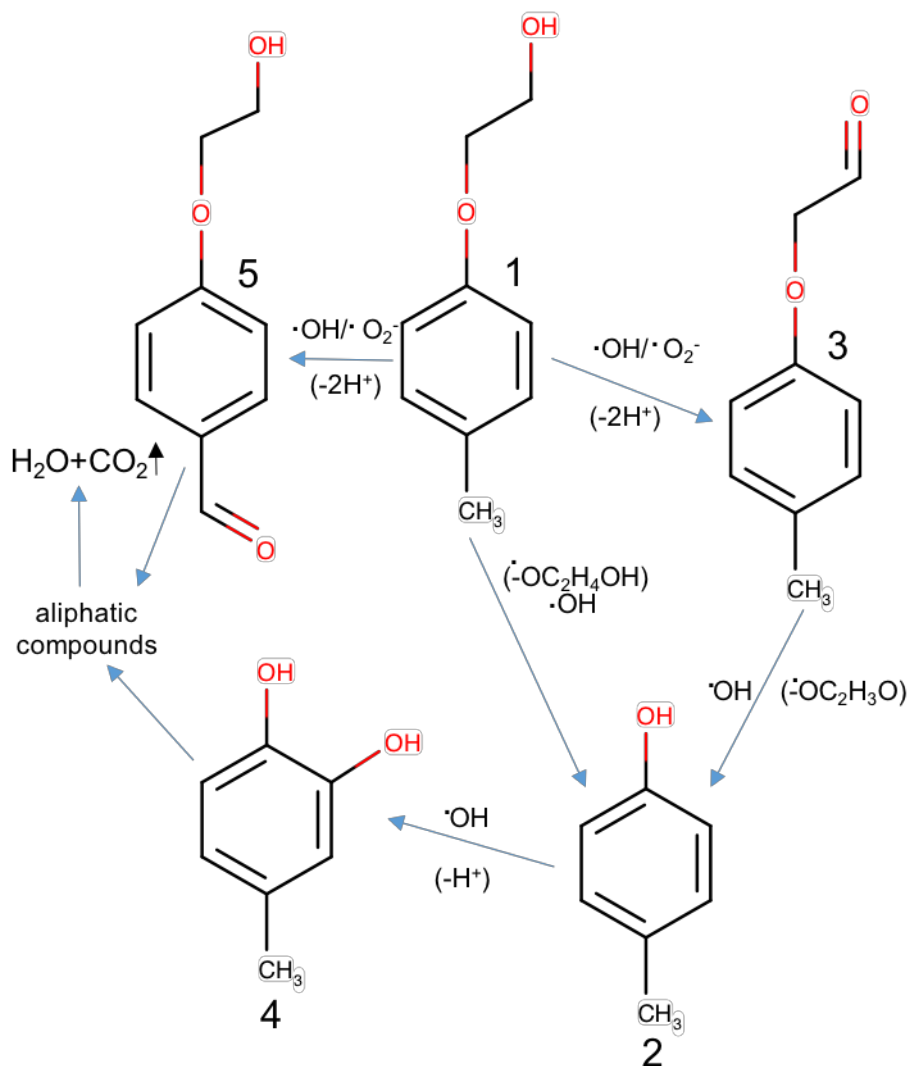
Also, MPET degradation rate shows its dependence on the calcination temperature for the refluxed TiO_2 anatase spheres (Fig. 6). The photocatalytic activity of this sample rises along

RESULTS AND DISCUSSION

with the increase of titania crystal size, despite the loss of SSA (Fig. S4). In the previous work, we found that small amounts of nitrogen is retained in the samples prepared by the precipitation from titanium peroxo complex and calcined at temperatures not higher than 500 °C [48]. This fact indicates that the crystal defects, are probable centres of electron-hole pairs recombination, caused by nitrogen-doping or the crystal growth process, are gradually eliminated at elevated temperatures. Obviously, the performance of TiPrR samples in MPET photodegradation is better than the titania spheres, which have not undergone the post-synthetic treatment, and the total decomposition of the substrate is achieved after 300 min of UV irradiation for TiPrR800, considered the most active sample of this series (Fig. 6c). By considering that the major difference between the samples, directly calcined after the synthesis and previously refluxed, is due to their SSA and pore size distribution, so it is logical to suggest that the enhanced photodegradation rate observed for TiPrR samples is derived from the accessibility of the photocatalyst's surface to MPET molecules. We suggest that the decisive role in the improved reaction performance is played by the pores with diameters between 10 and 20 nm, formed as a consequence of the post-synthetic treatment (Fig. 2). The commercial TiO₂ Aeroxide P25 is considered as the "golden standard" because of its outstanding photocatalytic activity under UV irradiation, which is due to the presence of anatase-rutile interface and its high crystallinity and good dispersibility in a liquid media. In this studied reaction, Aeroxide P25 proves itself as a highly efficient material capable of complete decomposition of MPET in 180 min under UV irradiation (Fig. 6c, Table 2). In order to thoroughly evaluate the photocatalytic activity of such compounds, it is not enough to track the decomposition of a substrate, but it is also very important to determine the reaction pathways and intermediate compounds formed during the photodegradation process. We have detected four major intermediate aromatic compounds during MPET photodecomposition, which include p-cresol (2), p-methylphenoxyacetaldehyde (3), p-methylcatechol (4) and HEB (5) (Scheme 1). The degradation pathways are depicted in Scheme 1 and the mass spectra of the compounds are presented in the SI (Fig. S5). Unsurprisingly, the elimination of ether group is the prevailing decomposition pathway, the same observations were made by Bahnemann et al. when studied phenoxyacetic acid photodegradation [52]. The rupture of the ether bond favours the formation of p-cresol, which is the dominant intermediate of this reaction. p-Cresol is a toxic compound which presence in

RESULTS AND DISCUSSION

water is highly undesirable. According to United States Environmental Protection Agency (USEPA), aquatic organisms should not be affected unacceptably if the four-day average concentration of p-cresol does not exceed 53 $\mu\text{g/L}$ more than once every three years on the average and if the one-hour average concentration does not exceed 480 $\mu\text{g/L}$ more than once every three years on the average [53]. This indicates on a serious problem of eliminating not only the initial emerging pollutant, but the toxic intermediate at a very low concentration level as well [54-57]. Most of the tested photocatalysts do not guarantee the complete elimination of p-cresol during the reaction time (Fig. 6d). Aeroxide P25 is capable of totally decomposing MPET, as well as p-cresol, within 360 min, while TiPrR800 reaches this level of performance after 480 min of UV irradiation (Figs. 6d). The p-cresol decomposition also has its sub-product, as the benzene ring hydroxylation takes place, thus p-methylcatechol (4) is formed. However, p-methylcatechol (4) is produced in trace quantities, and it is decomposed somewhat faster than p-cresol, due to the lower stability of the more hydroxylated benzene ring.



Scheme 1 – MPET photocatalytic degradation pathway.

RESULTS AND DISCUSSION

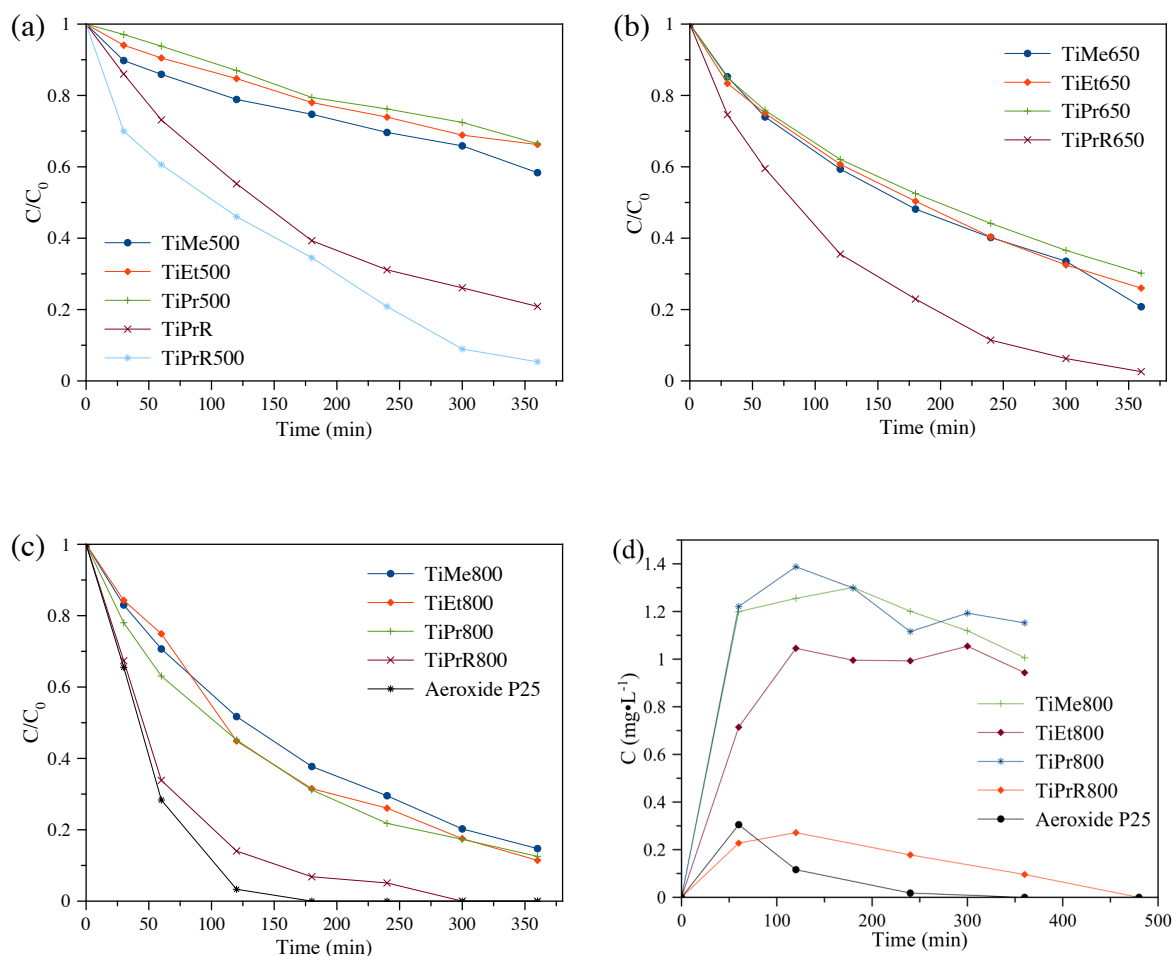


Figure 6 – Degradation curves of MPET under UV light in the presence of the samples: calcined at 500 °C (a), 650 °C (b), 800 °C (c), Aeroxide P25 (c), and p-Cresol evolution curves in the presence of different photocatalysts (d).

The formation of p-methylphenoxyacetaldehyde (3) and HEB (5) is less favourable than that of p-cresol (2), due to the presence of weak ether group, which is susceptible to interact with reactive species. The oxidation of MPET to the compounds (3) evolves according to the mechanism described by Bahnemann et al [16,17], while (5) is produced by oxidation of methyl group of MPET. Then compound (3) is decomposed to p-cresol through the ether bond breaking mechanism, while (5) by oxidizing is most likely to produce aliphatic compounds, since no 4-hydroxybenzaldehyde is detected (Scheme 1). Also, we have found that the degradation of MPET is accompanied by a slight reduction of pH of the suspension

RESULTS AND DISCUSSION

from 5.5 to 4.1, which is superior or equal to the PZC of TiPrR800 having a value of 4.1 (Fig. S6). The mineralization of MPET into CO₂ and H₂O was estimated by TOC measurement. The TOC removal data follow the same pattern as the MPET degradation curves. The highest value of the substrate mineralization is observed for P25 photocatalyst (63 % after 6 h), followed by TiPrR800 with 36 % (Fig. 7a). TiPrR800 sample appears to be the most active photocatalyst among all synthesised samples (Fig. 7a). Extending the irradiation time up to 14 h in the presence of TiPrR800 time allows achieving the TOC removal of 57 %, which is close to the value obtained for P25 within 6 h (Fig. 7b). Although the P25 might seem an ideal photocatalyst, it has a very notable drawback complicating the implementation of real-life applications. Due to its small particle size of about 20 nm and, consequently, high dispersibility in the liquid media, it suffers from poor recyclability or demands special measures for its separation after the photocatalytic reaction [58]. As it is shown in Fig. 8 and Fig. S7, more than half of the starting amount used of P25 is lost after the first reaction cycle; however, P25 retained a high level of activity. Then, almost all the P25 catalyst is washed away after the second reaction run, leading to the drastic loss of activity.

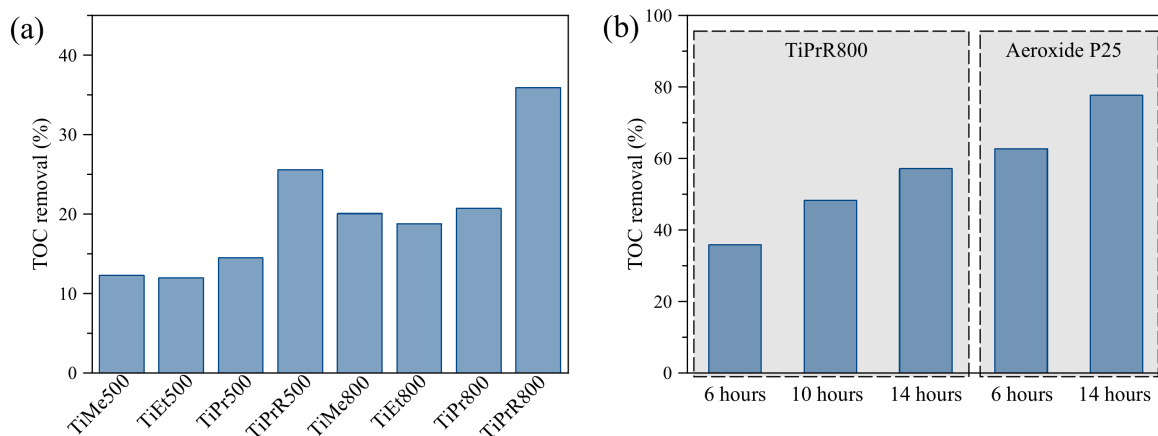


Figure 7 – TOC removal data for the synthesized samples after 6 hours of the reaction (a) and at different reaction time (b).

On the other hand, the titania spheres maintain their morphology after the reaction runs (Fig. S8) and demonstrate more stable performance during four consecutive cycles, retaining

RESULTS AND DISCUSSION

60 % of the starting amount of the photocatalyst after the fourth reaction run and maintaining TOC removal between 32 and 41 % (Fig. 8 and Fig. S7).

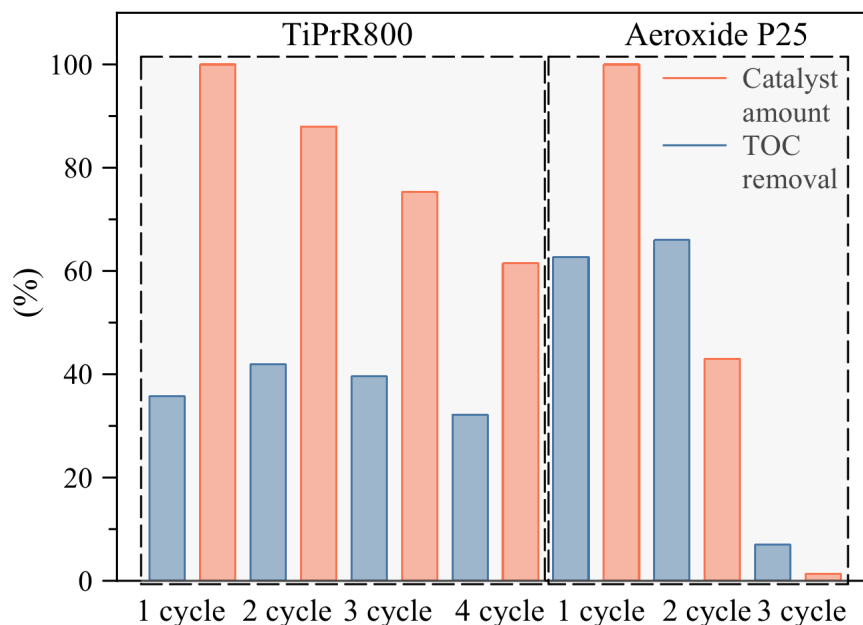


Figure 8 – TOC removal and amounts of TiPrR800 and Aeroxide P25 photocatalysts during 4 consecutive reaction cycles.

Evidently, the photooxidation of MPET is a complex process leading to the formation of a variety of aromatic and aliphatic intermediates, making it difficult to establish a level of harm each compound might cause in the environment. Hence, the estimation of toxicity is necessary to ensure viability of the proposed materials and photodegradation method. Figure 9 demonstrates that P25 Aeroxide gradually reduces toxicity of the initial MPET solution, while TiPrR800 produces more toxic partial oxidation compounds after 2 and 4 h of the reaction, but finally degrading them, thus lowering the toxicity below the starting value. Higher toxicity of the partial oxidation products of TiO_2 -assisted photo-degradation of herbicides and pharmaceuticals than the substrates themselves was attributed by Antonopoulou et al to the synergetic effect of several reaction intermediates [59,60]. The similar effect might take place in the present case, as the maximum of toxicity for the solutions photocatalytically treated in the presence of TiPrR800 is found for the 2 h of

irradiation, which coincides with the reaction time when the highest concentration of the major oxidation side-product is observed (Fig. 6d), however we cannot attribute this increased toxicity to any certain compound (Fig. S9). Besides the toxicity of the organic compounds formed during the reaction, the possible influence of photocatalyst particles on the inhibition of the bacteria is also must be estimated. The disaggregation of the photocatalysts takes place under the UV-irradiation, and some small nanoparticles might be able to pass the filtering systems. The toxicity of filtered water suspensions of the commercial photocatalyst and titania spheres after the UV-irradiation shows higher inhibition of the bacteria in case of Aeroxide P25 (Fig. S10). This finding is in accordance with other works demonstrating significant toxic effect of TiO₂ nanoparticles on live organisms was established [61,62].

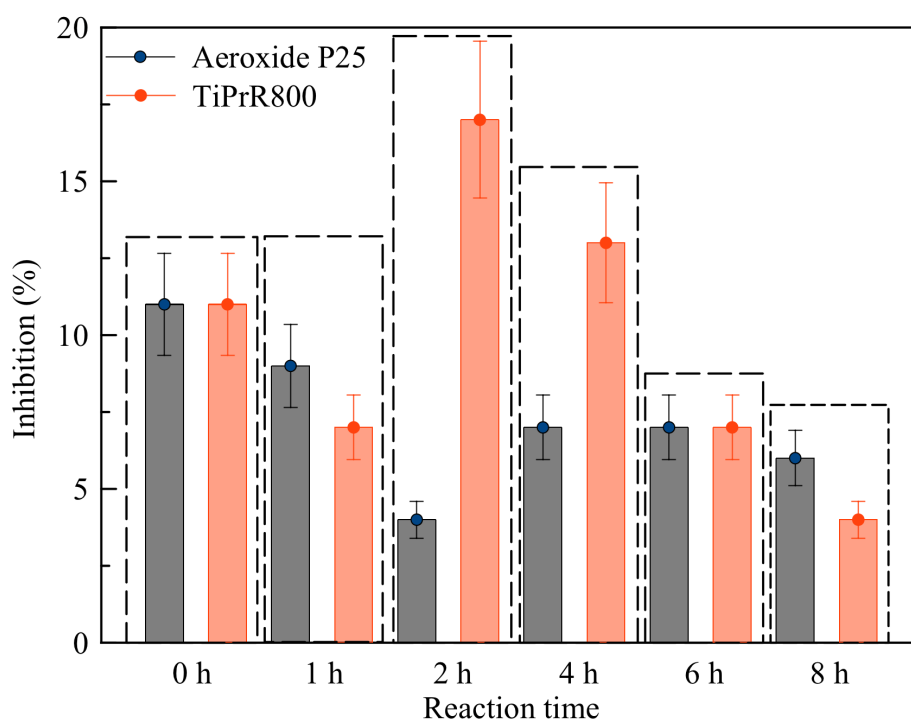


Figure 9 – % Inhibition of bioluminescence of *Vibrio fischeri* bacteria as a function of photocatalytic treatment in the presence of Aeroxide P25 and TiPrR800.

4. Conclusions

We have demonstrated that the use of aliphatic alcohols with different carbon chain length, during the solvent-exchange procedure, allows manipulating the particle size of the TiO₂ spheres. The resulted titania photocatalysts are mildly active due to their nonporous nature. However, the developed post-synthetic reflux procedure successively converts the prepared titania spheres into more efficient photocatalytic mesoporous material.

The determined pathway of MPET photocatalytic decomposition, under UV light and assisted by TiO₂ photocatalysts, includes the formation of toxic p-cresol intermediate. It has been established that the commercial photocatalyst Aeroxide P25 and our prepared mesoporous TiO₂ spheres are able to decompose totally and efficiently the initial substrate as well as intermediate p-cresol, thus leaving no toxic compounds behind after the photocatalytic reaction. Although the above-mentioned photocatalysts are both effective, the synthesized mesoporous titania spheres have an advantage over P25, since they are easily separated from the reaction mixture after the photocatalytic run, hence they can be reused multiple times without losing their activity.

Acknowledgement

We gratefully acknowledge financial support from the Spanish MINECO (MAT2016-78155-C2-1-R, MAT2013-40950-R, CTQ2011-29272-C04-02), and the Government of the Principality of Asturias (GRUPIN14-060; GRUPIN14-078; and “Severo Ochoa” PhD grant BP-14-029 to M.I.) and FEDER. South Ural State University acknowledges financial support from Ministry of Education and Science of the Russian Federation (grant No 16.2674.2014/K). IK is grateful for the support by Act 211 Government of the Russian Federation, contract № 02.A03.21.0011. We thank Cogersa for carrying out the toxicity measurements.

References

1. Y. Patiño, E. Díaz, S. Ordóñez, Performance of different carbonaceous materials for emerging pollutants adsorption, *Chemosphere*, **2015**, 119, 124–130.
2. Y. Patiño, E. Díaz, S. Ordóñez, E. Gallegos-Suarez, A. Guerrero-Ruiz, I. Rodríguez-Ramos, Adsorption of emerging pollutants on functionalized multiwall carbon nanotubes *Chemosphere*, **2015**, 136, 174–180.
3. S. Esplugas, D.M. Bila, L.G.T. Krause, M. Dezotti, Ozonation and advanced oxidation technologies to remove endocrine disrupting chemicals (EDCs) and pharmaceuticals and personal care products (PPCPs) in water effluents, *J. Hazard. Mater.*, **2007**, 149, 631–642.
4. H.-S. Chang, K.-H. Choo, B. Lee, S.-J. Choi, The methods of identification, analysis, and removal of endocrine disrupting compounds (EDCs) in water, *J. Hazard. Mater.*, **2009**, 172, 1–12.
5. Q. Wang, T. Jin, Z. Hu, L. Zhou, M. Zhou, TiO₂-NTs/SnO₂-Sb anode for efficient electrocatalytic degradation of organic pollutants: Effect of TiO₂-NTs architecture, *Sep. Purif. Technol.*, **2013**, 102, 180–186.
6. RIFM Expert Panel, D. Belsito, D. Bickers, M. Bruze, P. Calow, M.L. Dagli, A.D. Fryer, H. Greim, Y. Miyachi, J.H. Saurat, I.G. Sipes, A toxicological and dermatological assessment of aryl alkyl alcohols when used as fragrance ingredients, *Food Chem. Toxicol.*, **2012**, 50, S52–S99.
7. A.O. Kondrakov, A.N. Ignatev, F.H. Frimmel, S. Bräse, H. Horn, A.I. Revelsky, Formation of genotoxic quinones during bisphenol A degradation by TiO₂ photocatalysis and UV photolysis: A comparative study, *Appl. Catal. B: Environ.*, **2014**, 160–161, 106–114.
8. G. Li, X. Nie, Y. Gao, T. An, Can environmental pharmaceuticals be photocatalytically degraded and completely mineralized in water using g-C₃N₄/TiO₂ under visible light irradiation?—Implications of persistent toxic intermediates, *Appl. Catal., B: Environ.*, **2016**, 180, 726–732.
9. W.M.M. Mahmoud, A.P. Toolaram, J. Menz, C. Leder, M. Schneider, K. Kummerer, Identification of phototransformation products of thalidomide and mixture toxicity

assessment: an experimental and quantitative structural activity relationships (QSAR) approach, *Water Res.*, **2014**, 49, 11–22.

10. S. Yurdakal, G. Palmisano, V. Loddo, V. Augugliaro, L. Palmisano, Nanostructured rutile TiO₂ for selective photocatalytic oxidation of aromatic alcohols to aldehydes in water, *J. Am. Chem. Soc.*, **2008**, 130, 1568–1569.

11. I. Tamiolakis, I. N. Lykakis, G. S. Armatas, Mesoporous CdS-sensitized TiO₂ nanoparticle assemblies with enhanced photocatalytic properties: Selective aerobic oxidation of benzyl alcohols, *Catal. Today*, **2015**, 250, 180–186.

12. G. Palmisano, S. Yurdakal, V. Augugliaro, V. Loddo, L. Palmisano, Photocatalytic selective oxidation of 4-methoxybenzyl alcohol to aldehyde in aqueous suspension of home-prepared titanium dioxide catalyst, *Adv. Synth. Catal.*, **2007**, 349, 964–970.

13. V. Augugliaro, H. Kisch, V. Loddo, M. J. López-Muñoz, C. Márquez-Álvarez, G. Palmisano, L. Palmisano, F. Parrino, S. Yurdakal, Photocatalytic oxidation of aromatic alcohols to aldehydes in aqueous suspension of home-prepared titanium dioxide: 1. Selectivity enhancement by aliphatic alcohols, *Appl. Catal. A*, **2008**, 349, 182–188.

14. M. Addamo, V. Augugliaro, M. Bellardita, A. D. Paola, V. Loddo, G. Palmisano, L. Palmisano, S. Yurdakal, Environmentally friendly photocatalytic oxidation of aromatic alcohol to aldehyde in aqueous suspension of brookite TiO₂, *Catal. Lett.*, **2008**, 126, 58–62.

15. I. Tamiolakis, I.N. Lykakis, A.P. Katsoulidis, G.S. Armatas, One-pot synthesis of highly crystalline mesoporous TiO₂ nanoparticle assemblies with enhanced photocatalytic activity, *Chem. Commun.*, **2012**, 48, 6687–6689.

16. M. Qamar, R.B. Elsayed, K.R. Alhooshani, M.I. Ahmed, D.W. Bahnemann, Chemoselective and highly efficient conversion of aromatic alcohols into aldehydes photo-catalyzed by Ag₃PO₄ in aqueous suspension under simulated sunlight, *Catal. Commun.*, **2015**, 58, 34–39.

17. M. Qamar, R.B. Elsayed, K.R. Alhooshani, M.I. Ahmed, D.W. Bahnemann, Highly efficient and selective oxidation of aromatic alcohols photocatalyzed by nanoporous hierarchical Pt/Bi₂WO₆ in organic solvent-free environment, *ACS Appl. Mater. Interfaces*, **2015**, 7, 1257–1269.

18. H. Kisch, *Semiconductor Photocatalysis: Principles and Applications*, first ed., Wiley-VCH, Weinheim, **2015**.
19. V. Etacheri, C.D. Valentin, J. Schneider, D. Bahnemann, S.C. Pillai, Visible-light activation of TiO₂ photocatalysts: advances in theory and experiments, *J. Photochem. Photobiol. C: Photochem. Rev.*, **2015**, 25, 1–29.
20. L. G. Devi, R. Kavitha, A review on non metal ion doped titania for the photocatalytic degradation of organic pollutants under UV/solar light: Role of photogenerated charge carrier dynamics in enhancing the activity, *Appl. Catal., B*, **2013**, 140–141, 559–587.
21. C. Ahn, J. Park, D. Kim, S. Jeon, Monolithic 3D titania with ultrathin nanoshell structures for enhanced photocatalytic activity and recyclability, *Nanoscale*, **2013**, 5, 10384–10389.
22. C. Haw, W. Chiu, S.A. Rahman, P. Khiew, S. Radiman, R.A. Shukor, M.A.A. Hamid, N. Ghazali, The design of new magnetic-photocatalyst nanocomposites (CoFe₂O₄-TiO₂) as smart nanomaterials for recyclable-photocatalysis applications, *New J. Chem.*, **2016**, 40, 1124–1136.
23. D.H. Quiñones, A. Rey, P.M. Álvarez, F.J. Beltrán, P.K. Plucinski, Enhanced activity and reusability of TiO₂ loaded magnetic activated carbon for solar photocatalytic ozonation, *Appl. Catal., B*, **2014**, 144, 96–106.
24. N. Kaur, S. K. Shahi, V. Singh, Synthesis, characterization and photocatalytic activity of magnetically separable γ -Fe₂O₃/N,Fe codoped TiO₂ heterojunction for degradation of Reactive Blue 4 dye, *RSC Adv.*, **2015**, 5, 61623–61630.
25. S. Linley, T. Leshuk, F.X. Gu, Synthesis of magnetic rattle-type nanostructures for use in water treatment, *ACS Appl. Mater. Interfaces*, **2013**, 5, 2540–2548.
26. B. Barrocas, O.C. Monteiro, M.E. Melo Jorge, S. Sérgio, Photocatalytic activity and reusability study of nanocrystalline TiO₂ films prepared by sputtering technique, *Appl. Surf. Sci.*, **2013**, 264, 111–116.
27. K.P.O. Mahesh, D.-H. Kuo, B.-R. Huang, M. Ujihara, T. Imae, Chemically modified polyurethane-SiO₂/TiO₂ hybrid composite film and its reusability for photocatalytic degradation of Acid Black 1 (AB 1) under UV light, *Appl. Catal. A*, **2014**, 475, 235–241.
28. D. Chen, R.A. Caruso, Recent Progress in the Synthesis of Spherical Titania Nanostructures and Their Applications, *Adv. Funct. Mater.*, **2013**, 23, 1356–1374.

29. J. Chen, Z. Hua, Y. Yan, A.A. Zakhidov, R.H. Baughman, L. Xu, Template synthesis of ordered arrays of mesoporous titania spheres, *Chem. Commun.*, **2010**, 46, 1872–1874.
30. B. Liu, K. Nakata, M. Sakai, H. Saito, T. Ochiai, T. Murakami, K. Takagi, A. Fujishima, Hierarchical TiO₂ spherical nanostructures with tunable pore size, pore volume, and specific surface area: facile preparation and high-photocatalytic performance, *Catal. Sci. Technol.*, **2012**, 2, 1933–1939.
31. P.T.N. Nguyen, C. Salim, W. Kurniawan, H. Hinode, A non-hydrolytic sol-gel synthesis of reduced graphene oxide/TiO₂ microsphere photocatalysts, *Catal. Today*, **2014**, 230, 166–173.
32. J.H. Pan, Q. Wang, D.W. Bahnemann, Hydrous TiO₂ spheres: an excellent platform for the rational design of mesoporous anatase spheres for photoelectrochemical applications, *Catalysis Today*, **2014**, 230, 197–204.
33. B.F. Huang, D. Chen, X.Li. Zhang, R.A. Caruso, Y-B. Cheng, Dual-Function scattering layer of submicrometer-sized mesoporous TiO₂ beads for high-efficiency dye-sensitized solar cells, *Adv. Funct. Mater.*, **2010**, 20, 1301–1305.
34. K-F. Du, D. Yang, Y. Sun, Controlled fabrication of porous titania beads by a sol-gel templating method, *Ind. Eng. Chem. Res.*, **2009**, 48, 755–762.
35. H. Liu, Z. Bi, X-G. Sun, R.R. Unocic, M.P. Paranthaman, S. Dai, G.M. Brown, Mesoporous TiO₂-B microspheres with superior rate performance for lithium ion batteries, *Adv. Mater.*, **2011**, 23, 3450–3454.
36. L. Dou, L. Gao, X. Yang, X. Song, Hierarchical architectures TiO₂: Pollen-induced synthesis, remarkable crystalline-phase stability, tunable size, and reused photo-catalysis, *J. Hazard. Mater.*, **2012**, 203–204, 363–369.
37. S. Ullah, E.P. Ferreira-Neto, A.A. Pasa, C.C.J. Alcântara, J.J.S. Acuña, S.A. Bilmes, M.L.M. Riccio, R. Landers, T.Z. Fermino, U.P. Rodrigues-Filho, Enhanced photocatalytic properties of core@shell SiO₂@TiO₂ nanoparticles, *Appl. Catal. B*, **2015**, 179, 333–343.
38. D.G. Schukin, R.A. Caruso, Template synthesis and photocatalytic properties of porous metal oxide spheres formed by nanoparticle infiltration, *Chem. Mater.*, **2004**, 16, 2287–2292.

-
39. T. Leshuk, S. Linley, G. Baxter, F. Gu, Mesoporous hollow sphere titanium dioxide photocatalysts through hydrothermal silica etching, *ACS Appl. Mater. Interfaces*, **2012**, 4, 6062–6070.
40. D. Chen, L. Cao, F. Huang, P. Imperia, Y-B. Cheng, R.A. Caruso, Synthesis of monodisperse mesoporous titania beads with controllable diameter, high surface areas, and variable pore diameters (14–23 nm), *J. Am. Chem. Soc.*, **2010**, 132, 4438–4444.
41. H-J. Kim, J-D. Jeon, S-Y. Kwak, Highly dispersed mesoporous TiO₂ spheres via acid treatment and its application for dye-sensitized solar cells, *Powder Technol.*, **2013**, 243, 130–138.
42. S. Tanaka, D. Nogami, N. Tsuda, Y. Miyake, Synthesis of highly-monodisperse spherical titania particles with diameters in the submicron range, *J. Colloid Interface Sci.*, **2009**, 334, 188–194.
43. X. Jiang, T. Herricks, Y. Xia, Monodispersed spherical colloids of titania: synthesis, characterization, and crystallization, *Adv. Mater.*, **2003**, 15, 1205–1209.
44. M. Pal, J.G. Serrano, P. Santiago, U. Pal, Size-controlled synthesis of spherical TiO₂ nanoparticles: morphology, crystallization, and Phase Transition, *J. Phys. Chem. C.*, **2007**, 111, 96–102.
45. E. Matijević, M. Budnik, L. Meites, Preparation and mechanism of formation of titanium dioxide hydrosols of narrow size distribution, *J. Colloid Interface Sci.*, **1977**, 61, 302–311.
46. I.E. Saliby, L. Erdei, H.K. Shon, J.B. Kim, J.-H. Kim, Preparation and characterisation of mesoporous photoactive Na-titanate microspheres, *Catal. Today*, **2011**, 164, 370–376.
47. L. Kong, C. Wang, H. Zheng, X. Zhang, Y. Liu, Defect-induced yellow color in Nb-doped TiO₂ and its impact on visible-light photocatalysis, *J. Phys. Chem. C.*, **2015**, 119, 16623–16632.
48. I. Krivtsov, M. Ilkaeva, V. Avdin, Z. Amghouz, S. Khainakov, J.R. García, E. Díaz, S. Ordóñez, Peroxo method for preparation of composite silica–titania spheres, *RSC Adv.*, **2015**, 5, 36634–36641.
49. Microtox®Manual, 1998.

50. R. Morozov, I. Krivtsov, V. Avdin, Z. Amghouz, S.A. Khainakov, J.R. García, Peroxo method for preparation of composite silica–titania spheres, *J. Non-Cryst. Solids*, **2016**, 435, 8–16.
51. W. Stober, A. Fink, E. Bohn, Controlled growth of monodisperse silica spheres in the micron size range, *J. Colloid Interface Sci.*, **1968**, 26, 62–69.
52. H.K. Singh, M. Saquib, M.M. Haque, M. Muneer, D.W. Bahnemann, Titanium dioxide mediated photocatalysed degradation of phenoxyacetic acid and 2,4,5-trichlorophenoxyacetic acid, in aqueous suspensions, *J. Mol. Catal. A: Chem.*, **2007**, 264, 66–72.
53. https://www.epa.gov/sites/production/files/2015-06/documents/in_al_489_06241999.pdf (accessed 24.09.16)
54. H.-W. Chen, Y. Ku, Y.-L. Kuo, Effect of Pt/TiO₂ characteristics on temporal behavior of o-cresol decomposition by visible light-induced photocatalysis, *Water. Res.*, **2007**, 41, 2069–2078.
55. K.-H. Wang, Y.-H. Hsieh, L.-J. Chen, The heterogeneous photocatalytic degradation, intermediates and mineralization for the aqueous solution of cresols and nitrophenols, *J. Hazard. Mater.*, **1998**, 59, 251–260.
56. S. Rasalingam, H.S. Kibombo, C.-M. Wu, R. Peng, J. Baltrusaitis, R.T. Koodali, Competitive role of structural properties of titania–silica mixed oxides and a mechanistic study of the photocatalytic degradation of phenol, *Appl. Catal. B*, **2014**, 148–149, 394–405.
57. M.F. Atitar, A.A. Ismail, S.A. Al-Sayari, D. Bahnemann, D. Afanasev, A.V. Emeline, Mesoporous TiO₂ nanocrystals as efficient photocatalysts: Impact of calcination temperature and phase transformation on photocatalytic performance, *Chem. Eng. J.*, **2015**, 264, 417–424.
58. Y. Lv, L. Yu, H. Huang, Y. Feng, D. Chen, X. Xie, Application of the soluble salt-assisted route to scalable synthesis of ZnO nanopowder with repeated photocatalytic activity, *Nanotechnology*, **2012**, 23, 065402.
59. M. Antonopoulou, I. Konstantinou, Photocatalytic treatment of metribuzin herbicide over TiO₂ aqueous suspensions: Removal efficiency, identification of transformation

products, reaction pathways and ecotoxicity evaluation, *J. Photochem. Photobiol. A: Chem.*, **2014**, 294, 110–120.

60. M. Antonopoulou, I. Konstantinou, Photocatalytic degradation and mineralization of tramadol pharmaceutical in aqueous TiO₂ suspensions: Evaluation of kinetics, mechanisms and ecotoxicity, *Appl. Catal. A*, **2016**, 515, 136–143.

61. G.P.S. Marcone, Á.C. Oliveira, G. Almeida, G.A. Umbuzeiro, W.F. Jardim, Ecotoxicity of TiO₂ to *Daphnia similis* under irradiation, *J. Hazard. Mater.*, **2012**, 211–212, 436–442.

62. V.K. Sharma, Aggregation and toxicity of titanium dioxide nanoparticles in aquatic environment - A Review, *J. Environ. Sci. Health. A Tox. Hazard. Subst. Environ. Eng.*, **2009**, 44, 1485–1495.

SUPPLEMENTARY INFORMATION

**Photocatalytic degradation of 2-(4-methylphenoxy)ethanol over
TiO₂ spheres**

Marina Ilkaeva^{a,b}, Igor Krivtsov^{a,b,*}, Eva Díaz^c, Zakariae Amghouz^d, Yolanda Patiño^c, Sergei Khainakov^d, José R. García^a and Salvador Ordóñez^c

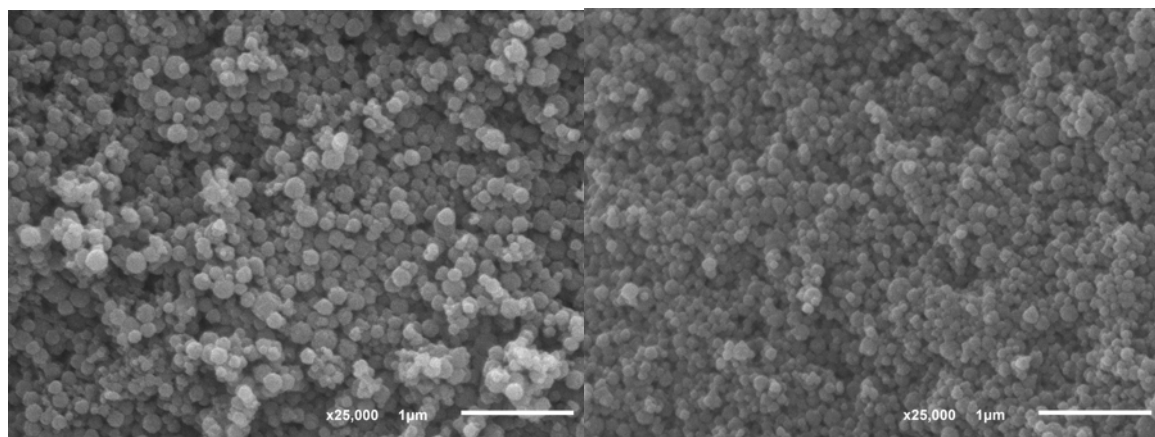
^a *Department of Organic and Inorganic Chemistry, University of Oviedo-CINN, 33006, Oviedo, Spain*

^b *Nanotechnology Education and Research Center, South Ural State University, 454080, Chelyabinsk, Russia*

^c *Department of Chemical and Environmental Engineering, University of Oviedo, 33006, Oviedo, Spain*

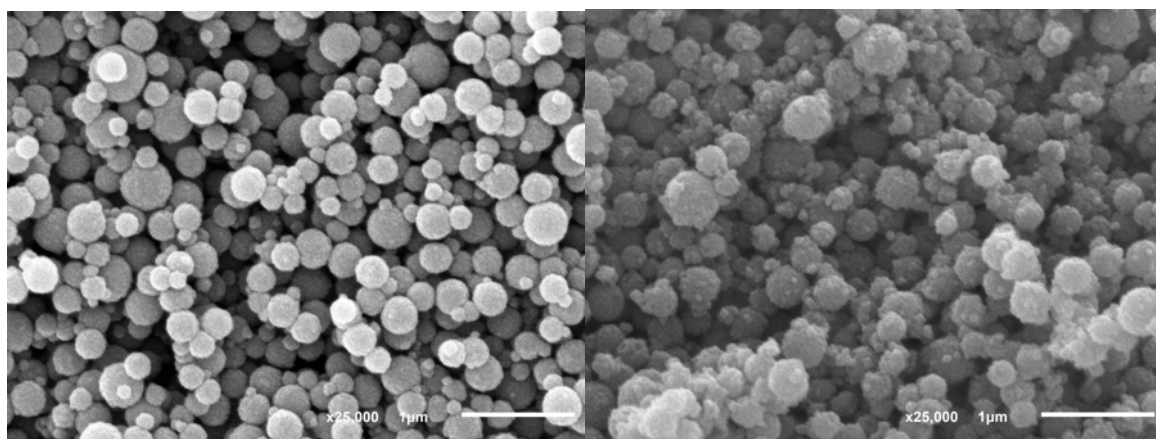
^d *Scientific Technical Services, University of Oviedo, 33006, Oviedo, Spain*

* Corresponding author. *E-mail address:* uo247495@uniovi.es; zapasoul@gmail.com (I. Krivtsov)



a

b



c

d

Figure S1 – SEM images of as-synthesized samples: TiMe800 (a), TiEt800 (b), TiPr800 (c), TiPrR800 (d).

RESULTS AND DISCUSSION

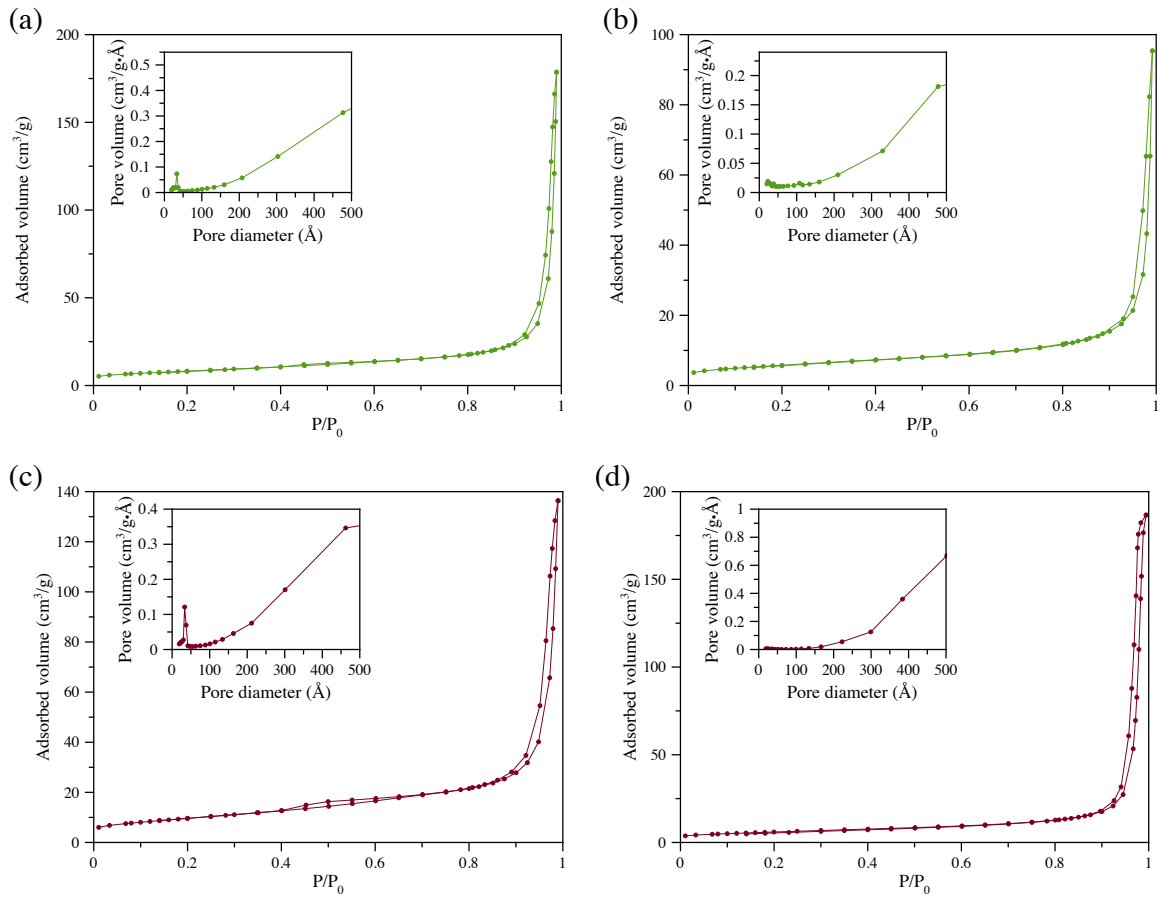


Figure S2 – N_2 adsorption-desorption isotherms and average pore size distribution: TiMe500 (a), TiMe800 (b), TiEt500 (c), TiEt800 (d).

RESULTS AND DISCUSSION

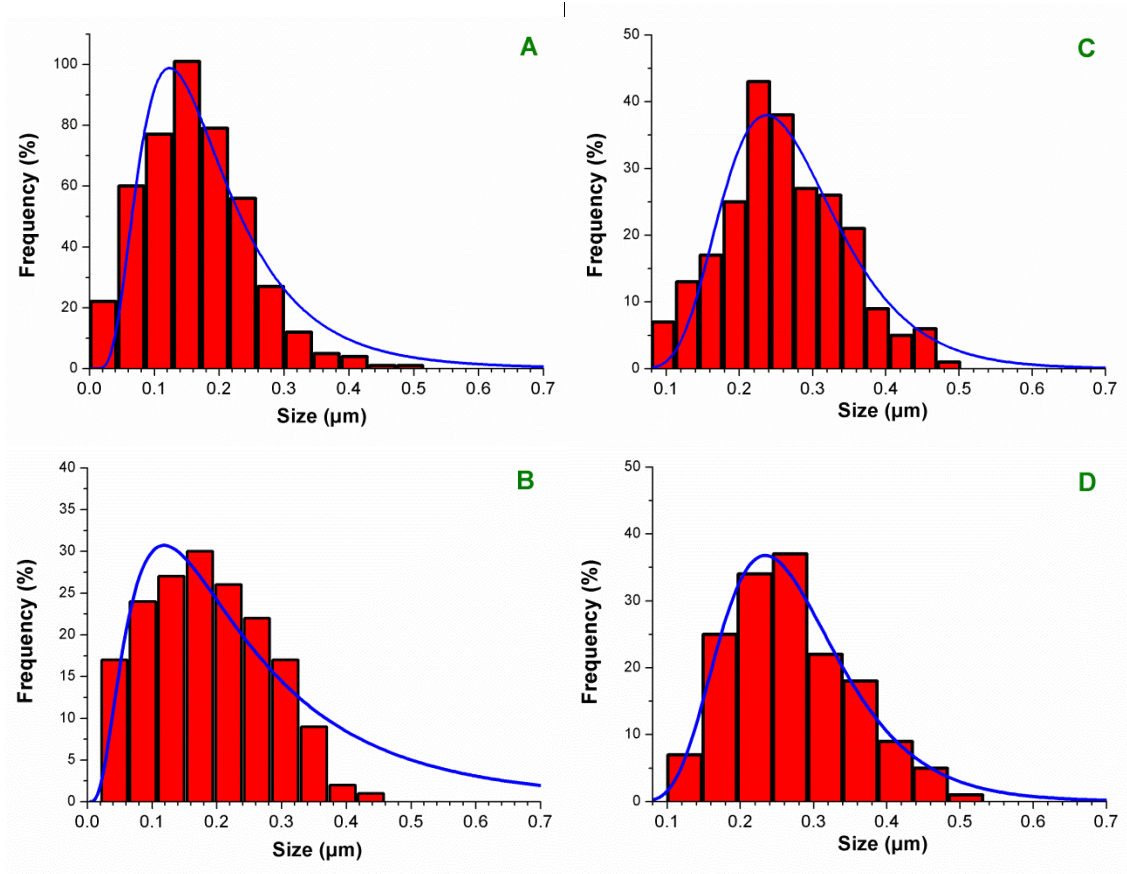


Figure S3 – Histograms of spherical particle size distribution for TiPr (a), TiPr800 (b), TiPrR (c) and TiPrR800 (d).

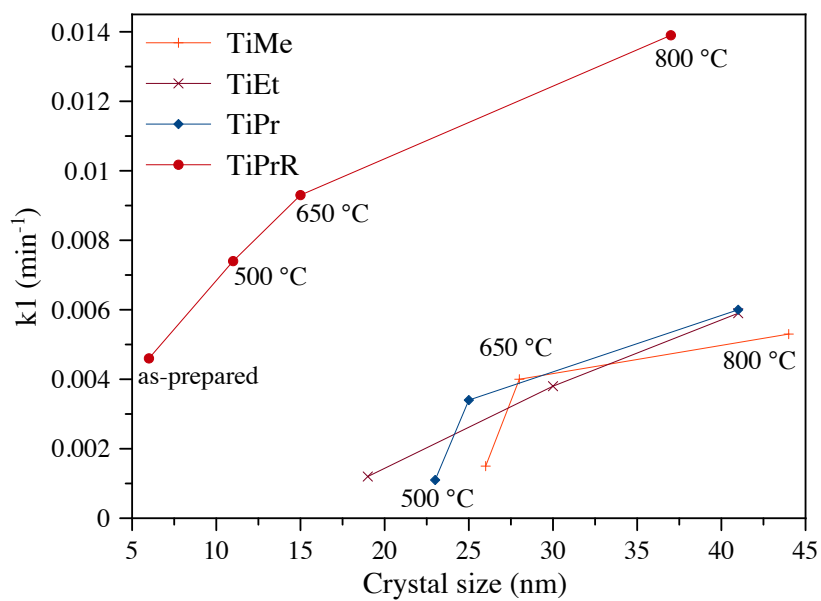
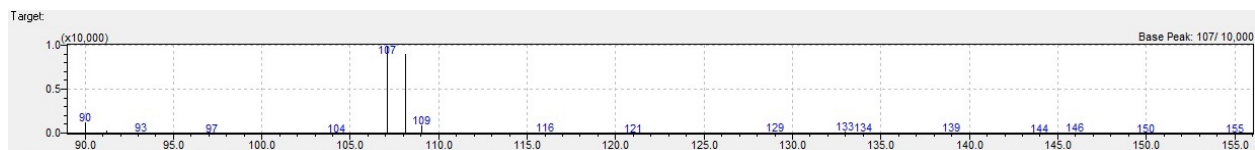
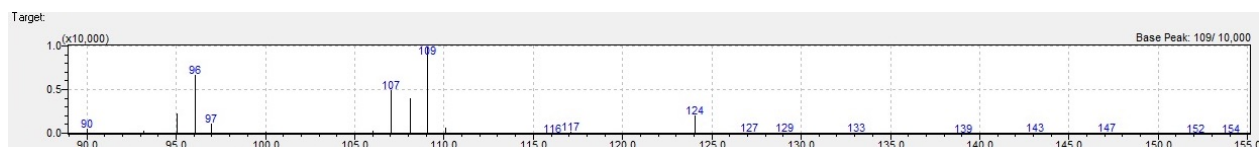


Figure S4 – Dependence of the photocatalytic activity and crystall size of the TiPrR and TiPr samples calcined at different temperatures.

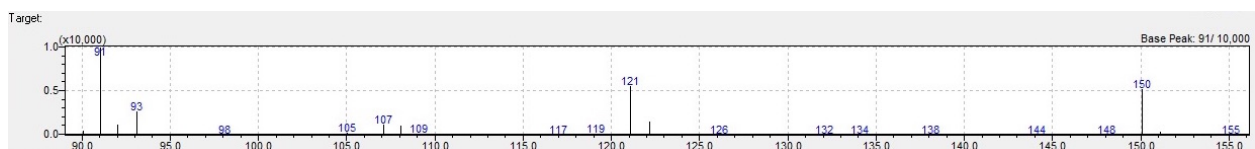
RESULTS AND DISCUSSION



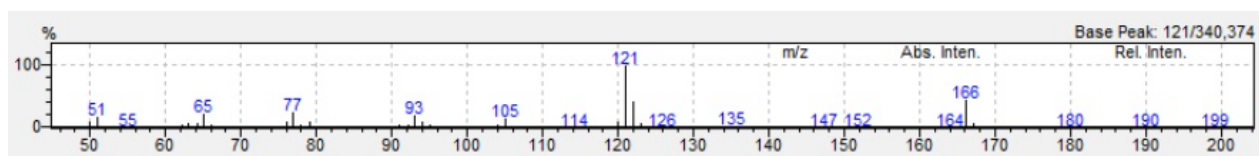
a



b



c



d

Figure S5 – Mass spectra for the proposed compounds detected during photocatalytic degradation of the MPET: p-cresol (a), 4-methylcatechol (b), p-methylphenyloxyacetaldehyde (c), and HEB (d).

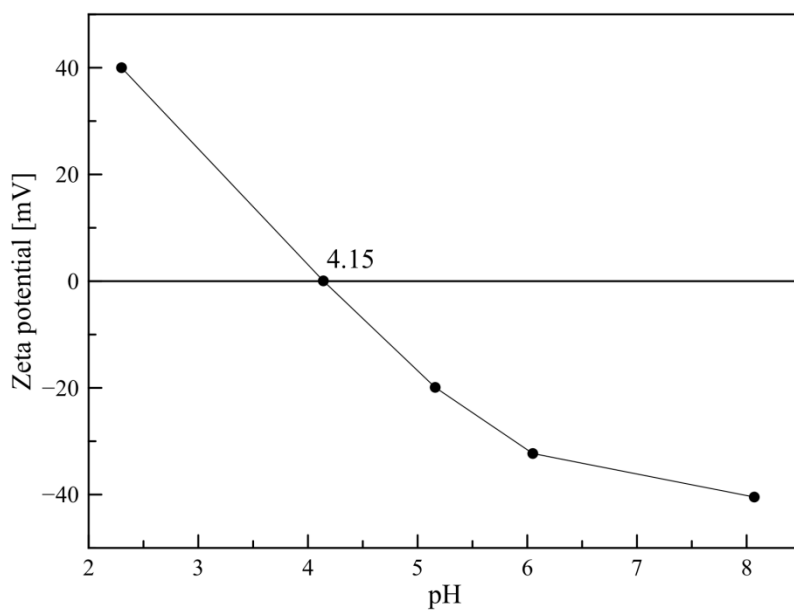


Figure S6 – Point of zero charge determination for TiPrR800.

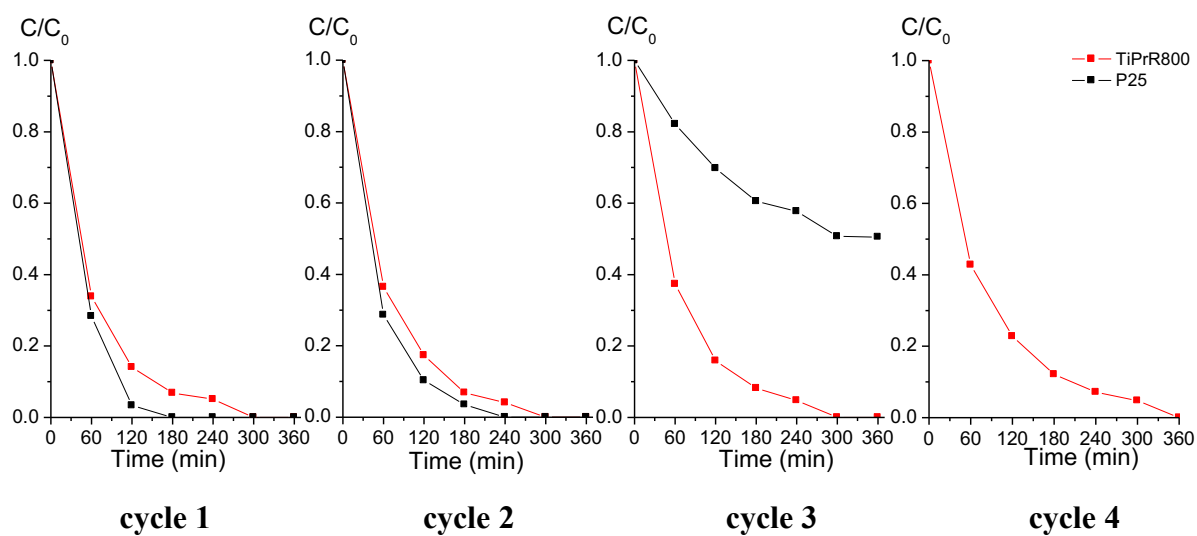


Figure S7 – Reutilization of TiPrR800 and Aeroxide P25 photocatalysts in MPET photodegradation.

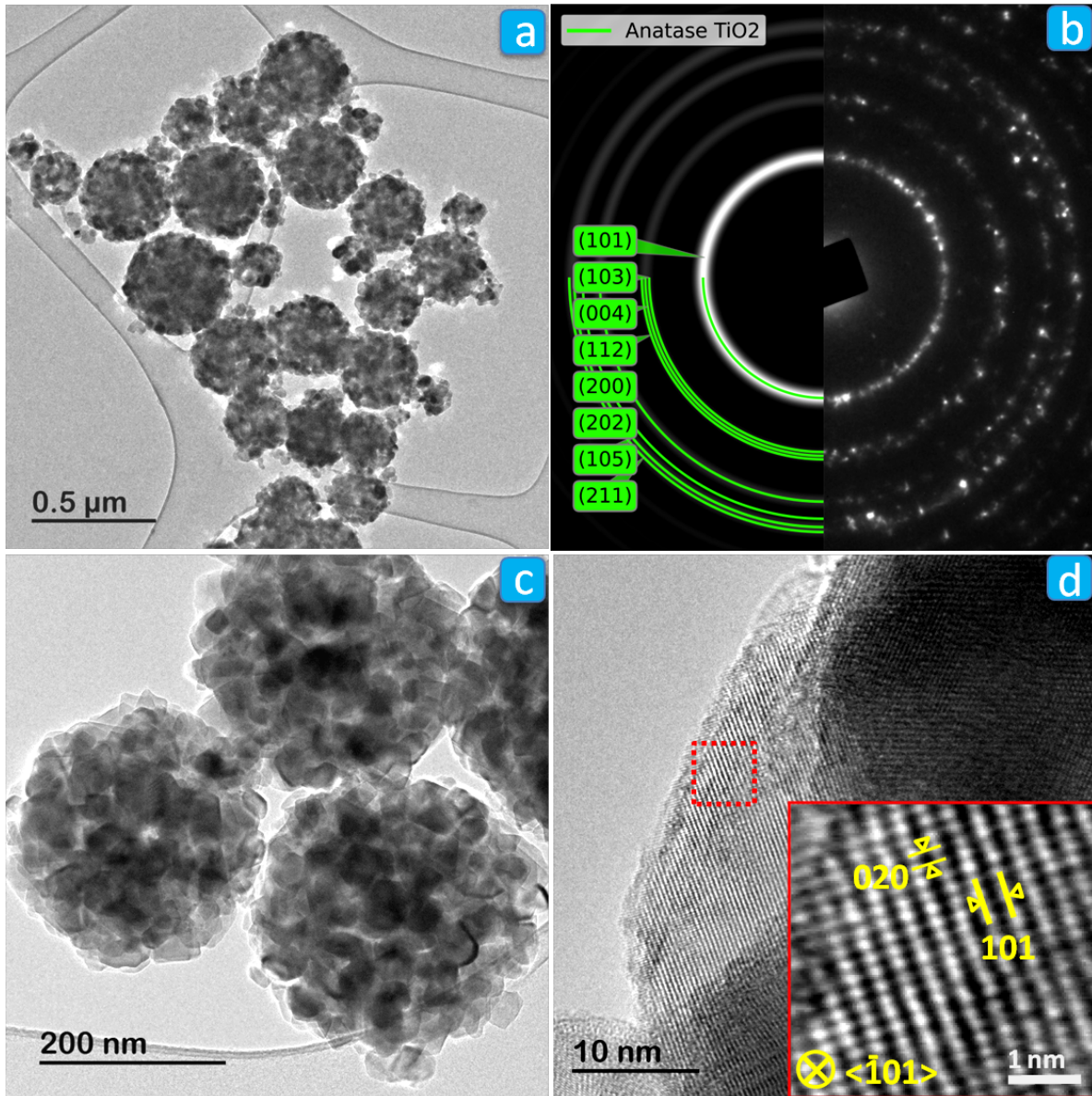


Figure S8 – TEM analysis of TiPrR800 sample after four consecutive photocatalytic runs: (a,c) TEM images, (b) SAED pattern (left: simulated; right: experimental), and (d) HRTEM image showing the anatase TiO_2 {101} facet.

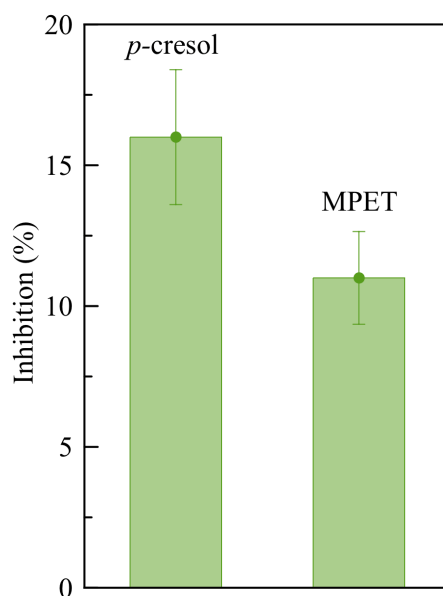


Figure S9 – % Inhibition of bioluminescence of *Vibrio fischeri* bacteria at *p*-cresol (1.5 mgL⁻¹) and MPET (20 mgL⁻¹).

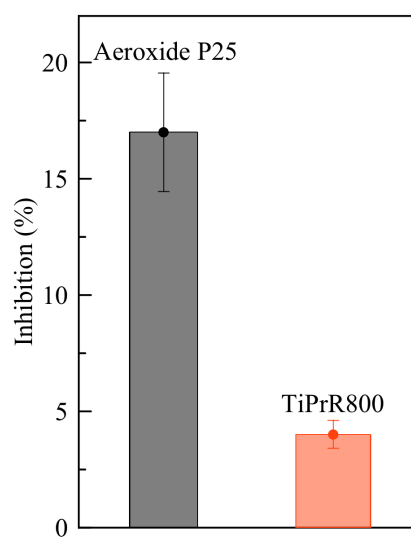


Figure S10 – % Inhibition of bioluminescence of *Vibrio fischeri* bacteria of the filtered suspensions of Aeroxide P25 and TiPrR800 after 8 h of irradiation.

RESULTS AND DISCUSSION

Table S1 – Mean size of the spherical particles obtained by Log-normal distribution function fit.

Sample	Mean size (μm)
TiPr	0.17(1)
TiPr800	0.21(3)
TiPrR	0.263(7)
TiPrR800	0.262(3)

Table S2 – Samples unit cell parameters (\AA).

		a				c			
sample	T ($^{\circ}\text{C}$)	as prepared	500	650	800	as prepared	500	650	800
	TiEt	-	3.7810	3.7773	3.7810	-	9.4809	9.4929	9.5075
TiPr	-	3.7796	3.7825	3.7796	-	9.5026	9.5123	9.5026	
TiMe	-	3.7818	3.7803	3.7818	-	9.4978	9.4978	9.5050	
TiPrR	3.7959	3.7759	3.7810	3.7803	9.4857	9.4905	9.5001	9.5026	

4.2 Modified Polymeric Carbon Nitride for Organic Molecules Selective Photo-Oxidation

In this chapter, the properties of pristine PCN and PCN-H₂O₂ and their ability to selectively photo-oxidise a variety of organic substrates are discussed. For a long period of time, significantly more attention had been paid to the investigation of the processes of photo-degradation of water contaminants than to the field of organic molecules partial photo-oxidation by semiconductor materials. An obvious advantage of the selective photo-conversion is the production of valuable compounds via the light-initiated reactions using mild oxidants. Photo-transformation of such substrates as benzyl alcohol, 4-methoxybenzyl alcohol, 2-(4-methylphenoxy)ethanol and biomass derived compound, 5-hydroxymethylfurfural, in the presence of semiconductors based on PCN to the corresponding aldehydes was studied. The results of this research is presented in the following publications. The applicability of the proposed synthetic methods for the PCN based materials production as well as their utilization in the photocatalytic conversion of organic molecules extend beyond the simple laboratory tests. The successful scaling-up of these approaches for the pilot-plant partial oxidation of aromatic alcohols at the Solar Pilot Plant makes PCN a promising candidate for the implementation of light-driven oxidation on the industrial level.

4.2.1 PCN-H₂O₂ adduct for C-H bond chemoselective photo-oxidation of alkylphenoxyethoxylates

As it was discussed in Introduction Chapter, carbon nitride possesses a valence band potential, which does not permit a direct water oxidation to •OH radicals [144], hence reducing the presence of notoriously unselective oxidative species in water suspension of photocatalysts with organic compounds. It is generally supposed that the main oxidative species in partial oxidation reactions under UV irradiation are •O₂⁻ radicals. All these observations make PCN a suitable material to be applied for selective conversion of organic molecules even in water medium.

RESULTS AND DISCUSSION

The selective oxidation of the methyl group substituent of aromatic compounds to the correspondent carbonyl and carboxyl functionalities is a process of an immense importance for the activation of raw materials in organic synthesis [155]. The presence of competitive easily oxidised substituents in a phenyl ring such as electron donating $-C-OH$, $C=O$, $-O-C$, or $-NH_2$ groups puts obstacles on the way to achieving the activation of a more inert $C-H$ bond. Many of the existing oxidation protocols are complicated and expensive, they often require the presence of toxic oxidants and/or organic solvents, also external heat must be supplied for the reaction to take place. Thus, they are energy consuming and not environmentally benign.

In the following work, the stated problem was solved by the utilisation of carbon nitride semiconductor, non-toxic and inexpensive material, which allowed to reach 57% of the selectivity in the reaction of $C-H$ bond oxidation of 2-(4-methylphenoxy)ethanol that resulted in the 4-(2-hydroxyethoxy)benzaldehyde (HEB) product formation under UV irradiation in water medium. It was found that the modification of PCN with H_2O_2 led to the enhanced selectivity to this product of 82-87%. It was proposed on the bases of the experimental evidence obtained by XRD, XPS, MAS NMR techniques and theoretical calculations that the reaction between PCN and H_2O_2 gave the $PCN-H_2O_2$ adduct, in which H_2O_2 was bonded to the non-condensed NH_2 -species. The steric hindrance for the direct interaction of carbon nitride amino-groups with the oxyethanol substituent of MPET promoted the selectivity towards the HEB formation.

Article II

“Carbon nitride assisted chemoselective C–H bond photo-oxidation of
alkylphenolethoxylates in water medium”

Green Chemistry

19 (4299–4304)

Year 2017

DOI: 10.1039/c7gc01588g rsc.li/greenchem

Impact Index: 9.125

Carbon nitride assisted chemoselective C–H bond photo-oxidation of alkylphenoxyethoxylates in water medium

M. Ilkaeva,^a I. Krivtsov,^{*a,b} E. Bartashevich,^c S.A. Khainakov,^d J.R. García,^a E. Díaz,^e S. Ordóñez^e

^a *Departments of Organic and Inorganic Chemistry, Physical and Analytical Chemistry, University of Oviedo-CINN, 33006 Oviedo, Spain.*

E-mail: UO247495@uniovi.es, Tel.: +34 985 103 030.

^b *Nanotechnology Education and Research Center, South Ural State University, 454080 Chelyabinsk, Russia.*

^c *Department of Theoretical and Applied Chemistry, South Ural State University, 454080 Chelyabinsk, Russia.*

^d *SCTs Facilities, University of Oviedo, 33006 Oviedo, Spain.*

^e *Department of Chemical and Environmental Engineering, University of Oviedo, 33006 Oviedo, Spain.*

†Electronic Supplementary Information (ESI) available. See DOI: 10.1039/x0xx00000x

The unprecedented ability of g-C₃N₄ to chemoselectively photo-oxidise the methyl group of 2-(4-methylphenoxy)ethanol instead of the easily oxidised oxyethanol fragment has been demonstrated. When g-C₃N₄ is treated by H₂O₂, its selectivity enhances due to the blocking of surface sites responsible for the adsorption and subsequent oxidation of oxyethanol substituent.

Selective oxidation of methyl group substituent of aromatic compounds to the corresponding carbonyl and carboxyl functionalities is a process of an immense importance for activation of raw materials in organic synthesis [1]. C–H bond oxidation of alkyl side-chains in aromatic hydrocarbons is well-developed, and many catalytic approaches are successfully applied for this purpose [2]. The presence of competitive easily oxidised substituents in a benzyl ring such as electron-donating –C–OH, –C=O, –O–C, or –NH₂ groups complicates achieving activation of a more inert C–H bond. Thus, a variety of

RESULTS AND DISCUSSION

methods utilizing homogeneous oxidation [3], photoactive complexes [4], metal oxide-supported noble metal nanoparticles [5], enzymes [6] and electrochemical oxidation in ionic liquids [7] is developed to overcome this obstacle. Many of the existing oxidation protocols are complicated and expensive, they often demand the presence of toxic oxidants and/or organic solvents, and external heat must be supplied for the reaction to take place. Hence, they are energy consuming and not environmentally benign.

Use of molecular oxygen as a green oxidant and UV or visible-light irradiation as an energy source for partial oxidation of organic molecules along with application of inexpensive, non-toxic, easily recoverable and zero-waste semiconductor photocatalysts such as TiO₂ or g-C₃N₄ have recently attracted attention [8]. So far the published data on photo-conversion of organic molecules in the presence of semiconductor photocatalysts are limited to the oxidation of the hydroxyl group of aromatic and aliphatic alcohols to the carbonyl group [9], sulfides to sulfoxides [10], and by the oxidation of benzene or the alkyl group of hydrocarbon compounds [11]. Although Verma et al. reported that carbon nitride promoted photo-oxidation of C–H groups of substituted toluenes, they stated that g-C₃N₄ was not active in the absence of vanadium oxide and H₂O₂ [11a].

The diversification of benign and energy-saving oxidation process such as photocatalysis is of utmost importance in order to deal with new challenges. Here, we report the unprecedented chemoselective g-C₃N₄-promoted photo-oxidation of the methyl group of an amphiphilic molecule 2-(4-methylphenoxy)ethanol (MPET) leading to the formation of 4-(2-hydroxyethoxy)benzaldehyde (HEB) using atmospheric O₂ as an oxidant. MPET has been chosen as a model compound because it allows modelling and assessing its interaction with the photocatalyst surface, having the functional groups of different polarity. Moreover, HEB, the product of this oxidation reaction, finds its application in pharmaceutical production [12], but is most commonly used as a building block in polymer synthesis for drug delivery [13]. This chemical is normally produced by synthesis in organic solvents with the use of external heat and halogenated compounds [14], hence the development of greener and more economic methods of its production is of interest.

RESULTS AND DISCUSSION

Comparison of the performance of the two most widespread photocatalysts in MPET photo-oxidation reveals staggering difference in their reaction pathways (Fig. 1). *p*-Cresol and HEB are found to be the principal partially oxidised MPET products, if commercial titania Aeroxide P25 is used as a photocatalyst [15]. However, the selectivity for both compounds is below 10% (Fig. 1, Table 1), which is obviously of interest for environmental purposes [15], but not for chemical synthesis. Graphitic carbon nitride prepared by direct condensation of melamine at 520 °C (MCN), on the other hand, favours producing relatively large quantities of HEB, achieving the selectivity to this product up to 50% (Fig. 1, Table 2). High selectivity observed for the carbon nitride photocatalyst can be explained either by the action of the reactive species generated during the irradiation and different to those produced by TiO₂, or by the specific interaction of the substrate and photocatalyst surfaces. This question will be addressed later in the communication.

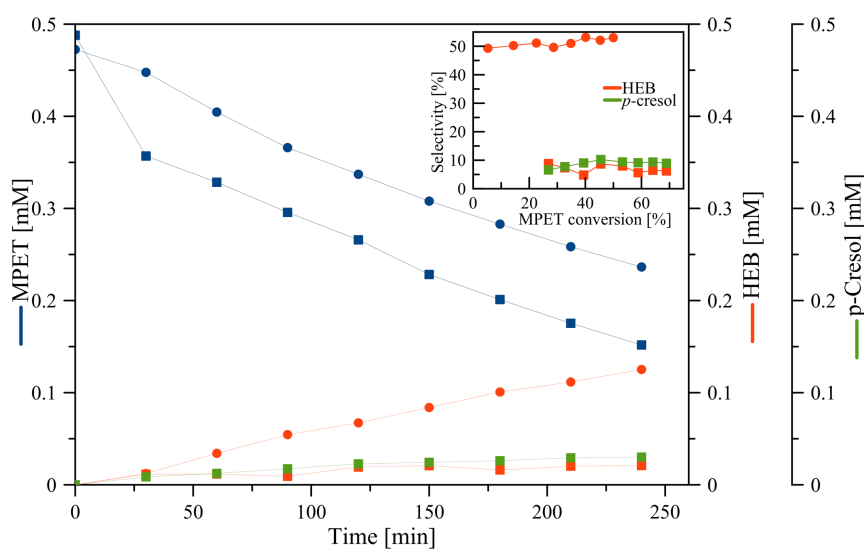
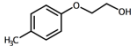
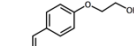
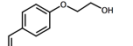
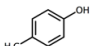
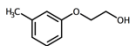
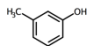
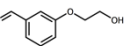
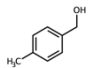
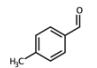
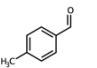
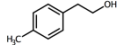
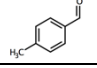
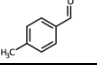
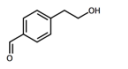
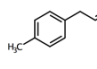
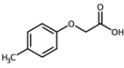
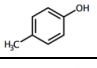
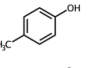
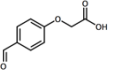
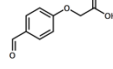


Figure 1 – Photooxidation of MPET in the presence of (•) MCN and (■) P25.

RESULTS AND DISCUSSION

Table 1 – Substrates and the products of photo-oxidation reactions in the presence of TiO₂ and g-C₃N₄ photocatalysts

substrate	oxidation products of P25 promoted reactions	oxidation products of TE and TE_O promoted reactions
	 Selectivity 8 %	 Selectivity 57 % (TE) Selectivity 82 % (TE_O)
	 Selectivity 10 %	
		 Selectivity 39 % (TE) Selectivity 38 % (TE_O)
		
		 
		
		 
		

RESULTS AND DISCUSSION

Table 2 – MPET apparent reaction rate constant (k), conversion degree, HEB selectivity at 30% of MPET conversion.

sample	k [min ⁻¹]	MPET conversion after 4 h of the reaction [%]	HEB selectivity at 30 % of MPET conversion [%]
P25	0.0050	68	8
MCN	0.0029	50	50
TE	0.0060	75	57
TE_O	0.0052	72	82

With the purpose of improving the reaction rate and selectivity toward HEB formation we applied several earlier reported treatment procedures. Among them there were thermal exfoliation (TE) [16], hydrothermal treatment with NaOH [17], g-C₃N₄ protonation with HCl [18], alkaline metal doping [19], and H₂O₂ treatment of the pristine g-C₃N₄ (MCN_O) similar to that reported by Li et al. [20], although carried out under milder conditions (for details, see Supplementary Material). Some of the g-C₃N₄ modification methods result in the improved reaction rate, and TE sample shows a slight increase of the selectivity, which is due to the partial elimination of uncondensed species [16b], though a significant enhancement of the HEB production is only observed for MCN_O sample (Fig. S1, Fig. S2), reaching the selectivity value of 87% (Fig. S1).

Obviously, the as-prepared carbon nitride and the one treated by H₂O₂ are not active enough due to their low specific surface areas (SSA) (Table 3). Thus, g-C₃N₄ thermal exfoliation at 500 °C (TE) and the subsequent H₂O₂ treatment (TE_O) have been implemented, in order to obtain a more efficient photocatalyst. The apparent reaction rate constant of MPET conversion, showed by TE sample, is slightly reduced after the H₂O₂ treatment (Fig. 2(A), Table 2), while the formation of HEB is noticeably increased (Fig. 2(B)). Although the selectivity toward HEB shows some decrease at high conversion values, it is in the range of 72-83% during the whole time of the reaction (Fig. 2(C,D)).

RESULTS AND DISCUSSION

Table 3 – SSA, BG and XPS data for MCN, TE, TE_O data.

sample	SSA [m ² ·g ⁻¹]	BG [eV]	XPS data		
			N2/N1 ratio	elemental composition	
				C/N	O [at%]
MCN	8	2.73	0.21	0.70	3.3
TE	154	2.80	0.20	0.71	3.7
TE_O	68	2.63/2.15	0.18	0.71	6.3

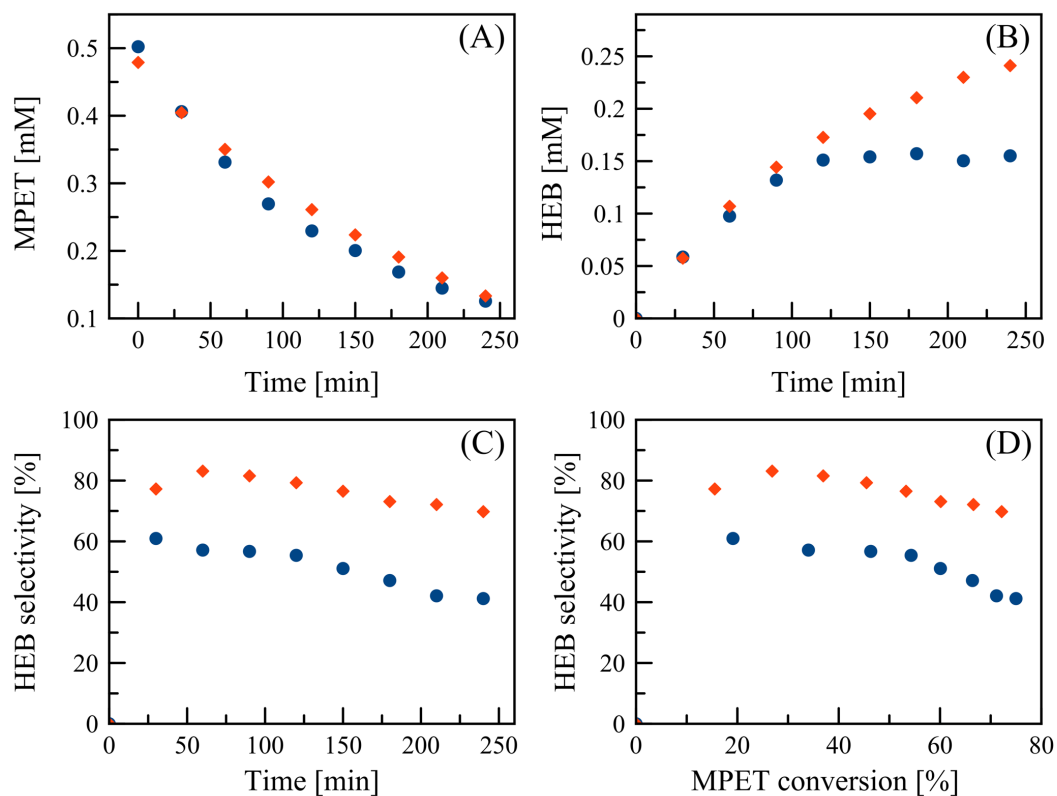


Figure 2 – MPET photo-oxidation in the presence of (●) TE and (◆) TE_O. (A) MPET conversion, (B) HEB production, (C) HEB selectivity, (D) MPET conversion vs HEB selectivity.

RESULTS AND DISCUSSION

According to EPR studies reported by Long et al. [21], the principal reactive species responsible for photo-oxidation of organic molecules by g-C₃N₄ is a superoxide radical. In this particular case of MPET to HEB photo-oxidation it is confirmed by the application of a set of scavengers for •O₂⁻, •OH, photo-generated holes and electrons (Fig. S4). The reaction carried out under N₂ reveals that 14% of MPET is decomposed and no HEB is formed (Fig. S4), which might be a consequence of the direct photo-generated hole oxidation of the substrate and could be the reason for less than 100% selectivity.

The possibility that the active surface species formed in the result of the H₂O₂ interaction with carbon nitride might be consumed promoting the MPET to HEB oxidation is verified by the utilization of the TE_O photocatalyst in four consecutive cycles (Fig. S5). A slight decrease of the conversion is observed during the photocatalyst reuse, although the selectivity does not suffer any significant changes, demonstrating that there are no H₂O₂ or other reactive species able to oxidise the substrate consumed during the oxidation, and the nature of the reaction is indeed photocatalytic. Unfortunately, up to now, the attempts to avoid the conversion loss in the reaction cycles have not been successful.

For better understanding of the chemoselectivity of this reaction the analysis of TE and TE_O-assisted photo-oxidation products of several other substrate molecules such as 3-(2-methylphenoxy)ethanol, 4-methylbenzyl alcohol, 2-(4-methylphenyl)ethanol, and (4-methylphenoxy)acetic acid has been carried out (Table 1). The position of a methyl group in respect to the competitive oxyethanol fragment has a great effect on the conversion degree and selectivity towards the product of its oxidation. Expectedly, in a view of the results reported by Yurdakal et al. for the case of aromatic alcohols photocatalytic oxidation [22], the conversion rate, as well as selectivity, is reduced for the case of 3-(2-methylphenoxy)ethanol photo-oxidation to 3-(2-hydroxyethoxy)benzaldehyde. TE and TE_O demonstrate nearly equal conversion and selectivity values, which are of 46 % and 39% for TE, and 42 % and 38 % for TE_O, respectively (Fig. S10). The use of P25 photocatalyst, on the other hand, inevitably leads to formation of m-cresol (Fig. S6). Expectedly, g-C₃N₄ preferably oxidise benzylic OH rather than C–H bond of the methyl group of 4-methylbenzyl alcohol (Fig. S7). The presence in 2-(4-methylphenyl)ethanol of the longer ethanol substituent bearing OH-group on an alkyl carbon atom results in that its photo-conversion produces two products 4-

RESULTS AND DISCUSSION

methylbenzaldehyde and 4-(2-hydroxyethyl)benzaldehyde, which are formed by oxidation of the benzylic carbon of the ethanol fragment and the C–H bond of the methyl group, while no alcohol functionality oxidation is observed (Fig. S8). Contrary to that, in the presence of titania P25 Aeroxide the oxidation of OH group occurs forming (4-methylphenyl)acetaldehyde (Table 1, Fig. S9). Despite in cases of 2-(4-methylphenyl)ethanol and MPET photo-conversion, C–H bond oxidation takes place, the presence of oxyethanol fragment favours better selectivity for the methyl group oxidation. Nonetheless, the presence of oxyethanol substituent in the substrate molecule does not guarantee the selectivity of the methyl group oxidation. Photocatalytic conversion of (4-methylphenoxy)acetic acid shows low selectivity for methyl group oxidation and demonstrates completely different reaction mechanism producing p-cresol and several other unidentified intermediates (Fig. S10). Thus, photo-oxidation of benzylic C–H bond and methyl group occurs also for other class of organic compounds, however the tailoring of selectivity for certain products demands other means of photocatalyst modification.

Since the reactive species responsible for the MPET photo-oxidation to HEB are the same for the TE and TE_O samples, it is likely that the interaction of the g-C₃N₄ surface with MPET governs the selectivity to methyl group oxidation, and the enhancement of the selectivity toward HEB production observed for the carbon nitride treated with H₂O₂ might be related to the modification of the carbon nitride surface sites. To explore this hypothesis, we have undertaken a detailed study of how the hydrogen peroxide modification influences carbon nitride properties. Contrary to other investigation describing g-C₃N₄ hydrothermal modification with H₂O₂ [20], where the exfoliation and the reduction of crystallinity of carbon nitride were observed, the mild conditions of the treatment applied in this work do not lead to the same result. Surprisingly, the PXRD pattern of TE_O shows the intensity increase of the diffraction maxima characteristic of (002) crystallographic plane of g-C₃N₄ phase and its shift from 27.5 to 27.8 degrees indicating the reduction of interplanar distance in g-C₃N₄ (Fig. 3(A)). Higher crystallinity and smaller interplanar distance found for TE_O is also the cause of the reduced SSA value compared to the thermally exfoliated carbon nitride TE (Table 3, Fig. 3(A)). In accordance with it, the XPS data reveal the lower ratio of N-(C)₃ (N₂) to C=N-C (N₁) species reflecting the increased condensation degree of the TE_O sample

RESULTS AND DISCUSSION

with respect to TE (Table 3, Fig. S11). Expectedly, the changes of the bulk carbon nitride properties after modification by H_2O_2 affect the electronic structure and photo-generated charge separation of TE_O. Thus, the absorption edge of TE_O in respect to that of TE is found shifted to the visible-light range (Fig. S12) and the corresponding band-gap (BG) values are estimated to be 2.63 eV with the mid-gap of 2.15 eV for TE_O and 2.80 eV for TE (Table 3, Fig. S12). The treatment by H_2O_2 suppresses the photoluminescence (PL) of TE_O (Fig. S13), thus explaining that high photocatalytic activity maintained by H_2O_2 -treated carbon nitride is due to better charge separation, despite the drastic reduction of SSA.

Apart from the fact that the bulk properties of the material are changed, the treatment also leads to the noticeable modification of the carbon nitride surface. From the XPS surface composition analysis it is seen that the C/N ratio of 0.67 remains unchanged after the treatment, but the oxygen content rises from 3.7 at% for TE to 6.3 at% in case of TE_O (Table 3). Moreover, the O 1s peak in the spectrum of TE_O shows the shift of the maximum from 532.2 eV, found for TE, to 531.8 eV, indicating the existence of different oxygen species to those presented in TE (Fig. 3(B)). Recently the melamine- H_2O_2 (MHP) complex was crystallized and its structure was elucidated by Chernyshov et al. [23], it was also described by Chehardoli et al. and applied for a controllable homogeneous oxidation [24]. In the present case the formed compound is insoluble and does not release H_2O_2 while in water or acetonitrile media. ^1H MAS NMR evidences the presence of ^1H (0.55 ppm) most probably belonging to unbridged OH groups [23] at the surface of the TE sample, considering that the presence of hydrogenated carbon in g- C_3N_4 is unlike [24] (Fig. 3(C)). This peak is absent on the spectrum of the TE_O sample, which might be a result of some adsorbed species removal because of SSA reduction or to the surface modification by H_2O_2 . The maximum at 4.06 ppm apart from NH_2 groups might be attributed to the adsorbed H_2O , while 8.90 ppm clearly indicates the presence of NH and NH_2 functionalities. The significant shift of both maxima for TE_O to 4.53 and 9.24 ppm arises from the interaction of the carbon nitride surface species, in particular amino-groups, with hydrogen peroxide (Fig. 3(C)). A characteristic ^1H peak of H_2O_2 cannot be clearly distinguished because of its possible overlapping with ^1H of the amino-groups. A characteristic ^1H peak of H_2O_2 cannot be clearly distinguished because of its possible overlapping with ^1H of the amino-groups. The presence of the tri-s-triazine

RESULTS AND DISCUSSION

breathing mode at $850\text{-}800\text{ cm}^{-1}$ indicates that the thermally exfoliated carbon nitride retains the $g\text{-C}_3\text{N}_4$ block structure after being treated by hydrogen peroxide (Fig. S14). The FTIR spectrum of TE_O presents a number of peak displacements at $1200\text{-}1600$ and $900\text{-}800\text{ cm}^{-1}$ corresponding to the changes of interaction between tri-s-triazine units due to the enhanced crystallinity of the sample (Fig. S14). It draws attention to the reduction of the relative intensity of the N–H bond stretching vibration characteristics of primary amines in the range of $3000\text{-}3200\text{ cm}^{-1}$ for TE_O with respect to the TE FTIR spectrum (Fig. 3(D)), which probably is the consequence of the surface $\text{NH}_2\text{-H}_2\text{O}_2$ complex formation. Thermogravimetric analysis shows the increased mass loss in the low-temperature region for the TE_O sample, thus confirming the presence of some surface species not presented in the pristine and thermally exfoliated $g\text{-C}_3\text{N}_4$ (Fig. S15).

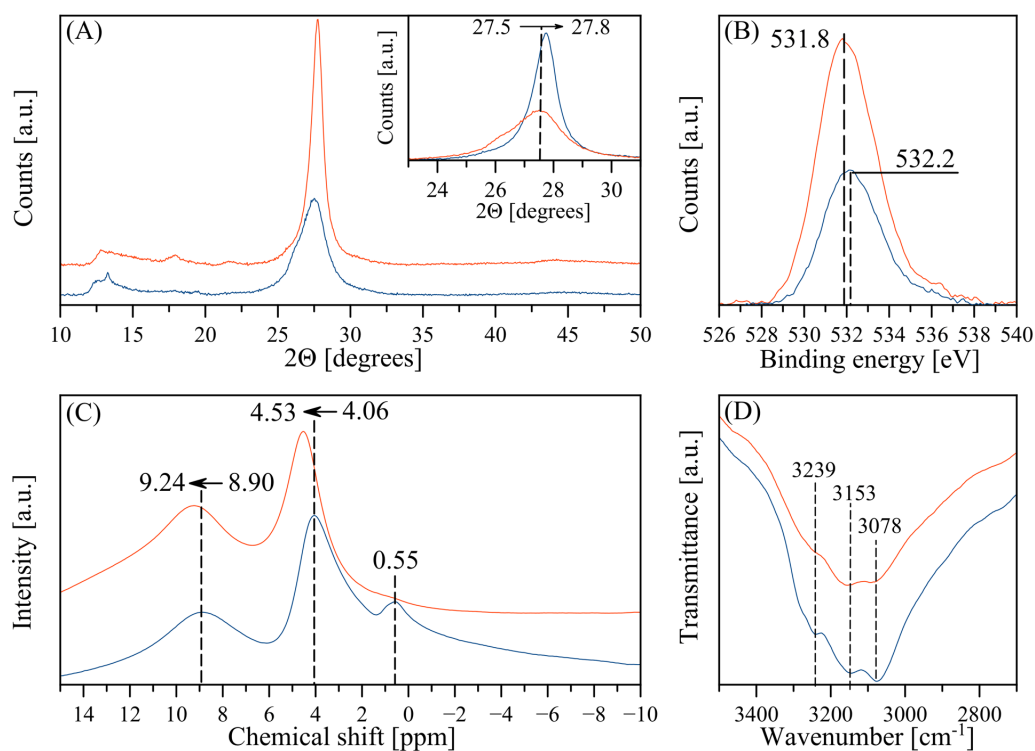


Figure 3 – (A) PXRD patterns, (B) XPS O 1s, (C) ^1H MAS NMR, and (D) FTIR, spectra of (blue) TE and (red) TE_O samples.

The computational study is indispensable for understanding of the substrate-photocatalyst interactions. It has helped us to confirm the affinity of oxyethanol substituent of MPET to the

surface amino-groups and the blockage of these surface sites by one H_2O_2 molecule. For modelling the features of the carbon nitride interactions with MPET and H_2O_2 molecules, the simple dimelem fragment representing the terminal surface groups of carbon nitride is chosen. The model structure of the dimelem molecule perfectly shows the presence of the 2D cavity with lateral size $\sim 6 \text{ \AA}$ between the neighboring nitrogen atoms. Molecular electrostatic potential (MEP) mapped on the iso-surface of the electron density (ED) illustrates pronounced complementarity of nucleophilic and electrophilic fragments in the dimelem cavity and MPET molecule (Fig. S16). The formation of dimelem complexes with polar functional groups of aromatic molecules was earlier suggested by Tan et al [25]. Our calculations demonstrate that MPET forms a stable complex with the dimelem via the relatively strong hydrogen bonds between the polar oxyethanol substituent and $\text{Nsp}^2\text{-Csp}^2\text{-Nsp}^3\text{-H}$ site (Fig. 4, TableS1). Coordination of MPET in this way would result in its oxidation by the formed radical species or directly via photogenerated hole oxidation, thus hindering the formation of the desired product HEB.

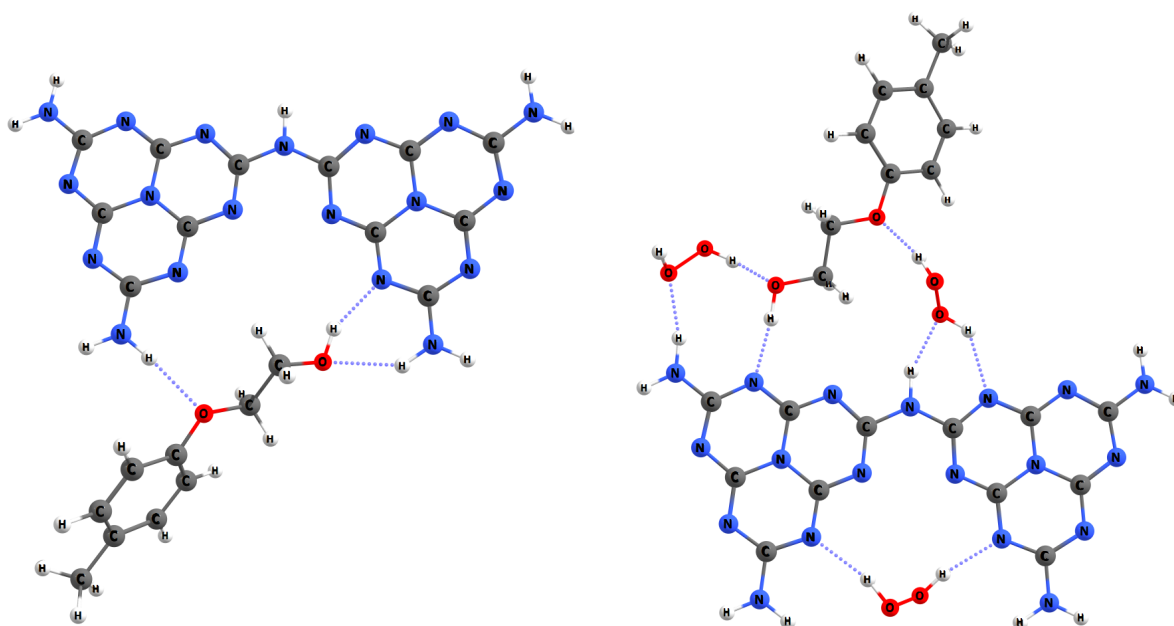


Figure 4 – The model structures of: Left: «dimelem – MPET» complex. Right: «dimelem – H_2O_2 – MPET» complex.

RESULTS AND DISCUSSION

One molecule of H_2O_2 can be attached to the 2D cavity and several molecules of H_2O_2 are able to form hydrogen bonds with the dimelem nitrogen atoms and amino-groups (Fig. 4). The strength of MPET holding by the direct contacts with the dimelem molecule decreases in this case (Table S1). Thus, the modification of carbon nitride by hydrogen peroxide influences the interactions between dimelem and MPET. Hence, the polar part of MPET becomes protected from the radical attack or direct hole oxidation.

Even the as-prepared $\text{g-C}_3\text{N}_4$ has high selectivity to C–H bond oxidation, thus indicating the preferable interaction of oxidant species generated by carbon nitride with the methyl group of MPET. The set of the applied methods has proved the coordination of H_2O_2 on the carbon nitride surface species. The $\text{g-C}_3\text{N}_4\text{-H}_2\text{O}_2$ complex formation creates a steric hindrance for the direct interaction between the polar group of MPET and the amino-groups of carbon nitride. This makes possible suppressing the oxidation of the oxyethanol substituent and enhancing the selectivity of MPET to HEB photo-oxidation even more.

Amphiphilic character of the studied molecule, used in the present study, leads to the favourable oxidation of its methyl group by $\text{g-C}_3\text{N}_4$ -generated $\bullet\text{O}_2^-$ radicals, thus high values of MPET to HEB selectivity reaching 82% are achieved. The presence of amino-groups on the photocatalyst surface is detrimental to the selectivity to HEB formation, as these species tend to coordinate MPET molecule via hydrogen bonding with its polar group and to oxidise it by h^+ or radical species.

The demonstrated extraordinary ability of $\text{g-C}_3\text{N}_4$ to selectively oxidise the alkyl group of alkylphenoxyolate and alkyl alcohol molecule in water medium, using O_2 as an oxidant, opens new applications for this unique photocatalyst in the field of organic synthesis. However, in order to get a more profound understanding of the reaction mechanism, it is necessary to test a wider selection of substrates. Moreover, the present study clearly demonstrates that the control of the hydrogen bonding between the functional groups on the photocatalyst surface and the substrate is of paramount importance for the partial photo-oxidation.

Acknowledgement

This work was financially supported by Spanish MINECO (MAT2013-40950-R, CTQ2014-52956-C3-1-R and MAT2016-78155-C2-1-R) and Gobierno del Principado de Asturias (GRUPIN14-060, GRUPIN14-078 and Severo Ochoa PhD grant BP-14-029 to MI), and FEDER. EB is grateful for the Ministry of Education and Science of the Russian Federation (grant 4.1157.2017/PP). IK thanks the Ministry of Education and Science of the Russian Federation (grant No 4.9722.2017/8.9).

Notes and references

1. Comprehensive Organic Transformations: A Guide to Functional Group Preparations, ed. R. C. Larock, Wiley-VCH, New York, **1999**.
2. (a) L. Kesevan, R. Tiruvalam, M.H. Ab Rahim, M.I. bin Saiman, D.I. Enache, R.L. Jenkins, N. Dimitratos, J.A. López-Sánchez, S.H. Taylor, D.W. Knight, C.K. Kiely and G.J. Hutchings, Solvent-Free Oxidation of Primary Carbon-Hydrogen Bonds in Toluene Using Au-Pd Alloy Nanoparticles, *Science*, **2011**, 331, 195–199; (b) W. Partenheimer, Methodology and scope of metal/bromide autoxidation of hydrocarbons, *Catal. Today*, **1995**, 23, 69–158; (c) R.L. Brutchey, I.J. Drake, A.T. Bell and T.D. Tilley, Liquid-phase oxidation of alkylaromatics by a H-atom transfer mechanism with a new heterogeneous CoSBA-15 catalyst, *Chem. Comm.*, **2005**, 29, 3736–3738; (d) Y. Wang, H. Li, J. Yao, X. Wang and M. Antonietti, Synthesis of boron doped polymeric carbon nitride solids and their use as metal-free catalysts for aliphatic C–H bond oxidation, *Chem. Sci.*, **2011**, 2, 446–450.
3. (a) M. Ghaffarzadeh, M. Bolourtchian, M. Gholamhosseni and F. Mohsenzadeh, Synthesis of arylaldehydes: Br₂/DMSO catalytic system for the chemoselective oxidation of methylarenes, *Appl. Catal., A*, **2007**, 333, 131–135; (b) N. Tada, K. Hattori, T. Nobuta, T. Miura and A. Itoh, Facile aerobic photooxidation of methyl group in the aromatic nucleus in the presence of an organocatalyst under VIS irradiation, *Green Chem.*, **2011**, 13, 1669–1671; (c) S-I. Hirashima and A. Itoh, Aerobic visible light-oxidation of aromatic methyl groups to carboxylic acids, *Photochem. Photobiol. Sci.*, **2007**, 6, 521–524.

4. G. Pandey, R. Laha and D. Singh, Benzylic C(sp³)-H functionalization for C-N and C-O bond formation via visible light photoredox catalysis, *J. Org. Chem.*, **2016**, 81, 7161–7171.
5. A. Tanaka, K. Hashimoto and H. Kominami, Preparation of Au/CeO₂ exhibiting strong surface plasmon resonance effective for selective or chemoselective oxidation of alcohols to aldehydes or ketones in aqueous suspensions under irradiation by green light, *J. Am. Chem. Soc.*, **2012**, 134, 14526–14533.
6. (a) E. Fritz-Langhals and B. Kunath, Synthesis of aromatic aldehydes by laccase-mediator assisted oxidation, *Tetrahedron Lett.*, **1998**, 39, 5955–5956; (b) A. Potthast, T. Rosenaq, C.-L. Chen and J.S. Gratzl, Selective enzymic oxidation of aromatic methyl groups to aldehydes, *J. Org. Chem.*, **1995**, 60, 4320–4321.
7. Y. Zhu, Y. Zhu, H. Zeng, Z. Chen, R.D. Little and C. Ma, A promising electro-oxidation of methyl-substituted aromatic compounds to aldehydes in aqueous imidazole ionic liquid solutions, *J. Electroanal. Chem.*, **2015**, 751, 105–110.
8. (a) Y. Wang, X. Wang and M. Antonietti, Polymeric graphitic carbon nitride as a heterogeneous organocatalyst: from photochemistry to multipurpose catalysis to sustainable chemistry, *Angew. Chem. Int. Ed.*, **2012**, 51, 68–89; (b) V. Augugliaro, M. Bellardita, V. Loddo, G. Palmisano, L. Palmisano and S. Yurdakal, Overview on oxidation mechanisms of organic compounds by TiO₂ in heterogeneous photocatalysis, *J. Photochem. Photobiol., C*, **2012**, 13, 224–245.
9. (a) S. Yurdakal, G. Palmisano, V. Loddo, V. Augugliaro and L. Palmisano, Nanostructured rutile TiO₂ for selective photocatalytic oxidation of aromatic alcohols to aldehydes in water, *J. Am. Chem. Soc.*, **2008**, 130, 1568–1569; (b) F. Su, S.C. Mathew, G. Lipner, X. Fu, M. Antonietti, S. Blechert and X. Wang, mpg-C₃N₄-Catalyzed selective oxidation of alcohols using O₂ and visible light, *J. Am. Chem. Soc.*, **2010**, 132, 16299–16301.
10. P. Zhang, Y. Wang, H. Li, and M. Antonietti, Metal-free oxidation of sulfides by carbon nitride with visible light illumination at room temperature, *Green Chem.*, **2012**, 14, 1904–1908.
11. (a) S. Verma, R.B.N. Baig, M.N. Nadagouda and R.S. Varma, Photocatalytic C-H activation of hydrocarbons over VO@g-C₃N₄, *ACS Sustainable Chem. Eng.*, **2016**, 4,

2333–2336; (b) Z. Ding, X. Chen, M. Antonietti and X. Wang, Synthesis of transition metal-modified carbon nitride polymers for selective hydrocarbon oxidation, *ChemSusChem*, **2011**, 4, 274–281; (c) P. Zhang, Y. Gong, H. Li, Z. Chen and Y. Wang, Selective oxidation of benzene to phenol by FeCl₃/mpg-C₃N₄ hybrids, *RSC Adv.*, **2013**, 3, 5121–5126.

12. W. Yi, R. Cao, W. Peng, H. Wen, Q. Yan, B. Zhou, L. Ma and H. Song, Synthesis and biological evaluation of novel 4-hydroxybenzaldehyde derivatives as tyrosinase inhibitors, *Eur. J. Med. Chem.*, **2010**, 45, 639–646;

13. (a) A.W. Jackson, C. Stakes and D.A. Fulton, The formation of core cross-linked star polymer and nanogel assemblies facilitated by the formation of dynamic covalent imine bonds, *Polym. Chem.*, **2011**, 2, 2500–2511; (b) Y-L. Zhao, Z. Li, S. Kabehie, Y.Y. Botros, J.F. Stoddart, and J.I. Zink, pH-Operated nanopistons on the surfaces of mesoporous silica nanoparticles, *J. Am. Chem. Soc.*, **2010**, 132, 13016–13025; (c) D. Xiong, N. Yao, H. Gu, J. Wang, and L. Zhang, Stimuli-responsive shell cross-linked micelles from amphiphilic four-arm star copolymers as potential nanocarriers for “pH/redox-triggered” anticancer drug release, *Polymer*, **2017**, 144, 161–172.

14. (a) US Patent 5408009; (b) A. Burkhardt, and H. Ritter, Organocatalytic formation of optically active polymers: enantioselective aldol reaction of aldehyde-containing copolymers in the presence of l-proline, *Polym. Int.*, **2015**, 64, 329–334.

15. M. Ilkaeva, I. Krivtsov, E. Díaz, Z. Amghouz, Y. Patiño, S. Khainakov, J.R. García, S. Ordóñez, Photocatalytic degradation of 2-(4-methylphenoxy)ethanol over TiO₂ spheres, *J. Hazard. Mater.*, **2017**, 332, 59–69.

16. (a) P. Niu, L. Zhang, G. Liu and H.M. Cheng, Graphene-Like carbon nitride Nnanosheets for improved photocatalytic activities, *Adv. Funct. Mater.*, **2012**, 22, 4763–4770; (b) I. Krivtsov, E. García-López, G. Marci, L. Plamisano, Z. Amghouz, J.R. García, E. Díaz, S. Ordóñez, Selective photocatalytic oxidation of 5-hydroxymethyl-2-furfural to 2,5-furandicarboxyaldehyde in aqueous suspension of g-C₃N₄, *Appl. Catal. B.*, **2017**, 204, 430–439.

17. T. Sano, S. Tsutsui, K. Koike, T. Hirakawa, Y. Teramoto, N. Negishi and K. Takeuchi, Activation of graphitic carbon nitride (g-C₃N₄) by alkaline hydrothermal

treatment for photocatalytic NO oxidation in gas phase, *J. Mater. Chem. A*, **2013**, 1, 6489–6496.

18. Y. Zhang, A. Thomas, M. Antonietti and X. Wang, Activation of carbon nitride solids by protonation: morphology changes, enhanced ionic conductivity, and photoconduction experiments, *J. Am. Chem. Soc.*, **2009**, 131, 50–51.

19. Y. Li, S. Ouyang, H. Xu, X. Wang, Y. Bi, Y. Zhang and J. Ye, Constructing solid–gas-interfacial fenton reaction over alkalized-C₃N₄ photocatalyst to achieve apparent quantum yield of 49% at 420 nm, *J. Am. Chem. Soc.*, **2016**, 138, 13289–13297.

20. J. Li, B. Shen, Z. Hong, B. Lin, B. Gao and Y. Chen, A facile approach to synthesize novel oxygen-doped g-C₃N₄ with superior visible-light photoreactivity, *Chem. Commun.*, **2012**, 48, 12017–12019.

21. B. Long, Z. Ding and X. Wang, Carbon nitride for the selective oxidation of aromatic alcohols in water under visible light, *ChemSusChem.*, **2013**, 6, 2074–2078.

22. S. Yurdakal and V. Augugliaro, Partial oxidation of aromatic alcohols via TiO₂ photocatalysis: the influence of substituent groups on the activity and selectivity, *RSC Adv.*, **2012**, 2, 8375–8380.

23. I. Yu. Chernyshov, M.V. Vener, P.V. Prihodchenko, A. G. Medvedev, O. Lev and A.V. Churakov, Peroxosolvates: formation criteria, H₂O₂ hydrogen bonding, and isomorphism with the corresponding hydrates, *Cryst. Growth Des.*, **2017**, 17, 214–220.

24. G. Chehardoli and M. A. Zolfigol, Melamine Hydrogen Peroxide (MHP): novel and efficient reagent for the chemo- and homoselective and transition metal–free oxidation of thiols and sulfides, *Phosphorus, Sulfur Silicon Relat. Elem.*, **2010**, 185, 193–203.

25. M.X. Tan, L. Gu, N. Li, J.Y. Ying, Y. Zhang, Mesoporous poly-melamine-formaldehyde (mPMF) – a highly efficient catalyst for chemoselective acetalization of aldehydes, *Green Chem.*, **2013**, 15, 1127–1132.

Supplementary Material

Carbon nitride assisted chemoselective C–H bond photo-oxidation of alkylphenoxyethoxylates in water medium

M. Ilkaeva,^{a,b} I. Krivtsov,^{*a,b} E. Bartashevich,^c S.A. Khainakov,^d J.R. García,^a E. Díaz,^e S. Ordóñez^e

^a *Departments of Organic and Inorganic Chemistry, Physical and Analytical Chemistry, University of Oviedo-CINN, 33006, Oviedo, Spain.*

^b *Nanotechnology Education and Research Center, South Ural State University, 454080, Chelyabinsk, Russia.*

^c *Department of Theoretical and Applied Chemistry, South Ural State University, 454080, Chelyabinsk, Russia.*

^d *SCTs Facilities, University of Oviedo, 33006 Oviedo, Spain.*

^e *Department of Chemical and Environmental Engineering, University of Oviedo, 33006 Oviedo, Spain.*

^{*} *Corresponding author, E-mail: UO247495@uniovi.es, Tel.: +34 985 103 030.*

1. Materials

Melamine, t-butyl alcohol, p-benzoquinone, p-cresol (all of 99 % purity), ethyl acetate (HPLC grade, 99.9 %), acetonitrile (HPLC grade, 99.9 %) and 30 wt % hydrogen peroxide were purchased from Aldrich. Hydrochloric acid 37-38 wt % water solution was obtained from J.T. Baker. Methanol, sodium hydroxide, potassium chloride were obtained from VWR Chemicals. For the photocatalytic test, 2-(4-methylphenoxy)ethanol (MPET), 4-(2-hydroxyethoxy)benzaldehyde (HEB) (both 98 %), 3-(2-methylphenoxy)ethanol (98 %), and 3-(2-hydroxyethoxy)benzaldehyde (95 %) were obtained from TCI Europe NV. 4-methylbenzyl alcohol, 2-(4-methylphenyl)ethanol, (4-methylphenoxy)acetic acid and 4-formylphenoxyacetic acid were purchased from Alfa Aesar.

2. Photocatalyst preparation

Bulk graphitic carbon nitride (g-C₃N₄) samples were prepared via the thermal condensation method from melamine following the procedure reported in [1]. 10 g of melamine was placed in a ceramic crucible covered with a lid and heated in a muffle furnace at 2 °C min⁻¹ up to 520 °C, then left for 2 h at the reached temperature and slowly cooled down. The g-C₃N₄ sample derived from melamine was labelled as MCN. The bulk carbon nitride prepared from melamine (MCN) was used as the precursor for the thermally exfoliated g-C₃N₄ [2]. For this purpose, 6 g of bulk carbon nitride was powdered in a mortar, evenly spread on the bottom of a ceramic bowl with a diameter of 14 cm, calcined in a static air atmosphere at 500 °C by using a temperature ramp of 2 °C min⁻¹ and maintained for 4 h. The thermally exfoliated carbon nitride was coded as TE. MCN and TE samples were treated with hydrogen peroxide on the following way. To 1 g of MCN or TE samples 20 mL of H₂O₂ (30%) was added, then the suspension was mildly heated (70 °C) while stirring until the complete evaporation of the liquid, and finally, the solid samples were thoroughly washed with deionized water and dried at 70 °C in an oven. The H₂O₂-treated samples MCN and TE were designated as MCN_O and TE_O, respectively.

Also, the carbon nitride samples were treated with NaOH, HCl and KCl using the procedures reported in refs. 3, 4, and 5, respectively; they were designated as MCN_Na, MCN_W and MCN_K, respectively. For MCN_Na preparation, 1 g of MCN was placed in an autoclave and treated at autogenous pressure for 24 h at 180 °C; for MCN_W synthesis, 1 g of MCN was placed in 37% solution of HCl and stirred for 4 h; MCN_K was prepared by the thermal condensation of 10 g of melamine in presence of 7.5 g of KCl and 0.28 g of KOH at 520 °C for 2 h. All the samples were washed with distilled water and dried at 70 °C for 24 h before using applying them in the reactions.

3. Photocatalyst characterization

Powder XRD patterns were recorded in an X'pert PANalytical diffractometer, using Ni-filtered Cu-K α radiation source. Specific surface areas (SSA) were calculated in accordance with the standard Brunauer-Emmet-Teller (BET) method from the nitrogen adsorption data using a Micromeritics ASAP 2020. Infrared spectra of the samples were recorded with 4 cm⁻¹

resolution using an ATR module of a Varian 620-IR spectrometer. Diffuse reflectance spectra (DRS) were obtained in air at room temperature in the 250–800 nm wavelengths range by means of a Shimadzu UV-2700 spectrophotometer, with BaSO₄ as the reference material. Mettler Toledo TGA/SDTA851 was used to investigate the thermal decomposition of g-C₃N₄ under an O₂ flow of 50 mL·min⁻¹ with the heating rate 10 °C min⁻¹ in the temperature range 25–1000 °C. The binding energies of C, N and O and the surface elemental composition in the TE and TE_O samples were measured by X-ray photoelectron spectroscopy (XPS) by using a SPECS system equipped with a Hemispherical Phoibos analyzer operating in a constant pass energy, using MgK α radiation ($h\nu = 1253.6$ eV). The solid state ¹H MAS NMR spectra were registered at spinning rate of 12 kHz using a Bruker Avance III 400WB spectrometer.

4. Photocatalysis procedure

The irradiation experiments were carried out in a Pyrex cylindrical photoreactor (internal diameter: 32 mm, height: 188 mm) containing 150 mL of aqueous suspension, irradiated by six external Actinic BL TL MINI 15 W/10 Philips fluorescent lamps emitting in the 340–420 wavelength range with the main emission peak at 365 nm. The reaction was carried out at about 25 °C and the reactor was provided by a thimble where water was allowed to circulate. Selected experiments were carried out in absence of O₂ by continuously bubbling N₂ throughout the runs to estimate the influence of O₂ on the reaction. The initial MPET concentration was 0.5 mM at the natural pH. The amount of a solid photocatalyst used for the experiments was 40 mg (80 mg for the recyclability study), except for the pristine carbon nitride MCN and MCN_O, for which 75 mg was used, due to their poorer light absorbance compared to the other samples. In this way, all the entering photons were virtually absorbed by the suspension. Some experiments were performed by reusing one of the best materials (TE_O) in order to verify its performance in a series of the consecutive reaction runs. Selected scavengers were used, in order to establish the reactive species responsible for MPET conversion and the selectivity to HEB. Methanol (MeOH) was used as a hole scavenger, t-butyl alcohol (t-BuOH) as an •OH radical scavenger and p-benzoquinone to scavenge •O₂⁻ radicals. The concentration of methanol, p-benzoquinone and tert-butyl alcohol scavengers was 2 mM. Samples of the irradiated solution were withdrawn at fixed time

intervals. Then, the solution was filtered from the photocatalyst with 0.25 μm PTFE filter, extracted with ethyl acetate (at a volume ratio 1:1). Liquid aliquots were analyzed by a GC–MS technique, using a Shimadzu 2100 Ultra GC–MS equipped with a Teknokroma TRB-5MS (95%) dimethyl (5%) diphenyl polysiloxane copolymer column to identify and to determine the concentration of MPET, HEB and p-cresol. Standards purchased from Sigma-Aldrich and TCI with a purity >98% were used to identify the products formed during the reaction and to obtain the calibration curves. HPLC analysis of (4-methylphenoxy)acetic acid photo-oxidation products was carried out using an Agilent 1200 Series instrument equipped with Agilent Eclipse CDB-C18 column. The determination was done in the flow of acetonitrile (20 %) and 13 mM trifluoroacetic acid (80 %) at 40 °C

5. Calculations

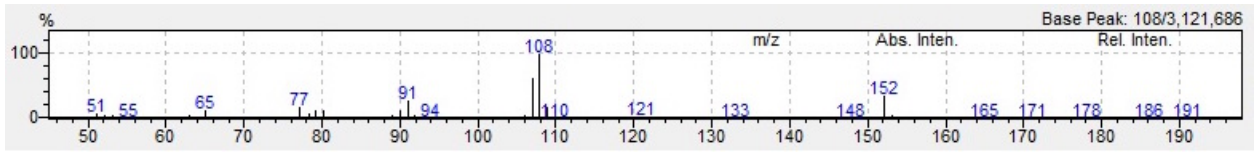
Geometry optimization of dimelem, MPET molecules and their molecular complexes (Table S1) with and without hydrogen peroxide was carried out by Kohn-Sham method in B3LYP/6-311+G (d, p) approximation in the Firefly 8.0.1 program [6] with visualization in Chemcraft [7] package. The absence of imaginary vibration frequencies controlled in all cases. The resulting wave functions were used for QTAIM [8] analysis. The summarizing energy of interacted fragments was estimated with EML approach [9,10] as a sum of corresponding hydrogen bond energies between considered compounds in complexes. For that the potential energy density, $v(\text{rb})$, at the bond critical points rb , of the electron density were calculated (see Table S1). The electron density (ED) and molecular electrostatic potential [11] (MEP) distributions were performed using Multiwfn [12] and MoleCoolQT [13] programs.

RESULTS AND DISCUSSION

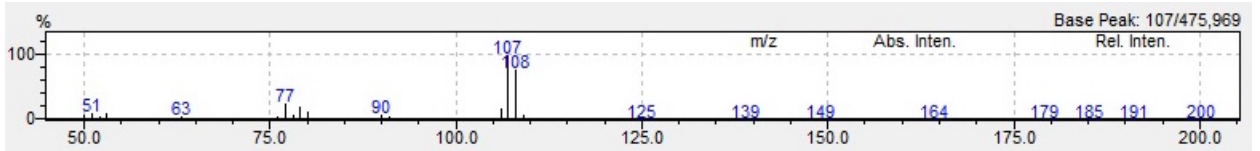
Table S1 – Summarizing energy ($\text{kcal}\cdot\text{mol}^{-1}$) of HBs, the electron density (a.u.) and the potential energy density (a.u.) at the bond critical points in considerate complexes (see Fig. 4)

Dimelem – MPET	Dimelem – MPET		Dimelem – H ₂ O ₂		MPET – H ₂ O ₂	
dimelem–MPET (direct interactions)	-15.4		-		-	
HBs	$\rho(r_b)$	$v(r_b)$	-		-	
N...H-O	0.0329	-0.0254	-		-	
N-H...O	0.0172	-0.0112	-		-	
N-H...O	0.0146	-0.0092	-		-	
N...H-C	0.0067	-0.0033	-		-	
Dimelem–3H ₂ O ₂ – MPET	-8.6		-18.7		-20.7	
HBs	$\rho(r_b)$	$v(r_b)$	$\rho(r_b)$	$v(r_b)$	$\rho(r_b)$	$v(r_b)$
N...H-O	0.0326	-0.02429	-	-	-	-
N...H-C	0.0062	-0.00318	-	-	-	-
N...H-O	-	-	0.0246	-0.0169	-	-
N-H...O	-	-	0.0268	-0.0207	-	-
N-H...O	-	-	0.0289	-0.0220	-	-
O...H-O	-	-	-	-	0.0072	-0.0045
O...H-O	-	-	-	-	0.0435	-0.0401
O...H-C	-	-	-	-	0.0272	-0.0212

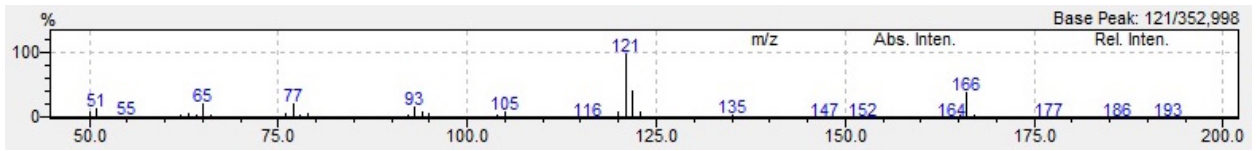
RESULTS AND DISCUSSION



a



b



c

Figure S1 – Mass spectra for the MPET (a), p-cresol (b) and HEB (c) compounds.

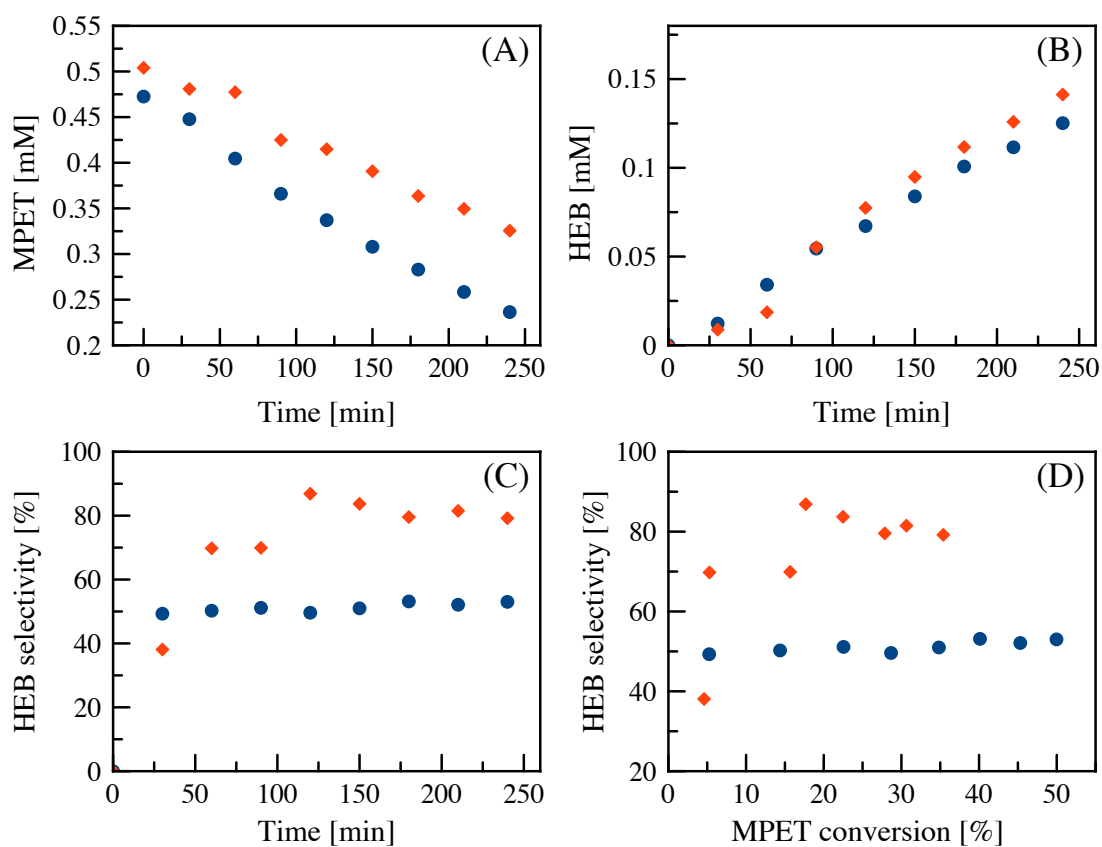


Figure S2 – MPET conversion (A); HEB formation (B); and selectivity to HEB versus irradiation time (C) or selectivity to HEB versus MPET conversion (D) in the presence of the non-exfoliated MCN (—) and H₂O₂-treated MCN_O (—).

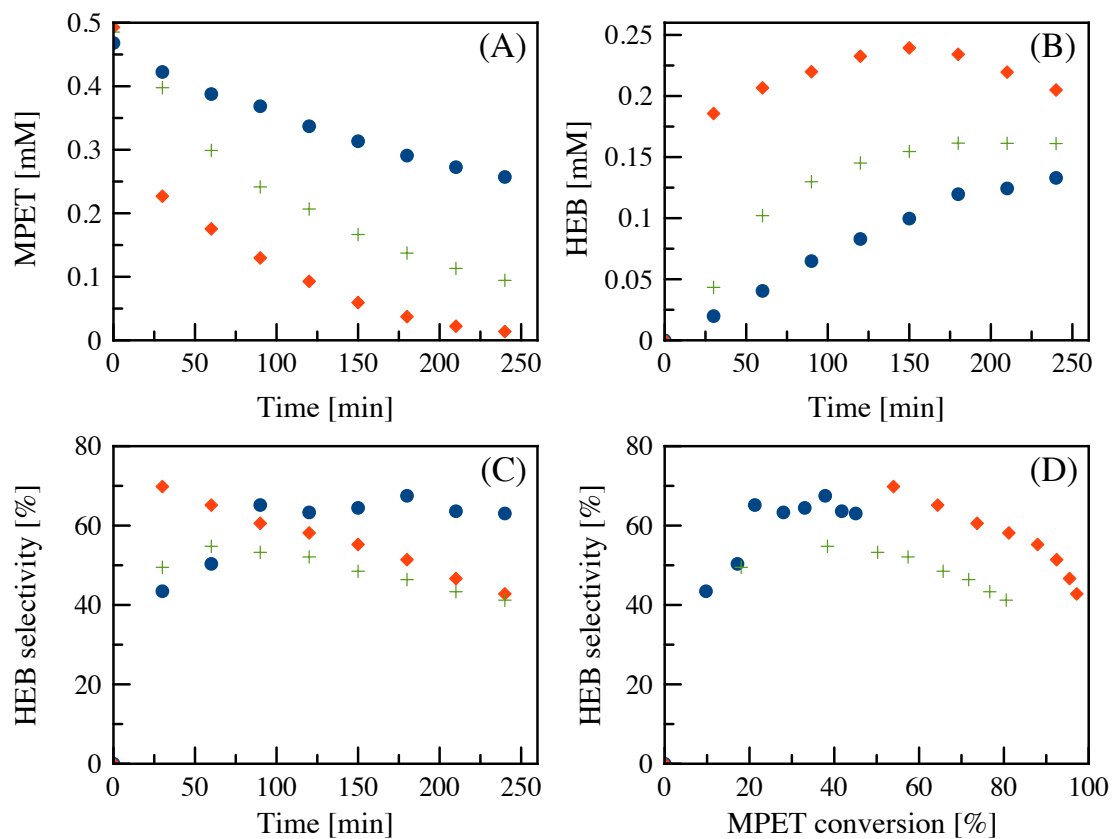


Figure S3 – MPET conversion (A); HEB formation (B); and selectivity to HEB versus irradiation time (C) or selectivity to HEB versus MPET conversion (D) in the presence of the MCN_K (—), MCN_W (—) and MCN_Na (—).

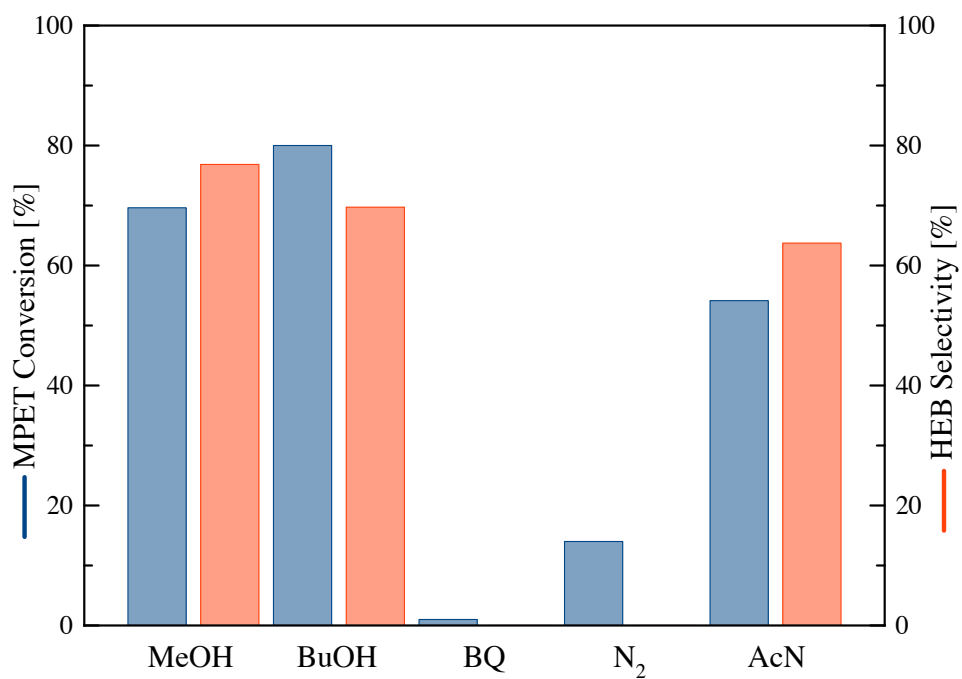


Figure S4 – Effect of using the scavengers (of charges and/or radicals) and acetonitrile (AcN) instead of water on the MPET conversion and the corresponding selectivity to HEB, after 240 min of irradiation in the presence of TE₂O.

RESULTS AND DISCUSSION

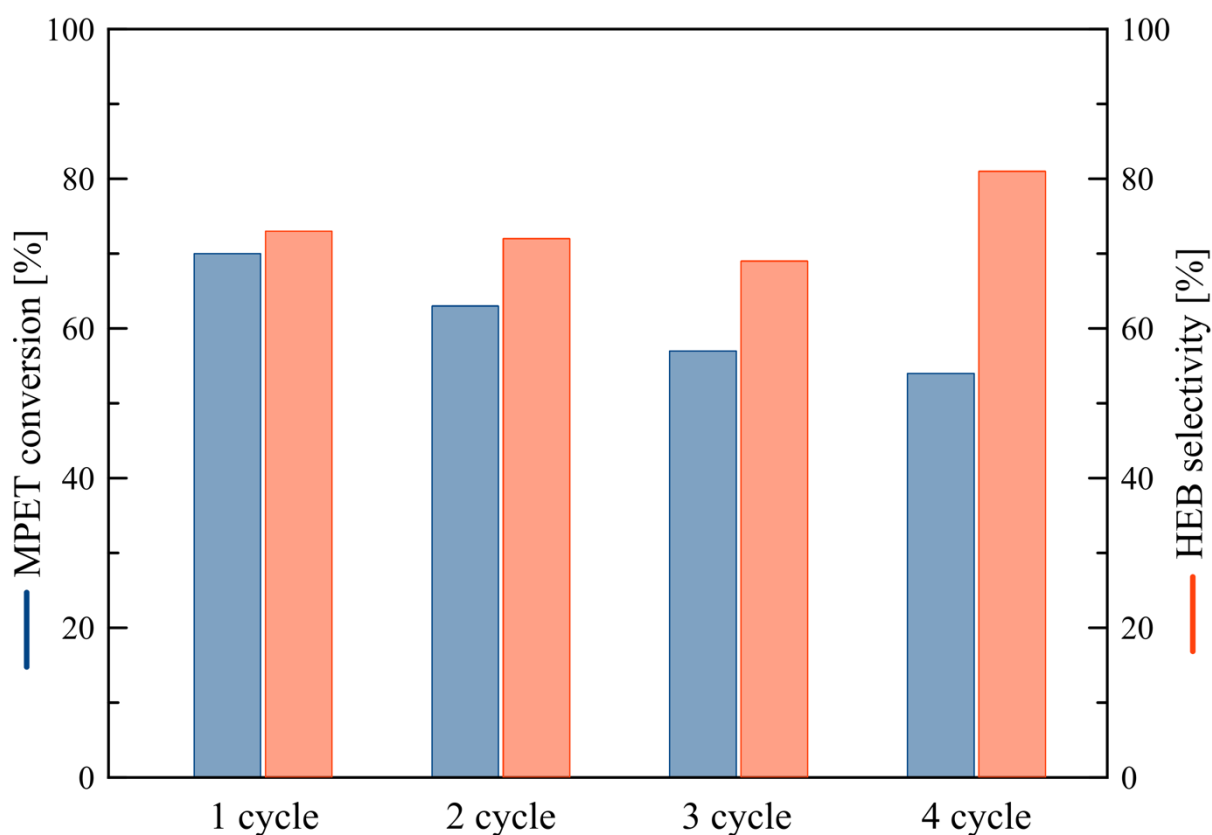


Figure S5 – The recyclability of TE₂O in MPET conversion. The data is presented for 240 min of irradiation.

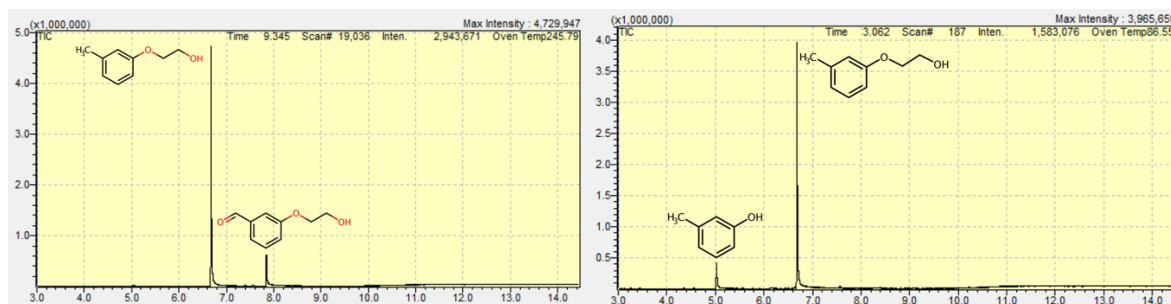


Figure S6 – To the left: Typical GC-MS data of the products of 3-(2-methylphenoxy)ethanol photo-oxidation in the presence of TE and TE₂O photocatalysts after 4 h of irradiation. To the right: GC-MS data for 3-(2-methylphenoxy)ethanol photo-oxidation in the presence of P25.

RESULTS AND DISCUSSION

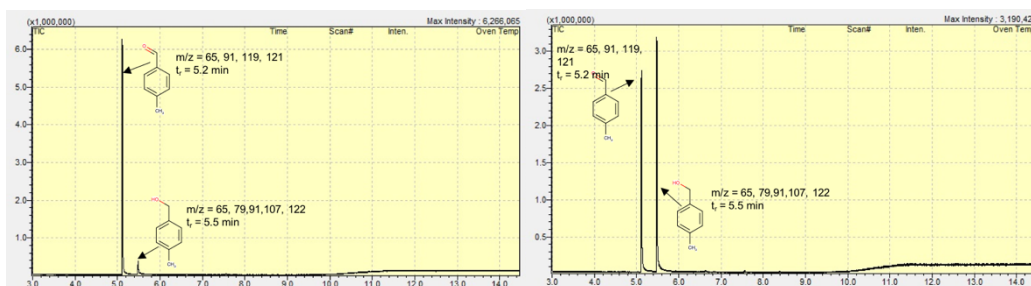


Figure S7 – GC-MS data of the products of 4-methylbenzyl alcohol photo-oxidation in the presence of TE (left) and TE_O (right) photocatalysts after 4 h of irradiation.

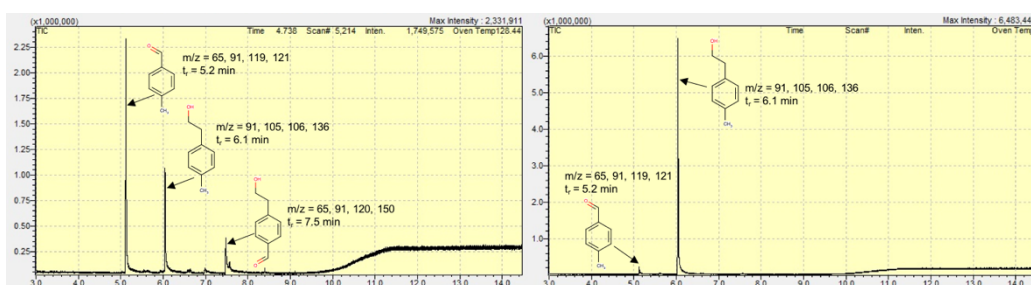


Figure S8 – GC-MS data of the products of 2-(4-methylphenyl)ethanol photo-oxidation in the presence of TE (left) and TE_O (right) photocatalysts after 4 h of irradiation.

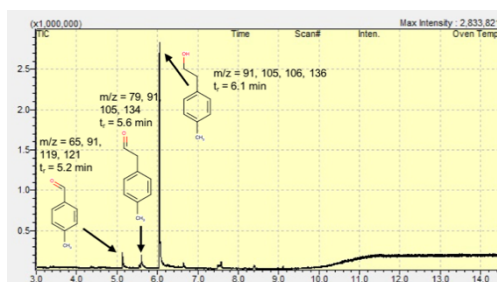


Figure S9 – GC-MS data of the products of 2-(4-methylphenyl)ethanol photo-oxidation in the presence of P25 Aeroxide photocatalyst after 4 h of irradiation.

RESULTS AND DISCUSSION

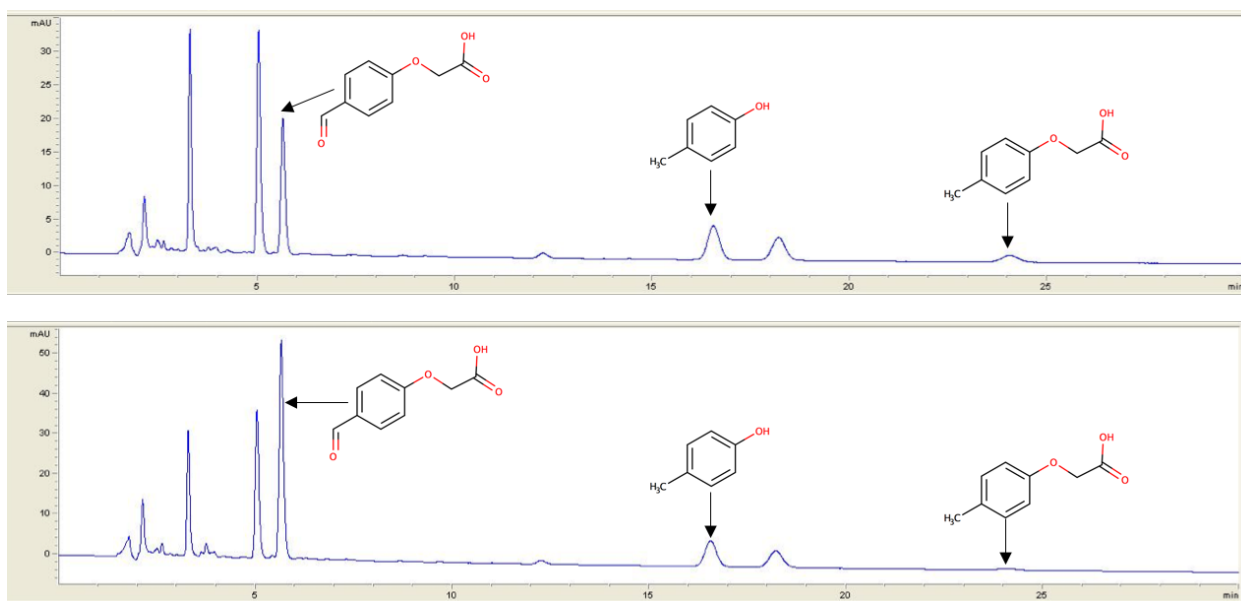


Figure S10 – HPLC chromatogram (230 nm) of products of (4-methylphenoxy)acetic acid oxidation in the presence of TE (top) and TE_O (bottom) photocatalysts after 4 h of irradiation.

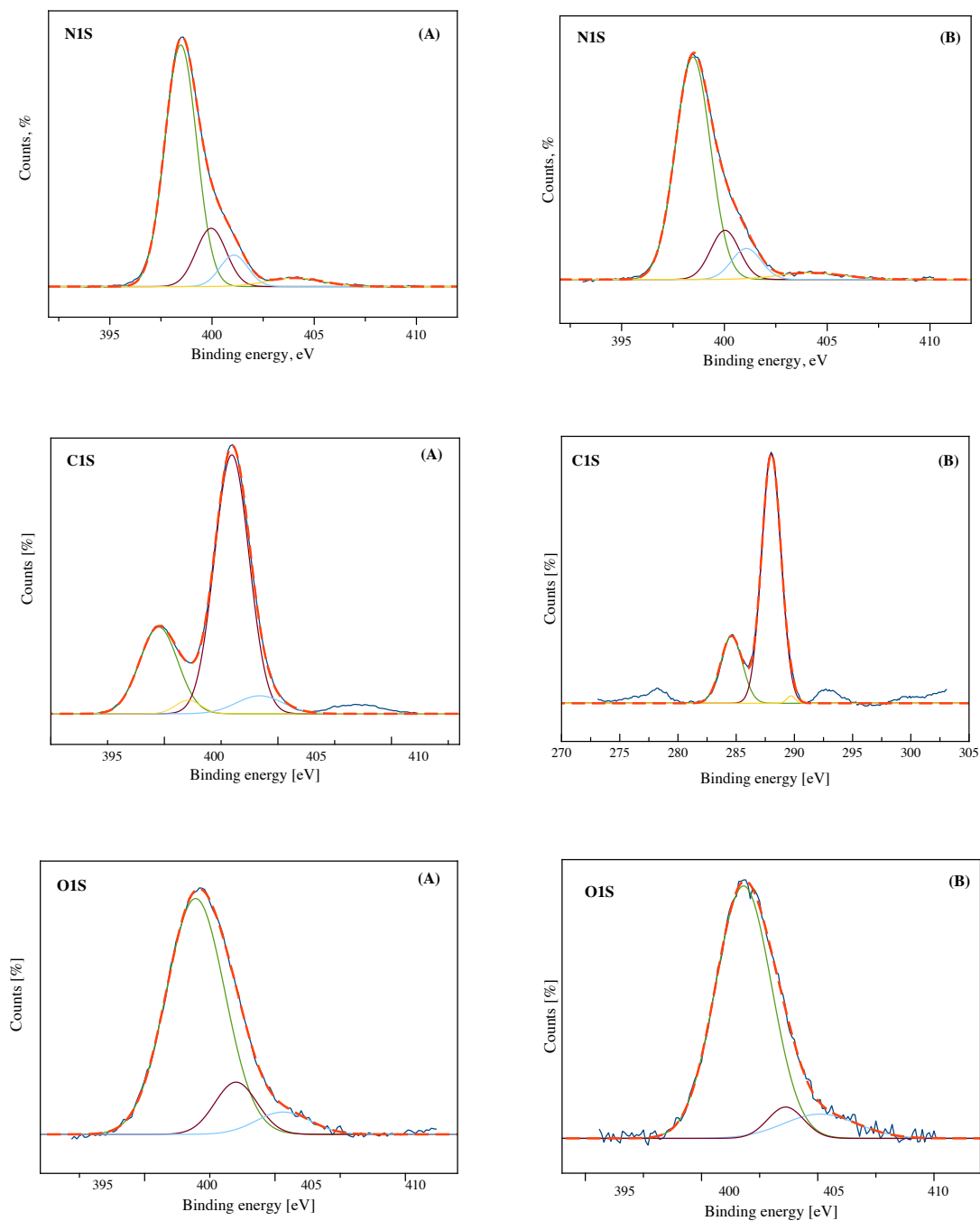


Figure S11 – XPS spectra of N 1s (A), C 1s (B) and O 1s (C) regions of the TE and TE_O samples.

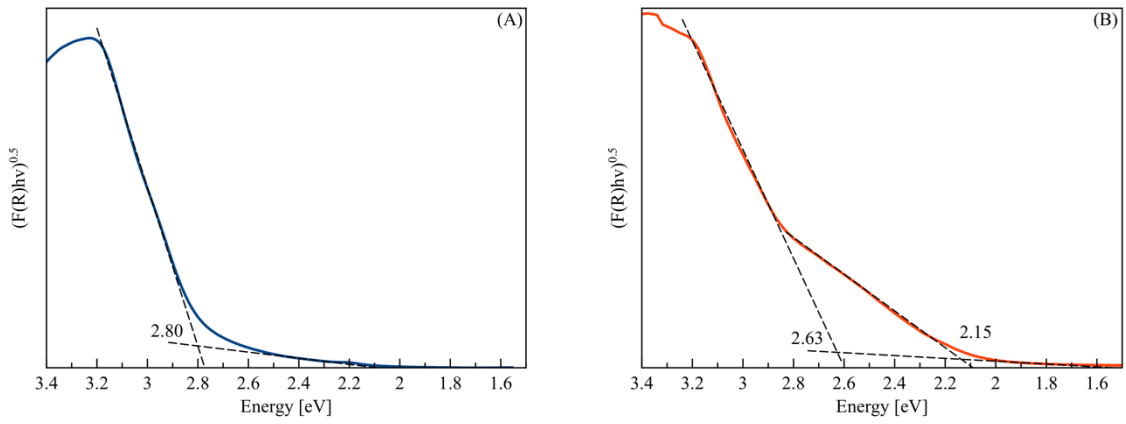


Figure S12 – Kubelka-Munk transformed DR UV-vis spectra of (A) TE and (B) TE_O samples.

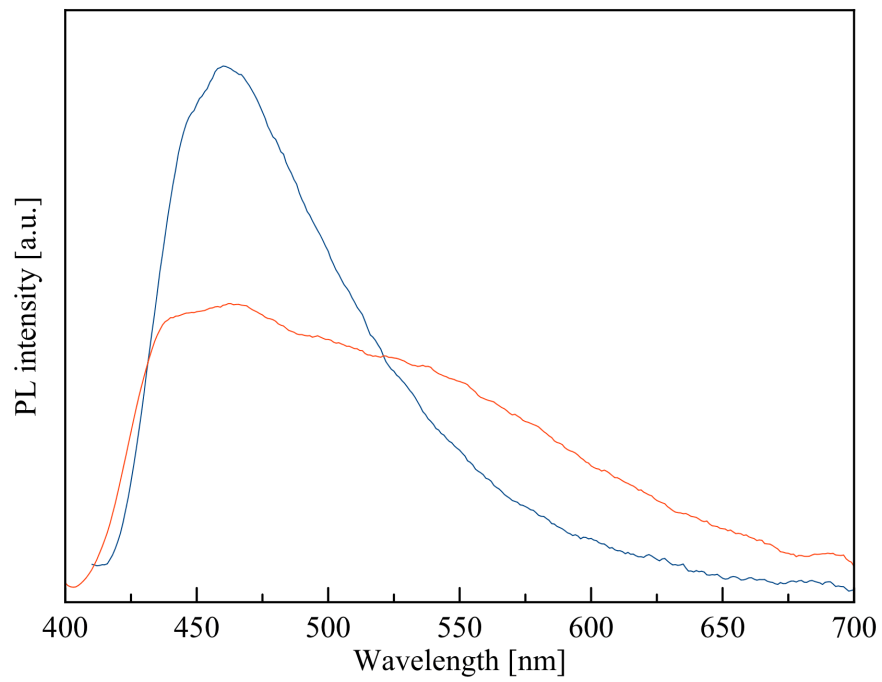


Figure S13 – PL spectra of (—) TE and (—) TE_O samples at 365 nm excitation.

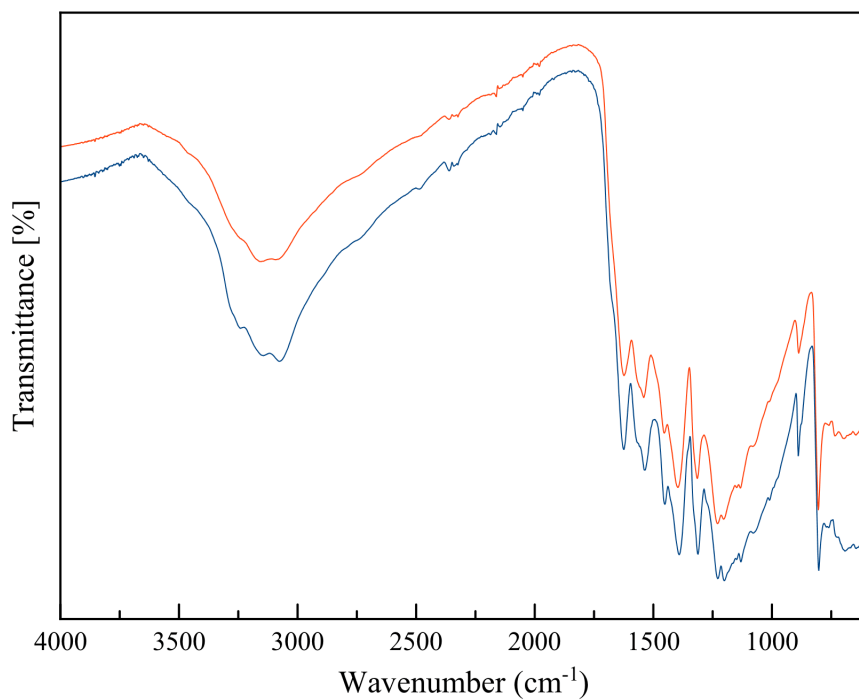


Figure S14 – FTIR of (—) TE and (—) TE_O samples.

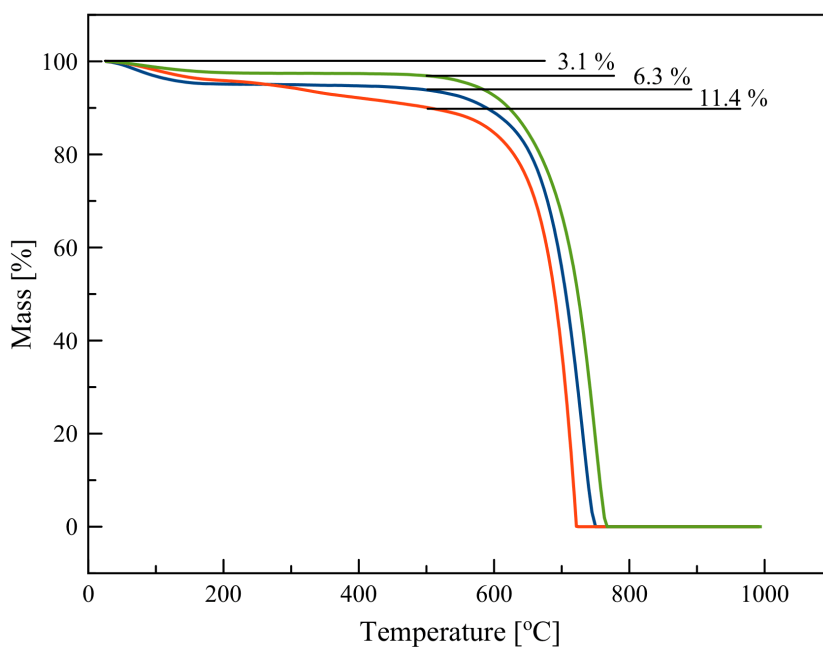


Figure S15 – Thermogravimetric study of (—) MCN, (—) TE, and (—) TE_O samples.

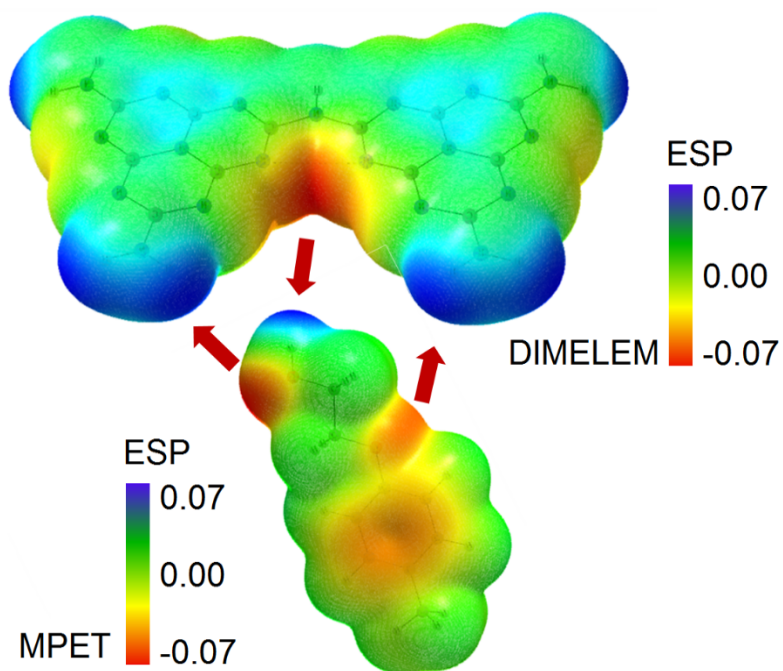


Figure S16 – Fragments complementarity of the dimelem and MPET that promotes to complex formation shown with molecular electrostatic potential (MEP) mapped on the isosurface of the electron density (ED) 0.001 a.u.

References

1. K. Wang, Q. Li, B. Liu, B. Cheng, W. Ho and J. Yu, Sulfur-doped g-C₃N₄ with enhanced photocatalytic CO₂-reduction performance, *Appl. Catal. B*, **2015**, 176–177, 44–52.
2. (a) P. Niu, L. Zhang, G. Liu and H.M. Cheng, Graphene-Like Carbon Nitride Nanosheets for Improved Photocatalytic Activities, *Adv. Funct. Mater.*, **2012**, 22, 4763–4770; (b) F. Dong, Y. Li, Z. Wang and W.K. Ho, Enhanced visible light photocatalytic activity and oxidation ability of porous graphene-like g-C₃N₄ nanosheets via thermal exfoliation, *Appl. Surf. Sci.*, **2015**, 358, 393–403; (c) I. Krivtsov, E.I. García-López, G. Marci, L. Palmisano, Z. Amghouz, J.R. García, S. Ordóñez and E. Díaz, Selective photocatalytic oxidation of 5-hydroxymethyl-2-furfural to 2,5-furandicarboxyaldehyde in aqueous suspension of g-C₃N₄, *Appl. Catal., B*, **2017**, 204, 430–439.
3. T. Sano, S. Tsutsui, K. Koike, T. Hirakawa, Y. Teramoto, N. Negishi and K. Takeuchi, Activation of graphitic carbon nitride (g-C₃N₄) by alkaline hydrothermal treatment for photocatalytic NO oxidation in gas phase, *J. Mater. Chem. A*, **2013**, 1, 6489–6496.
4. Y. Zhang, A. Thomas, M. Antonietti and X. Wang, Activation of carbon nitride solids by protonation: morphology changes, enhanced ionic conductivity, and photoconduction experiments, *J. Am. Chem. Soc.*, **2009**, 131, 50–51.
5. Y. Li, S. Ouyang, H. Xu, X. Wang, Y. Bi, Y. Zhang and J. Ye, Constructing solid–gas–interfacial fenton reaction over alkalinized-C₃N₄ Photocatalyst to achieve apparent quantum yield of 49% at 420 nm, *J. Am. Chem. Soc.*, **2016**, 138, 13289–13297.
6. A. A. Granovsky. Firefly version 8. <http://classic.chem.msu.su/gran/firefly/index.html>
7. G. A. Andrienko, Chemcraft v.1.6, <http://www.chemcraftprog.com/index.html>
8. R.F.W. Bader, Atoms in Molecules. A Quantum Theory, Oxford University Press, New York, USA, **1990**.
9. E. Espinosa, E. Molins, C. Lecomte, Hydrogen bond strengths revealed by topological analyses of experimentally observed electron densities, *Chem. Phys. Lett.*, **1998**, 285, 170–173.

10. K.A. Lyssenko, A.A. Korlyukov, D.G. Golovanov, S.Yu. Ketkov, M.Yu. Antipin, Estimation of the Barrier to Rotation of Benzene in the $(\eta_6\text{-C}_6\text{H}_6)_2\text{Cr}$ Crystal via Topological Analysis of the Electron Density Distribution Function, *J. Phys. Chem. A*, **2006**, 110, 6545–6551.
11. Z. Shields, J.S. Murray, P. Politzer, Directional tendencies of halogen and hydrogen bonds, *Int. J. Quant. Chem.*, **2010**, 110, 2823–2832.
12. T. Lu, F. Chen, Multiwfn: A multifunctional wavefunction analyzer, *J. Comput. Chem.*, **2012**, 33, 580–592.
13. C. B. Hubschle and B. Dittrich, MoleCoolQt – a molecule viewer for charge-density research, *J. Appl. Crystallogr.*, **2011**, 44, 238–240.

4.2.2 PCN–H₂O₂ adduct for selective photo-oxidation of 5-hydroxymethylfurfural to 2,5-furandicarboxaldehyde

Cellulose, an abundant biomass compound, can be valorized by undergoing hydrolysis producing hexose sugars which, after being subsequently dehydrated, give a biomass platform molecule 5-hydroxymethyl furfural (HMF). While HMF itself has few applications, the products of its oxidation 2,5-furandicarboxylic acid (FDCA) and 2,5-furandicarboxaldehyde (FDC) possess certain properties making them valuable for polymers production. While a lot of catalytic processes have been developed for the biomass valorisation, reports on photocatalytic biomass-derived molecules transformations, especially in water medium, are scarce.

As was mentioned in Introduction, replacing organic solvents with water is an important challenge, since it makes the process cost-effective and environmentally benign. Despite this fact, carbon nitride mostly has been used for conversion of aromatic alcohols [154,195,196,174] and hydrocarbons [175,197–199] in organic solvents, while its efficient application in aqueous phase remains a challenge [10,53,201].

The outstanding performance of the PCN–H₂O₂ adduct in the partial photocatalytic oxidation of 5-hydroxymethylfurfural (HMF) allows reaching the selectivity to 2,5-furandicarboxaldehyde (FDC) of 80% under UV irradiation and up to 89% under natural solar light in water medium. The following work presents a detailed study of the structural and physicochemical properties of the PCN–H₂O₂ adduct addressing the questions of its thermal stability and durability in the reaction mixture. The XRD, XPS, TPD and Solid State NMR methods confirmed the presence of the bonded hydrogen peroxide to the NH_x-species and its effect on the hydrogen bonding in the adduct samples. It was proposed that the non-condensed carbon nitride species are responsible for the generation of •OH radicals leading to the decrease of the reaction selectivity, but in the PCN–H₂O₂ adduct these sites are blocked by the coordinated H₂O₂, thus hindering either the hydroxyl radical production or catalyst interaction with these sites, hence allowing to avoid the unselective substrate conversion. The successful performance of the applied photocatalyst in the selective photocatalytic conversion

RESULTS AND DISCUSSION

of HMF to a high added value FDC in a green solvent under natural illumination makes a significant contribution to the development of environmentally friendly technologies for biomass valorization.

Article III

“Selective photocatalytic oxidation of 5-hydroxymethylfurfural to 2,5-furandicarboxaldehyde by polymeric carbon nitride-hydrogen peroxide adduct”

Journal of Catalysis

359 (212–222)

Year 2018

DOI: 10.1016/j.jcat.2018.01.012

Impact Index: 6.844

Selective Photocatalytic Oxidation of 5-Hydroxymethylfurfural to 2,5-Furandicarboxaldehyde by Polymeric Carbon Nitride-Hydrogen Peroxide Adduct

M. Ilkaeva,^a I. Krivtsov,^{*a,b} E.I. García-López,^c G. Marci,^c O. Khainakova,^a J.R. García,^a L. Palmisano,^c E. Díaz,^d S. Ordóñez^d.

^a Departments of Organic and Inorganic Chemistry, Physical and Analytical Chemistry, University of Oviedo-CINN, 33006 Oviedo, Spain.

^b Nanotechnology Education and Research Center, South Ural State University, 454080 Chelyabinsk, Russia.

^c “Schiavello-Grillone” Photocatalysis Group. Dipartimento di Energia, Ingegneria dell’informazione e modelli Matematici (DEIM), Università di Palermo, Viale delle Scienze, 90128 Palermo, Italy.

^d Department of Chemical and Environmental Engineering, University of Oviedo, 33006 Oviedo, Spain.

Corresponding author e-mail: krivtsovigor@uniovi.es; Tel: +34 985 103 030

Abstract

Polymeric carbon nitride-hydrogen peroxide adduct (PCN-H₂O₂) has been prepared, thoroughly characterised and its application for selective photocatalytic conversion of 5-hydroxymethylfurfural (HMF) to 2,5-furandicarboxaldehyde (FDC) in aqueous suspension has been studied. The PCN-H₂O₂ adduct is stable in aqueous suspension under UV and solar irradiation up to 100 °C. It is also stable up to 200 °C if heated in air, while at temperatures close to 300 °C its decomposition takes place. Based on the obtained characterisation data it has been proposed that H₂O₂ attaches to the non-polymerised carbon nitride species and to the heptazine nitrogen atoms, thus producing strong hydrogen bonding within the PCN-H₂O₂ adduct. The blockage of the surface amino-groups in PCN-H₂O₂ by H₂O₂ hinders the interaction of HMF with these sites, which are responsible for unselective substrate conversion. PCN-H₂O₂, although being less active, possesses a superior selectivity in natural solar light assisted oxidation of HMF to FDC reaching 80% with respect to its thermally etched PCN counterpart, which gives rise to a 40-50% selectivity. We believe that the exceptional performance of the applied photocatalyst in the selective photocatalytic conversion of HMF to a high added value FDC in a green solvent under natural illumination

makes a significant contribution to the development of environmentally friendly technologies for biomass valorisation.

Keywords: *photocatalysis; carbon nitride; selective photo-oxidation; 5-hydroxymethylfurfural; 2,5-furandicarboxaldehyde*

Introduction

Wood industry and agricultural sector release a large amount of by-products and wastes, which if processed appropriately, can be converted into a range of valuable chemicals or fuels. This renewable feedstock known under the general term “biomass”, despite being used for multiple purposes, is still in the spotlight of the research community, inasmuch as newly emerged technologies allow benefiting from its more complete use. Cellulose, an abundant biomass compound, can be upgraded by undergoing hydrolysis producing hexose sugars, which after being subsequently dehydrated give the biomass platform molecule 5-hydroxymethyl furfural (HMF) [1,2]. While HMF itself has few applications, the products of its oxidation 2,5-furandicarboxylic acid (FDCA) and 2,5-diformylfuran, also known as 2,5-furandicarboxaldehyde (FDC), possess properties making them valuable for biopolymer production [3-7]. Many catalytic procedures have been developed for obtaining both FDCA [8,9] and FDC [9-14] by oxidising HMF, but photocatalysis is among the most economic and greener alternatives as it benefits from a nearly free energy source, which is solar radiation, and does not require toxic oxidants. The outburst of interest toward semiconductor-assisted selective photo-oxidation has already resulted in an impressive number of exhaustive reviews on mechanisms and applied aspects of this process [15-20]. Light-initiated transformation of biomass aiming to produce fuel has recently been reported by Wakerley et al. [21], while the approaches for its chemical upgrading has been reviewed in [22-23].

HMF itself was subjected to the electrophotocatalytic [24] and photocatalytic conversion in aqueous phase using TiO₂ as the photocatalyst, and FDC was found to be the main oxidation product of this reaction [25,26]. Although TiO₂ and especially N-doped TiO₂ promoted the formation of FDC from HMF, the selectivity of this process was low reaching 30% for the

best photocatalysts, owing to the formation on the TiO₂ surface of highly oxidative hydroxyl radicals inducing the substrate mineralisation [26]. Obviously, an alternative material for such transformation was in demand. It has not been long since polymeric carbon nitride (PCN) (the recommended term for graphitic carbon nitride, g-C₃N₄) [27] photocatalyst has emerged [28]. In addition to its high ability to reduce water protons to molecular hydrogen, it possesses a valence band (VB) potential which does not permit direct water oxidation to •OH radicals [28], hence reducing the presence of notoriously unselective oxidative species in water suspension of photocatalysts with organic compounds. Despite this attractive property, this material has mostly been used for conversion of aromatic alcohols [29-32] and hydrocarbons [33-36] in organic solvents, while reports on its performance in aqueous phase are scarce [37-38]. Recently, the enhanced selectivity of PCN for aqueous phase HMF to FDC photo-oxidation with respect to that previously achieved in the presence of TiO₂ [25] has been reported [39-40]. A detrimental effect of the presence of non-polymerised carbon nitride species on the selectivity of photo-oxidation has also been observed [39]. Thermal etching applied to bulk PCN, principally with the purpose of increasing its specific surface area (SSA), also eliminated excessive NH and NH₂ moieties from the PCN surface resulting in the growth of selectivity toward the FDC production from 30% to 50% under solar irradiation [39]. The importance of controlling the interaction of substrate with the surface functional groups of PCN was even more stressed for chemoselective C–H bond oxidation of alkylphenoxyethoxylate molecules [41]. In this paper, we report the application of the PCN-H₂O₂ adduct for highly selective photocatalytic oxidation of HMF to FDC in aqueous medium under both UV and natural solar light irradiation.

Experimental Section

Materials

Melamine (99%), 30 wt% hydrogen peroxide water solution, 5-hydroxymethylfurfural (HMF) (≥99%), 2,5-furandicarboxyaldehyde (FDC) (≥99%), and 5-formyl-2-furoic acid (FFA) (≥99%) were purchased from Aldrich.

Synthesis

The bulk PCN was prepared via the thermal condensation method using melamine as the precursor according to the procedure described by Wang et al. [42]. Briefly, 10 g of melamine was placed in a covered ceramic crucible and heated in a muffle furnace at $2\text{ }^{\circ}\text{C min}^{-1}$ up to $520\text{ }^{\circ}\text{C}$. Once the temperature was reached it was left for 2 h and slowly cooled down afterwards. By this procedure, 6 g of PCN was obtained. Bulk PCN was then subjected to thermal etching as previously reported [39,43], in order to produce high SSA PCN. For this purpose, 6 g of the bulk carbon nitride was powdered in a mortar, evenly spread on the bottom of a ceramic bowl with a diameter of 12 cm, heated in a static air atmosphere at $500\text{ }^{\circ}\text{C}$ by using a temperature ramp of $3\text{ }^{\circ}\text{C min}^{-1}$ and maintained for 4 h at the reached temperature before being cooled down. This procedure yielded 2.8 g of the thermally etched PCN sample, designated as TE. Finally, the PCN- H_2O_2 adduct, whose preparation and characterisation were reported elsewhere [41], was synthesized. For this, 2.8 g of TE was stirred in 50 mL of H_2O_2 aqueous solution (30 wt%) in an open beaker while heating at $70\text{ }^{\circ}\text{C}$ until complete evaporation of the liquid was achieved. The obtained solid was washed thoroughly with deionized water, until H_2O_2 was no longer detected in the washing liquid, filtered and finally dried at $80\text{ }^{\circ}\text{C}$ for 24 h giving the PCN- H_2O_2 adduct (TEO). After that, aliquots of the TEO sample, 0.87 g in each case, were treated at 200, 300, and $400\text{ }^{\circ}\text{C}$ in air for 2 h, and the resulting samples were coded as TEO_x , where “x” indicated the treatment temperature. For the sake of comparison, two more samples were synthesized. Thermally etched TEO450 was prepared by treating the TEO sample at $450\text{ }^{\circ}\text{C}$ in air. H_2O_2 modification of TE was also carried out using reflux treatment at $70\text{ }^{\circ}\text{C}$ (TEO_R). Melamine-hydrogen peroxide adduct (MHP) was prepared and used as the reference for the assignment of carbon nitride surface species formed after the reaction with hydrogen peroxide. For this purpose, 10 g of melamine was mixed with 50 mL of 30 wt% H_2O_2 and let stirring while heated at $70\text{ }^{\circ}\text{C}$ until the solvent was evaporated. The obtained solid was dried at $70\text{ }^{\circ}\text{C}$ for 24 h.

Characterisation

Powder XRD patterns were registered in an X'pert PANalytical diffractometer, using a Ni-filtered Cu-K α radiation source and PixCel1D (tm) detector. Infrared spectra of the samples were recorded with 4 cm⁻¹ resolution using an ATR module of a Varian 620-IR spectrometer. The surface elemental composition of the PCN and PCN-H₂O₂ samples, their valence band (VB) potentials, and the binding energies of C, N and O were measured by X-ray photoelectron spectroscopy (XPS) on a SPECS system equipped with a Hemispherical Phoibos analyser operating in a constant pass energy, using MgK α radiation ($h\nu = 1253.6$ eV). The absence of C–C bonds in carbon nitride made possible taking a signal of adventitious carbon at 284.8 eV as a reference. The elemental composition was estimated from the deconvoluted high-resolution data as to remove the contribution of adventitious carbon. The value of conduction band potential of the PCN samples was estimated by subtracting the value of band gap energy (BG) from that of the valence band energy (VB). The solid-state ¹³C, ¹H MAS NMR, and ¹H-¹³C CPMAS NMR spectra were registered at the spinning rates of 5 kHz for ¹³C, and 8 kHz for the other measurements using a Bruker Avance III 400WB spectrometer. A Shimadzu UV-2401 PC spectrophotometer equipped with an integrated sphere was used to obtain diffuse reflectance spectra (DRS) from the prepared samples supported on BaSO₄ pellets. The BG was estimated by applying the Kubelka-Munk function to the DRS data considering PCN as an indirect semiconductor. Photoluminescence spectra were recorded for the obtained materials by means of a standard spectrofluorimeter Edinburgh Instruments FLSP920 equipped with a 450 W Xe lamp as an excitation source (365 and 455 nm wavelengths were selected for the samples excitation). A Micromeritics ASAP 2020 was used to obtain adsorption-desorption isotherms of N₂ at 77 K. Specific surface area (SSA) was calculated from the nitrogen adsorption data by BET equation. Before the experiment, the samples were outgassed under vacuum at 200 °C. The temperature programmed desorption mass-spectroscopic (TPD-MS) analysis was carried out with help of a Micromeritics Autochem II 2920 system coupled with a ThermoStar mass spectrometer. For the analysis, 100 mg of a powdered PCN was put onto a fibreglass support inside a quartz U-tube, purged for 60 min with argon gas flowing through the sample at the rate of 10 mL min⁻¹ at 35 °C and then heated at 10 °C min⁻¹ up to 400 °C. The concentration

of H₂O₂ released into water suspension by the PCN-H₂O₂ adduct was estimated photocolourimetrically by using titanium oxysulfate based method.

Photocatalytic oxidation of HMF

Partial photocatalytic oxidation of HMF to FDC under UV-light was carried out by using the experimental set-up described elsewhere [39]. A water-cooled Pyrex reactor containing 150 mL of aqueous suspension was irradiated with six Actinic BL TL MINI 15 W/10 Philips fluorescent lamps having an irradiation maximum at 365 nm. The initial HMF concentration was 0.5 mM at the natural pH if not stated otherwise. The amount of solid photocatalyst used for the experiments was 100 mg. In this way, all the entering photons were virtually absorbed by the suspension. The impinging radiation energy in the range 315–400 nm was measured by a radiometer Delta Ohm DO9721 with a UVA probe and its average value was 3.9 W m⁻². The performance of the most efficient photocatalyst (TEO) was tested in a series of three consecutive reaction runs. The suspension of TEO was left for 24 h to separate the photocatalyst after the photocatalytic reaction. Then, the limp solution was removed, 150 mL of fresh HMF 0.5 mM solution was introduced into the reactor and the test was repeated. Samples of the irradiated solution were withdrawn at fixed time intervals and immediately filtered through 0.25 µm membranes (polypropylene, VWR) to separate the photocatalyst particles. Liquid aliquots were analysed by a Thermo Scientific Dionex UltiMate 3000 HPLC equipped with a Diode Array detector and a REZEK ROA organic acid H⁺ column with aqueous 2.5 mM H₂SO₄ solution mobile phase at a flow rate of 0.6 mL min⁻¹. The concentrations of HMF, FDC and FFA were determined. Standards purchased from Sigma-Aldrich with a purity >99% were used to identify the products formed during the reaction and to obtain the calibration curves. The calibration curves for all the compounds built up to the concentration of 2 mM were linear with a correlation coefficient ≥ 0.99.

The photocatalytic reactions under natural solar irradiation were carried out on clear sunny days from March to May in Palermo (Italy) from 9:30 to 13:30. Typically, 75 mL of 0.5 mM HMF solution and 50 mg of the PCN or PCN-H₂O₂ samples were introduced into a round-shaped Pyrex batch reactor having a total volume of 125 mL and a diameter of 10 cm. Additionally, the TEO sample was tested under the same conditions, but at initial HMF

concentrations of 1mM and 2 mM. The suspensions of the PCN samples in HMF solution were continuously magnetically stirred and probes of approximately 2.5 mL were withdrawn every 30 min and analysed by using the previously described analytical procedure. The photon flux in the range of 315-400 nm, which largely determines the reactivity of PCN under present conditions [39], was measured every 10 min throughout the photocatalytic runs, and the cumulative energy (E) was estimated based on the obtained data. The E value allows the comparison of photoreactivity results obtained under natural sunlight irradiation at different meteorological conditions. It is given by:

$$E = \int_0^t I(t) dt \quad (1)$$

in which “I(t)” is the instantaneous photon flow and “t” the irradiation time. The values of “I(t)” were calculated from the recorded values of irradiance, UVG(t), by using the following relationship:

$$I(t) = UVG(t) \cdot S \quad (2)$$

in which “S” is the total irradiated surface and “UVG” is the irradiance (in the 315-400 nm wavelength range) [44].

The detection of hydroxyl radicals was carried out by a standard terephthalic acid (TA) method [45]. For this, 12 mg of PCN was suspended in 150 mL of 3 M solution of TA in 0.01 M of NaOH. The suspension was irradiated in the same set-up described above, the samples were withdrawn at fixed time intervals and PL spectra of the formed hydroxyterephthalic acid were recorded at excitation wavelength of 310 nm.

Results and Discussion

XRD and FTIR

According to the XRD patterns of the thermally etched PCN and the PCN-H₂O₂ adduct samples shown in Figure 1, the typical PCN reflections of (002), (100), and (101) planes are observed. Noteworthy, the full-width at half-maximum (FWHM) of the diffraction peak at 27.7° (2θ) is decreased to 1.46° for the TEO sample with respect to that of TE (1.66°),

indicating the change in preferential orientation or bonding in the adduct, also noted elsewhere [41] (Fig. 1 inset). This finding differs from other works reporting the use of H_2O_2 for hydrothermal carbon nitride treatment, where harsh conditions favoured exfoliation of PCN, consequently reducing the intensity of diffraction maxima [46,47]. Thermal treatment at 200 and 400 °C applied to the TEO sample does not lead to further changes of FWHM of the (002) peak, which is maintained in the range of 1.40° to 1.46° (Fig. 1 inset). For the PCN- H_2O_2 subjected to 400 °C (TEO400) a shift of the peak position is clearly seen on the XRD pattern of this sample (Fig. 1 inset), implying that thermal etching has already taken place at 400 °C [48].

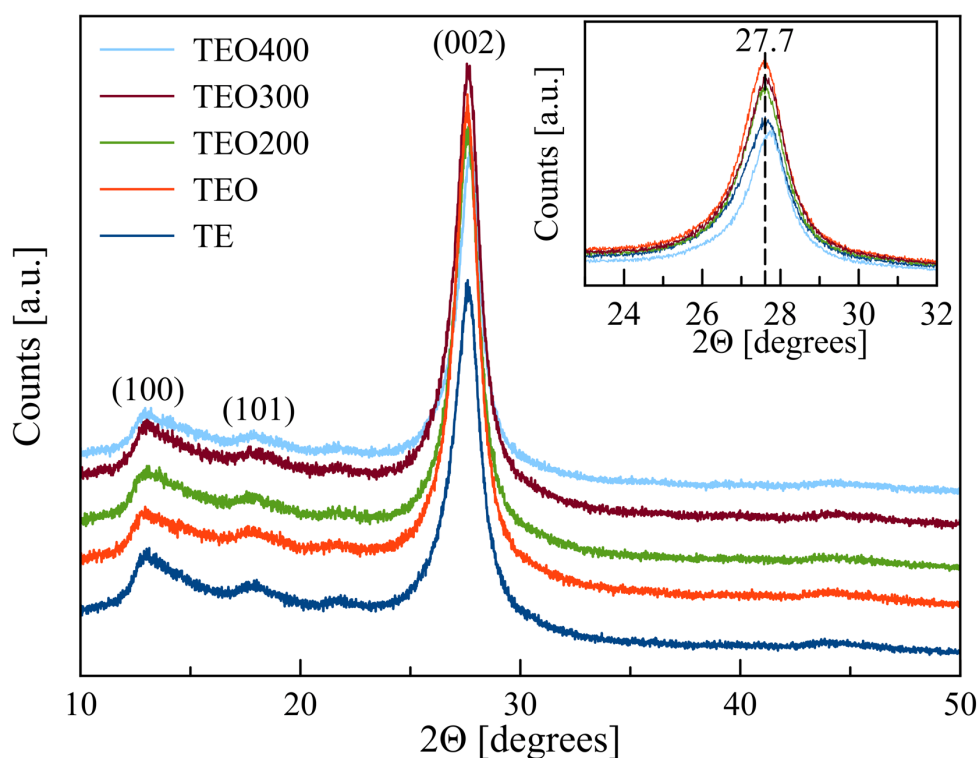


Figure 1 – XRD patterns of the prepared PCN and PCN- H_2O_2 samples.

FTIR study is in agreement with the discussed XRD results, as it confirms that no major changes in polymeric C_3N_4 structure occur neither after the reaction with H_2O_2 nor after the subsequent heating (see Electronic Supplementary Information, Fig. S1). The range of wavenumbers from 1100 to 1700 cm^{-1} is typical of C–N stretching vibrations in heptazine

heterocycles (Fig. S1), and it remains almost identical whatever treatment is applied to the TE or TEO samples.

XPS study

The C 1s XPS spectra (Fig. S2) show that the positions of the corresponding maxima do not change and the profiles of the spectra are not significantly modified after the applied treatment. The XPS probing of the N 1s region results in a broad maximum, which can be deconvoluted into the three major contributions from C–N=C (N1), N–(C)₃ (N2) and C–N–H (N3) species (Fig. S3). The ratio of N1 to N3 remains nearly constant for all the samples, whereas it is not the case of the N1/N2 ratio (Table S1). Due to the significant peak width and the possible superposition of the signals from several N-containing moieties, it is difficult to unambiguously attribute the observed changes to certain groups in PCN-H₂O₂. However, one can suggest that the decrease of the N1 to N2 ratio for TEO is a consequence of the enhanced condensation degree of PCN, while the following changes manifested by the samples subjected to thermal treatment at 200 and 300 °C result most likely from the reaction of evolving hydrogen peroxide with carbon nitride (Table S1).

In accordance with the previously reported data [41], XPS results show the increased surface oxygen content in TEO contrary to its unmodified counterpart, the TE sample (Table 1). Interestingly, the concentration of surface oxygen decreases slightly after the material is heated at 200 °C, but it drops down, even below the value obtained for TE, in the samples heated up to 300 and 400 °C (Table 1).

RESULTS AND DISCUSSION

Table 1 – XPS data, electronic structure and SSA values of the PCN and PCN-H₂O₂ samples

Sample	XPS surface composition [at%]	O 1s peak position [eV]	BG [eV]	VB [eV]	CB [eV]	SSA [m ² ·g ⁻¹]
TE	C _{42.3} N _{54.4} O _{3.3}	532.5	2.76	1.59	-1.17	94
TEO	C _{40.8} N _{53.8} O _{5.4}	531.6	2.74/2.19	1.44	-1.30	70
TEO200	C _{39.6} N _{55.8} O _{4.6}	531.6	2.67/2.16	1.52	-1.15	23
TEO300	C _{41.0} N _{56.6} O _{2.4}	531.5	2.72	1.52	-1.20	30
TEO400	C _{41.7} N _{55.8} O _{2.5}	532.3	2.81	1.65	-1.16	168
MHP		531.3				

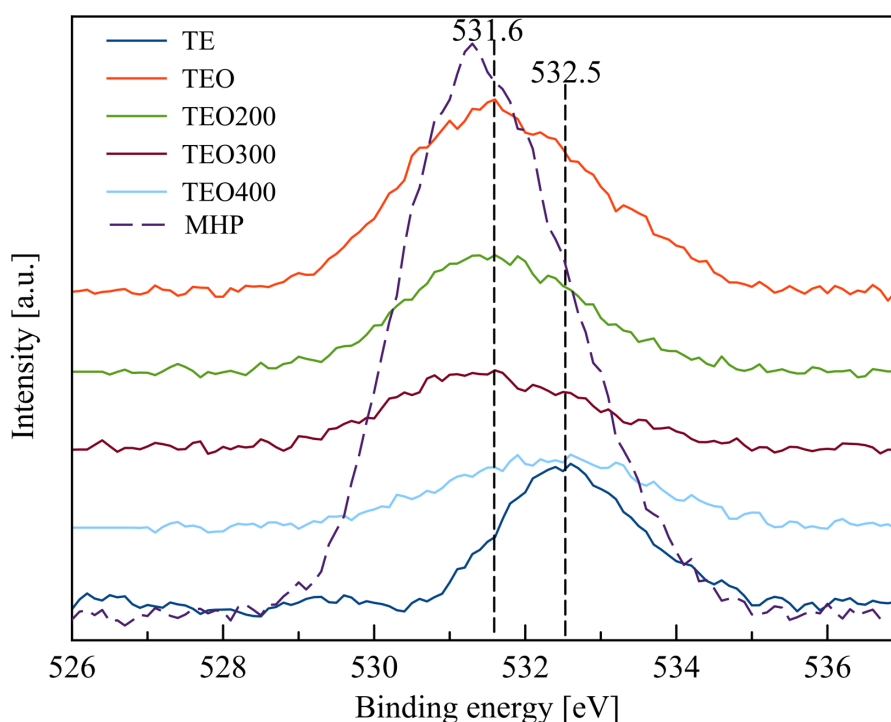


Figure 2 – XPS spectra of O 1s region of the PCN and PCN-H₂O₂ samples.

The nature of the oxygen-containing species in the PCN-H₂O₂ samples is determined from the O 1s XPS spectra. It appears that the peak of O 1s, centred at 532.5 eV for the TE sample,

RESULTS AND DISCUSSION

is displaced to 531.6 eV for TEO (Fig. 2). The position of the peak remains unchanged even after the PCN-H₂O₂ adduct is heated up to 300 °C. The XPS spectrum of TEO400 clearly indicates that the O 1s maximum returns to the same value of binding energy as that of the starting material (Fig. 2). The similar shift of the O 1s peak was earlier reported for H₂O₂-treated carbon nitrides [46,47], however, the assignment of these oxygen-containing moieties is a controversial matter. Li et al. [47], who subjected PCN to hydrothermal treatment in H₂O₂ solution, attributed the appearance of the peak at 531.6 eV to the formation of N–C–O or adsorbed O₂ species. Liu et al. [46] suggested that the cause was an O-doping of the heptazine skeleton. The absence of any noticeable changes in the chemical states of C and N atoms in the PCN-H₂O₂ samples prepared in this work compared to the thermally etched PCN, and the fact that the adsorbed oxygen is expected to appear in XPS spectra at about 532 eV [49] suggest to hold on to the earlier proposed hypothesis [41]. The reaction of melamine with hydrogen peroxide produces the crystalline MHP adduct [50,51], whose structure is reported by Chernyshov et al. [52]. In a very similar way, H₂O₂ can interact with the surface carbon nitride species [41]. Here, we corroborate this hypothesis by comparing the O 1s XPS data obtained for the crystalline MHP complex, whose structure is confirmed by the XRD measurement (Fig. S4), and the PCN-H₂O₂ samples (Fig. 2). The O 1s peak of MHP complex is centred at 531.3 eV nearly coinciding with the O 1s maximum found for the TEO, TEO200, and TEO300 samples; however, the contribution of other oxygen species also present in PCN causes its shift to 531.5–531.6 eV (Fig. 2, Table 1). A drastic reduction of the oxygen content observed for TEO300 can be attributed to the elimination of a greater part of bonded H₂O₂, although the fact that the position of the O 1s maximum remains unchanged could indicate the presence of small quantities of H₂O₂ retained in the material. Thus, considering the surface elemental composition and the position of the O 1s maximum, one can conclude that the reaction of PCN with H₂O₂ produces a PCN-H₂O₂ adduct stable in air up to 200 °C.

Solid-state MAS ¹H, ¹³C, and ¹H-¹³C CPMAS NMR studies

The chemical shifts of the two maxima at 156.7 and 165.0 ppm on the ¹³C MAS NMR spectra correspond to carbon atoms bonded to three nitrogen atoms of the aromatic carbon nitride structural units (C_i) and to those bearing non-polymerised NH₂ and partially

RESULTS AND DISCUSSION

polymerised NH fragments (C_e), respectively (Fig. 3, Fig. 4A). This is confirmed by the ^1H - ^{13}C CPMAS NMR, where the signal at 165.0 ppm is significantly enhanced (Fig. 4B).

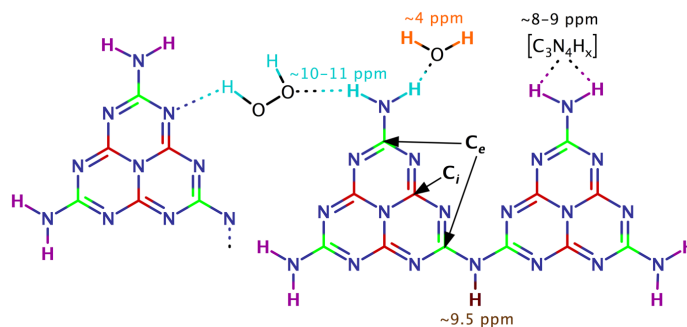


Figure 3 – Proposed model of interactions in the PCN- H_2O_2 adduct.

The ^{13}C MAS NMR peak positions do not suffer any noticeable displacements after the material is reacted with H_2O_2 or subsequently heated (Fig. 4A). The C_i to C_e integrated area ratio of 1.0 is also constant for all of the tested samples (Table 2). It confirms that the bulk structure of PCN is retained and the relative quantity of the uncondensed units is also unchanged, in spite of the procedures the material underwent.

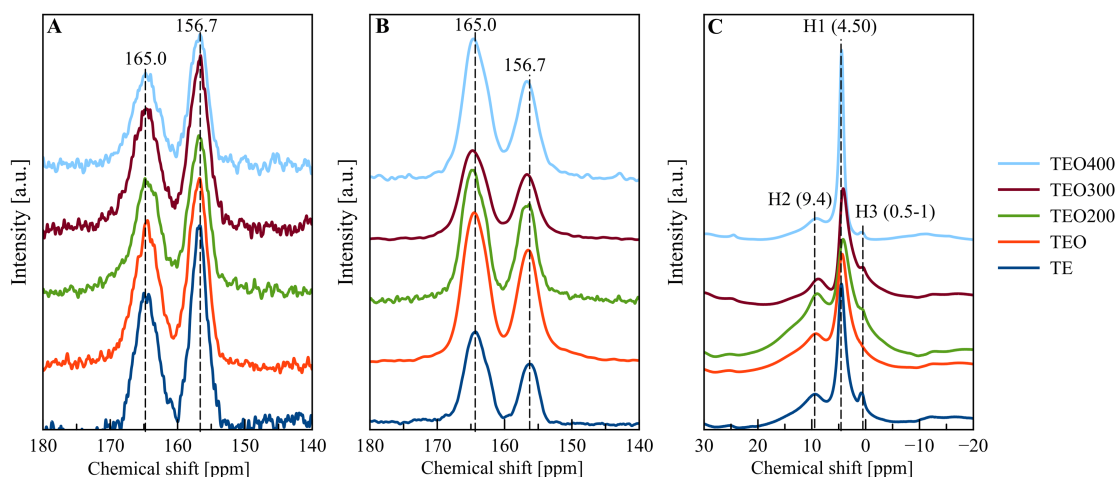


Figure 4 – (A) ^{13}C MAS NMR, (B) ^1H - ^{13}C CPMAS NMR and (C) ^1H MAS NMR spectra of the PCN and PCN- H_2O_2 samples.

RESULTS AND DISCUSSION

Table 2 – Solid state MAS NMR data obtained for the PCN and PCN-H₂O₂ samples.

Samples	¹³ C MAS NMR C _i /C _e ratio	Position of H1 peak [ppm]	HWHM of H1 maximum [Hz]	HWHM of H2 maximum [Hz]	¹ H MAS NMR H2/H1 ratio
TE	1.02	4.5	340	1100	0.63
TEO	0.96	4.3	548	1624	1.06
TEO200	1.00	4.1	520	1888	1.91
TEO300	0.99	4.0	368	748	0.30
TEO400	1.00	4.5	196	904	0.45

One of the characteristic features of PCN is a strong hydrogen bonding of NH₂ and NH functionalities to N atoms of another heptazine [27,53]. There is still no consensus in the assignment of the most intense ¹H maximum in polymerised C₃N₄ heptazines. On the basis of theoretical calculations, it is suggested that the peak at about 4.3 ppm corresponds to the free amino-groups of PCN [54]. However, the alternative view, founded on the experimental data collected from polymerised heptazine (melon), attributes it to the protons of hydrogen-bonded water molecules [53,55]. The decrease of the intensity of this maximum under in-situ heat treatment at 150 °C in NMR apparatus is in accord with the above hypothesis [56]. Although adsorbed water is not a part of the structural PCN unit, the type of its interaction with PCN gives information about the state of the surface species in the photocatalysts. A relatively narrow maximum, of 340 Hz of half-width at half-maximum (HWHM) of the H1 peak centred at approximately 4.5 ppm observed for the TE sample is noticeably broadened to 548 and 520 Hz for the TEO and TEO200 samples, respectively. This could indicate the involvement of water adsorption sites in hydrogen bonding with other species present in PCN-H₂O₂ (Fig. 4C, Fig. S5A-C, Table 2). For TEO300 and TEO400 the corresponding HWHM value is reduced again (Fig. S5D,E, Table 2). This finding suggests that the modification of water adsorption sites in TEO and TEO200 is due to the changes in the hydrogen bonding network caused by the attachment of hydrogen peroxide molecules to the amino-groups and heptazine nitrogen atoms (Fig. 3). On the other hand, TEO400 having its

melon layers well-separated and hydrogen bonding between them significantly reduced demonstrates a narrow peak at 4.5 ppm, which can be attributed to the adsorption of water molecules on well-defined surface sites.

The defect sites in PCN, i.e. NH₂ and NH species, according to Syefarth et al. [55], reveal themselves at 10 and 9.5 ppm, respectively, and a very similar range of chemical shifts, from 8.4 to 10.9, was also proposed by Hu et al [54]. (Fig. 3). On the ¹H MAS NMR spectrum of the MHP adduct, the main peak is centred at 10.9 ppm, and it can be assigned to the protons of H₂O₂ as well as to the developed hydrogen bonding in a melamine peroxosolvate crystal, where one molecule of H₂O₂ is able to interact with six melamine molecules [52] (Fig. S6). The much lower concentration of H₂O₂ in the PCN-H₂O₂ materials and interference of the protons of the NH- and NH₂-groups make it difficult to fully understand the contribution of this peak to the spectra. The deconvolution of the spectra by three Lorentz functions centred at about 4.5 (H1), 9.4 (H2), and 1.0 (H3) ppm indicates that the peak at 9.4 ppm for the TEO and TEO200 samples is significantly broadened and its contribution to the spectra is greater than that of the other PCN samples (Fig. S5, Table 2). This finding can be attributed to the protons of H₂O₂ bonded to carbon nitride and to the displacement of the chemical shift maxima of the NH₂ moieties, due to the formation of hydrogen bonding between amino-groups and heptazine nitrogens mediating H₂O₂ (Fig. 3). The peak at approximately 1.0 ppm (H3) could be assigned to H₂O adsorbed on isolated basic sites of carbon nitride as it occurs on the surface of basic oxides [57].

Electronic structure

The BG of the thermally etched carbon nitride (TE) is 2.76 eV (Fig. 5A, Table 1), which is close to the value reported earlier for the same type of photocatalysts [39]. The VB of this sample is positioned at 1.59 eV, lower than that of the bulk PCN synthesised via the same process [38] (Fig. 5A inset, Table 1). The treatment of the thermally etched polymeric C₃N₄ with H₂O₂ does not change the BG value significantly, although a new absorption edge at lower energies of approximately 2.19 eV appears (Fig. 5B, Table 1). This could be explained by the formation of midgap states in the electronic structure of the PCN-H₂O₂ adduct, which is also deduced from the reduced value of its VB (Fig. 5B, inset). The heat treatment of TEO

RESULTS AND DISCUSSION

causes a slight decrease in the concentration of oxygen belonging to the bonded H_2O_2 (Table 1). Nevertheless, the absorption edge at 2.16 eV is retained (Fig. 5C, Table 1). Moreover, it is obvious that the sample undergoes some other changes, as its BG value decreases to 2.67 eV, while its VB has a potential of 1.52 eV (Fig. 5C inset, Table 1). By considering the strong hydrogen bonding in the TEO and TEO200 samples which is evidenced by NMR studies, it can be hypothesised that the changes in their electronic structures are due to a strong interaction between adjacent carbon nitride units which interact with H_2O_2 . The increase of thermal treatment temperature up to 300 °C results in an almost complete disappearance of the midgap absorption edge observed for the above discussed samples, and in the BG value equal to that of the parent material, TE (Fig. 5D, Table 1). Notably, the VB position maintains the same value of 1.52 eV (Fig. 5D inset, Table 1). The shift of the (002) diffraction maximum observed for TEO400 (Fig. 1) could be related to its thermal etching at high temperatures in an oxidative atmosphere. Indeed, the increase of the BG and VB values is in accord with this hypothesis as the same effect of thermal etching on the BG was also observed elsewhere [39].

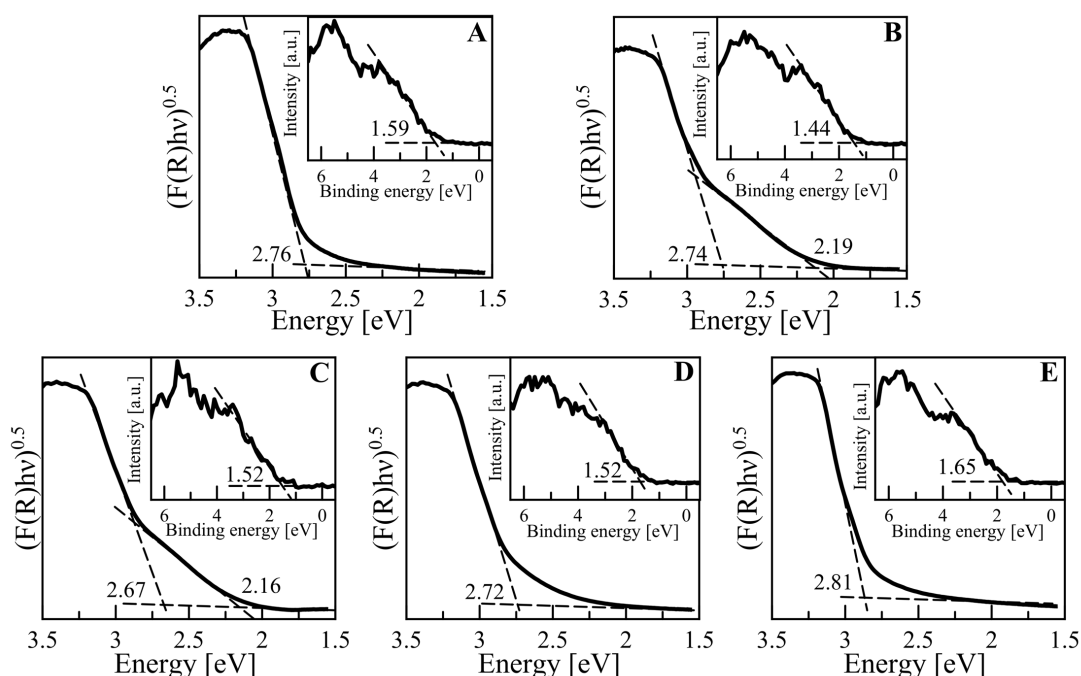


Figure 5 – DR spectra and XPS VB spectra (inset) of (A) TE, (B) TEO, (C) TEO200, (D) TEO300, and (E) TEO400.

The PL spectra registered after the excitation at 365 nm show photoluminescence quenching for the PCN-H₂O₂ samples, which can be explained by the favoured charge separation on strongly hydrogen bonded carbon nitride units. In addition, the appearance of a new PL band for the PCN-H₂O₂ adducts can be noticed (Fig. S7).

N₂ physisorption

All the prepared samples show the adsorption isotherms of IV type with a hysteresis loop of a mixed H3-H4 type corresponding to mesoporous materials with broad pore-size distribution (Fig. S8). The porous structure itself barely changes after the PCN-H₂O₂ adduct is formed and the subsequent thermal treatment is applied, however, the differences in SSA values are drastic (Fig. S8, Table 1). The SSA of TEO is reduced to 70 m²·g⁻¹ compared to 94 m²·g⁻¹ of TE (Table 1). The SSAs of TEO200 and TEO300 are smaller, i.e. 23 and 30 m²·g⁻¹, respectively (Table 1, Fig. S8). It has already been proposed while discussing the XRD and DRS data that TEO400 shows the features characteristic of thermally etched carbon nitride. Indeed, the increase of its SSA value up to 168 m²·g⁻¹ unambiguously confirms this supposition (Table 1, Fig. S8).

TPD-MS analysis of the PCN and PCN-H₂O₂ samples

The MS analysis of the volatile substances evolved during the thermal treatment of the TE and TEO samples under inert atmosphere shows the presence of 18 amu attributed to adsorbed or chemically bonded H₂O in PCN (Fig. S9A). For the TE sample water removal ends at about 200 °C, while the additional smaller peak observed for TEO around 300 °C could be due to H₂O formed in the result of the bonded H₂O₂ decomposition (Fig. S9A inset). The materials release CO₂ (44 amu) at different temperatures that might be attributed to the modification of the basic adsorption surface sites in the PCN-H₂O₂ or to the release of O₂ during the PCN-H₂O₂ heating, which can partially oxidise surface carbon nitride species (Fig. S9B). Three more gaseous products with mass numbers 32, 30, and 28 amu, respectively assigned to O₂, NO, and N₂, are detected only for the TEO sample (Fig. S9C-E). These species are produced as a result of the bonded H₂O₂ decomposition and the oxidation of the surface carbon nitride groups (Fig. S9C-E). The findings corresponding to the O₂ and N₂ generation during the adduct decomposition are consistent with the proposed thermal

degradation pathway of another H₂O₂ complex compound urea-hydrogen peroxide adduct [58]. Summarizing, the PCN-H₂O₂ is likely to contain a weakly bonded hydrogen peroxide, which decomposes at temperatures below 200 °C producing H₂O and O₂ but also strongly bonded peroxy species, whose thermal degradation gives rise to oxidation of the surface C–NHx-groups producing gaseous NO, CO₂ and N₂.

HMF partial photo-oxidation to FDC under UV-irradiation

The adsorption capacity of the photocatalysts did not exceed 1% of the initial HMF concentration. Photolyses of the substrate and of the principal reaction product were determined for the used photocatalytic set-up earlier [39]. The possible release of H₂O₂ by the PCN-H₂O₂ photocatalysts into water suspensions was tested. No H₂O₂ was found in the aqueous suspension of photocatalysts when it was heated up to 50 °C, while negligible quantities, not exceeding 6.6 μmol of H₂O₂ per 1 g of the PCN-H₂O₂ adduct, were released at boiling point.

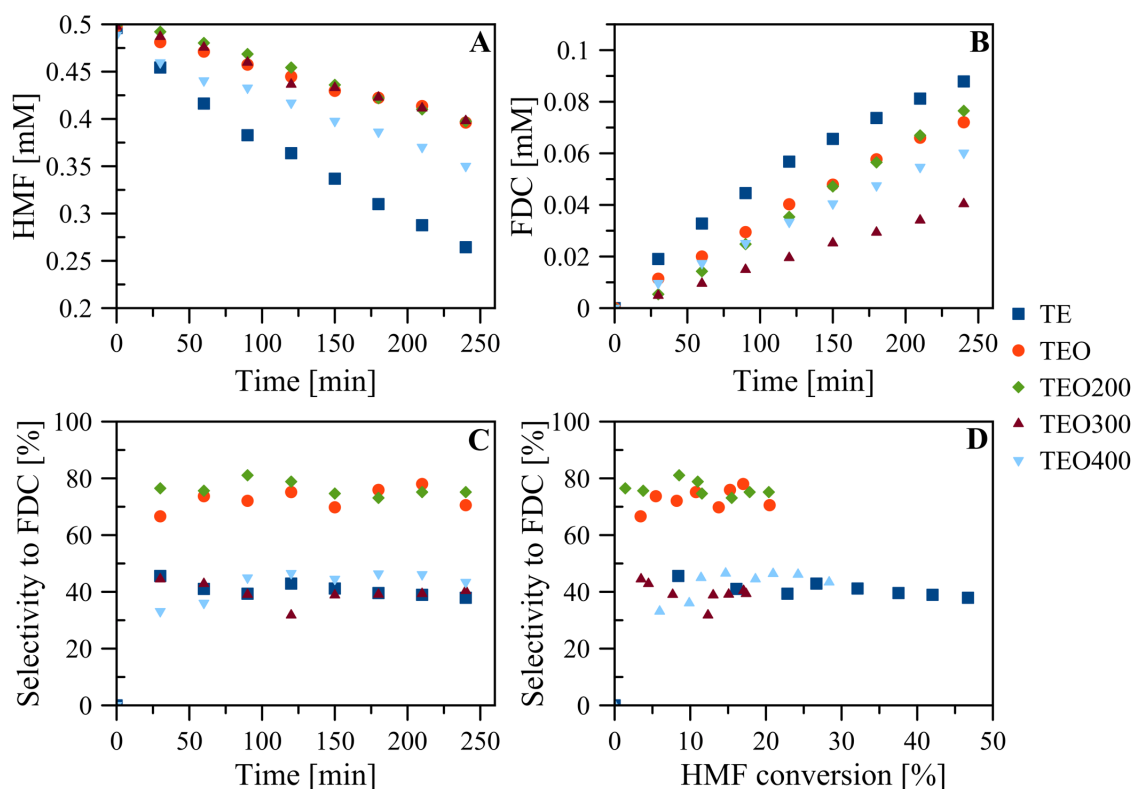


Figure 6 – (A) HMF and (B) FDC concentrations and (C) selectivity to FDC formation versus reaction time; (D) selectivity to FDC versus HMF conversion for the prepared photocatalysts under UV irradiation.

Expectedly, under UV irradiation the thermally etched PCN (TE) shows high HMF conversion approaching 47%, which is close to that reported elsewhere [39]. Also, it is the most active sample among all the tested ones (Fig. 6A, Table 3). The treatment of TE with hydrogen peroxide results in almost three times less active photocatalyst (TEO), due probably to its reduced SSA ($70 \text{ m}^2 \cdot \text{g}^{-1}$) (Fig. 6A, Table 3) and to the blockage of certain carbon nitride surface sites to which H_2O_2 is attached. Despite the further reduction of the SSA observed for the thermally treated PCN- H_2O_2 adducts at 200 °C (TEO200) and 300 °C (TEO300), the HMF conversion degree barely changes (Fig. 6A). The explanation of this finding could be found in the improved charge transfer and charge separation occurring on strongly hydrogen bonded melon units. The activity of the TEO400 sample, however, was found higher than that of TEO300, but still less significant than that of TE (Fig. 6A). Although the SSA of TEO400 is the highest among all of the tested materials, this property does not exclusively

RESULTS AND DISCUSSION

determine the photocatalytic performance of carbon nitride materials. Considering other differences in the TE and TEO400 features, the only one able to explain the decreased photoactivity is the low surface oxygen content and lower O 1s binding energy value of the latter (Table 1). It might be an indication of a higher strength of TEO400 basic sites, hence the presence of strongly bonded adsorbed oxygen species [59], whose removal from the surface in a form of radicals is hindered.

Table 3 – HMF initial conversion rate (r) under UV irradiation, HMF conversion and selectivity values under UV and natural solar light irradiation.

Sample	UV				Natural solar light				Selectivity at 20% of HMF conversion [%]	
	Initial HMF conversion rate $\cdot 10^2$ [mM min ⁻¹]	Initial FDC formation rate $\cdot 10^2$ [mM min ⁻¹]	0.99 kJ (4 h)		0.99 kJ (~ 2 h)		1.8 kJ (~ 4 h)		UV	Natural solar light
			HMF Conversion [%]	Selectivity to FDC [%]	HMF Conversion [%]	Selectivity to FDC [%]	HMF Conversion [%]	Selectivity to FDC [%]		
TE	0.130	0.058	47	38	47	40	74	31	40	45
TEO	0.047	0.036	21	71	21	88	37	83	71	88
TEO200	0.037	0.029	20	75	30	77	51	75	75	73
TEO300	0.040	0.016	20	48	16	52	33	46	47	50
TEO400	0.069	0.021	28	43	34	42	58	35	46	44

The highest amount of FDC produced during the photocatalytic HMF conversion was observed for the TE sample, while for TEO300 this value was the lowest one (Fig. 6B, Table 3). Despite the reduced conversion degree, TEO demonstrates significantly improved selectivity for the FDC production reaching 71% at 20% of HMF conversion, while the corresponding value for the thermally etched PCN is only 40% (Table 3, Fig. 6C). Moreover, the selectivity is also maintained on a nearly the same level throughout the reaction (Fig. 6C).

Subjecting the PCN-H₂O₂ adduct to thermal treatment at 200 °C (TEO200) does not affect the selectivity to FDC formation (Fig. 6C). For the TEO300 and TEO400 samples, the selectivity is very similar to that of TE (Fig. 6C). This can be attributed to the drop in the content of oxygen corresponding to the presence of H₂O₂ in the PCN-H₂O₂ adduct (Table 1). The relation of selectivity to FDC formation versus HMF conversion represented in Figure 6D indicates that the PCN-H₂O₂ adduct samples have higher selectivity to FDC production at the same conversion extent than TE, TEO300 and TEO400 (Table 3). For the TEO and TEO200 photocatalysts, similar values of the rates of HMF conversion and FDC formation are obtained, indicating that HMF to FDC oxidation is the primary process occurring in the irradiated suspension (Table 3). For the other materials (TE, TEO300, TEO400) the respective values differ by more than a factor of 2 because parallel reactions take place (Table 3). There are several factors responsible for HMF to FDC selectivity being below 100 %. Once FDC is produced in the reaction suspension, it is slowly photolysed to FFA (Fig. S10). Another factor contributing to the selectivity loss, especially in case of the TE, TEO300 and TEO400 samples, is the direct oxidation of HMF to aliphatic carboxylic acids, detected but not identified in the present work.

The sample prepared by the thermal etching of the PCN-H₂O₂ adduct at 450 °C (TEO450) has also been studied. Although it shows an HMF conversion degree higher than that of TE, it does not demonstrate any improvement of the selectivity (Fig. S11). The alternative method of H₂O₂-modification via refluxing the suspension of H₂O₂ and TE resulted in the formation of the TEO_R photocatalyst having mild reaction rate and selectivity of about 60%, which is lower than that observed for TEO (Fig. S11).

The recoverability of the TEO photocatalyst was tested in three consecutive reaction cycles under UV irradiation. TEO maintains the same conversion degree and the selectivity to FDC formation equal to 19-21% and 68-82%, respectively, thus proving itself as an efficient photocatalyst for the partial photo-assisted HMF oxidation (Fig. S12).

HMF partial photo-oxidation to FDC under solar light

PCN is an attractive photocatalyst for reactions occurring under solar light, due to the electronic structure which allows its activation under visible-light irradiation. Unsurprisingly,

RESULTS AND DISCUSSION

the reaction rate under sunlight is significantly improved for all of the tested materials with respect to that achieved under the UV lamps, which is attributed to the higher UV photon flux of the outdoor irradiation (Fig. 7A, Table 3). The most active TE sample is capable of oxidising almost all of the substrate within the reaction time, while other photocatalysts show degrees of conversion nearly twice increased with respect to those obtained under the UV-source used (Fig. 7A, Table 3). The comparison of the cumulative energies entering the UV and solar-light reactors shows that the photocatalytic activity is almost directly proportional to the energy of irradiation with wavelengths from 315 to 400 nm (Table 3). However, the performance of TEO200 stands aside of the common trend, which is most probably due to its narrower BG with respect to those of the other tested photocatalysts (Fig. 7A, Table 3). The concentration of FDC, for the TE and TEO400 samples, increases with the cumulative energy up to about 1.65 kJ, after which a plateau is observed (Fig. 7B). This finding can be explained by considering the high extent of conversion achieved in the presence of these samples because the product itself becomes a target for photo-produced radical species after most of the substrate is oxidised. As far as the selectivity is concerned, no significant differences can be noticed between the results obtained under UV irradiation and solar light (Fig. 7C). The selectivity toward FDC approaches 100% at low HMF conversion values in the presence of the TEO sample, while it ranges between 70 to 80% for moderate and high conversions in the cases of the TEO and TEO200 samples. These figures are higher than the corresponding ones attained by the thermally etched PCN (TE), TEO300 and TEO400 samples (Fig. 7D).

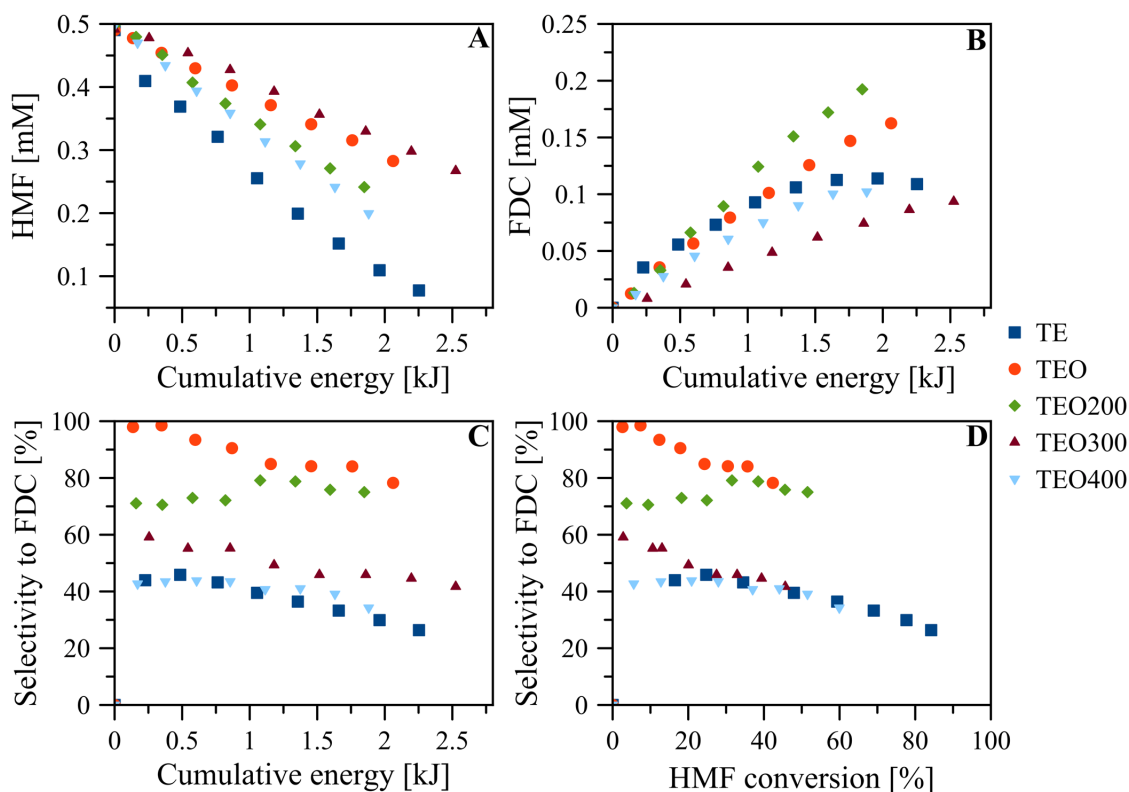


Figure 7 – (A) HMF and (B) FDC concentrations and (C) selectivity to FDC formation versus cumulative energy; (D) selectivity to FDC versus HMF conversion for the prepared photocatalysts under solar light irradiation.

Additional tests to prove the effectiveness of the TEO sample for the conversion of HMF to FDC at enhanced concentrations of the substrate (1 and 2 mM) were performed. The quantity of HMF converted is found to be in a nearly direct dependency from the initial HMF concentration (Fig. 8A). TEO converts 15.6 μmol of HMF when the initial substrate concentration is 0.5 mM, while 30.5 and 56.3 μmol are converted when the initial concentrations are 1.0 and 2.0 mM, respectively (Fig. 8A). Figure 8B shows that the selectivity to FDC decreases by increasing HMF initial concentration (Fig. 8B), however, it appears to be on the same level when plotted against the quantity of HMF reacted (Fig. 8C).

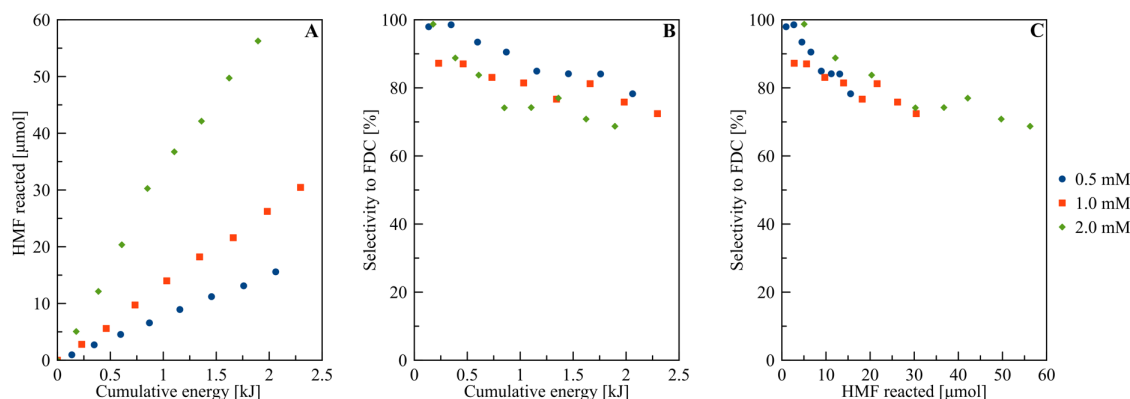


Figure 8 – (A) HMF reacted and (B) selectivity to FDC versus cumulative energy; (C) selectivity to FDC formation versus amount of HMF reacted in the presence of the TEO photocatalyst under solar light irradiation at varying initial HMF concentrations.

A dramatic effect on the selectivity of the photo-oxidation of HMF to FDC, consequent to the formation of the PCN- H_2O_2 adduct, could be attributed to the type of interaction of the substrate molecules with some carbon nitride surface sites. In a previous study on the HMF photo-oxidation in the presence of thermally exfoliated PCN, the selectivity to FDC up to 75% was obtained in the organic solvent [39], and this value is close to that found in the present work for the PCN- H_2O_2 adducts in aqueous medium. The presence of water could have a detrimental effect on the reaction selectivity. Indeed, the test for hydroxyl radicals generation by TA method confirms their formation, and in particular that TE produces higher quantities of $\bullet\text{OH}$ than TEO (Fig. S13). It is commonly accepted that PCN cannot form $\bullet\text{OH}$ radicals by directly oxidising water with photo-generated holes, whilst it is possible by the action of photo-generated electrons mediating H_2O_2 formation [60]. Nonetheless, we have not observed the photocatalytic production H_2O_2 in the absence of the substrate. Another pathway could also be considered: the non-polymerised C_3N_4 species bearing Brønsted basic sites, i.e. amino-groups, form hydrogen bonds in water suspension, giving positively charged $-\text{NH}^{3+}$ surface moieties [61] (Fig. 9A). The coordination of water in this way allows it being attacked by the photo-generated holes ripping off electrons from the H_2O molecules and forming $\bullet\text{OH}$ radicals, which are not produced on the polymerised aromatic units of carbon nitride, due to the low potential of its VB [28] (Fig. 9A). For the thermally etched PCN photocatalyst, the NH_2 functionalities, where the produced $\bullet\text{OH}$ radicals are localized, are

accessible for the interaction with HMF, which can be attached to the uncondensed carbon nitride species in a similar way as it was proposed for an aromatic compound [41]. The reaction of HMF with hydroxyl radical leads to the ring opening and the formation of aliphatic intermediates, observed but not studied in this work, thus reducing the selectivity of the photo-oxidation reaction toward the formation of FDC (Fig. 9B). On the other hand, H₂O₂ blocks the amino-groups of the PCN-H₂O₂ adducts, thus creating a steric hindrance for the HMF molecule interaction with the carbon nitride surface sites (Fig. 9C). Therefore, the PCN-H₂O₂ samples favour higher selectivity to FDC formation, whilst the HMF conversion rates appear lower, due to the absence of hydroxyl radicals action and to the smaller SSAs of these photocatalysts (Fig. 9C).

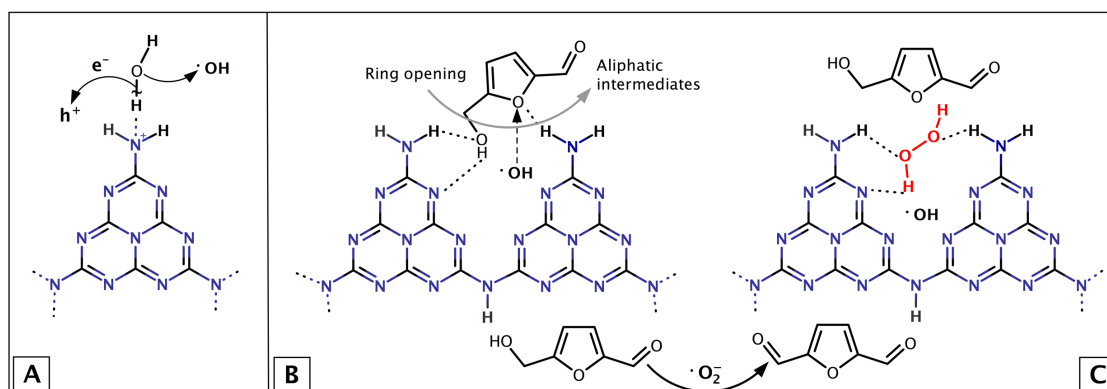


Figure 9 – (A) Hypothetical mechanism of hydroxyl radical formation on PCN basic sites; (B) proposed types of interaction and photo-oxidation of HMF on PCN, and (C) on PCN-H₂O₂.

Conclusions

PCN reacts with H₂O₂ producing PCN-H₂O₂ adduct stable up to 200 °C in air. The formed material does not release H₂O₂ into the suspension in aqueous medium and under irradiation, thus ensuring its usability for photocatalytic applications. The result of H₂O₂ bonding to the carbon nitride partially polymerised and non-polymerised sites is the development of hydrogen bonding network within the material. The formation of the adduct is also responsible for the blockage of NH₂ functional groups, which are detrimental for the selective

partial photocatalytic oxidation of HMF to FDC. The bonded H₂O₂ creates a steric hindrance for the HMF interaction with amino-groups, where •OH radicals, driving to furanic ring opening and hence unselective oxidation of the substrate, are probably localized. Although it reduces the activity of PCN-H₂O₂, the elimination from the reaction process of the pathway involving the action of hydroxyl radicals leads to the enhancement of the selectivity toward the FDC production under outdoor illumination from 45% to 88% at 20% of HMF conversion. Moreover, the prepared PCN-H₂O₂ adduct photocatalyst proved itself recoverable and efficient in the solar light assisted conversion of HMF even at high initial concentrations of the substrate. The present work has underlined the importance of the modification of the surface species of PCN for its improved performance in partial photo-oxidation reactions.

Conflicts of interest

There are no conflicts to declare.

Acknowledgements

We gratefully acknowledge financial support from the Spanish MINECO (MAT2013-40950-R, MAT2016-78155-C2-1-R, CTQ2014-52956-C3-1-R, and Severo Ochoa PhD grant BP-14-029 to M.I.) and FEDER. IK acknowledges financial support from Ministry of Education and Science of the Russian Federation (grant No 4.9722.2017/8.9) and grateful for the support by Act 211 Government of the Russian Federation, contract № 02.A03.21.0011.

Notes and references

1. S. Suganuma, K. Nakajima, M. Kitano, D. Yamaguchi, Hydrolysis of Cellulose by Amorphous Carbon Bearing SO₃H, COOH, and OH Groups, *J. Am. Chem. Soc.*, **2008**, 130, 12787–12793.
2. J.N. Chheda, Y. Roman-Leshkov, J.A. Dumesic, Production of 5-hydroxymethylfurfural and furfural by dehydration of biomass-derived mono- and poly-saccharides, *Green Chem.*, **2007**, 9, 342–350.

3. G.Z. Papageorgiou, D.G. Papageorgiou, Z. Terzopoulou, D.N. Bikiaris, Production of bio-based 2,5-furan dicarboxylate polyesters: Recent progress and critical aspects in their synthesis and thermal properties, *Eur. Polym. J.*, **2016**, 83, 202–229.
4. A.F. Sousa, C. Vilela, A.C. Fonseca, M. Matos, C.S.R. Freire, G.-J.M. Gruter, J.F.J. Coelho, A.J.D. Silvestre, Biobased polyesters and other polymers from 2,5-furandicarboxylic acid: a tribute to furan excellency, *Polym. Chem.*, **2015**, 6, 5961–5983.
5. I. Delidovich, P.J.C. Hausoul, L. Deng, R. Pfützenreuter, M. Rose, R. Palkovits, Alternative monomers based on lignocellulose and their use for polymer production, *Chem. Rev.*, **2016**, 116, 1540–1599.
6. A.S. Amarasekara, D. Green, L.D. Williams, Renewable resources based polymers: Synthesis and characterization of 2,5-diformylfuran–urea resin, *Eur. Polym. J.*, **2009**, 45, 595–598.
7. T. Xiang, X. Liu, P. Yi, M. Guo, Y. Chen, C. Wesdemiotis, Y. Pang, Schiff base polymers derived from 2,5-diformylfuran, *Polym. Int.*, **2013**, 62, 1517–1523.
8. J.M.R. Gallo, D.M. Alonso, M.A. Mellmer, J.A. Dumesic, Production and upgrading of 5-hydroxymethylfurfural using heterogeneous catalysts and biomass-derived solvents, *Green Chem.*, **2013**, 15, 85–90.
9. X. Tong, Y. Ma, Y. Li, Biomass into chemicals: Conversion of sugars to furan derivatives by catalytic processes, *Appl. Catal. A: Gen.*, **2010**, 385, 1–13.
10. I. Sadaba, Y.Y. Gorbanev, S. Kegnæs, S. Reddy, Catalytic performance of zeolite-supported vanadia in the aerobic oxidation of 5-hydroxymethylfurfural to 2,5-diformylfuran, *ChemCatChem.*, **2013**, 5, 284–293.
11. C. Carlini, P. Patrono, A. Maria, R. Galletti, Selective oxidation of 5-hydroxymethyl-2-furaldehyde to furan-2,5-dicarboxaldehyde by catalytic systems based on vanadyl phosphate, *Appl. Catal. A: Gen.*, **2005**, 289, 197–204.
12. J. Nie, J. Xie, H. Liu, Efficient aerobic oxidation of 5-hydroxymethylfurfural to 2,5-diformylfuran on supported Ru catalysts, *J. Catal.*, **2013**, 301, 83–91.

13. F. Neat, N. Petrea, R. Petre, V. Somoghi, M. Florea, V.I. Parvulescu, Oxidation of 5-hydroxymethyl furfural to 2,5-diformylfuran in aqueous media over heterogeneous manganese based catalysts, *Catal. Today*, **2016**, 278, 66–73.
14. M. Chatterjee, T. Ishizaka, A. Chatterjee, H. Kawanami, Dehydrogenation of 5-hydroxymethylfurfural to diformylfuran in compressed carbon dioxide: an oxidant free approach, *Green Chem.*, **2017**, 19, 1315–1326.
15. Y. Shiraishi, T. Hirai, Selective organic transformations on titanium oxide-based photocatalysts, *J. Photochem. Photobiol. C: Photochem. Rev.*, **2008**, 9, 157–170.
16. X. Lang, W. Ma, C. Chen, H. Ji, J. Zhao, Selective Aerobic Oxidation Mediated by TiO₂ Photocatalysis, *Acc. Chem. Res.*, **2014**, 47, 355–363.
17. V. Augugliaro, G. Camera-roda, V. Loddo, L. Palmisano, J. Soria, S. Yurdakal, Heterogeneous Photocatalysis and Photoelectrocatalysis: From Unselective Abatement of Noxious Species to Selective Production of High-Value Chemicals, *J. Phys. Chem., Lett*, **2015**, 6, 1968–1981.
18. G. Palmisano, A. Albini, G. Marci, L. Palmisano, D. Ravelli, New synthetic routes in heterogeneous photocatalysis, *RSC Energy Environ. Series.*, **2016**, 15, 303–344.
19. X. Lang, J. Zhao, Heterogeneous visible light photocatalysis for selective organic transformations, *Chem Soc Rev.*, **2014**, 43, 473–486.
20. J. Kou, C. Lu, J. Wang, Y. Chen, Z. Xu, R.S. Varma, Selectivity enhancement in heterogeneous photocatalytic transformations, *Chem. Rev.*, **2017**, 117, 1445–1514.
21. D.W. Wakerley, M.F. Kuehnel, K.L. Orchard, K.H. Ly, T.E. Rosser, E. Reisner, Solar-driven reforming of lignocellulose to H₂ with a CdS/CdOx photocatalyst, *Nature Energ.*, **2017**, 2, 17021.
22. S.-H. Li, S. Liu, J.C. Colmenares, Y.-J. Xu, A sustainable approach for lignin valorization by heterogeneous photocatalysis, *Green Chem.*, **2016**, 18, 594–607.
23. G. Chatel, S. Valange, R. Behling, J.C. Colmenares, A Combined approach using sonochemistry and photocatalysis: how to apply sonophotocatalysis for biomass conversion?, *ChemCatChem.*, **2017**, 9, 2615–2621.
24. L. Ozcan, P. Yalcin, O. Alagoz, S. Yurdakal, Selective photoelectrocatalytic oxidation of 5-(hydroxymethyl)-2-furaldehyde in water by using Pt loaded nanotube structure of TiO₂ on Ti photoanodes, *Catal. Today.*, **2017**, 281, 205–213.

25. S. Yurdakal, B. S. Tek, O. Alagöz, V. Augugliaro, V. Loddo, G. Palmisano, L. Palmisano, Photocatalytic Selective Oxidation of 5-(Hydroxymethyl)-2-furaldehyde to 2,5-Furandicarbaldehyde in Water by Using Anatase, Rutile, and Brookite TiO₂ Nanoparticles, *ACS Sustain. Chem. Eng.*, **2013**, 1, 456–461.
26. I. Krivtsov, M. Ilkaeva, E. Salas-Colera, Z. Amghouz, J.R. García, E. Díaz, S. Ordoñez, S. Villar-Rodil, Consequences of Nitrogen Doping and Oxygen Enrichment on Titanium Local Order and Photocatalytic Performance of TiO₂ Anatase, *J. Phys. Chem. C.*, **2017**, 121, 6770–6780.
27. F.K. Kessler, Y. Zheng, D. Schwarz, C. Merschjann, W. Schnick, X. Wang, M.J. Bojdys, Functional carbon nitride materials — design strategies for electrochemical devices, *Nature Mater.*, **2017**, 2, 17030.
28. X. Wang, K. Maeda, A. Thomas, K. Takanabe, G. Xin, J.M. Carlsson, K. Domen, M. Antonietti, A metal-free polymeric photocatalyst for hydrogen production from water under visible light, *Nat. Mater.*, **2008**, 8, 76–80.
29. X. Dai, M. Xie, S. Meng, X. Fu, S. Chen, Coupled systems for selective oxidation of aromatic alcohols to aldehydes and reduction of nitrobenzene into aniline using CdS/g-C₃N₄ photocatalyst under visible light irradiation, *Appl. Catal. B: Environ.*, **2014**, 158–159, 382–390.
30. F. Su, S. C. Mathew, G. Lipner, X. Fu, M. Antonietti, S. Blechert, X. Wang, mpg-C₃N₄-Catalyzed selective oxidation of alcohols using O₂ and visible light, *J. Am. Chem. Soc.*, **2010**, 123, 16299–16301.
31. J. Xu, L. Luo, G. Xiao, Z. Zhang, H. Lin, X. Wang, J. Long, Layered C₃N₃S₃ polymer/graphene hybrids as metal-free catalysts for selective photocatalytic oxidation of benzylic alcohols under visible light, *ACS Catal.*, **2014**, 4, 3302–3306.
32. S. Verma, R.B.N. Baig, M.N. Nadagouda, R.S. Varma, Selective oxidation of alcohols using photoactive VO@g-C₃N₄, *ACS. Sustain. Chem. Eng.*, **2016**, 4, 1094–1098.
33. X. Chen, J. Zhang, X. Fu, M. Antonietti, X. Wang, Fe-g-C₃N₄-Catalyzed oxidation of benzene to phenol using hydrogen peroxide and visible light, *J. Am. Chem. Soc.*, **2009**, 131, 11658–11659.

-
34. X.-H. Li, X. Wang, M. Antonietti, Solvent-Free and metal-free oxidation of toluene using O₂ and g-C₃N₄ with nanopores: nanostructure boosts the catalytic selectivity, *ACS Catal.*, **2012**, 2, 2082–2086.
35. X.-H. Li, J.-S. Chen, X. Wang, J. Sun, M. Antonietti, Metal-Free activation of dioxygen by graphene/g-C₃N₄ nanocomposites: functional dyads for selective oxidation of saturated hydrocarbons, *J. Am. Chem. Soc.*, **2011**, 133, 8074–8077.
36. Z. Ding, X. Chen, M. Antonietti, X. Wang, Carbon Nitride for the selective oxidation of aromatic alcohols in water under visible light, *ChemSusChem.*, **2011**, 4, 274–281.
37. B. Long, Z. Ding, X. Wang, Carbon nitride for the selective oxidation of aromatic alcohols in water under visible light, *ChemSusChem.*, **2013**, 6, 2074–2078.
38. M. Bellardita, E.I. García-López, G. Marci, I. Krivtsov, J.R. García, L. Palmisano, Selective photocatalytic oxidation of aromatic alcohols in water by using P-doped g-C₃N₄, *Appl. Catal. B: Environ.*, **2018**, 220, 222–233.
39. I. Krivtsov, E.I. García-López, G. Marci, L. Palmisano, Z. Amghouz, J.R. García, E. Díaz, S. Ordóñez, Selective photocatalytic oxidation of 5-hydroxymethyl-2-furfural to 2,5-furandicarboxyaldehyde in aqueous suspension of g-C₃N₄, *Appl. Catal., B: Environ.*, **2017**, 204, 430–439.
40. A. Akhundi, E.I. García-López, G. Marci, A. Habibi-Yangjeh, L. Palmisano, Comparison between preparative methodologies of nanostructured carbon nitride and their use as selective photocatalysts in water suspension, *Res. Chem. Intermed.*, **2017**, 43, 5153–5168.
41. M. Ilkaeva, I. Krivtsov, E.V. Bartashevich, S. Khainakov, J.R. García, E. Díaz, S. Ordóñez, Carbon nitride assisted chemoselective C–H bond photo-oxidation of alkylphenoethoxylates in water medium, *Green Chem.*, **2017**, 19, 4299–4304.
42. K. Wang, Q. Li, B. Liu, B. Cheng, W. Ho, J. Yu, Sulfur-doped g-C₃N₄ with enhanced photocatalytic CO₂-reduction performance, *Appl. Catal. B: Environ.*, **2015**, 176–177, 44–52.
43. P. Niu, L. Zhang, G. Liu, H.-M. Chen, Graphene-like carbon nitride nanosheets for improved photocatalytic activities, *Adv. Funct. Mater.*, **2012**, 22, 4763–4770.

-
44. V. Augugliaro, E.I. García-López, V. Loddo, S. Malato-Rodriguez, I. Maldonado, G. Marci, R. Molinari, L. Palmisano, Degradation of lincomycin in aqueous medium: Coupling of solar photocatalysis and membrane separation, *Solar Energy*, **2005**, 79, 402–408.
 45. T. Hirakawa, Y. Nosaka, Properties of $O_2^{\cdot-}$ and OH^{\cdot} formed in TiO_2 aqueous suspensions by photocatalytic reaction and the influence of H_2O_2 and some ions, *Langmuir*, **2002**, 18, 3247–3254.
 46. S. Liu, D. Li, H. Sun, H. Ming, M. O. Tadé, S. Wang, Oxygen functional groups in graphitic carbon nitride for enhanced photocatalysis, *J. Colloid Interface Sci.*, **2016**, 468, 176–182.
 47. J. Li, B. Shen, Z. Hong, B. Lin, B. Gao, Y. Chen, Enhanced visible light photocatalytic activity and oxidation ability of porous graphene-like $g-C_3N_4$ nanosheets via thermal exfoliation, *Chem. Comm.*, **2012**, 4, 12017–12019.
 48. F. Dong, Y. Li, Z. Wang, W. Ho, Enhanced visible light photocatalytic activity and oxidation ability of porous graphene-like $g-C_3N_4$ nanosheets via thermal exfoliation, *Appl. Surf. Sci.*, **2015**, 358, 393–403.
 49. B. Marchon, J. Carrazza, H. Heinemann, G. A. Somorjai, TPD and XPS studies of O_2 , CO_2 , and H_2O adsorption on clean polycrystalline graphite, *Carbon*, **1988**, 26, 507–514.
 50. T. Nagaishi, M. Matsumoto, S. Yoshigana, Thermal decomposition of the addition compound of melamine with hydrogen peroxide, *J. Therm. Anal. Calorim.*, **1990**, 36, 55–60.
 51. G. Chehardoli, M.A. Zolfigol, Melamine Hydrogen Peroxide (MHP): Novel and Efficient Reagent for the Chemo- and Homoselective and Transition Metal-Free Oxidation of Thiols and Sulfides, *Phosphorus, Sulfur Silicon Relat. Elem.*, **2010**, 185, 193–203.
 52. I.Yu. Chernyshov, M.V. Vener, P.V. Prihodchenko, A.G. Medvedev, O. Lev, A.V. Churakov, Peroxosolvates: formation criteria, H_2O_2 hydrogen bonding, and isomorphism with the corresponding hydrates, *Cryst. Growth Des.*, **2017**, 17, 214–220.

-
53. L. Seyfarth, J. Senker, An NMR crystallographic approach for the determination of the hydrogen substructure of nitrogen bonded protons, *Phys. Chem. Chem. Phys.*, **2009**, 11, 3522–3531.
54. Y. Hu, Y. Shim, J. Oh, S. Park, S. Park, Y. Ishii, Synthesis of ^{13}C -, ^{15}N -labeled graphitic carbon nitrides and NMR-based evidence of hydrogen-bonding assisted two-dimensional assembly, *Chem. Mater.*, **2017**, 29, 5080–5089.
55. L. Seyfarth, J. Seyfarth, B. V. Lotsch, W. Schnick, J. Senker, Tackling the stacking disorder of melon—structure elucidation in a semicrystalline material, *Phys. Chem. Chem. Phys.*, **2010**, 12, 2227–2237.
56. W.J. Gammon, G.L. Hoatson, B.C. Holloway, R.L. Vold, A.C. Reilly, Bonding in hard and elastic amorphous carbon nitride films investigated using ^{15}N , ^{13}C , and ^1H NMR spectroscopy, *Phys. Rev. B.*, **2003**, 68, 195401.
57. M.A. Aramendía, J.A. Benítez, V. Borau, C. Jiménez, J.M. Marinas, J.R. Ruiz, F. Urbano, Study of MgO and Pt/MgO Systems by XRD, TPR, and ^1H MAS NMR, *Langmuir*, **1999**, 15, 1192–1197.
58. R. Matyas, J. Selesovsky, V. Pelikan, M. Szala, S. Cudzilo, W. A. Trzcinsky, M. Gozin, Explosive properties and thermal stability of urea-hydrogen peroxide adduct, *Propellant. Explosiv. Pyrotech.*, **2017**, 42, 198–203.
59. E. Díaz, E. Muñoz, A. Vega, S. Ordóñez, Enhancement of the CO_2 retention capacity of Y zeolites by Na and Cs treatments: effect of adsorption temperature and water treatment, *Ind. Eng. Chem. Res.*, **2008**, 47, 412–418.
60. J. Liu, T. An, Z. Chen, Z. Wang, H. Zhou, T. Fan, D. Zhang, M. Antonietti, Carbon nitride nanosheets as visible light photocatalytic initiators and crosslinkers for hydrogels with thermoresponsive turbidity, *J. Mater. Chem. A.*, **2017**, 5, 8933–8938.
61. S. Li, K. Su, Z. Li, B. Cheng, Selective oxidation of 5-hydroxymethylfurfural with H_2O_2 catalyzed by a molybdenum complex, *Green Chem.*, **2016**, 18, 2122–2128.

SUPPLEMENTARY INFORMATION

**Selective Photocatalytic Oxidation of 5-Hydroxymethylfurfural to
2,5-Furandicarboxaldehyde by Polymeric Carbon Nitride-
Hydrogen Peroxide Adduct**

Marina Ilkaeva,^a Igor Krivtsov,^{*a,b} Elisa I. García-López,^c Giuseppe Marci,^c Olena Khainakova,^a José Rubén García,^a Leonardo Palmisano,^c Eva Díaz,^d Salvador Ordóñez^d

^aDepartments of Organic and Inorganic Chemistry, Physical and Analytical Chemistry, University of Oviedo-CINN, 33006 Oviedo, Spain.

^bNanotechnology Education and Research Center, South Ural State University, 454080 Chelyabinsk, Russia.

^c“Schiavello-Grillone” Photocatalysis Group. Dipartimento di Energia, Ingegneria dell’informazione e modelli Matematici (DEIM), Università di Palermo, Viale delle Scienze, 90128 Palermo, Italy.

^dDepartment of Chemical and Environmental Engineering, University of Oviedo, 33006 Oviedo, Spain.

*Corresponding author: krivtsovigor@uniovi.es, Tel.: +34 985 103 030

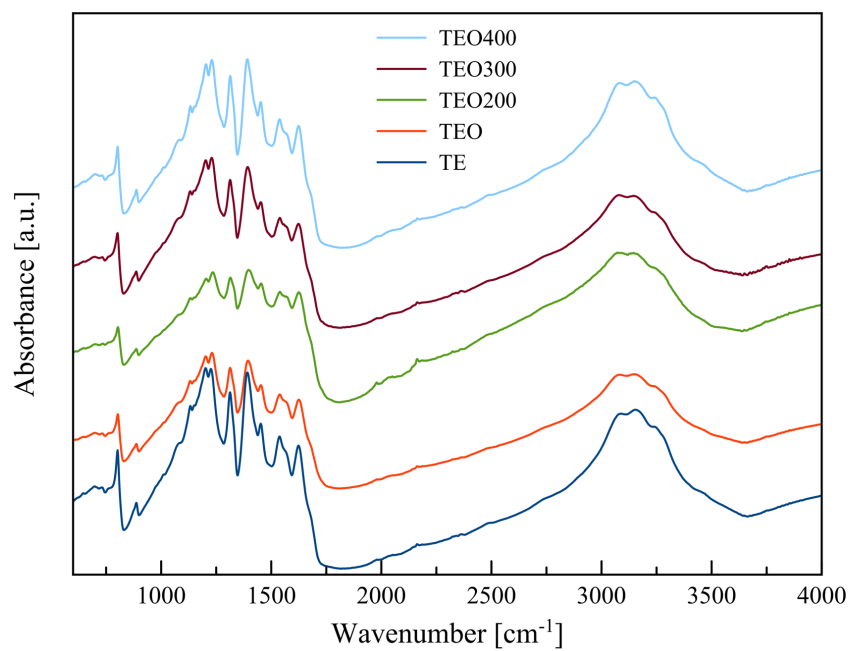
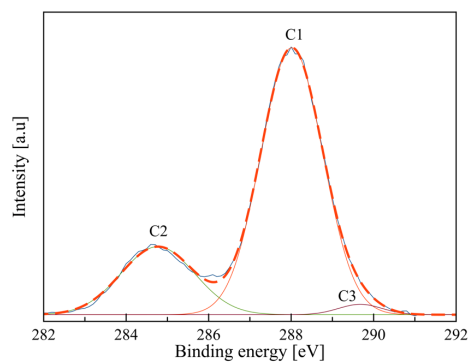
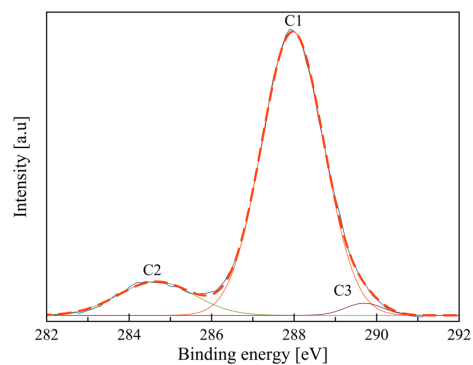


Figure S1 – FTIR spectra of the prepared PCN samples.

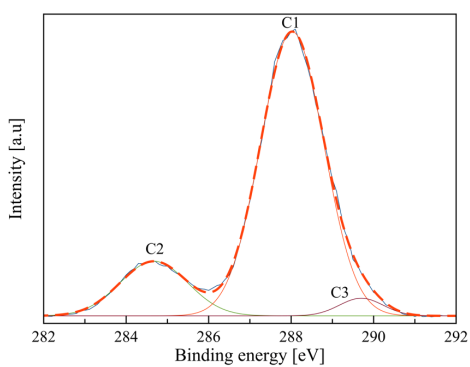
RESULTS AND DISCUSSION



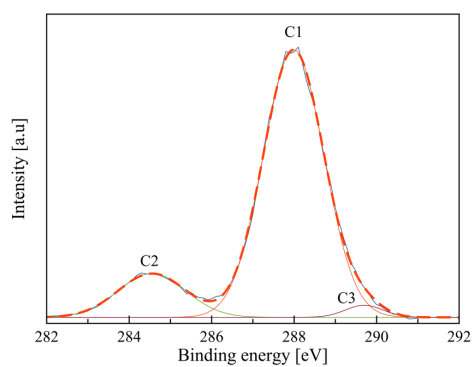
TE



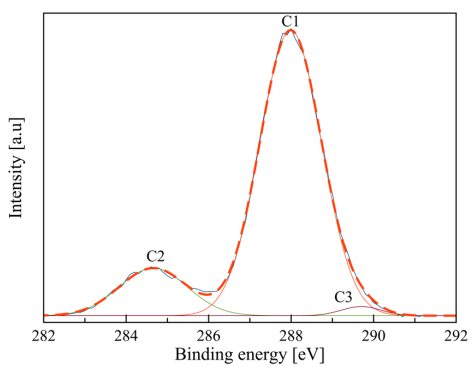
TEO



TEO200



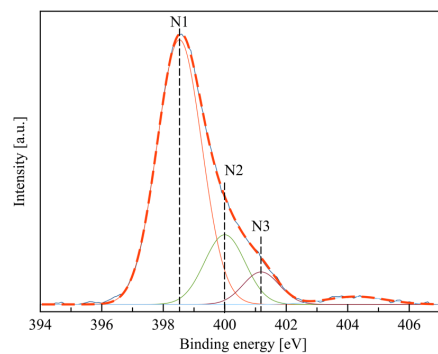
TEO300



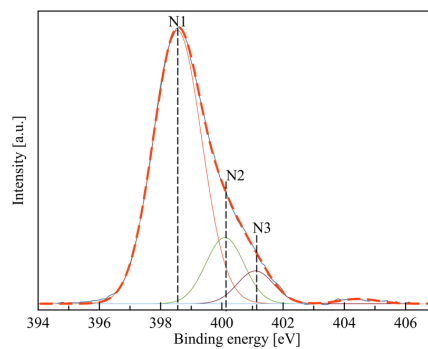
TEO400

Figure S2 – XPS C 1s spectra of the prepared PCN samples.

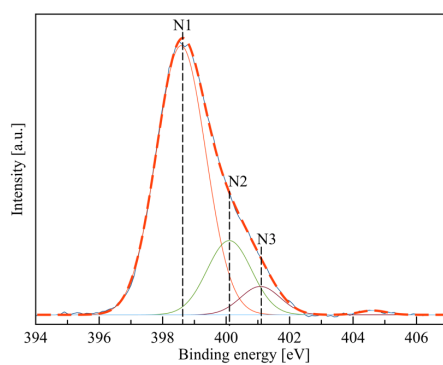
RESULTS AND DISCUSSION



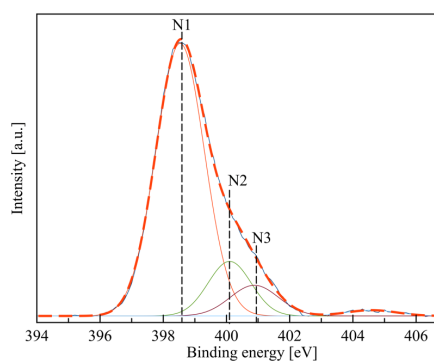
TE



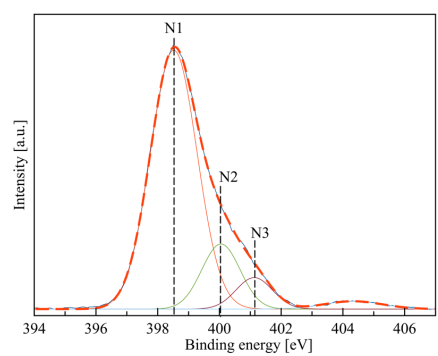
TEO



TEO200



TEO300



TEO400

Figure S3 – XPS N 1s spectra of the prepared PCN samples.

Table S1 – XPS N 1s peak deconvolution results.

Sample	N1/N2/N3 area ratio	N2 position/ N2 HWHM [eV]
TE	1/0.24/0.10	400.3/1.11
TEO	1/0.20/0.09	400.4/0.98
TEO200	1/0.25/0.08	400.3/1.00
TEO300	1/0.18/0.11	400.3/0.99
TE400	1/0.20/0.10	400.3/1.02

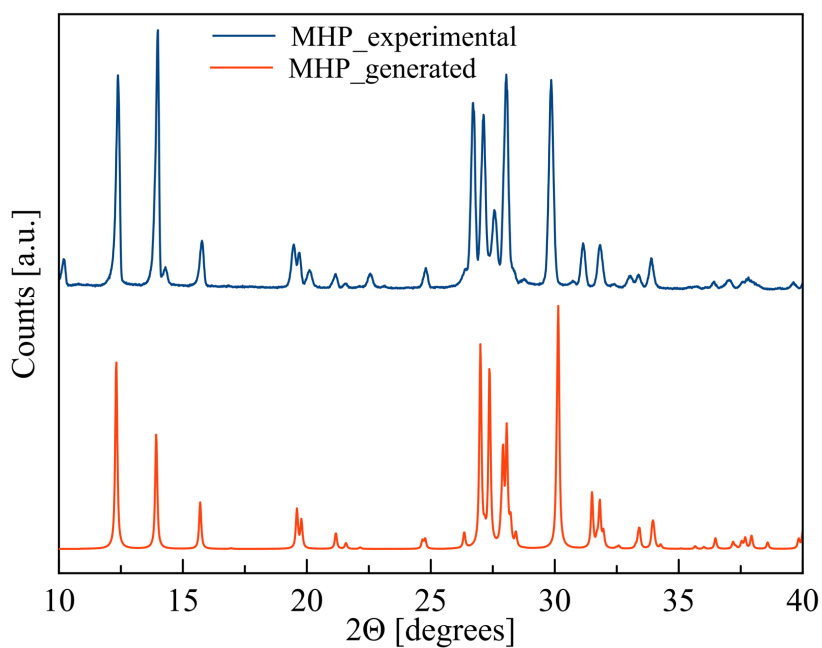


Figure S4 – Comparison of PXRD pattern of MHP complex prepared in this work and the one generated from single crystal XRD data [1].

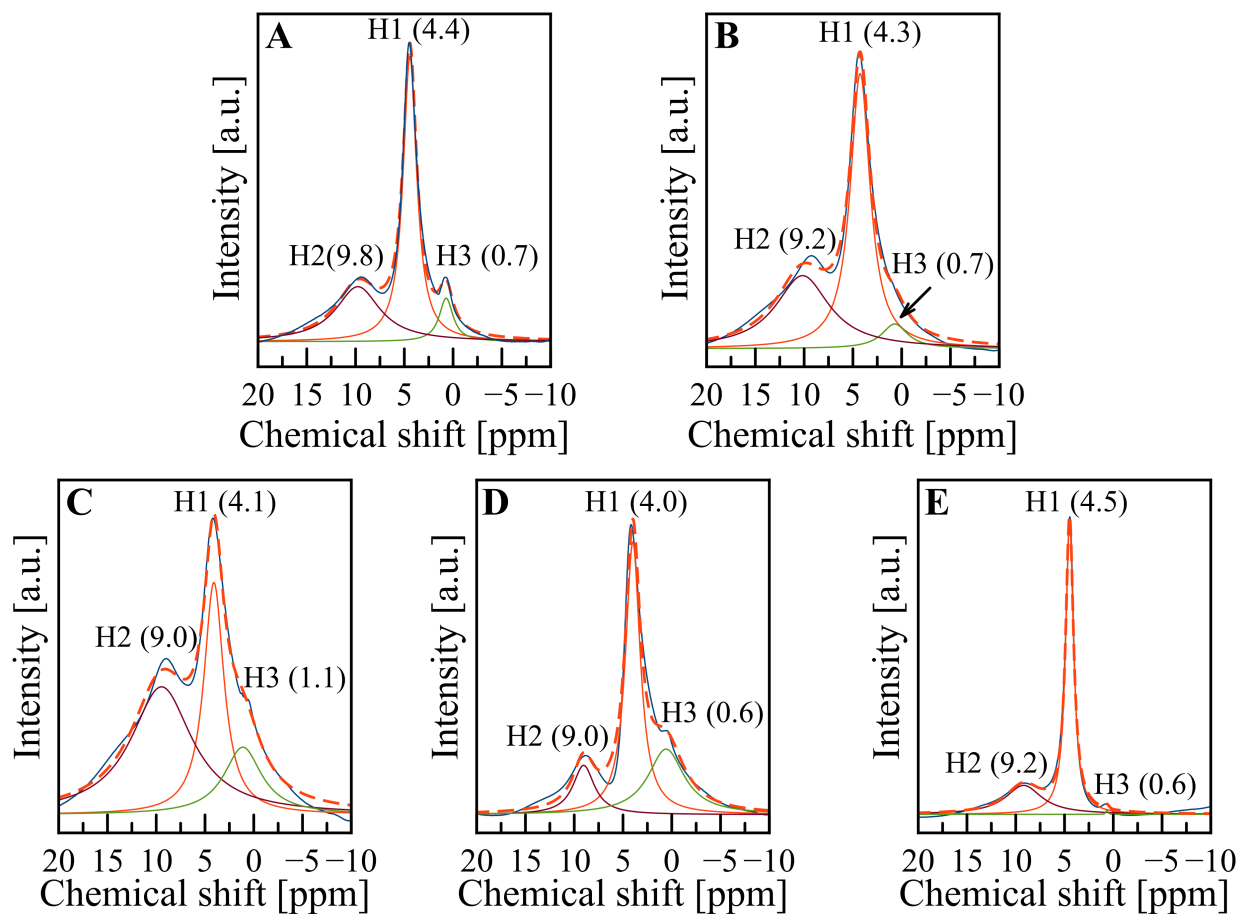
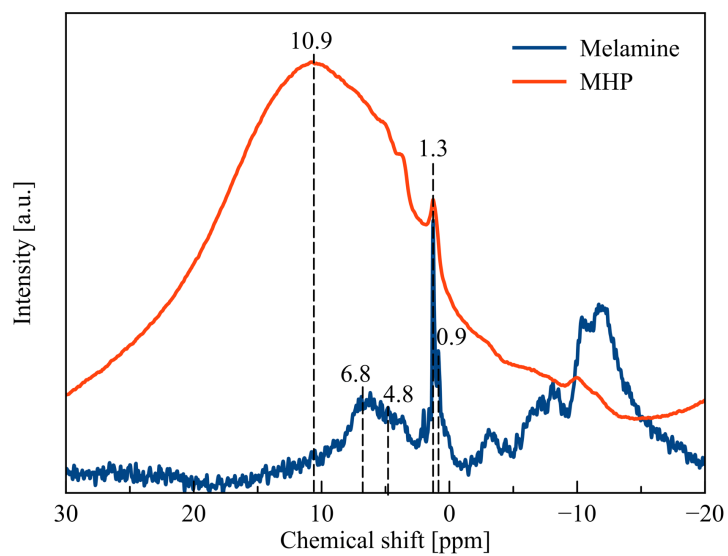
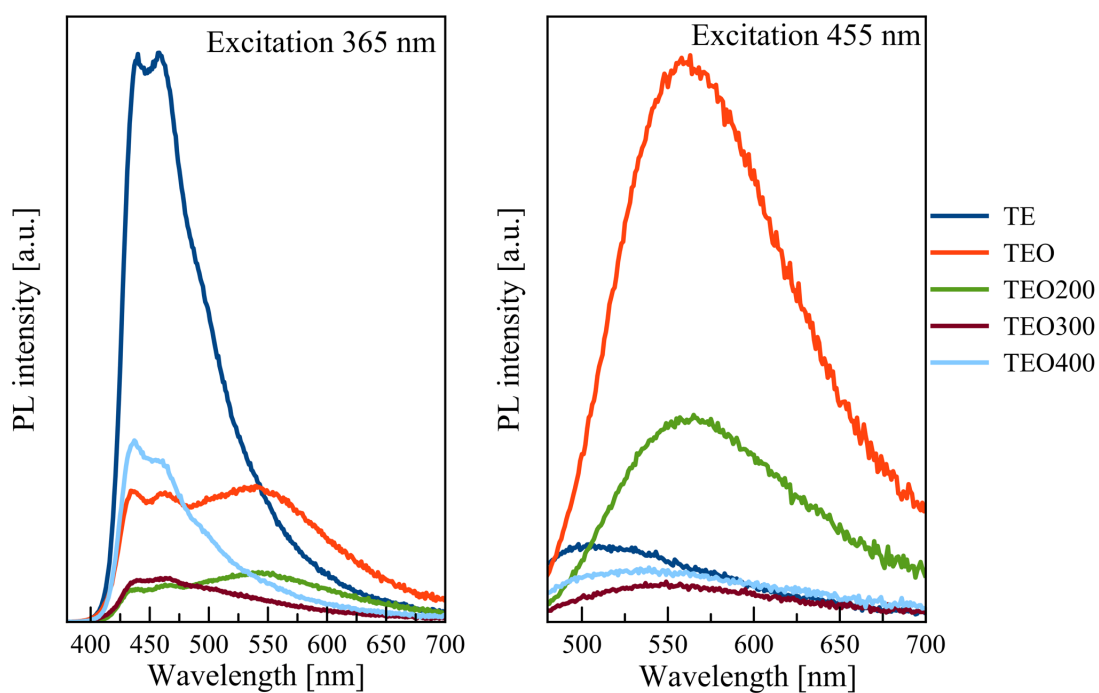


Figure S5 – Deconvolution of ^1H MAS NMR spectra of (A) TE, (B) TEO, (C) TEO200, (D) TEO300 and (E) TEO400 samples.

Figure S6 – ^1H MAS NMR spectra of melamine and MHP.Figure S7 – PL spectra of the PCN and PCN- H_2O_2 samples recorded at excitations at 365 nm (left) and 455 nm (right).

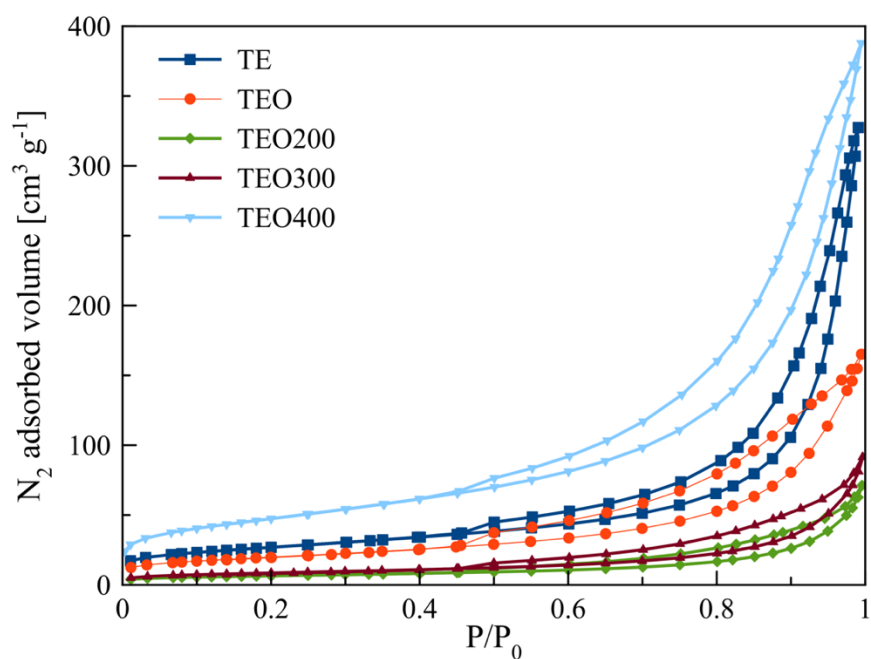


Figure S8 – Physisorption of N_2 at 77K on the prepared PCN and PCN- H_2O_2 samples.

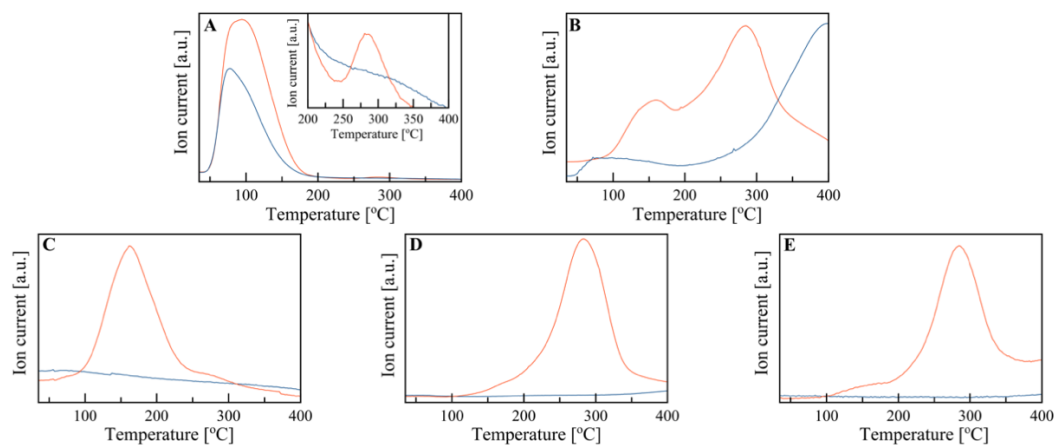


Figure S9 – TPD-MS analysis of the TE (blue) and TEO (red) samples; (A) 18 amu, (B) 44 amu, (C) 32 amu, (D) 30 amu, (E) 28 amu.

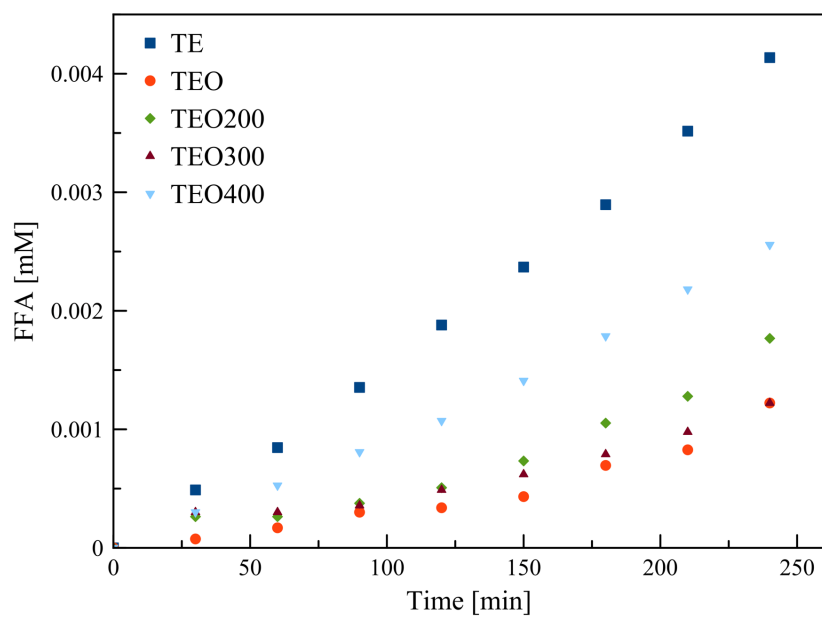


Figure S10 – Formation of FFA during the UV-assisted photocatalytic oxidation of HMF in the presence of the PCN and PCN-H₂O₂ photocatalysts.

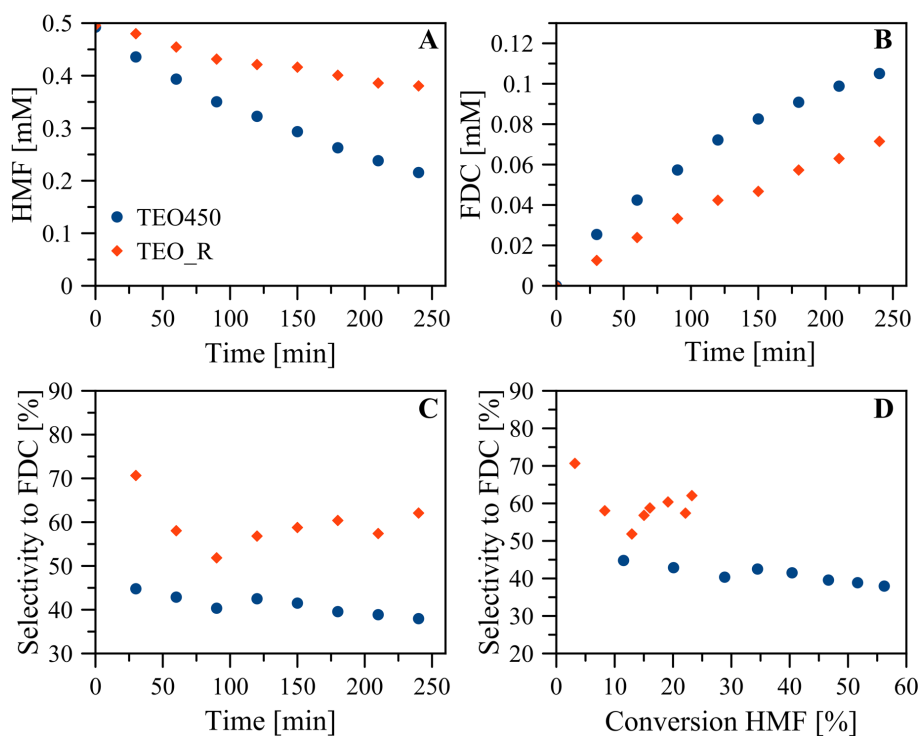


Figure S11 – (A) HMF and (B) FDC concentrations versus time; (C) selectivity to FDC formation versus time, and (D) selectivity to FDC versus HMF conversion for TEO 450 and TEO_R photocatalysts under UV irradiation.

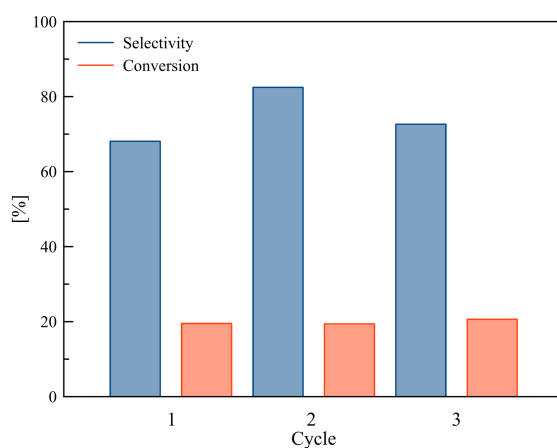


Figure S12 – Reusability of the TEO photocatalyst for the HMF partial photo-oxidation to FDC under UV irradiation.

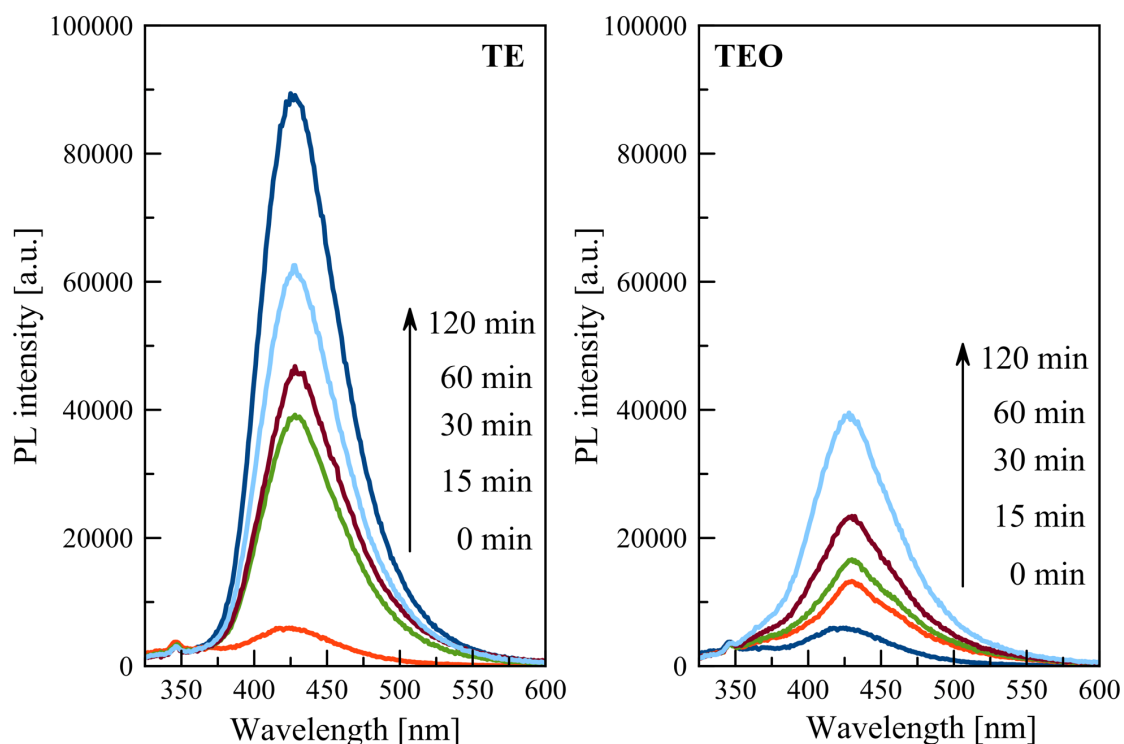


Figure S13 – The fluorescence spectra of 2-hydroxy terephthalic acid formation by reaction of TA with hydroxyl radicals as a function of time for the TE (left) and TEO (right) samples.

References

1. I.Yu. Chernyshov, M.V. Vener, P.V. Prikhodchenko, A.G. Medveddev, O. Lev, A.V. Churakov, Peroxosolvates: formation criteria, H₂O₂ hydrogen bonding, and isomorphism with the corresponding hydrates, *Cryst. Growth Des.*, **2017**, 17, 214–220.

4.2.3 PCN-H₂O₂ adduct for selective photo-oxidation of 5-hydroxymethylfurfural and aromatic alcohols in solar pilot plant

Numerous photocatalysts efficiently converting aromatic alcohols to aldehydes have been synthesised in laboratories, however, the scaling-up of the procedures for their preparation supposes a serious challenge. The viability of industrial applications of catalysts, apart from the activity and selectivity, must be also justified by the easiness of their preparation and low cost of the implemented method. Moreover, in the field of photocatalysis it is especially important that the designed material would be activated by as broader range of the solar spectrum as possible. Polymeric carbon nitride due to its BG of about 2.7 eV and favourable VB position allowing the formation of only mildly oxidative species is an ideal candidate for this role. In the presented below research the PCN and PCN-H₂O₂ photocatalysts were synthesised using inexpensive melamine and hydrogen peroxide as precursors. The simplicity of the preparation procedure allowed to obtain significant amount (up to 100 g of each type) of the catalysts, thus satisfying the requirements for carrying out a pilot-plant test. If the research in the field of photocatalytic water decontamination on a large scale has advanced significantly in the recent years, the studies concerning the use of solar radiation to drive selective photochemical reactions are scarce [315]. In the following work we addressed the question of selective photo-oxidation of HMF to FDC in the presence of the PCN and PCN-H₂O₂ photocatalyst in Compound Parabolic Collector (CPC) photoreactor under natural solar irradiation and in water medium at the Almeria Solar Platform. Additionally, the selective conversion of 4-methoxybenzyl alcohol (MBA), benzyl alcohol (BA) molecules to the corresponding aldehydes was also tested in the same conditions as to demonstrate the applicability of the proposed technique to a broader range of organic substrates. The selectivity of HMF to FDC photo-oxidation in CPC was in the range of 70-90%, which is comparable with the laboratory tests reported earlier. The varying concentrations of the photocatalysts, as well as the substrates, proved the viability of the use of partial photocatalytic oxidation of aromatic alcohols to produce high-value products under real-life conditions. The Langmuir-Hinshelwood mechanism was applied to build the kinetic model on the basis of the obtained experimental data.

Article IV

“Selective photocatalytic oxidation of 5-hydroxymethyl-2-furfural in aqueous suspension of polymeric carbon nitride and its adduct with H₂O₂ in a solar pilot plant”

Catalysis Today

In Press

Year 2018

DOI: 10.1016/j.cattod.2018.03.013

Impact Index: 4.636

Selective photocatalytic oxidation of 5-hydroxymethyl-2-furfural in aqueous suspension of polymeric carbon nitride and its adduct with H₂O₂ in a solar pilot plant

Marina Ilkaeva¹, Igor Krivtsov^{1,2}, José R. García¹, Eva Díaz³, Salvador Ordóñez³, Elisa I. García-López^{4,*}, Giuseppe Marci⁴, Leonardo Palmisano⁴, M. Ignacio Maldonado^{5,6}, Sixto Malato^{5,6}

¹ Department of Physical and Analytical and Organic and Inorganic Chemistry, University of Oviedo-CINN, 33006 Oviedo, Spain.

² Nanotechnology Education and Research Center, South Ural State University, 454080 Chelyabinsk, Russia

³ Department of Chemical and Environmental Engineering, University of Oviedo, 33006 Oviedo, Spain.

⁴ "Schiavello-Grillone" Photocatalysis Group. Dipartimento di Energia, Ingegneria dell'informazione e modelli Matematici (DEIM), Università di Palermo, Viale delle Scienze, 90128 Palermo, Italy.

⁵ Plataforma Solar de Almería-CIEMAT, Tabernas, Spain.

⁶ CIESOL, Centro de Investigación en Energía Solar, Joint Centre University of Almería-CIEMAT, 04120 Almería, Spain

elisaisabel.garcialopez@unipa.it

Abstract

This work reports a study on the reactivity of polymeric carbon nitride and (PCN) and PCN-H₂O₂ adduct samples for sunlight photocatalytic selective oxidation reactions. The characterization of these materials was reported in a previous paper where the reactivity towards the partial oxidation of 5-hydroxymethylfurfural (HMF) was studied by using two different laboratory scale photoreactors; one irradiated by UV lamps and the other one by natural sunlight. In the present study it has been confirmed the effectiveness of these C₃N₄ based materials for the selective partial oxidation of HMF to FDC (2,5-furandicarboxaldehyde) in aqueous medium in a pilot plant photoreactor irradiated by natural solar light. The reactivity results and, in particular, the selectivity to FDC formation have

been very encouraging, mostly by considering that the reaction was carried out in water. Moreover, they are comparable with those obtained in the laboratory scale photoreactors irradiated by both UV lamps and natural sunlight. Interestingly, the pristine PCN sample has shown the higher HMF conversion with respect to that of the PCN-H₂O₂ adduct, but the last one is more selective to the FDC formation. A kinetic study indicates that the pseudo-first-order rate constant of HMF oxidation is higher in the case of pristine photocatalyst and that the equilibrium adsorption constants of HMF is higher in the case of PCN-H₂O₂ adduct catalyst. Finally, the partial oxidation of two aromatic alcohols, i.e. benzyl alcohol (BA) and 4-methoxy benzyl alcohol (4-MBA) to benzaldehyde (BAL) and 4-methoxy benzaldehyde (4-MBAL), respectively, has also been studied.

Keywords: Solar photocatalysis, carbon nitride; selective photocatalytic oxidation; 5-hydroxymethyl-2-furfural, 2,5-furandicarboxaldehyde; 4-methoxy-benzyl alcohol; benzyl alcohol

Introduction

The application of photocatalytic reactions to water and air remediation has been widely studied and thoroughly reviewed [1]. The use of TiO₂ as photocatalyst has been demonstrated to be an excellent technology to unselectively degrade many pollutants giving rise to their complete mineralization. However, photocatalysis is also capable to selectively oxidize or reduce a substrate producing a higher value compound in water solution, with no toxic by-products and the possible use of solar light as the radiation source. Many case studies on different organic substrates demonstrating the feasibility of this new approach have been reported until now [2]. The heterogeneous photocatalytic oxidation of alcohols to aldehydes has been carried out in some cases with high yields [3] although in most of the cases in organic media [4]. TiO₂ under UV irradiation in aqueous medium readily forms hydroxyl radicals (\bullet OH), which unselectively attack organic species until their mineralization to CO₂ and H₂O. Consequently, the use of an alternative photocatalytic material with a lower oxidant ability can be a good strategy to avoid the complete oxidation of the substrate. In this context, a photocatalyst with appropriate thermodynamic requirements, which has recently attracted

RESULTS AND DISCUSSION

attention as a potential candidate to photocatalyse selective partial oxidations is C_3N_4 , i.e. polymeric carbon nitride (PCN) [5-9]. The electronic structure of carbon nitride allows its application in selective photocatalytic oxidation reactions of organic compounds [10], particularly for aromatic alcohols in the presence of O_2 [11,12]. The favorable energies of its conduction and valence bands and the absence of hydroxyl groups on its surface, which would promote the direct formation of the unselective $\bullet OH$ radicals, make this material an optimal photocatalyst for selective oxidation of alcohols in aqueous medium. The difference in the position of the valence band of TiO_2 and C_3N_4 seems particularly important to justify why PCN can be better used as photocatalyst in partial oxidation reactions. Indeed, the electrons promoted into the conduction band of C_3N_4 are thermodynamically capable to reduce O_2 to form the superoxide radical $\bullet O_2^-$ or H_2O_2 . On the contrary, the potential of the holes generated in the valence band is not sufficient to oxidize OH^- forming $\bullet OH$ radicals [10]. Natural solar radiation can be applied to activate C_3N_4 photocatalyst, because its band gap is in the range of 2.8-3.0 eV, depending on the preparation method. The use of solar light is particularly relevant to develop innovative and economically consistent processes and, at the same time, to move toward sustainable chemistry with a reduced environmental impact.

5-Hydroxymethyl-2-furfural (HMF) is one of the most versatile “biomass platform molecule” produced from abundant and inexpensive lignocellulose-derived glucose [13]. The presence of alcohol and aldehyde functional groups on the furanic ring gives HMF the possibility to be a precursor of several high-value chemicals [14]. In particular, HMF can be partially oxidized to 2,5-furandicarboxaldehyde (FDC), 5-hydroxymethyl-2-furancarboxylic acid (HMFA) and 2,5-furandicarboxylic acid (FDCA), which are valuable molecules for the polymer industry [15]. Selective oxidation of the alcohol functional group without affecting other functionalities, keeping intact the furan ring, results particularly challenging. The oxidation of the alcohol group forming the corresponding aldehyde (FDC) is an interesting task because this molecule is used as a monomer to synthesize adhesives, binders, foams, antifungal agents, heterocyclic ligands and resins [16]. Generally, the process requires toxic oxidants and generate a large amount of hazardous wastes making it environmentally and economically undesirable. These processes have been substituted by catalytic oxidation; however, the application of high temperatures, as well as expensive noble metals makes this

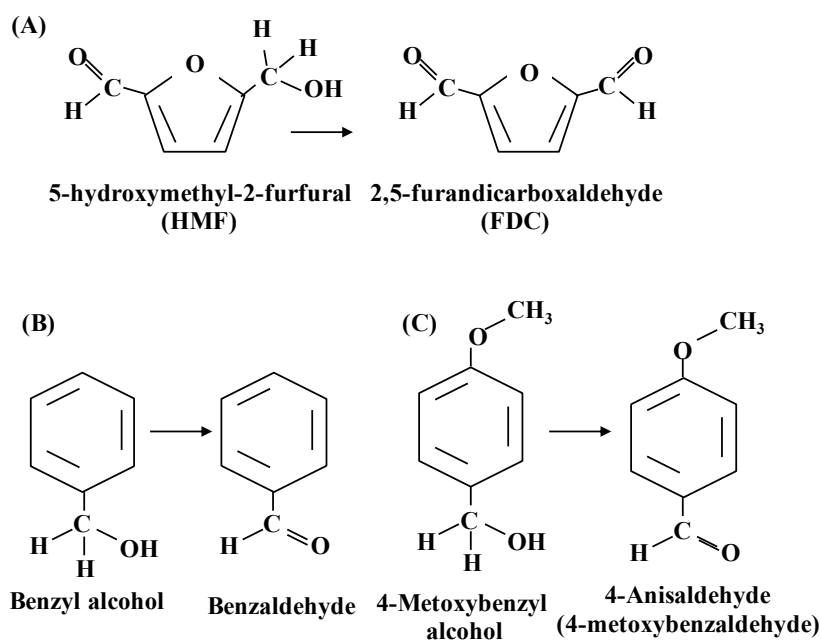
RESULTS AND DISCUSSION

reaction energy-consuming and environmentally unfriendly [17]. Hu et al. reviewed the different aspects of the synthesis of FDC starting from fructose or HMF [18].

There were several efforts to improve the knowledge on the photocatalytical formation of HMF, and in most cases FDC was the principal reaction product [21-23], whilst FDCA was produced only in the presence of a metal-organic cocatalyst [24]. To control the selectivity of HMF oxidation to FDC is quite easy in organic solvents where hydroxyl radicals are not formed [25], but to carry out the same reaction in aqueous medium is a more difficult task. Low-crystalline and N-doped TiO₂ were found to be suitable photocatalysts for this reaction under UV-light in aqueous medium, however only 30-40 % selectivity was achieved [21,26]. The application of C₃N₄ not only allowed to increase this figure up to 50 %, but also to efficiently use natural sunlight [23]. The following step in the improvement of selectivity toward FDC production was achieved by PCN-H₂O₂ adduct, which was previously synthesized and characterized [27]. It was found that, despite the VB potential of PCN does not permit direct H₂O oxidation to hydroxyl radicals, they could be formed on the unpolymerized carbon nitride functionalities subsequently reacting with the organic substrate causing its unselective oxidation. Hydrogen peroxide attached to these species creates a steric hindrance for substrate interacting with the NH₂-containing groups, hence preventing the attack of •OH to the substrate [27].

Although the investigation of selective photocatalytic oxidations has advanced significantly in the last two decades, still the research is limited to laboratory studies and only few reports on scaling-up of this process (using TiO₂) exist [26]. Here, we will demonstrate the applicability of the PCN and PCN-H₂O₂ adduct photocatalysts for pilot plant scale partial photocatalytic oxidation of HMF to FDC under natural sunlight. Moreover, we will show that the use of the pilot plant compound parabolic collector (CPC) photoreactor for partial photocatalytic oxidation can be extended to syntheses of other valuable chemicals earlier carried out on laboratory scale [27]. For this reason the photo-oxidation of benzyl alcohol (BA) and 4-methoxybenzyl alcohol (4MBA) to their respective aldehydes, i.e. benzaldehyde (BAL) and 4-methoxybenzaldehyde (4MBAL) will be also discussed (Scheme 1). The two aromatic alcohols were chosen because they bear different substituent groups which influence, as before reported, their conversion and selectivity [12]. Indeed, the presence of

the methoxy group in para position (4-methoxy benzyl alcohol versus benzyl alcohol), increased both reaction rate and selectivity to aldehyde both in the presence of TiO₂ [13] and C₃N₄ [12]. Notably, the aldehydes which can be obtained from the photo-oxidation of aromatic alcohols are important intermediates in the chemical, pharmaceutical and agricultural industry. The photocatalytic partial oxidation of benzyl alcohol in water to obtain BAL was also reported by using TiO₂ [14,15] and C₃N₄ based photocatalysts [12,16]. A selectivity to BAL formation of ca. 38-42 % was achieved in studies carried out in the presence of TiO₂, while oxidation of 4-MBA to 4-MBAD in water assisted by TiO₂ gave rise to a selectivity of 60 % [13] or 72 % [15], depending on the type of TiO₂ used.



Scheme 1 – Structure of the alcohols and their corresponding aldehydes.

2. Experimental

2.1. Photocatalyst Preparation and characterization

Bulk carbon nitride (BCN) was prepared by thermal condensation starting from melamine [21]. The scaled-up preparation of BCN proceeded by placing 60 g of melamine in a covered ceramic crucible and by heating it in an oven up to 520 °C at 2 °C·min⁻¹. The temperature was maintained for 6 h, and after that the system was slowly cooled down giving about 36 g of BCN. The obtained BCN consisting of a yellow powder underwent a successive heating in

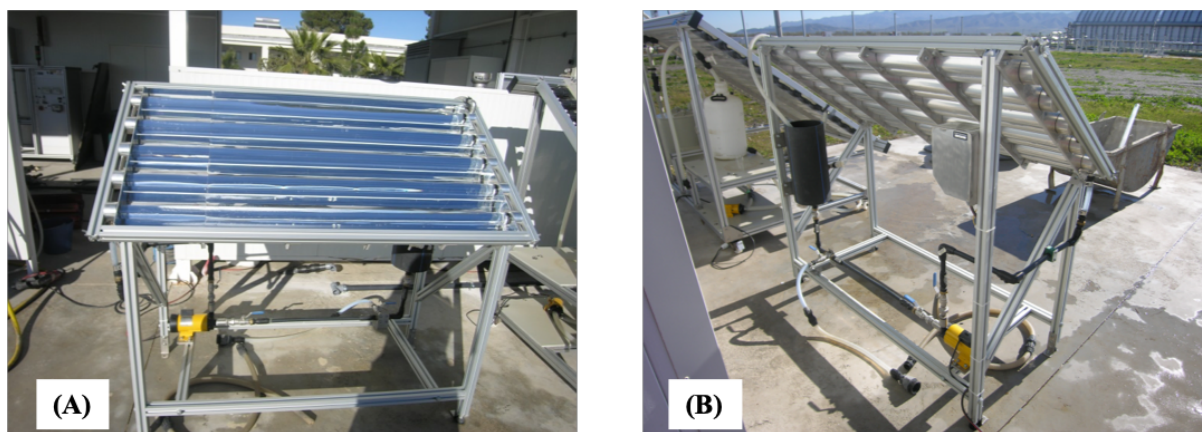
air atmosphere, to obtain thermally etched PCN (TE) with improved physicochemical features [28,29]. It was prepared starting from 20 g of the powdered BCN, which was evenly spread on an aluminium sheet with dimensions 15x22 cm, then heated in air up to 520 °C at 3 °C min⁻¹ and kept for 7 h at this temperature before being cooled down. The thermal etching produced ca. 9 g of TE, and the procedure was repeated until 200 g of the thermally etched PCN (TE) was obtained, then TE was powdered and thoroughly mechanically mixed. After that, the pale yellow TE powder was divided into two aliquots, one of them was left as it was, while the other one was treated with H₂O₂ according to the procedure reported elsewhere [25,30]. Briefly, 500 mL of aqueous H₂O₂ solution (wt 30%) containing 100 g of TE was stirred in an open beaker under heating at 70 °C to evaporate the liquid. Once dry, the powder was washed with water until the complete absence of H₂O₂ in the washing liquid, filtered and dried at 80 °C for 24 h. The finally obtained dark yellow-to-orange powder was labelled as TEO. The properties of the solids were fully characterized elsewhere [25]. The SSAs of the TE and TEO samples resulted to be 129 and 59 m²·g⁻¹, respectively.

2.2. Photocatalytic set-up and procedure

The photocatalytic experiments were carried out in a pilot plant scale CPC solar photoreactor located at the Plataforma Solar de Almería (Spain). The CPC was not a concentrating one, i.e. the ratio between the sun exposed surface and that of the reactor was approximately equal to 1.1. The set-up consisted of a plug flow photoreactor (PFP) in a total recycle loop with a not-reacting stirred tank whose function was providing aeration and sample withdrawing for analyses. The plug flow photoreactor (PFP) was equipped with CPC having five UV-transparent glass tubes (inner diameter 45 mm, outer diameter 50 mm, irradiated length 1460 mm) connected in series and placed on a fixed support inclined 37° (latitude of the PSA) with respect to the horizontal plane and facing south to maximize the daily incidence of solar radiation. The aqueous suspension was continuously fed to the PFP upwards from the not-reacting tank by means of a centrifugal pump. The suspension flow rate, maintained constant for all the runs, was 12 L·min⁻¹. The Reynolds number value was equal to ca. 5700, indicating a turbulent regime of the flow inside the tubes. The total volume of suspension (V_t) charged in the whole system was 15.5 L, whereas the irradiated volume, i.e. the volume of suspension contained in the glass tubes, was 11.6 L. The irradiated volume

RESULTS AND DISCUSSION

was 75% of the total one (dead volume was accounted for to 25%). The total irradiated area in the photo-reactor was 1.055 m² and the suspension slightly heated throughout the experiments, reaching temperatures of ca. 42-45 °C at the end of the run. A picture of the photoreactor and the reaction set-up is presented in Scheme 2.



Scheme 2 – Pilot plant photoreactor (A) and set-up (B).

Aqueous solutions of HMF (0.5, 1, 2 and 4 mM) at natural pH were used for the experiments. For selected runs BA and 4-MBA (2 mM) were also used as the substrates. The photocatalytic activity of the TE and TEO powders was studied together with that of TiO₂ Evonik P25, which was tested for the sake of comparison. The loading of the TE and TEO photocatalysts in the photoreactor ranged between 0.1 and 0.4 g·L⁻¹. Before starting the photoreactivity runs the aqueous suspension was allowed to recirculate under dark for 20 min to establish the adsorption/desorption equilibrium between the organic substrate and the solid photocatalyst. Subsequently, the CPC was uncovered and the system was irradiated for 5 h under sunlight. Samples of the suspension were withdrawn immediately after starting the irradiation and at fixed time intervals (0.5 h). The samples were withdrawn from the not-reacting tank so that they were representative of the conditions in the inlet. They were filtered through 0.25 μm membranes (HA, Millipore) to separate the photocatalyst particles and to analyze the concentration of the substrate and the reaction products. The analyses were carried out by an Agilent 1100 HPLC equipped with a Diode Array detector to identify and to determine concentrations of HMF, FDC and 5-formyl-2-furoic acid (FFA). A REZEK ROA

RESULTS AND DISCUSSION

Organic acid H⁺ column was used with a mobile phase of aqueous 2.5 mM H₂SO₄ solution at a flow rate of 1 mL·min⁻¹. The aromatic molecules, i.e. BA, 4-MBA, BAL and 4-MBAL were analyzed by the same HPLC, but equipped with a Phenomenex KINETEK 5 μm C18 instead. The eluent (0.6 mL·min⁻¹) consisted of a mixture of acetonitrile and 13 mM trifluoroacetic acid (20:80 v:v). Standards purchased from Sigma-Aldrich with a purity > 99% were used to identify the products and to obtain the calibration curves. Additionally, dissolved organic carbon (DOC) analyses were performed by using a Shimadzu TOC-VCSN. The method for monitoring the evolution of H₂O₂ during the reaction was based on the formation of a coloured complex between 0.5 mL of TiOSO₄ 1.5% (Aldrich) and hydrogen peroxide present in 4.5 mL of the reacting solution. Then, the concentration of H₂O₂ was photometrically determined by measuring the absorbance at 410 nm using a spectrophotometer UNICAM UV2. The recyclability study was carried out according to the following procedure: At the end of each run the catalyst was left to decant inside the reactor and the supernatant was removed. After that, the reactor was filled with a fresh HMF solution and the subsequent reaction started.

As all of the experiments were carried out under natural solar radiation, it should be considered that the radiation intensity changed throughout the experiments, depending on time and meteorological conditions. Consequently, to properly compare the results, the experimental data were normalized to the amount of energy entering the photoreactor. In the present work this parameter is used instead of the irradiation time to represent the evolution of the concentration of the different substrates during the solar experiments. A Kipp & Zonen CUV4 (300-400 nm) radiometer, oriented at 37° South, was applied to automatically measure every minute the power (W·m⁻²) of the impinging radiation in the 300-400 nm range. The solar energy accumulated per volume unit throughout the experiment (E_n), expressed in kJ·L⁻¹, was calculated by considering the irradiated area of the photoreactor and the total volume by using Equation (1):

$$E_n = E_{n-1} + \Delta t_n W_s (A_i/V_t) \quad (1)$$

where t_n represents the irradiation time for each sample, W_s the average solar radiation measured by the radiometer in each time interval, Δt_n, V_t is the total reactor volume (15.5 L) and A_i the irradiated area of the reactor (1.055 m²).

3. Results and discussion

3.1. Photocatalytic oxidation of HMF by using PCN and PCN-H₂O₂

Preliminary adsorption measurements of HMF and FDC under dark in the presence of TE and TEO samples indicated that the extent of adsorption was negligible for both substrates. Blank experiments under solar irradiation of HMF for 5 h in the absence of photocatalyst showed a decomposition of HMF of ca. 10 % without any selectivity to FDC. On the other hand, ca. 20 % of FDC transformed into FFA under the same experimental conditions, as before observed in the lab scale photoreactor [31]. Nevertheless, it should be considered that the contribution of photolysis in the presence of photocatalyst is always less significant due to the shielding effect of the suspended powder.

The stability of the TEO catalyst under irradiation and dark conditions (in the absence of the substrates) was studied by suspending it in water under vigorous stirring at ca. 50 and 80 °C for 4 h and measuring the amount of H₂O₂ released in water. Only trace quantities of H₂O₂ were detected in all cases. Considering that the temperature during the photocatalytic runs under solar irradiation was much lower than 80 °C, this experiment ensured the applicability of the TEO sample for the reaction.

To establish the optimal photocatalyst loading which is necessary to absorb all of the photons impinging on the photoreactor, some photocatalytic tests of HMF oxidation have been carried out in the presence of different amounts (0.1 to 0.4 g·L⁻¹) of both the TEO and TE powders, while maintaining HMF initial concentration at 0.5 mM for all these runs. In Figure 1 (A) the changes of HMF concentration versus the cumulative photonic energy, E_n , in the presence of different loadings of TEO in the photoreactor are reported. No significant differences can be observed for the experiments carried out in the presence of 0.2, 0.33 or 0.4 g·L⁻¹ of the photocatalyst, whilst the reaction is noticeably slower for the case of using 0.1 g·L⁻¹ of TEO. Throughout the photo-oxidation of HMF, FDC is produced together with small amounts of FFA. FDC concentration increases with cumulative energy, as it is shown in Figure 1 (B). The plots of selectivity to FDC versus cumulative energy and HMF conversion at varying TEO loadings are reported in Figures 1 (C) and (D), respectively. It can be noticed that the selectivity to FDC is ca. 90 % at ca. 20 % of HMF conversion for all the loadings

RESULTS AND DISCUSSION

except for $0.1 \text{ g}\cdot\text{L}^{-1}$, but afterwards it decreases, although never below ca. 71% at maximum conversion degree (see Table 1). The obtained values are very high by considering that the reaction is carried out in water and they are very close to those measured by some of us under UV and solar light irradiation using laboratory scale photoreactors [25].

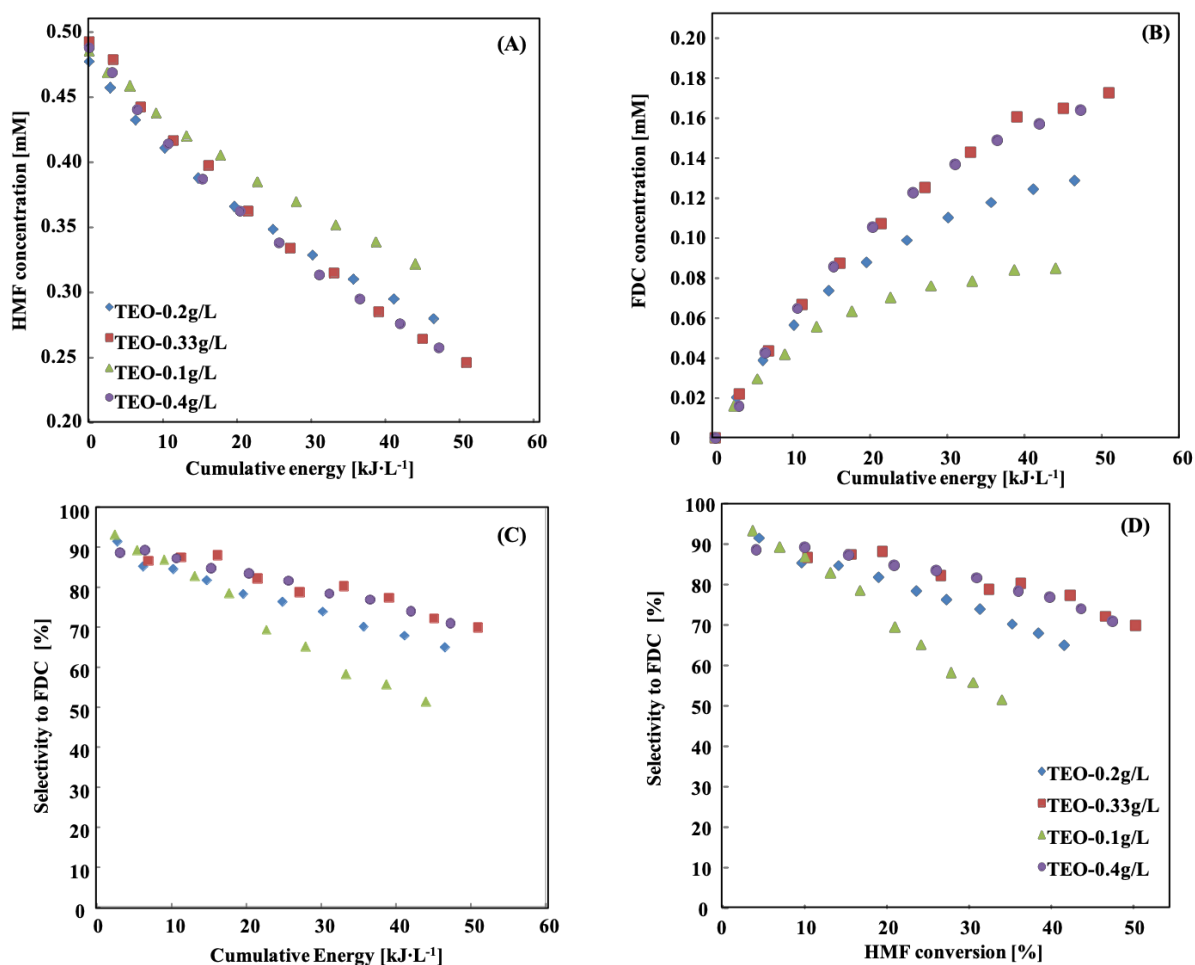


Figure 1 – HMF concentration (A), FDC concentration (B), selectivity to FDC versus cumulative energy (C), and selectivity to FDC versus HMF conversion (D) in the presence of different loadings of TEO: $0.1 \text{ g}\cdot\text{L}^{-1}$ (\blacktriangle); $0.2 \text{ g}\cdot\text{L}^{-1}$ (\blacklozenge); $0.33 \text{ g}\cdot\text{L}^{-1}$ (\blacksquare) and $0.4 \text{ g}\cdot\text{L}^{-1}$ (\bullet).

Initial HMF concentration: 0.5 mM .

A similar dependency of HMF conversion from the photocatalyst loading is observed for the TE sample. In the presence of $0.1 \text{ g}\cdot\text{L}^{-1}$ of TE, the rate of HMF oxidation is significantly lower than for the other cases (Fig. 2 (A)). Moreover, the FDC concentration in the reactor

RESULTS AND DISCUSSION

(Fig. 2 (B)) and the selectivity toward FDC is also inferior to the values obtained for higher TE loadings (Fig. 2 (C)). The plot of selectivity to FDC formation versus HMF conversion clearly indicates that the TE photocatalyst is less selective than its PCN-H₂O₂ counterpart, the TEO sample, for any given conversion degree (Fig. 2 (D)).

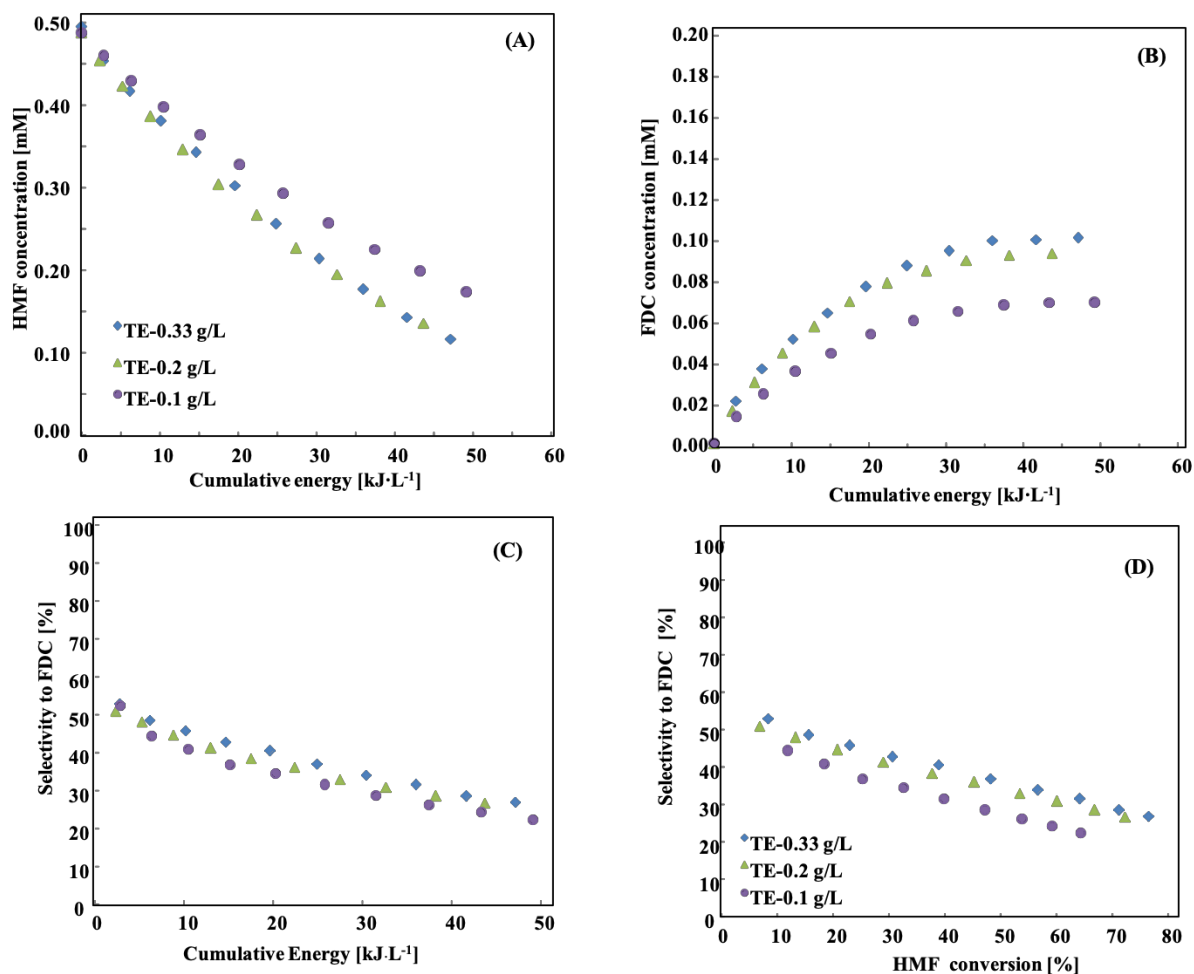


Figure 2 – HMF concentration (A), FDC concentration (B), selectivity to FDC versus cumulative energy (C), and selectivity to FDC versus HMF conversion (D) in the presence of different loadings of TE: 0.1 g·L⁻¹ (●); 0.2 g·L⁻¹ (▲); 0.33 g·L⁻¹ (◆). Initial HMF concentration: 0.5 mM.

Table 1 shows the HMF conversion and the selectivity to FDC results obtained for different TE and TEO loadings in the photocatalytic runs at 45 kJ·L⁻¹ of cumulative energy. As far as the TEO catalyst is concerned, the conversion increases with the increasing amounts of

RESULTS AND DISCUSSION

carbon nitride in the reactor, although it is maintained on the same level for runs carried out with 0.33 and 0.4 g·L⁻¹ of PCN-H₂O₂. In addition, the selectivity to FDC increases reaching a plateau for photocatalyst loadings higher or equal to 0.33 g·L⁻¹ (71 % at 47 % of HMF conversion, after 45 kJ·L⁻¹ of cumulative energy), indicating that this photocatalyst concentration corresponds to an optimal value. Also, in the case of TE, the optimal catalyst loading is 0.33 g·L⁻¹, but the photoactivity of this material is much higher with respect to that of TEO, reaching the HMF conversion of 77 % under the same experimental conditions, although demonstrating lower selectivity to FDC of only 28 % (Table 1). Interestingly, also in this case the reactivity of TE is close to that measured by some of us in a solar and in an UV-irradiated laboratory-scale photoreactors [25]. It is worth noticing that PCN and PCN-H₂O₂ possess low capability to mineralize the substrate (Table 1). Notably, an experiment carried out under the same experimental conditions but in the presence of 0.2 g·L⁻¹ of TiO₂ Evonik P25 (this amount was the optimum for P25 as was previously established for the same photoreactor [32,33] showed the total mineralization of HMF at ca. 25 kJ·L⁻¹, being the selectivity versus FDC virtually zero at any cumulative energy value of the run.

RESULTS AND DISCUSSION

Table 1 – Photoreactivity results for the TEO, TE and TiO₂ Evonik P25 (for the sake of comparison) photocatalysts with 0.5 mM HMF initial concentration. HMF conversion (X_{HMF}), selectivity towards FDC (S_{FDC}), and dissolved organic carbon (DOC) decrease after 45 kJ·L⁻¹ (25 kJ·L⁻¹ in the case of P25) of cumulative energy entering the photoreactor.

Photocatalyst loading [g·L ⁻¹]	X_{HMF} [%]		S_{FDC} [%]		DOC [%]	
	TEO	TE	TEO	TE	TEO	TE
0.1	34	62	51	25	5	8
0.2	41	77	65	28	2	11
0.33	47	77	71	28	4	13
0.4	47	-	71	-	3	-
	P25		P25		P25	
0.2	100		0		100	

A perusal of the data reported in Figs. 1 (A), (B) and 2 (A), (B) indicates that a straight-line fits both the initial variation of HMF concentration and the FDC formation, although the latter deviates from this trend at high cumulative energy values due to its transformation into FFA.

Table 2 reports the values of the initial reaction rates of HMF photo-oxidation and FDC formation at the varying loadings of TEO and TE. These values are also shown in Figures 3(A) and (B) for the TEO and TE photocatalysts, respectively. From Table 2 and Fig. 3 it can be observed that the initial HMF disappearance rate is always nearly the same as the initial

RESULTS AND DISCUSSION

formation rate of FDC in all of the runs, but only in the case of the TEO catalyst. This finding suggests that in the presence of TEO the oxidation of HMF proceeds by one-step reaction giving rise to FDC. On the contrary, the initial reaction rate of HMF is nearly twice as higher than the initial FDC formation rate in the case of the TE photocatalyst, indicating on the presence of parallel reactions. One can suppose that the formation of open-chain aliphatic compounds might take place. As it is evidenced from the HPLC study, several intermediate compounds, other than FDC and FFA, supposedly attributed to the class of carboxylic acids, are produced while HMF is being oxidized with the assistance of TE. However, the formation of FFA is not likely to be attributed to any parallel pathway of HMF photo-oxidation, since its production correlates well with the FDC concentration in the reactor. It is highly probable that FFA is the principal product of the photolysis of FDC, as previously was suggested [21].

Table 2 – HMF initial oxidation rate (r_{HMF}) and FDC initial formation rate (r_{FDC}) in the presence of the TEO and TE photocatalysts with HMF 0.5 mM initial concentration.

Photocatalyst loading [g·L ⁻¹]	r_{HMF} [mmol·kJ ⁻¹] 10 ³		r_{FDC} [mmol·kJ ⁻¹] 10 ³	
	TEO	TE	TEO	TE
0.1	4.90	8.80	5.10	4.10
0.2	6.40	11.0	6.10	6.00
0.33	7.30	10.9	6.60	6.00
0.4	7.10	-	6.40	-

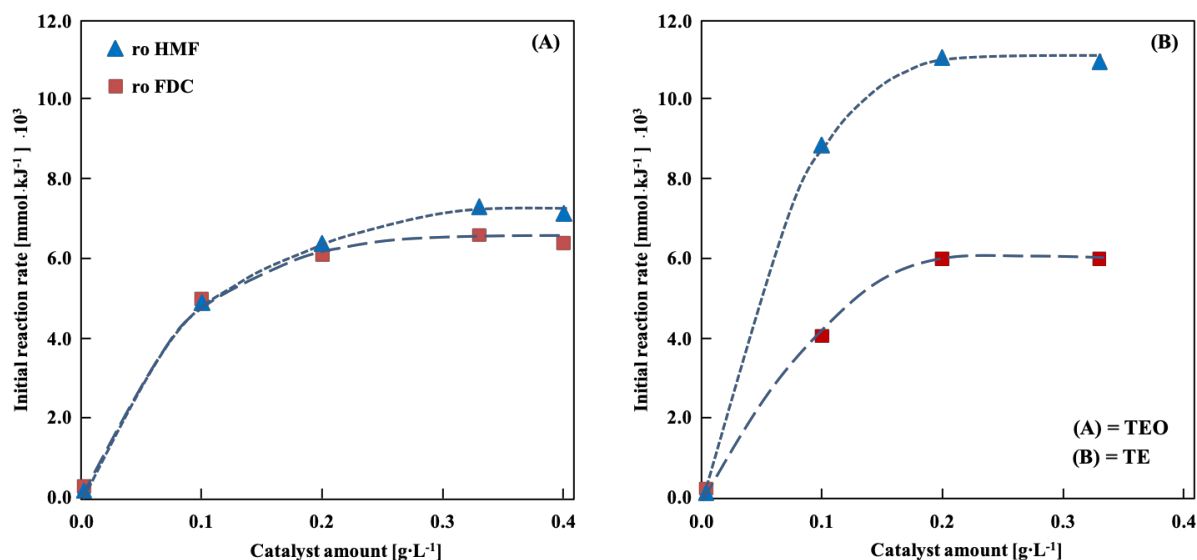


Figure 3 – Initial HMF degradation rate (▲) and initial FDC formation rate (■) versus the loading of the TEO (A) and TE (B) photocatalysts. Initial HMF concentration: 0.5 mM.

Once the optimal photocatalyst loading equal to $0.33 \text{ g} \cdot \text{L}^{-1}$ for both of the used materials had been established, a systematic investigation of the influence of the initial HMF concentration on the reaction rate and on the selectivity to FDC was carried out. Figures 4 and 5 report the concentrations of HMF and FDC versus the incident cumulative photonic energy and the selectivity to FDC versus both the cumulative energy and the HMF conversion for the runs carried out applying different initial HMF concentrations in the presence of the TEO and TE photocatalysts, respectively.

As a general trend, it is observed that the increase of the initial HMF concentration favours the enhancement of the reaction rate of the HMF disappearance as well as that of the FDC formation (Figs. 4 (A), (B) and Figs. 5 (A), (B)). As far as the selectivity to FDC is concerned, it is seen that the TEO sample is still the most selective of the two (Figs. 4 (C), (D) and Figs. 5 (C), (D)). Notably, during the reaction the selectivity to FDC decreases with increasing the HMF conversion, and this is particularly evident in the case of the TE photocatalyst (Fig. 5). The selectivity to FDC is found to be lower for the highest HMF initial concentration at $45 \text{ kJ} \cdot \text{L}^{-1}$ of cumulative energy (Table 3). The most plausible explanation to this fact might be the presence in the reactor of high concentration of hydrogen peroxide produced according to the mechanism represented in Scheme 3. The concentration of

RESULTS AND DISCUSSION

hydrogen peroxide formed throughout the photoreactions carried out in the presence of TEO and TE, respectively, is reported in Figures 6 (A) and (B). High H_2O_2 content in the irradiated suspension can promote its reaction with photo-generated electrons leading to the production of highly oxidative $\cdot\text{OH}$ radicals, which are responsible for the ring-opening reaction as well as for the complete substrate mineralization (Table 3).

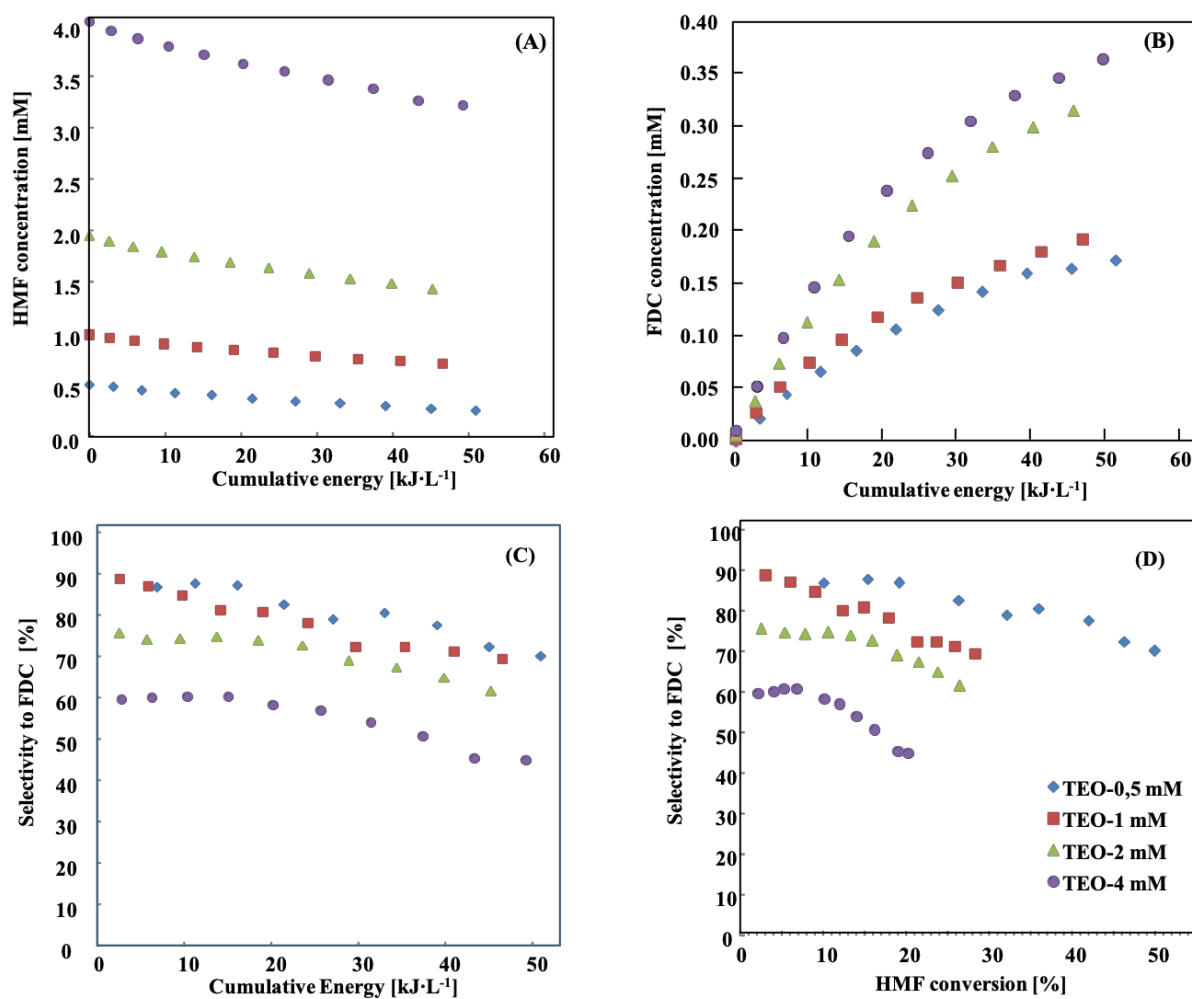


Figure 4 – HMF concentration (A), FDC concentration (B), selectivity to FDC versus cumulative energy (C) and selectivity to FDC versus HMF conversion (D) at different initial concentrations of HMF: 0.5 mM (◆); 1 mM (■); 2 mM (▲) and 4 mM (●). Loading of TEO: 0.33 g·L⁻¹.

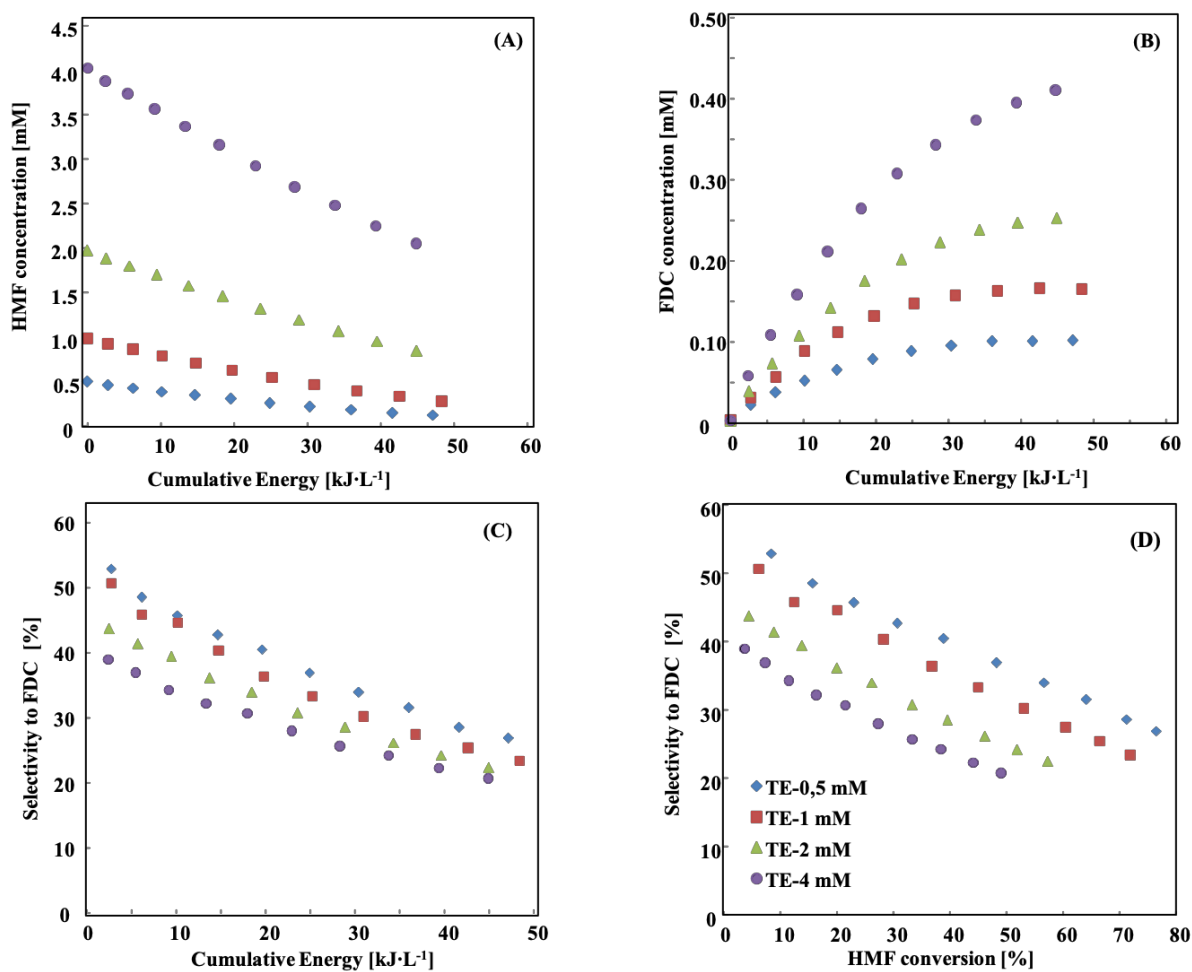
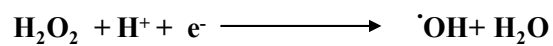
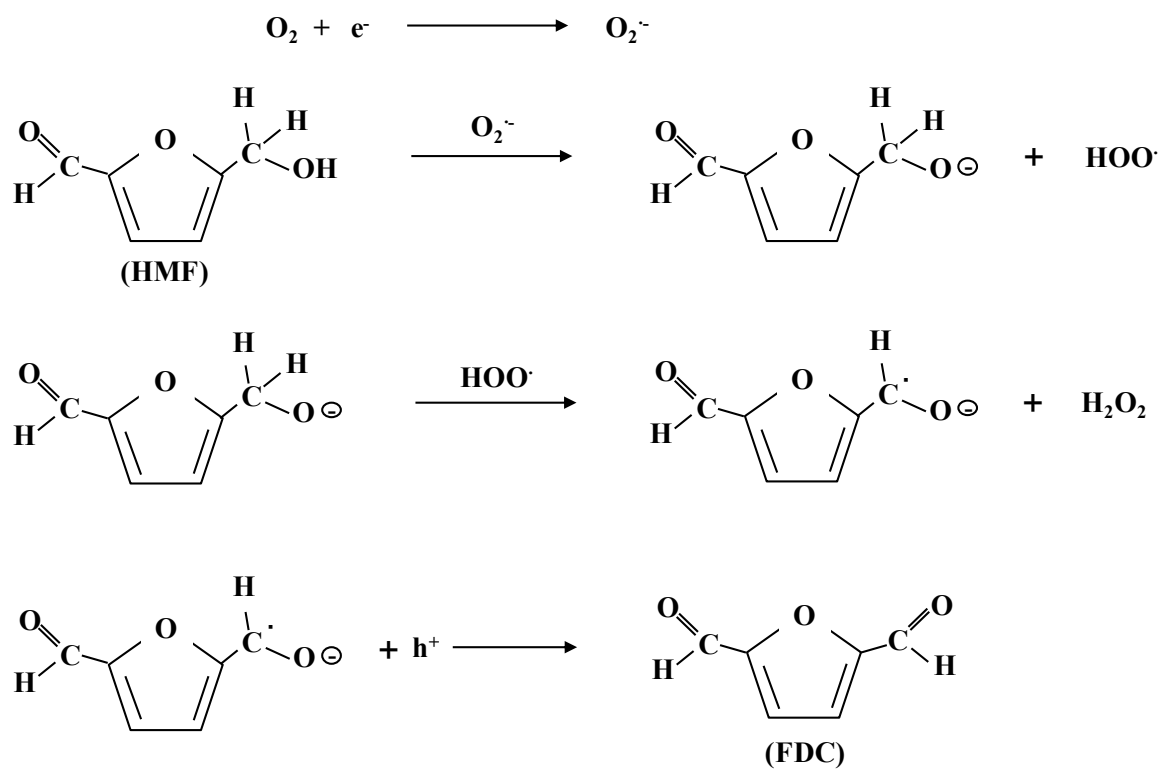


Figure 5 – HMF concentration (A), FDC concentration (B), selectivity to FDC versus cumulative energy (C) and selectivity to FDC versus HMF conversion (D) at different initial concentrations of HMF: 0.5 mM (◆); 1 mM (■); 2 mM (▲) and 4 mM (●). Loading of TE 0.33 g·L⁻¹.

RESULTS AND DISCUSSION

Table 3 – Photoreactivity results in the presence of 0.33 g·L⁻¹ of the TEO and TE photocatalysts at different HMF initial concentrations: HMF conversion (X_{HMF}), selectivity to FDC (S_{FDC}) and dissolved organic carbon (DOC) decrease after 45 kJ·L⁻¹ of cumulative energy.

HMF [mM]	X_{HMF} [%]		S_{FDC} [%]		DOC [%]	
	TEO	TE	TEO	TE	TEO	TE
0.5	47	77	71	28	4	13
1	26	69	70	24	2	11
2	26	57	61	22	2	9
4	20	49	45	21	2	6



Scheme 3 – Hypothesized mechanism of FDC and H₂O₂ formation during the course of the reaction.

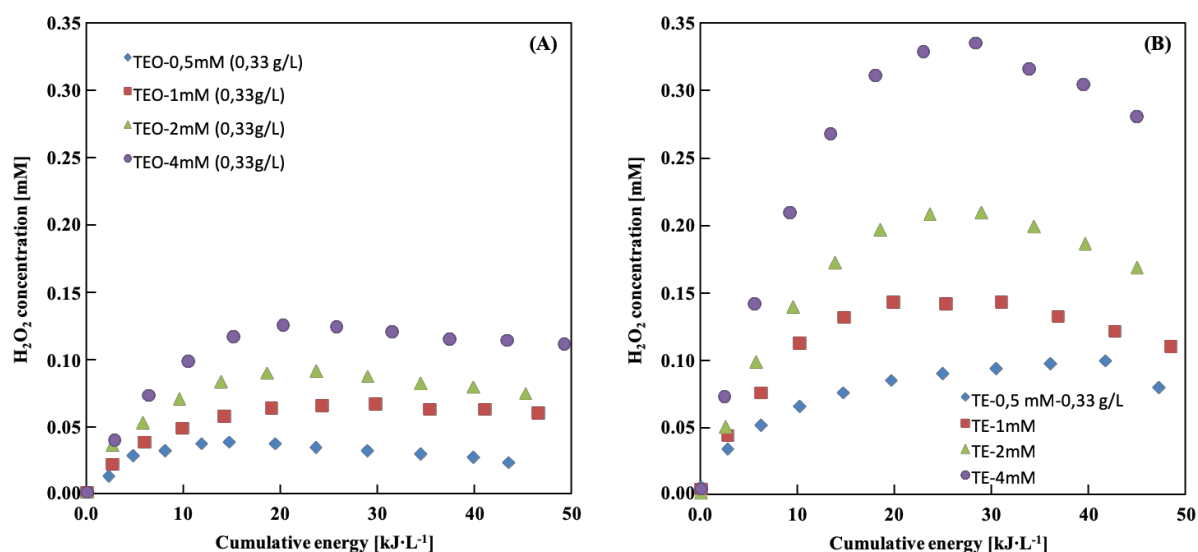


Figure 6 – H₂O₂ concentration versus cumulative energy for different initial concentrations of HMF: 0.5 mM (◆); 1 mM (■); 2 mM (▲) and 4 mM (●) for runs carried out in the presence of TEO (A) and TE (B) photocatalysts. Loading of catalyst 0.33 g·L⁻¹.

The initial reaction rates of HMF disappearance and FDC formation calculated from the reaction data are represented on Figure 7 and summarized in Table 4 for the runs carried out in the presence of the TEO and TE catalysts. The initial reaction rate both for HMF oxidation and for FDC formation increases by increasing the initial HMF concentration. For TEO catalyst the value of the initial reaction rate of HMF conversion is very close to that of FDC formation only for the runs with the lowest HMF initial concentration (0.5 and 1 mM). On the contrary, for higher initial HMF concentrations and for the TE catalyst in all the cases, the initial reaction rate of HMF conversion is higher than that of FDC formation, indicating the occurrence of parallel oxidation processes from the early reaction stages.

Table 4 also reports the initial formation rate of H₂O₂ in the presence of each of two photocatalysts. Interestingly, in the case of using the TEO photocatalyst, for which the HMF to FDC oxidation is the primary reaction and the only one at low conversion rates of HMF, the initial formation rates of FDC and H₂O₂ nearly coincide (Table 4). On the contrary, for the TE photocatalyst the initial formation rate of H₂O₂ is far superior to that of FDC (Table 4). It has been confirmed that, despite the TEO photocatalyst is prepared in the presence of H₂O₂, it does not release H₂O₂ in water under irradiation, nor if heated. Moreover, the

RESULTS AND DISCUSSION

material is stable throughout the reaction runs, as above discussed. Another possible way of H₂O₂ photocatalytic production is through the series of consecutive reduction reaction from water and oxygen [31]. However, no H₂O₂ has been detected in the irradiated aqueous suspensions of any of the PCN catalysts in the absence of organic substrate. H₂O₂ detected in the reaction suspensions appears in the result of organic substrate oxidation.

Table 4 – Photoreactivity results in the presence of 0.33 g·L⁻¹ of the TEO and TE photocatalysts at different HMF initial concentrations: HMF initial oxidation rate (r_{HMF}), FDC initial formation rate (r_{FDC}) and initial H₂O₂ formation rate ($r_{\text{H}_2\text{O}_2}$).

HMF [mM]	r_{HMF} [mmol·kJ ⁻¹] 10 ³		r_{FDC} [mmol·kJ ⁻¹] 10 ³		$r_{\text{H}_2\text{O}_2}$ [mmol·kJ ⁻¹] 10 ³	
	TEO	TE	TEO	TE	TEO	TE
0.5	7.30	10.9	6.60	6.00	6.50	10.4
1	8.70	20.6	6.90	10.0	6.90	13.9
2	15.0	29.9	11.9	12.1	12.0	18.7
4	20.0	51.0	13.6	19.3	12.9	27.6

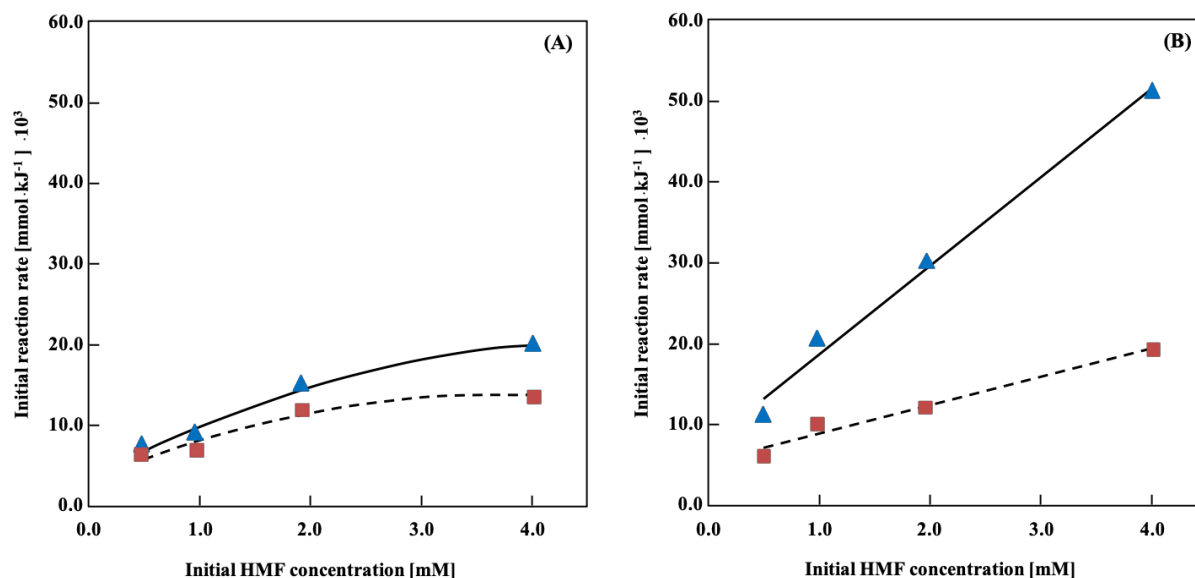


Figure 7 – Initial HMF degradation rate (▲) and initial FDC formation rate (■) versus HMF concentration in the presence of TEO (A) and TE (B) photocatalysts.

Catalyst loading of 0.33 g·L⁻¹.

The initial formation rates of FDC and H₂O₂ are very close when TEO catalyst is used, indicating the simultaneous formation of the two species during the early stages of the reaction, as it was observed as well by Shiraishi et al. [34]. Consequently, the mechanism depicted on Scheme 3 can be hypothesized. The superoxide radical, O₂^{•-}, that is the most abundant and the most likely oxidant species present in the reaction environment (see section 3.2 kinetic aspects), attacks the substrate forming HMF⁻ and a hydro-peroxide radical, which is transformed into H₂O₂ by abstracting a hydrogen atom from HMF⁻ giving rise, in turn, to the formation of a HMF^{•-} radical species, in a similar way to that was previously proposed in [35]. This last species can be oxidized by the hole forming FDC. This mechanism shows that for each mole of FDC produced, one mole of H₂O₂ is also obtained. In the presence of TE, the initial formation rate of H₂O₂ is higher than that of FDC. In this case, as above discussed, the occurrence of at least two parallel reactions is evident, consequently a similar mechanism, in which H₂O₂ is formed also during the other parallel reaction, can also be hypothesized.

In order to test the reusability of the most selective TEO catalyst, three consecutive runs were carried out. The decrease of both reactivity and selectivity is accounted for ca. 10 %

after each cycle. This behaviour is very different with respect to that observed in laboratory scale reactor, in which the catalysts maintained the same HMF conversion degree and the same selectivity to FDC during all the runs [21,25]. Probably, the impossibility to wash the photocatalysts and its loss after the runs in the solar pilot plant photoreactor are responsible for the lowered efficiency of PCN-H₂O₂.

3.2. Kinetic aspects

The inability of carbon nitride to produce •OH radicals by direct interaction of electron-holes with water does not favour the degradation of FDC, making HMF partial oxidation the prevailing process. In previous studies [21], the presence of molecular oxygen (aerobic atmosphere) was necessary to obtain FDC; indeed, the superoxide radical formed via reduction of O₂ by photo-generated electrons was established to be the main reactive species responsible for the HMF partial oxidation to FDC in water.

The rate determining step of the photo-oxidation process is hypothesised to be the reaction between O₂^{•-} and HMF on the catalyst surface. As the adsorbed oxygen acts as an electron trap thus hindering the electron–hole recombination, the O₂^{•-} radicals concentration depends on the fractional sites coverage by O₂. Two different types of sites are hypothesised to exist on the catalyst surface. The first ones can adsorb HMF while the second ones adsorb oxygen. In this hypothesis the initial reaction rate (*r*) for second-order surface oxidation of HMF can be written in terms of Langmuir–Hinshelwood kinetics as:

$$r = k'' \theta_{oxygen} \theta_{HMF} \quad \text{eq. 1}$$

in which *k''* is the surface second-order rate constant, and θ_{oxygen} and θ_{HMF} are the fractional sites coverages by oxygen and HMF, respectively. The fractional sites coverages by oxygen and HMF are given by:

$$\theta_{oxygen} = \frac{K_{Ox}c_{Ox}}{1 + K_{Ox}c_{Ox}} \quad \text{eq. 2}$$

$$\theta_{HMF} = \frac{K_{HMF}c_{HMF}}{1 + K_{HMF}c_{HMF}} \quad \text{eq. 3}$$

in which K_{Ox} and K_{HMF} are the equilibrium adsorption constants of oxygen and HMF, respectively, and c_{Ox} , and c_{HMF} , the oxygen and HMF concentrations in the aqueous phase. As all the experiments were performed in an open batch reactor in contact with atmospheric oxygen, it may be assumed that the θ_{oxygen} term is constant throughout the HMF photo-oxidation. eq. 1 can therefore be written as:

$$r = k' \theta_{HMF} \quad \text{eq.4}$$

in which k' is the surface pseudo-first-order rate constant and it is equal to $k'' \theta_{oxygen}$. By substituting eq. 3 into eq. 4, the following equation is obtained:

$$r = k' \frac{K_{HMF}c_{HMF}}{1 + K_{HMF}c_{HMF}} \quad \text{eq.5}$$

and consequently:

$$\frac{1}{r} = \frac{1}{k'} \frac{1 + K_{HMF}c_{HMF}}{K_{HMF}c_{HMF}} = \frac{1}{k'} + \frac{1}{k'K_{HMF}} \frac{1}{c_{HMF}} \quad \text{eq.6}$$

The experimental data of the reciprocal of the initial HMF concentration $\left(\frac{1}{c_{HMF}}\right)$ and the corresponding reciprocal of the initial reaction rate $\left(\frac{1}{r}\right)$ in the Cartesian coordinates plane $\left(\frac{1}{c_{HMF}}, \frac{1}{r}\right)$ for runs carried out in the presence of the TEO and TE catalysts, respectively, are shown in Figures 8 (A) and (B). In that plane, equation 6 represents a straight line whose slope is $\frac{1}{k'K_{HMF}}$ and whose intercept with the $\frac{1}{r}$ axis is $\frac{1}{k'}$ (Fig. 8).

By applying a least-square best fitting procedure to these data (dotted lines in Figure 8 represent the interpolating equation), it is possible to calculate k' and K_{HMF} values for the two catalysts used. These values are reported in Table 5. The fitting of the experimental data is very good, particularly in the case of the TE photocatalyst, validating the kinetic model. The results indicate that, the surface pseudo-first-order rate constant of HMF degradation is higher in the case of the TE photocatalyst but that the equilibrium adsorption constants of HMF is higher in the case of the TEO catalyst. This last finding suggests that the saturation of the catalytic sites can be reached more easily in the case of TEO, probably because, as

RESULTS AND DISCUSSION

hypothesized in the previous work [25], this catalyst present a lower number of active sites with respect to the TE photocatalyst, which is also expected in a view of its lower SSA.

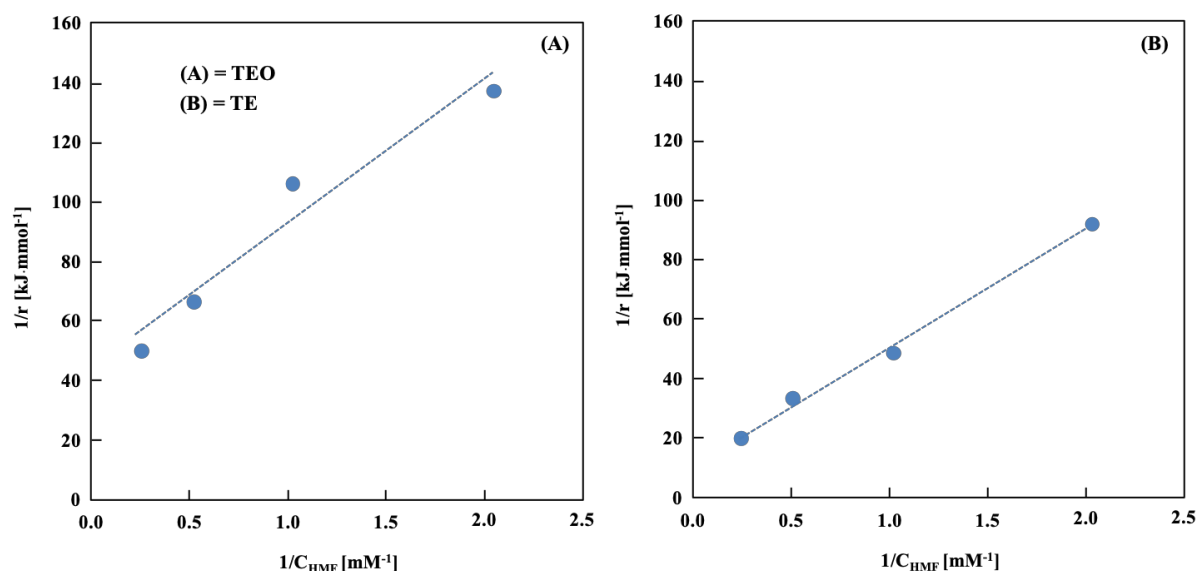


Figure 8 – Reciprocal of the initial HMF concentration ($\frac{1}{C_{HMF}}$) vs. the corresponding reciprocal of the initial reaction rate ($\frac{1}{r}$) for runs carried out in the presence of the TEO (A) and TE (B) photocatalysts, respectively. The dotted lines represent the interpolating equations obtained by applying the least-square best fitting procedure to the experimental data.

Table 5 – Surface pseudo-first-order rate constant (k') and HMF equilibrium adsorption constants (K_{HMF}) calculated for TEO and TE as photocatalyst.

	TEO	TE
$k' \cdot 10^6$ (mol·kJ ⁻¹)	22	95
K_{HMF} (M ⁻¹)	925	265

3.3. Photocatalytic oxidation of BA and 4MBA by using TE and TEO

Figure 9 reports the obtained results. It can be observed that, by using both photocatalysts, the conversion of 4MBA is faster with respect to that of BA as well as the formation of the corresponding aldehydes how it is shown in Figures 9 (A) and (B), respectively. Moreover, the reactivity of the TE material is higher with respect to that of TEO. The selectivity to the corresponding aldehydes, reported in Figure 9 (C), appears higher for BA than for 4MBA. However, if compared at the same conversion percentage of the alcohol (see Figure 9(D)) it is evident that: i) up to ca. 20 % of alcohol conversion the selectivity to both aldehydes is ca. 100 %; ii) for higher conversion degrees the selectivity is higher for 4MBAL (this last comparison was possible only by using TE catalyst because the maximum conversion of BA in the presence of TEO is only of 19 %). The higher conversion of 4MBA with respect to BA and selectivity to 4MBAL with respect to BAL were observed in the previous investigation using the C_3N_4 based photocatalysts [27]. Although, the presence, in 4MBA, of a methoxy group in para position with respect to the alcoholic one determines both an inductive and a delocalization effect that hinder the oxidant attack which can cause the substrate mineralization [27,36], since methoxy group is also ortho-para orienting, it induces the oxidant attack to the alcoholic group, thus favouring the aldehyde formation. By comparing this results with those obtained for HMF partial oxidation under the same conditions (see Table 6) it can be seen that: i) the conversion of HMF is intermediate to that of the aromatic alcohols and ii) the selectivity to the corresponding aldehydes is higher for the aromatic compounds. The higher selectivity to aromatic aldehyde with respect to FDC is not surprising, because it is well known that furanic ring of HMF is much less stable than the aromatic one, and, consequently, during the oxidative attack its breakage is most probable. This last finding can also explain why the conversion of HMF is higher with respect to that of BA in the photocatalytic tests.

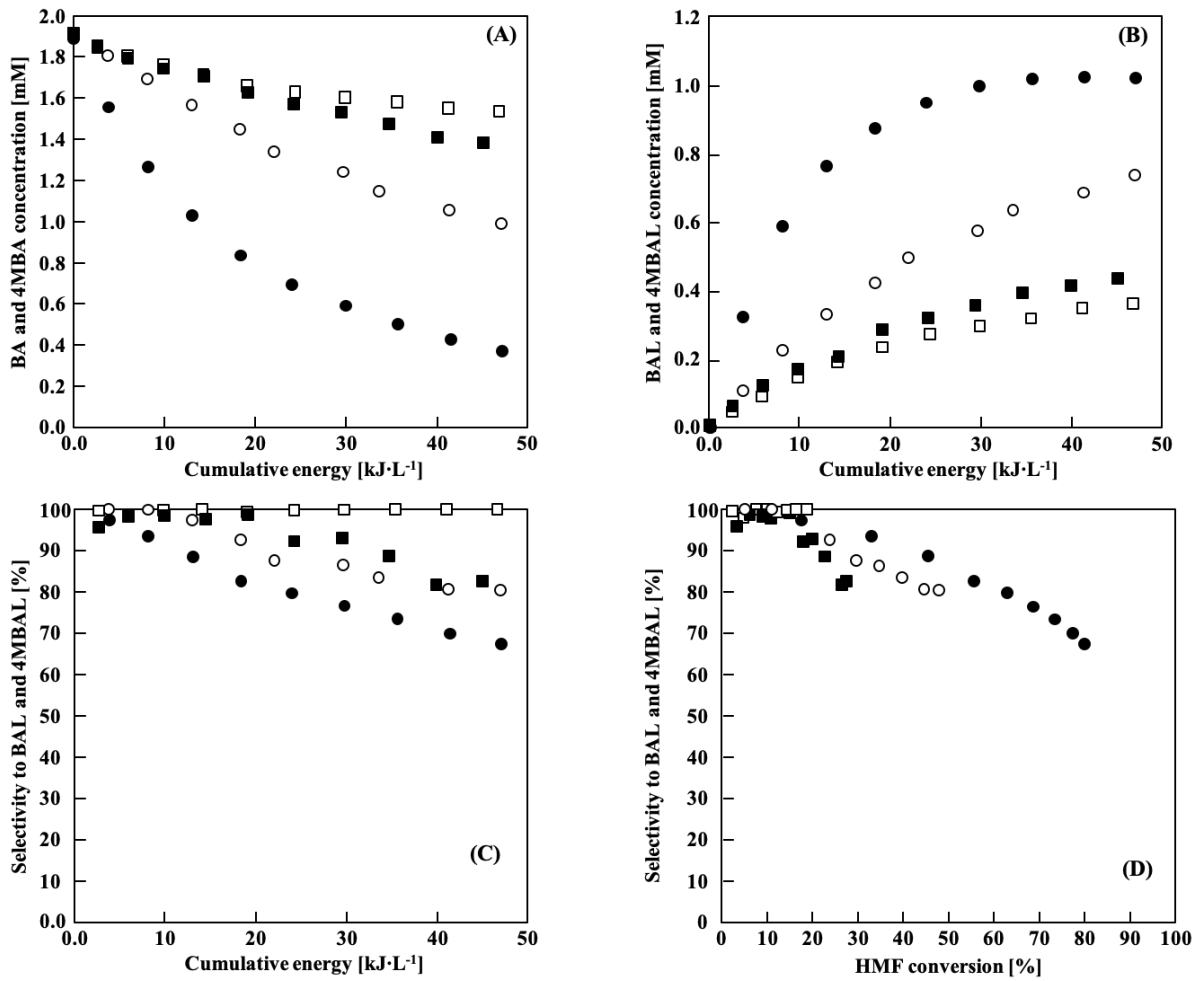


Figure 9 – BA (squares) and 4-MBA (circles) concentrations (A); BAL (squares) and 4-MBAL (circles) concentrations (B); selectivity to BAL (squares) and 4-MBAL (circles) versus cumulative energy (C) and selectivity to BAL (squares) and 4-MBAL (circles) versus BA and 4-MBA conversion, respectively (D) in the presence of 0.33 g·L⁻¹ of TE (full symbols) and TEO (void symbols). Initial alcohol concentration 2 mM.

RESULTS AND DISCUSSION

Table 6 – Photoreactivity results in the presence of 0.33 g·L⁻¹ of the TEO and TE photocatalysts for the three different substrates at 2 mM initial concentration: Initial alcohol oxidation rate (r_{alcohol}), initial aldehyde formation rate (r_{aldehyde}), alcohol conversion (X) and selectivity to the aldehyde (S) after 45 kJ·L⁻¹ of cumulative energy.

	TE			TEO		
	4-MBA	BA	HMF	4-MBA	BA	HMF
r_{alcohol} [mmol·kJ ⁻¹] 10 ³	85.8	16.6	29.9	29.1	15.0	15.0
r_{aldehyde} [mmol·kJ ⁻¹] 10 ³	84.0	16.6	12.1	28.9	15.0	11.9
X [%]	81	28	57	48	19	26
S [%]	67	83	22	81	100	61

4. Conclusions

In this work photocatalytic selective oxidation of HMF to FDC in the presence of PCN and PCN-H₂O₂ adduct has successfully been carried out in a solar pilot photoreactor. The reactivity results and, in particular, the selectivity to FDC formation are found promising for the development of partial photo-oxidation methods, especially by considering that the reaction is carried out in water. Moreover, they are comparable with those obtained in the laboratory scale photoreactor irradiated by both UV artificial lamps and natural sunlight. Interestingly, the pristine PCN sample has shown the higher HMF conversion with respect to that of the PCN-H₂O₂ adduct, but the last one is more selective to the FDC formation. Finally, the partial oxidation of benzyl alcohol and 4-methoxy benzyl alcohol to the corresponding aldehydes has also been achieved proving the applicability of the carbon nitride assisted sun-driven photocatalytic oxidation for a wide range of organic compounds.

5. Acknowledgments

Authors wish to thank CIEMAT-PSA and European Commission for the funding in the framework of the EU-DG RTD's project: SFERA II contract n° 312643. University of Oviedo acknowledge the financial support from Spanish MINECO (MAT2013-40950-R, CTQ2014-52956-C3-1-R and MAT2016-78155-C2-1-R) and Gobierno del Principado de Asturias (GRUPIN14-060, GRUPIN14-078 and Severo Ochoa PhD grant BP-14-029 to MI). IK thanks for the support the Ministry of Education and Science of the Russian Federation (grant no. 4.9722.2017/8.9).

REFERENCES

1. D. Spasiano, R. Marotta, S. Malato, P. Fernandez-Ibáñez, I. Di Somma, Solar photocatalysis: Materials, reactors, some commercial, and pre-industrialized applications. A comprehensive approach, *Appl. Catal. B Environ.*, **2015**, 170, 90–123.
2. X. Lang, X. Chen, J. Zhao, Heterogeneous visible light photocatalysis for selective organic transformations, *Chem. Soc. Rev.*, **2014**, 46, 473–486.
3. L. Palmisano, V. Augugliaro, M. Bellardita, A. Di Paola, E. García-López, V. Loddo, G. Marci, G. Palmisano, S. Yurkadal, Titania photocatalysts for selective oxidations in water, *ChemSusChem*, **2011**, 4, 1431–1438.
4. J.C. Colmenares, W. Ouyang, M. Ojeda, E. Kuna, O. Chernyayeva, D. Lisovytskiy, S. De, R. Luque, A. M. Balu, Mild ultrasound-assisted synthesis of TiO₂ supported on magnetic nanocomposites for selective photo-oxidation of benzyl alcohol, *Appl. Catal. B.*, **2016**, 183, 107–112.
5. X. Wang, K. Maeda, A. Thomas, K. Takanabe, G. Xin, J.M. Carlsson, K. Domen, M. Antonietti, A metal-free polymeric photocatalyst for hydrogen production from water under visible light, *Nature Mater.*, **2009**, 8, 76–80.

6. Y. Wang, Y. Di, M. Antonietti, H. Li, X. Chen, X. Wang, Excellent visible-light photocatalysis of fluorinated polymeric carbon nitride solids, *Chem. Mater.*, **2010**, *22*, 5119–5121.
7. K. Wang, Q. Li, B. Liu, B. Cheng, W. Ho, J. Yu, Sulfur-doped g-C₃N₄ with enhanced photocatalytic CO₂-reduction performance, *Appl. Catal. B.*, **2015**, 176–177, 44–52.
8. Y.W. Zhang, J.H. Liu, G. Wu, W. Chen, Porous graphitic carbon nitride synthesized *via* direct polymerization of urea for efficient sunlight-driven photocatalytic hydrogen production, *Nanoscale*, **2012**, *4*, 5300–5303.
9. Z. Yang, Y. Zhang, Z. Schnopp, Soft and hard templating of graphitic carbon nitride, *J. Mater. Chem. A.*, **2015**, *3*, 14081–14092.
10. X. Wang, S. Blechert, M. Antonietti, Polymeric graphitic carbon nitride for heterogeneous photocatalysis, *ACS Catal.*, **2012**, *2*, 1596–1606.
11. S. Verma, R.B.N Baig, M.N. Nadagouda, R.S. Varma, Selective oxidation of alcohols using photoactive VO@g-C₃N₄, *ACS Sustain. Chem. Eng.*, **2016**, *4*, 1094–1098.
12. B. Long, Z. Ding, X. Wang, Carbon nitride for the selective oxidation of aromatic alcohols in water under visible light, *ChemSusChem*, **2013**, *6*, 2074–2078.
13. J. Wang, J. Xi, Q. Xia, X. Liu, Y. Wang, Recent advances in heterogeneous catalytic conversion of glucose to 5-hydroxymethylfurfural via green routes, *Sci. China Chem.*, **2017**, *60*, 870–886.
14. M.J. Climent, A. Corma, S. Iborra, Conversion of biomass platform molecules into fuel additives and liquid hydrocarbon fuels, *Green Chem.*, **2014**, *16*, 516–547.
15. L. Hu, L. Linc, Z. Wu, S. Zhou, S. Liu, Recent advances in catalytic transformation of biomass-derived 5-hydroxymethylfurfural into the innovative fuels and chemicals, *Renew. Sus. Eng. Rev.*, **2017**, *74*, 230–257.
16. M. Chatterjee, T. Ishizaka, A. Chatterjee, H. Kawanami, Dehydrogenation of 5-hydroxymethylfurfural to diformylfuran in compressed carbon dioxide: an oxidant free approach, *Green Chem.*, **2017**, *19*, 1315–1326.
17. A.S. Amarasekara, D. Green, E. McMillan, Efficient oxidation of 5-hydroxymethylfurfural to 2,5-diformylfuran using Mn(III)-salen catalysts, *Catal. Commun.*, **2008**, *9*, 286–288.

18. L. Hu, G. Zhao, W. Hao, X. Tang, Y. Sun, L. Lin, S. Liu, Catalytic conversion of biomass-derived carbohydrates into fuels and chemicals *via* furanic aldehydes, *RSC Adv.*, **2012**, 2, 11184–11206.
19. S. Yurdakal, B.S. Tek, O. Alagoz, V. Augugliaro, V. Loddo, G. Palmisano, L. Palmisano, Photocatalytic selective oxidation of 5-(hydroxymethyl)-2-furaldehyde to 2,5-furandicarbaldehyde in water by using anatase, rutile, and brookite TiO₂ nanoparticles, *ACS Sust. Chem. Eng.*, **2013**, 1, 456–461.
20. L. Ozcan, P. Yalcin, O. Alagoz, S. Yurdakal, Selective photoelectrocatalytic oxidation of 5-(hydroxymethyl)-2-furaldehyde in water by using Pt loaded nanotube structure of TiO₂ on Ti photoanodes, *Catal. Today*, **2017**, 281, 205–213.
21. I. Krivstov, E.I. García-López, G. Marci, L. Palmisano, Z. Amghouz, J.R. García, S. Ordóñez, E. Díaz, Selective photocatalytic oxidation of 5-hydroxymethyl-2-furfural to 2,5-furandicarboxyaldehyde in aqueous suspension of g-C₃N₄, *Appl. Catal. B*, **2017**, 204, 430–439.
22. S. Xu, P. Zhou, Z. Zhang, C. Yang, B. Zhang, K. Deng, S. Bottle, H. Zhu, Selective oxidation of 5-hydroxymethylfurfural to 2,5-furandicarboxylic acid Using O₂ and a photocatalyst of Co-thioporphyrzine bonded to g-C₃N₄, *J. Am. Chem. Soc.*, **2017**, 139, 14775–14782.
23. H. Zhang, Q. Wu, C. Guo, Y. Wu, T. Wu, Photocatalytic selective oxidation of 5-hydroxymethylfurfural to 2,5-diformylfuran over Nb₂O₅ under visible light, *ACS Sus. Chem. Eng.*, **2017**, 5, 3517–3523.
24. I. Krivtsov, M. Ilkaeva, E. Salas-Colera, Z. Amghouz, J.R. García, E. Díaz, S. Ordóñez, S. Villar-Rodil, Consequences of nitrogen doping and oxygen enrichment on titanium local order and photocatalytic performance of TiO₂ anatase, *J. Phys. Chem. C*, **2017**, 121, 6770–6780.
25. M. Ilkaeva, I. Krivtsov, E.I. García-López, G. Marci, O. Khainakova, J.R. García, L. Palmisano, E. Díaz, S. Ordóñez, Selective photocatalytic oxidation of 5-hydroxymethylfurfural to 2,5-furandicarboxaldehyde by polymeric carbon nitride-hydrogen peroxide adduct, *J. Catalysis*, **2018**, 359, 212–222.

26. D. Spasiano, L.P.P. Rodriguez, J.C. Olleros, S. Malato, R. Marotta, R. Andreozzi, TiO₂/Cu(II) photocatalytic production of benzaldehyde from benzyl alcohol in solar pilot plant reactor, *Appl. Catal. B: Environ.*, **2013**, 136–137, 56–63.
27. M. Bellardita, E.I. García-López, G. Marci, I. Krivtsov, J.R. García, L. Palmisano, Selective photocatalytic oxidation of aromatic alcohols in water by using P-doped g-C₃N₄, *Appl. Catal. B*, **2018**, 220, 222–233.
28. P. Niu, L. Zhang, G. Liu, H.M. Cheng, Graphene-like carbon nitride nanosheets for improved photocatalytic activities, *Adv. Func. Mater.*, **2012**, 22, 4763–4770
29. A. Akhundi, E. I. García-López, G. Marci, A. Habibi-Yangjeh, L. Palmisano, Comparison between preparative methodologies of nanostructured carbon nitride and their use as selective photocatalysts in water suspension, *Res. Chem. Interm.*, **2017**, 43, 5153–5168.
30. M. Ilkaeva, I. Krivtsov, E. Bartashevich, S.A. Khainakov, J.R. García, E. Díaz, S. Ordóñez, Carbon nitride assisted chemoselective C–H bond photo-oxidation of alkylphenolethoxylates in water medium, *Green Chem.*, **2017**, 19, 4299–4304.
31. Y. Kofuji, Y. Isobe, Y. Shiraishi, H. Sakamoto, S. Tanaka, S. Ichikawa, T. Hirai, Carbon Nitride–Aromatic Diimide–Graphene Nanohybrids: Metal-Free Photocatalysts for Solar-to-Hydrogen Peroxide Energy Conversion with 0.2% Efficiency, *J. Am. Chem. Soc.*, **2016**, 138, 10019–10025.
32. S. Malato Rodriguez, J. Blanco Galvez, M.I. Maldonado Rubio, P. Fernandez Ibañez, D. Alarcon Padilla, M. Collares Pereira, J. Farinha Mendes, J. Correia de Oliveira, Engineering of solar photocatalytic collectors, *Solar Energy*, **2004**, 77, 513–524.
33. J. Colina-Márquez, F. Machuca-Martínez, G. Li Puma, Radiation absorption and optimization of solar photocatalytic reactors for environmental applications, *Env. Sci. Technol.*, **2010**, 44, 5112–5120.
34. Y. Shiraishi, S. Kanazawa, Y. Sugano, D. Tsukamoto, H. Sakamoto, S. Ichikawa, T. Hirai, Radiation Absorption and Optimization of Solar Photocatalytic Reactors for Environmental Applications, *ACS Catal.*, **2014**, 4, 774–780.
35. F. Su, S.C. Mathew, G. Lipner, X.Fu, M. Antonietti, S. Blechert, X. Wang, Radiation absorption and optimization of solar photocatalytic reactors for environmental applications, *J. Am. Chem. Soc.*, **2010**, 132, 16299–16301.

36. G. Palmisano, M. Addamo, V. Augugliaro, T. Caronna, A. Di Paola, E. García-López, V. Loddo, G. Marci, L. Palmisano, M. Schiavello, Selectivity of hydroxyl radical in the partial oxidation of aromatic compounds in heterogeneous photocatalysis, *Catal Today*, **2007**, 122, 118–127.

Chapter 5 Conclusions

In the present Ph. D. Thesis, the methodologies for the preparation of TiO₂ and polymeric carbon nitride based semiconductor photocatalysts and their application for emerging pollutants degradation and selective transformation of organic compounds to high-added value molecules, respectively, have been developed. The set of the synthetic and modification techniques applied in the present work targets the tuning of the morphological, textural and surface properties of the elaborated photocatalytic materials, thus providing the means for the fine control of their reaction performance.

1. With regard to the synthesis and photocatalytic application of titania spherical particles for organic pollutants degradation:
 - A new method for preparation of mesoporous TiO₂ anatase spherical nanoparticles (in the range of 50-260 nm) accomplished by the precipitation of hydrous titania from aqueous solution of titania peroxo complex with organic solvents and followed by post-synthetic reflux treatment has been developed.
 - The prepared titania spheres have demonstrated a degree of activity in the reaction of 2-(4-methylphenoxy)ethanol (MPET) photo-degradation close to that of the commercial titania Aeroxide P25.
 - The reusability test has shown that the activity of Aeroxide P25 decreases significantly after the third reaction due to poor recoverability, while the synthesised titania spheres can be repeatedly used for at least four cycles without any significant loss of their photocatalytic activity.
 - The mechanism of the photo-decomposition of MPET has been proposed and several partially oxidised products of it have been identified. The prepared mesoporous titania spheres have proved efficient not only for the initial

compound (MPET) photo-degradation but also for the toxic intermediate, *p*-cresol.

2. With regard to the synthesis and photocatalytic application of the PCN–H₂O₂ adduct material for chemoselective C–H bond photo-oxidation of alkylphenolethoxylates in water medium:
 - It has been proposed on the bases of experimental evidence and theoretical calculations that the treatment of polymeric carbon nitride (PCN) using H₂O₂ resulted in the PCN–H₂O₂ adduct formation, which contained H₂O₂ bonded to the non-condensed NH₂-species of PCN.
 - PCN oxidises the MPET benzylic carbon forming 4-(2-hydroxyethoxy)benzaldehyde (HEB) with selectivity of 57%, whereas the PCN–H₂O₂ adduct provides an enhanced selectivity to this product reaching the values in the range of 82-87%.
 - It has been proposed that the presence of the PCN–H₂O₂ surface complex creates a steric hindrance for the direct interaction between the oxyethanol group of MPET and the amino-groups of carbon nitride, thus promoting the selectivity towards the HEB formation.
3. With regard to the study of the PCN–H₂O₂ adduct performance in the partial photocatalytic oxidation of 5-hydroxymethyl-2-furaldehyde (HMF) for biomass valorisation:
 - The in-depth study of the PCN–H₂O₂ photocatalysts by XRD, XPS, TPD and Solid State NMR methods has confirmed the presence of the bonded hydrogen peroxide and its effect on the hydrogen bonding in the adduct samples.
 - It has been revealed that the synthesised photocatalyst PCN–H₂O₂ having hydrogen peroxide coordinated to its NH₂ surface species is stable up to 200 °C if heated in air, and it does not release H₂O₂ under irradiation or heating in water suspensions.
 - PCN–H₂O₂ photocatalyst has shown 80% of HMF to FDC (2,5-furandicarboxaldehyde) conversion selectivity under UV irradiation and up to 89% under natural solar light in water medium.

- It has been proposed that the non-condensed carbon nitride species are responsible for the generation of $\bullet\text{OH}$ radicals leading to the decrease of the reaction selectivity, but in the PCN– H_2O_2 adduct these sites are blocked by the coordinated hydrogen peroxide, thus allowing to avoid the unselective substrate conversion.
4. With regard to the study of partial photo-oxidation of HMF to FDC using PCN– H_2O_2 as photocatalyst under the real conditions on a pilot scale photoreactor at the Almería Solar Platform:
- The PCN– H_2O_2 adduct has been tested for partial selective oxidation of HMF, 4-methoxybenzyl alcohol (MBA), benzyl alcohol (BA) molecules to the corresponding aldehydes at the Almería Solar Platform in a 15.5 L volume Compound Parabolic Collector (CPC) photo-reactor under natural solar irradiation and in water medium.
 - The selectivity of HMF to FDC photo-oxidation in CPC has been found in the range 70-90%, which is comparable with the laboratory tests. The varying concentrations of the photocatalysts as well as the substrates have proved the viability of the partial photocatalytic oxidation of aromatic alcohols under real-life conditions.
 - It has been found that the kinetic model built on the basis of the obtained experimental data described by the Langmuir-Hinshelwood mechanism.

Conclusiones

En esta Tesis Doctoral se han desarrollado distintos métodos para la preparación de fotocatalizadores semiconductores basados en TiO_2 y nitruro de carbono polimérico y sus aplicaciones para la degradación de contaminantes emergentes y la transformación selectiva de compuestos orgánicos a moléculas de alto valor añadido. La selección de las técnicas sintéticas y post-sintéticas aplicadas en este trabajo pretende modular las propiedades morfológicas, texturales y superficiales del material fotocatalítico elaborado, proveyendo los medios para un control preciso de su comportamiento en las reacciones estudiadas.

1. En lo que se refiere a la síntesis y aplicación fotocatalítica de partículas esféricas de titania para la degradación de los contaminantes orgánicos:
 - Se ha desarrollado un nuevo método para la preparación de nanopartículas mesoporosas esféricas de TiO_2 anatasa (diámetro: 50-260 nm), que incluye la precipitación de titania hidratada desde una disolución acuosa conteniendo peróxido de titanio, asistida por un disolvente orgánico, y acompañada con un tratamiento post-sintético de reflujo.
 - Las esferas de titania han mostrado un nivel de actividad en la fotodegradación de 2-(4-metilfenoxi)etanol (MPET) comparable a la de la titania comercial, Aeroxide P25.
 - Los ensayos de reutilización han revelado que la actividad de Aeroxide P25 disminuye significativamente después de tres ciclos, mientras que las esferas de titania sintetizadas en este trabajo pueden ser utilizadas repetitivamente en al menos cuatro ciclos sin pérdida significativa de su actividad fotocatalítica.
 - Se ha propuesto el mecanismo de foto-decomposición de MPET y se han identificado productos parcialmente oxidados. El material preparado, basado

en esferas de titania, ha demostrado su eficiencia no solo en la fotodegradación del compuesto inicial (MPET) sino también en la del intermedio tóxico, *p*-cresol.

2. En lo que se refiere a la síntesis y aplicación del aducto nitruro de carbono-agua oxigenada para la foto-oxidación quimioselectiva de enlaces C–H de alquifenoletoxilatos en agua:

- Las evidencias experimentales y los cálculos teóricos indican que el tratamiento de nitruro de carbono polimérico con H_2O_2 resulta en la formación del aducto nitruro de carbono-agua oxigenada, por interacción de H_2O_2 y grupos NH_2 del nitruro de carbono polimérico.
- El nitruro de carbono polimérico oxida al carbono bencílico de la molécula MPET, obteniéndose 4-(2-hidroxietoxi)benzaldehído (HEB) con una selectividad del 57%, mientras que el aducto nitruro de carbono-agua oxigenada eleva dicha selectividad hasta el 82-87%.
- Se propone que el complejo superficial nitruro de carbono- H_2O_2 impide la interacción directa entre el grupo oxietanol del MPET y los grupos amino del nitruro de carbono, promoviendo la selectividad hacia la formación de HEB.

3. En lo que se refiere al estudio de comportamiento del aducto nitruro de carbono-agua oxigenada en la oxidación parcial fotocatalítica de 5-hidroximetil-2-furaldehído (HMF) para la valorización de biomasa:

- El aducto nitruro de carbono-agua oxigenada se ha caracterizado mediante diferentes técnicas experimentales (XRD, XPS, TPD, SS-NMR), confirmando la presencia de H_2O_2 enlazada en superficie.
- El aducto nitruro de carbono-agua oxigenada es estable hasta 200 °C en aire y, en suspensiones acuosas, no libera H_2O_2 bajo irradiación, incluso a temperaturas relativamente elevadas.
- Las especies no condensadas de nitruro de carbono parecen ser las responsables de la generación de radicales $\bullet OH$, causantes del descenso en la selectividad de la reacción mientras que, en el aducto nitruro de carbono-agua

oxigenada, estos sitios están bloqueados por el agua oxigenada coordinada, impidiendo la conversión no selectiva del sustrato.

4. En lo que se refiere al estudio de foto-oxidación parcial de HMF a FDC usando el aducto nitruro de carbono-agua oxigenada como fotocatalizador en un foto-reactor piloto de la Plataforma Solar de Almería:
 - El aducto nitruro de carbono-agua oxigenada se utilizó en la oxidación parcial selectiva de HMF, alcohol 4-metoxibencílico (MBA) y alcohol bencílico (BA) a sus aldehídos correspondientes, utilizando un foto-reactor de 15.5 L de volumen, en medio acuoso, bajo luz solar.
 - La selectividad de la foto-oxidación de HMF a FDC en el foto-reactor piloto fue del 70-90%, comparable a los resultados obtenidos en ensayos de laboratorio, confirmándose la viabilidad de la foto-oxidación parcial de alcoholes aromáticos en condiciones reales.
 - El modelo cinético construido a partir de datos experimentales indica que la reacción sigue un mecanismo Langmuir-Hinshelwood.

References

1. S. Braslavsky, A. Braun, A. Cassano, A. Emeline, M. Litter, L. Palmisano, V. Parmon, N. Serpone, Glossary of terms used in photocatalysis and radiation catalysis, *Pure Appl. Chem.*, **2011**, 83, 931–1014.
2. L. Palmisano, E. I. García-López, G. Marci, Inorganic materials acting as heterogeneous photocatalysts and catalysts in the same reactions, *Dalton Trans.*, **2016**, 29, 11596–11605.
3. A. Fujishima, K. Honda, Electrochemical photolysis of water at a semiconductor electrode, *Nature*, **1972**, 238, 37–38.
4. N. Serpone, A. V. Emeline, S. Horikoshi, V. N. Kuznetsov, V. K. Ryabchuk, On the genesis of heterogeneous photocatalysis: a brief historical perspective in the period 1910 to the mid-1980s, *Photochem. Photobiol. Sci.*, **2012**, 11, 1121–1150.
5. Textbook of photochemistry, J. Plotnikow, Verlag von Wilhelm Knapp, **1910**.
6. M. D. Hernández-Alonso, F. Fresno, S. Suárez, J. M. Coronado, Development of alternative photocatalysts to TiO₂: Challenges and opportunities, *Energy Environ. Sci.*, **2009**, 2, 1231–1257.
7. W.-J. Ong, L.-L. Tan, Y. H. Ng, S.-T. Yong, S.-P. Chai, Graphitic carbon nitride (g-C₃N₄)-based photocatalysts for artificial photosynthesis and environmental remediation: are we a step closer to achieving sustainability?, *Chem. Rev.*, **2016**, 116, 7159–7329.
8. L. Zeng, X. Guo, C. He, C. Duan, Metal–Organic frameworks: versatile materials for heterogeneous photocatalysis, *ACS Catal.*, **2016**, 6, 7935–7947.
9. J. Kou, C. Lu, J. Wang, Y. Chen, Z. Xu, R. S. Varma, Selectivity enhancement in heterogeneous photocatalytic transformations, *Chem. Rev.*, **2017**, 117, 1445–1514

REFERENCES

10. V. Augugliaro, M. Bellardita, V. Loddo, G. Palmisano, L. Palmisano, S. Yurdakal, Overview on oxidation mechanisms of organic compounds by TiO₂ in heterogeneous photocatalysis, *J. Photochem. Photobiol. C*, **2012**, 13, 224–245.
11. W. Wang, M. O. Tadé, Z. Shao, Nitrogen-doped simple and complex oxides for photocatalysis: A review, *Prog. Mater. Sci.*, **2018**, 92, 33–63.
12. J.C. Yu, W. Ho, J. Yu, H. Yip, P.K. Wong, J. Zhao, Efficient visible-light-induced photocatalytic disinfection on sulfur-doped nanocrystalline titania, *Environ. Sci. Technol.*, **2005**, 39, 1175–1179.
13. C. Zhao, M. Pelaez, D. D. Dionysiou, S. C. Pillai, J. A. Byrne, K. E. O’Shea, UV and visible light activated TiO₂ photocatalysis of 6-hydroxymethyl uracil, a model compound for the potent cyanotoxin cylindrospermopsin, *Catal. Today*, **2014**, 224, 70–76.
14. M. Miyauchi, H. Irie, M. Liu, X. Qiu, H. Yu, K. Sunada, K. Hashimoto, Visible-light-sensitive photocatalysts: nanocluster-grafted titanium dioxide for indoor environmental remediation, *J. Phys. Chem. Lett.*, **2016**, 7, 75–84.
15. M.R. Hoffmann, S.T. Martin, W. Choi, D.W. Bahnemann, Environmental applications of semiconductor photocatalysis, *Chem. Rev.*, **1995**, 95, 69–96.
16. M. Schiavello, V. Augugliaro, L. Palmisano, An experimental method for the determination of the photon flow reflected and absorbed by aqueous dispersions containing polycrystalline solids in heterogeneous photocatalysis, *J. Catal.*, **1991**, 127, 332–341.
17. M. L. Satuf, R. J. Brandi, A. E. Cassano, O. M. Alfano, Quantum efficiencies of 4-chlorophenol photocatalytic degradation and mineralization in a well-mixed slurry reactor, *Ind. Eng. Chem. Res.*, **2007**, 46, 43–51.
18. G. Sagawe, M. L. Satuf, R. J. Brandi, J. P. Muschner, C. Federer, O. M. Alfano, D. Bahnemann, A. E. Cassano, Analysis of photocatalytic reactors employing the photonic efficiency and the removal efficiency parameters: degradation of radiation absorbing and nonabsorbing pollutants, *Ind. Eng. Chem. Res.*, **2010**, 49, 6898–6908.
19. M. J. Muñoz-Batista, A. Kubacka, A. B. Hungria, M. Fernández-García, Heterogeneous photocatalysis: Light-matter interaction and chemical effects in quantum efficiency calculations, *J. Catal.*, **2015**, 330, 154–166.

REFERENCES

20. O. Fontelles-Carceller, M. J. Muñoz-Batista, M. Fernández-García, A. Kubacka, Interface effects in sunlight-driven Ag/g-C₃N₄ composite catalysts: study of the toluene photodegradation quantum, *ACS Appl. Mater. Interfaces*, **2016**, 8, 2617–2627.
21. U. Caudillo-Flores, M. J. Muñoz-Batista, F. Ung-Medina, G. Alonso-Núñez, A. Kubacka, J. A. Cortés, M. Fernández-García, Effect of the anatase-rutile contact in gas phase toluene photodegradation quantum efficiency, *Chem. Eng. J.*, **2016**, 299, 393–402.
22. O. Fontelles-Carceller, M. J. Muñoz-Batista, E. Rodríguez-Castellón, J. C. Conesa, M. Fernández-García, A. Kubacka, Measuring and interpreting quantum efficiency for hydrogen photo-production using Pt-titania catalysts, *J. Catal.*, **2017**, 347, 157–169.
23. Y. Du, J. Rabani, The measure of TiO₂ photocatalytic efficiency and the comparison of different photocatalytic titania, *J. Phys. Chem. B*, **2003**, 107, 11970–11978.
24. Y. Du, J. Rabani, Determination of quantum yields in two-dimensional scattering systems, *J. Photochem. Photobiol. A*, **2004**, 162, 575–578.
25. H. Kisch, On the problem of comparing rates or apparent quantum yields in heterogeneous photocatalysis, *Angew. Chem., Int. Ed.*, **2010**, 49, 9588–9589.
26. P. Johne, H. Kisch, Photoreduction of carbon dioxide catalysed by free and supported zinc and cadmium sulphide powders, *J. Photochem. Photobiol. A*, **1997**, 111, 223–228.
27. D. Curco, J. Gimenez, A. Addardak, S. Cervera-March, S. Esplugas, Effects of radiation absorption and catalyst concentration on the photocatalytic degradation of pollutants, *Catal. Today*, **2002**, 76, 177–188.
28. D. Friedmann, C. Mendive, D. Bahnemann, TiO₂ for water treatment: Parameters affecting the kinetics and mechanisms of photocatalysis, *Appl. Catal. B: Environ.*, **2010**, 99, 398–406.
29. Heterogeneous photocatalysis. From fundamentals to green applications. Eds.: J.C. Colmenares, Y-J. Xu, Springer, **2016**.
30. T. Berger, M. Sterrer, O. Diwald, E. Knözinger, D. Panayotov, T. L. Thompson, J. T. Yates, Light-induced charge separation in anatase TiO₂ particles, *J. Phys. Chem. B*, **2005**, 109, 6061–6068.

REFERENCES

31. N. A. Deskins, R. Rousseau, M. Dupuis, Localized electronic states from surface hydroxyls and polarons in TiO₂ (110), *J. Phys. Chem. C*, **2009**, 113, 14583–14586.
32. J. Schneider, M. Matsuoka, M. Takeuchi, J. Zhang, Y. Horiuchi, M. Anpo, D. W. Bahnemann, Understanding TiO₂ photocatalysis: mechanisms and materials, *Chem. Rev.*, **2014**, 114, 9919–9986.
33. D. W. Bahnemann, M. Hilgendorff, R. Memming, Charge carrier dynamics at TiO₂ particles: reactivity of free and trapped holes, *J. Phys. Chem. B*, **1997**, 101, 4265–4275.
34. C. Y. Wang, C. Böttcher, D. W. Bahnemann, J. K. Dohrmann, A comparative study of nanometer sized Fe(III)-doped TiO₂ photocatalysts: synthesis, characterization and activity, *J. Mater. Chem.*, **2003**, 13, 2322–2329.
35. M.A. Henderson, A surface science perspective on photocatalysis, *Surf. Sci. Rep.*, **2011**, 66, 185–297.
36. Y.-C. Liang, C.-C. Wang, C.-C. Kei, Y.-C. Hsueh, W.-H. Cho, T.-P. Perng, Modified TiO₂ for environmental photocatalytic applications: a review, photocatalytic activity of TiO₂ nanotube layers loaded with Ag and Au nanoparticles, *J. Phys. Chem. C*, **2011**, 115, 9498–9502.
37. G. L. Chiarello, M. H. Aguirre, E. Selli, Hydrogen production by photocatalytic steam reforming of methanol on noble metal-modified TiO₂, *J. Catal.*, **2010**, 273, 182–190.
38. D. Lawless, N. Serpone, D. Meisel, Role of hydroxyl radicals and trapped holes in photocatalysis. A pulse radiolysis study., *J. Phys. Chem.*, **1991**, 95, 5166–5170.
39. X. Yang, N. Tamai, How fast is interfacial hole transfer? In situ monitoring of carrier dynamics in anatase TiO₂ nanoparticles by femtosecond laser spectroscopy, *Phys. Chem. Chem. Phys.*, **2001**, 3, 3393–3398.
40. T. Morishita, A. Hibara, T. Sawada, Ultrafast charge transfer at TiO₂/SCN⁻(aq) interfaces investigated by femtosecond transient reflecting grating method, *J. Phys. Chem. B*, **1999**, 103, 5984–5987.
41. J. M. Warman, M. P. De Haas, P. Pichat, N. Serpone, Effect of isopropyl alcohol on the surface localization and recombination of conduction-band electrons in Degussa P25 titania: a pulse-radiolysis time-resolved microwave conductivity study, *J. Phys. Chem.*, **1991**, 95, 8858.

REFERENCES

42. Y. Tamaki, A. Furube, M. Murai, K. Hara, R. Katoh, M. Tachiya, Direct observation of reactive trapped holes in TiO₂ undergoing photocatalytic oxidation of adsorbed alcohols: evaluation of the reaction rates and yields., *J. Am. Chem. Soc.*, **2006**, 128, 416–417.
43. I. A. Shkrob, M. C. Sauer, D. Gosztola, Efficient, rapid photooxidation of chemisorbed polyhydroxyl alcohols and carbohydrates by TiO₂ nanoparticles in an aqueous solution, *J. Phys. Chem. B*, **2004**, 108, 12512–12517.
44. Y. Nosaka, A. Y. Nosaka, Kinetic processes in the presence of photogenerated charge carriers in photocatalysis. Fundamentals and Perspectives. Eds.: J. Schneider, D. Bahnemann, J. Ye, G. Li Puma, D. D. Dionysiou, RSC Energy and Environment Series, **2016**.
45. A. Y. Nosaka, T. Fujiwara, H. Yagi, H. Akutsu, Y. Nosaka, Photocatalytic reaction sites at the TiO₂ surface as studied by solid-state ¹H NMR spectroscopy, *Langmuir*, **2003**, 19, 1935–1937.
46. M.A. Henderson, A surface science perspective on photocatalysis, *Surf. Sci. Rep.*, **2011**, 66, 185–297.
47. F. D. Angelis, C. D. Valentin, S. Fantacci, A. Vittadini, A. Selloni, Theoretical studies on anatase and less common TiO₂ phases: bulk, surfaces, and nanomaterials, *Chem. Rev.*, **2014**, 114, 9708–9753.
48. Y. Du, N.A. Deskins, Z. Zhang, Z. Dohnalek, M. Dupuis, I. Lyubinetsky, Two pathways for water interaction with oxygen adatoms on TiO₂ (110), *Phys. Rev. Lett.*, **2009**, 102, 096102.
49. F. Parrino, P. Conte, C. De Pasquale, V. A. Laudicina, V. Loddo, L. Palmisano, Influence of adsorbed water on the activation energy of model photocatalytic reactions, *J. Phys. Chem. C*, **2017**, 121, 2258–2267.
50. Y.-F. Li, U. Aschauer, J. Chen, A. Selloni, Adsorption and reactions of O₂ on anatase TiO₂, *Acc. Chem. Res.*, **2014**, 47, 3361–3368.
51. E. Carter, A. F. Carley, D. M. Murphy, Evidence for O₂-radical stabilization at surface oxygen vacancies on polycrystalline TiO₂, *J. Phys. Chem. C*, **2007**, 111, 10630–10638.

REFERENCES

52. T. Berger, M. Sterrer, O. Diwald, E. Knözinger, Light-induced charge separation in anatase TiO₂ particles, *J. Phys. Chem. B*, **2005**, 109, 6061–6068.
53. I. Krivtsov, E. I. García-López, G. Marci, L. Palmisano, Z. Amghouz, J. R. García, S. Ordóñez, E. Díaz, Selective photocatalytic oxidation of 5-hydroxymethyl-2-furfural to 2,5-furandicarboxyaldehyde in aqueous suspension of g-C₃N₄, *Appl. Catal. B: Environ.*, **2017**, 204, 430–439.
54. M. Bellardita, E. I. García-López, G. Marci, I. Krivtsov, J. R. García, L. Palmisano, Selective photocatalytic oxidation of aromatic alcohols in water by using P-doped g-C₃N₄, *Appl. Catal. B: Environ.*, **2018**, 220, 222–233.
55. V. Augugliaro, H. Kisch, V. Loddo, M. J. López-Muñoz, C. Márquez-Álvarez, G. Palmisano, L. Palmisano, F. Parrino, S. Yurdakal, Photocatalytic oxidation of aromatic alcohols to aldehydes in aqueous suspension of home-prepared titanium dioxide 1. Selectivity enhancement by aliphatic alcohols, *Appl. Catal. A: General*, **2008**, 349, 182–188.
56. Y. Paz, Specificity in photocatalysis in Photocatalysis. Fundamentals and Perspectives. Eds.: J. Schneider, D. Bahnemann, J. Ye, G. Li Puma, D. D. Dionysiou, RSC Energy and Environment Series, **2016**.
57. Photocatalysis. Applications. Eds.: D. D. Dionysiou, G. Li Puma, J. Ye, J. Schneider, D. Bahnemann, RSC Energy and Environment Series, **2016**.
58. R. Loos, R. Carvalho, D. C. António, S. Comero, G. Locoro, S. Tavazzi, B. Paracchini, M. Ghiani, T. Lettieri, L. Blaha, B. Jarosova, S. Voorspoels, K. Servaes, P. Haglund, J. Fick, R. H. Lindberg, D. Schwesig, B. M. Gawlik, EU-wide monitoring survey on emerging polar organic contaminants in wastewater treatment plant effluents, *Water Res.*, **2013**, 47, 6475–6487.
59. M. J. Martínez Bueno, M. J. Gomez, S. Herrera, M. D., Hernando, A. Agüera, A. R. Fernández-Alba, Occurrence and persistence of organic emerging contaminants and priority pollutants in five sewage treatment plants of Spain: Two years pilot survey monitoring, *Environ. Pollut.*, **2012**, 164, 267–273.
60. S.C. Monteiro, A.B. Boxall, Factor affecting the degradation of pharmaceuticals in agricultural soils, *Environ. Toxicol. Chem.*, **2009**, 28, 2546–2554

-
61. Treatment of Micropollutants in Water and Wastewater, J. Virkutyte, R. S. Varma, V. Jegatheesan, IWA Publishing, **2010**.
 62. Y. Wu, Y. Jia, , Lu, X., 2013. Assessment of semi-volatile organic compounds in drinking water sources in Jiangsu. China., *Ecotoxicol. Environ. Saf.*, **2013**, 94, 138–146.
 63. A. Kumar, I. Xagorarakis, Pharmaceuticals, personal care products and endocrine-disrupting chemicals in U.S. surface and finished drinking waters: a proposed ranking system, *Sci. Total Environ.*, **2010**, 408, 5972–5989.
 64. G. Zhang, E. M. Wurtzler, X. He, M. N. Nadagouda, K. O'Shea, S. M. El-Sheikh, A. A. Ismail, D. Wendell, D. D. Dionysiou, Identification of TiO₂ photocatalytic destruction byproducts and reaction pathway of cylindrospermopsin, *Appl. Catal. B: Environ.*, **2015**, 163, 591–598.
 65. M. G. Antoniou, C. Zhao, K. E. O'Shea, G. Zhang, D. D. Dionysiou, C. Zhao, C. Han, M. N. Nadagouda, H. Choi, T. Fotiou, T. M. Triantis, A. Hiskia, Photocatalytic Degradation of Organic Contaminants in Water: Process Optimization and Degradation Pathways in Photocatalysis. Applications. Eds.: D. D. Dionysiou, G. Li Puma, J. Ye, J. Schneider, D. Bahnemann, RSC Energy and Environment Series, **2016**.
 66. M. Muneer, M. Qamar, M. Saquib, D. W. Bahnemann, Heterogeneous photocatalysed reaction of three selected pesticide derivatives, propham, propachlor and tebuthiuron in aqueous suspensions of titanium dioxide, *Chemosphere*, **2005**, 61, 457–468.
 67. U. I. Gaya, A. H. Abdullah, Heterogeneous photocatalytic degradation of organic contaminants over titanium dioxide: A review of fundamentals, progress and problems, *J. Photochem. Photobiol. C*, **2008**, 9, 1–12.
 68. Z. Guo, R. Ma, G. Li, Degradation of phenol by nanomaterial TiO₂ in wastewater, *Chem. Eng. J.*, **2006**, 119, 55.
 69. A. O. Kondrakov, A. N. Ignateva, F. H. Frimmel, S. Bräse, H. Horn, A. I. Revelsky, Formation of genotoxic quinones during bisphenol A degradation by TiO₂ photocatalysis and UV photolysis: A comparative study, *Appl. Catal. B: Environ.*, **2014**, 160–161, 106–114.

REFERENCES

70. G. Li, X. Nie, Y. Gao, T. An, Can environmental pharmaceuticals be photocatalytically degraded and completely mineralized in water using g-C₃N₄/TiO₂ under visible light irradiation?—Implications of persistent toxic intermediates, *Appl. Catal. B: Environ.*, **2016**, 180, 726–732.
71. H. K. Singh, M. Saquib, M. M. Haqua, M. Muneer, D. W. Bahnemann, Titanium dioxide mediated photocatalysed degradation of phenoxyacetic acid and 2,4,5-trichlorophenoxyacetic acid in aqueous suspensions, *J. Mol. Catal. A: Chem.*, **2007**, 264, 66–72.
72. W. Bahnemann, M. Muneer, M. M. Haque, Titanium dioxide-mediated photocatalysed degradation of few selected organic pollutants in aqueous suspensions, *Catal. Today*, **2007**, 124, 133–148.
73. M. Muneer, J. Theurich, D. Bahnemann, Titanium dioxide mediated photocatalytic degradation of 1,2-diethyl phthalate, *J. Photochem. Photobiol. A*, **2001**, 143, 213–219.
74. M. Muneer, D. Bahnemann, M. Qamar, M. A. Tariq, M. Faisal, Photocatalysed reaction of few selected organic systems in presence of titanium dioxide, *Appl. Catal. A: General*, **2005**, 289, 224–230.
75. M. Antonopoulou, I. Konstantinou, Photocatalytic degradation and mineralization of tramadol pharmaceutical in aqueous TiO₂ suspensions: Evaluation of kinetics, mechanisms and ecotoxicity, *Appl. Catal. A: General*, **2016**, 515, 136–143.
76. Microtox® Manual, **1998**.
77. G. P. S. Marcone, A. C. Oliveira, G. Almeida, G. A. Umbuzeiro, W. F. Jardim, Ecotoxicity of TiO₂ to *Daphnia similis* under irradiation, *J. Hazard. Mater.*, **2012**, 211–212, 436–442.
78. V.K. Sharma, Aggregation and toxicity of titanium dioxide nanoparticles in aquatic environment—A Review, *J. Environ. Sci. Health, A Tox. Hazard. Subst. Environ. Eng.*, **2009**, 44, 1485–1495.
79. Chemistry of Nanocrystalline Oxide Materials. Combustion Synthesis, Properties and Applications, K. C. Patil, M. S. Hegde, T. Rattan, S. T. Aruna, World Scientific, **2008**.

REFERENCES

80. Y. Kakuma, A.Y. Nosaka, Y. Nosaka, Difference in TiO₂ photocatalytic mechanism between rutile and anatase studied by the detection of active oxygen and surface species in water, *Phys. Chem. Chem. Phys.*, **2015**, 17, 18691–18698.
81. V. Etacheri, C. Di Valentin, J. Schneider, D. Bahnemann, S.C. Pillai, Visible-light activation of TiO₂ photocatalysts: Advances in theory and experiments, *J. Photochem. Photobiol. C: Photochem. Rev.*, **2015**, 25, 1–29.
82. A.S. Barnard, H. Xu, An environmentally sensitive phase map of titania nanocrystals, *ACS Nano*, **2008**, 2, 2237–2242.
83. H. Zhang, J.F. Banfield, Thermodynamic analysis of phase stability of nanocrystalline titania, *J. Mater. Chem.*, **1998**, 8, 2073–2076.
84. M. Hirano, K. Ota, H. Iwata, Direct formation of anatase (TiO₂)/silica (SiO₂) composite nanoparticles with high phase stability of 1300 °C from acidic solution by hydrolysis under hydrothermal condition, *Chem. Mater.*, **2004**, 16, 3725–3732.
85. C. Kang, L. Jing, T. Guo, H. Cui, J. Zhou, H. Fu, Mesoporous SiO₂-modified nanocrystalline TiO₂ with high anatase thermal stability and large surface area as efficient photocatalyst, *J. Phys. Chem. C*, **2009**, 113, 1006–1013.
86. J. Bahadur, D. Sen, S. Mazumder, P. U. Sastry, B. Paul, H. Bhat, S. G. Singh, One-step fabrication of thermally stable TiO₂/SiO₂ nanocomposite microspheres by evaporation-induced self-assembly, *Langmuir*, **2012**, 28, 11343–11353.
87. D. J. Reidy, J. D. Holmes, C. Nagle, M. A. Morris, A highly thermally stable anatase phase prepared by doping with zirconia and silica coupled to a mesoporous type synthesis technique, *J. Mater. Chem.*, **2005**, 15, 3494–3500.
88. F. Riboni, Maria V. Dozzi, M. C. Paganini, E. Giamello, E. Selli, Photocatalytic activity of TiO₂-WO₃ mixed oxides in formic acid oxidation, *Catal. Today*, **2017**, 287, 176–181.
89. M.R. Mohammadi, D. J. Fray, Sensor performance of nanostructured TiO₂-Cr₂O₃ thin films derived by a particulate sol-gel route with various Cr:Ti molar Ratios, *J. Electron. Mater.*, **2014**, 43, 3922–3932.
90. P. Periyat, S.C. Pillai, D.E. McCormack, J. Colreavy, S.J. Hinder, Improved high-temperature stability and sun-light-driven photocatalytic activity of sulfur-doped anatase TiO₂, *J. Phys. Chem. C*, **2008**, 112, 7644–7652.

-
91. P. Periyat, D. E. McCormack, S. J. Hinder, S. C. Pillai, One-pot synthesis of anionic (nitrogen) and cationic (sulfur) codoped high-temperature stable, *J. Phys. Chem. C*, **2009**, 113, 3246–3253.
 92. S. C. Padmanabhan, S. C. Pillai, J. Colreavy, S. Balakrishnan, D. E. McCormack, T. S. Perova, S. J. Hinder, J. M. Kelly, A Simple sol-gel processing for the development of high-temperature stable photoactive anatase titania, *Chem. Mater.*, **2007**, 19, 4474–4481.
 93. V. Etacheri, M. K. Seery, S. J. Hinder and S. C. Pillai, Oxygen rich titania: A dopant free, high temperature stable, and visible-light active anatase photocatalyst, *Adv. Funct. Mater.*, **2011**, 21, 3744–3752.
 94. I. Krivtsov, M. Ilkaeva, V. Avdin, Z. Amghouz, S. A. Khainakov, J. R. García, Eva Díaz, S. Ordóñez, Exceptional thermal stability of undoped anatase TiO₂ photocatalysts prepared by a solvent exchange method, *RSC Adv.*, **2015**, 5, 36634–36641.
 95. K. Nagaveni, M.S. Hegde, G. Madras, Structure and photocatalytic activity of Ti_{1-x}M_xO_{2±δ} (M = W, V, Ce, Zr, Fe, and Cu) synthesized by solution combustion method, *J. Phys. Chem. B*, **2004**, 108, 20204–20212.
 96. N. Pinna, M. Niederberger, Surfactant-free nonaqueous synthesis of metal oxide nanostructures, *Angew. Chem., Int. Ed.*, **2008**, 47, 5292–5304.
 97. M. Kakihana, M. Kobayashi, K. Tomita, V. Petrykin, Application of water-soluble titanium complexes as precursors for synthesis of titanium-containing oxides via aqueous solution processes, *Bull. Chem. Soc. Jpn.*, **2010**, 83, 1285–1308.
 98. M. Kakihana, K. Tomita, V. Petrykin, M. Tada, S. Sasaki, Y. Nakamura, Chelating of titanium by lactic acid in the water-soluble diammonium Tris(2-hydroxypropionato)titanate(IV), *Inorg. Chem.*, **2004**, 43, 4546–4548.
 99. M. Kobayashi, V. Petrykin, K. Tomita, M. Kakihana, Hydrothermal synthesis of brookite-type titanium dioxide with snowflake-like nanostructures using a water-soluble citratoperoxotitanate complex, *J. Cryst. Growth*, **2011**, 337, 30–37.
 100. I. V. Krivtsov, M. V. Ilkaeva, V. D. Samokhina, V. V. Avdin, S. A. Khainakov, D. A. Uchaev, J. R. Garcia, Synthesis of silica–titania composite oxide via “green” aqueous peroxo-route, *J. Sol–Gel. Sci. Technol.*, **2013**, 67, 665–669.

REFERENCES

101. I. A. de Castro, J. A. de Oliveira, E. C. Paris, T. R. Giraldo, C. Ribeiro, Production of heterostructured TiO₂/WO₃ nanoparticulated photocatalysts through a simple one pot method, *Ceram. Int.*, **2015**, 41, 3502–3510.
102. S. A. Bakar, C. Ribeiro, Low temperature synthesis of N-doped TiO₂ with rice-like morphology through peroxo assisted hydrothermal route: Materials characterization and photocatalytic properties, *Appl. Surf. Sci.*, **2016**, 377, 121–133.
103. S. A. Bakar, G. Byzanski, C. Ribeiro, Synergistic effect on the photocatalytic activity of N-doped TiO₂ nanorods synthesised by novel route with exposed (110) face, *J. A. Compd.*, **2016**, 666, 38–49.
104. I. Krivtsov, M. Ilkaeva, E. Salas-Colera, Z. Amghouz, J. R. García, E. Díaz, S. Ordóñez, S. Villar-Rodil, Consequences of nitrogen-doping and oxygen enrichment on titanium local order and photocatalytic performance of TiO₂ anatase, *J. Phys. Chem. C*, **2017**, 121, 6770–6780.
105. C. Liu, S. Yang, Synthesis of angstrom-scale anatase titania atomic wires, *ACS Nano*, **2009**, 3, 1025–1031.
106. M. Munz, Mark T. Langridge, K. K. Devarepally, D. C. Cox, P. Patel, N. A. Martin, G. Vargha, V. Stolojan, S. White, R. J. Curry, Facile synthesis of titania nanowires via a hot filament method and conductometric measurement of their response to hydrogen sulfide gas, *ACS Appl. Mater. Interfaces*, **2013**, 5, 1197–1205.
107. T. Nonoyama, T. Kinoshita, M. Higuchi, K. Nagata, M. Tanaka, K. Sato, K. Kato, TiO₂ synthesis inspired by biomineralization: control of morphology, crystal phase, and light-use efficiency in a single process, *J. Am. Chem. Soc.*, **2012**, 134, 8841–8847.
108. Y. Xiong, D. He, R. Jaber, P. J. Cameron, K. J. Edler, Sulfur-doped cubic mesostructured titania films for use as a solar photocatalyst, *J. Phys. Chem. C*, **2017**, 121, 9929–9937.
109. H. Choi, E. Stathatos, D. D. Dionysiou, Sol–gel preparation of mesoporous photocatalytic TiO₂ films and TiO₂/Al₂O₃ composite membranes for environmental applications, *Appl. Catal. B: Environ.*, **2006**, 63, 60–67.
110. B. Su, H. A. Caller-Guzman, V. Körstgens, Y. Rui, Y. Yao, N. Saxena, G. Santoro, S. V. Roth, P. Müller-Buschbaum, Macroscale and nanoscale morphology evolution

- during in situ spray coating of titania films for perovskite solar cells, *ACS Appl. Mater. Interfaces*, **2017**, 9, 43724–43732.
111. Y. Kumabe, M. Ohtani, K. Kobiro, Rapid one-pot synthesis of ultrafine titania nanocrystals and their conversion into transparent mesoporous thin layer films, *Micropor. Mesopor. Mat.*, **2018**, 261, 207–213.
112. D. Chen, R. A. Caruso, Recent progress in the synthesis of spherical titania nanostructures and their applications, *Adv. Funct. Mater.*, **2013**, 23, 1356–1374.
113. D. G. Shchukin, R. A. Caruso, Template synthesis and photocatalytic properties of porous metal oxide spheres formed by nanoparticle infiltration, *Chem. Mater.*, **2004**, 16, 2287–2292.
114. T. Leshuk, S. Linley, G. Baxter, F. Gu, Mesoporous hollow sphere titanium dioxide photocatalysts through hydrothermal silica etching, *ACS Appl. Mater. Interfaces*, **2012**, 4, 6062–6070.
115. D. Chen, L. Cao, F. Huang, P. Imperia, Y.-B. Cheng, R. A. Caruso, Synthesis of monodisperse mesoporous titania beads with controllable diameter, high surface areas, and variable pore diameters (14–23 nm), *J. Am. Chem. Soc.*, **2010**, 132, 4438–4444.
116. H.-J. Kim, J.-D. Jeon, S.-Y. Kwak, Highly dispersed mesoporous TiO₂ spheres via acid treatment and its application for dye-sensitized solar cells, *Powder Technol.*, **2013**, 243, 130–138.
117. S. Tanaka, D. Nogami, N. Tsuda, Y. Miyake, Synthesis of highly-monodisperse spherical titania particles with diameters in the submicron range, *J. Colloid Interface Sci.*, **2009**, 334, 188–194.
118. X. Jiang, T. Herricks, Y. Xia, Monodispersed spherical colloids of titania: synthesis, characterization, and crystallization, *Adv. Funct. Mater.*, **2003**, 15, 1205–1209.
119. M. Pal, J. G. Serrano, P. Santiago, U. Pal, Size-controlled synthesis of spherical TiO₂ nanoparticles: morphology, crystallization, and phase transition, *J. Phys. Chem. C*, **2007**, 111, 96–102.
120. Z. D. Lu, M. M. Ye, N. Li, W. W. Zhong, Y. D. Yin, Self-assembled TiO₂ Nanocrystal clusters for selective enrichment of intact phosphorylated proteins, *Angew. Chem., Int. Ed.*, **2010**, 49, 1862–1866.

-
121. F. Bai, D. S. Wang, Z. Y. Huo, W. Chen, L. P. Liu, X. Liang, C. Chen, X. Wang, Q. Peng, Y. D. Li, A versatile bottom-up assembly approach to colloidal spheres from nanocrystals, *Angew. Chem., Int. Ed.*, **2007**, 46, 6650–6653.
 122. Q. Zhang, J.-B. Joo, Z. Lu, M. Dahl, D. Oliveira, M. Ye, Y. Yin, Self-assembly and photocatalysis of mesoporous TiO₂ nanocrystal clusters, *Nano Res.*, **2011**, 4, 103–114.
 123. P. Z. Araujo, V. Luca, P. B. Bozzano, H. L. Bianchi, G. J. Soler-Illia, M. A. Blesa, Aerosol-assisted production of mesoporous titania microspheres with enhanced photocatalytic activity: the basis of an improved process, *ACS Appl. Mater. Interfaces.*, **2010**, 2, 1663–1673.
 124. B. Liu, K. Nakata, M. Sakai, H. Saito, T. Ochiai, T. Murakami, K. Takagi, A. Fujishima, Hierarchical TiO₂ spherical nanostructures with tunable pore size, pore volume, and specific surface area: facile preparation and high-photocatalytic performance, *Catal. Sci. Technol.*, **2012**, 2, 1933–1939.
 125. X. Wang, L. Bai, H. Liu, X. Yu, Y. Yin, C. Gao, A unique disintegration–reassembly route to mesoporous titania nanocrystalline hollow spheres with enhanced photocatalytic activity, *Adv. Funct. Mater.*, **2018**, 28, 1704208.
 126. J. Hu, M. Chen, X. Fanga, L. Wu, Fabrication and application of inorganic hollow spheres, *Chem. Soc. Rev.*, **2011**, 40, 5472–5491.
 127. Q. Zhang, W. Wang, J. Goebel, Y. Yin, Self-templated synthesis of hollow nanostructures, *Nanotoday*, **2009**, 4, 494–507.
 128. Y. Lv, L. Yu, H. Huang, Y. Feng, D. Chen, X. Xie, Application of the soluble salt-assisted route to scalable synthesis of ZnO nanopowder with repeated photocatalytic activity, *Nanotechnology*, **2012**, 23, 065402.
 129. C. Charbonneau, P. J. Holliman, M. L. Davies, T. M. Watson, D. A. Worsley, Facile self-assembly and stabilization of metal oxide nanoparticles, *J. Colloid Interface Sci.*, **2015**, 442, 110–119.
 130. J. Carbajo, A. Tolosana-Moranchel, J. A. Casas, M. Faraldos, A. Bahamonde, Analysis of photoefficiency in TiO₂ aqueous suspensions: Effect of titania hydrodynamic particle size and catalyst loading on their optical properties, *Appl. Catal. B: Environ.*, **2018**, 221, 1–8.

REFERENCES

131. C. Ahn, J. Park, D. Kim, S. Jeon, Monolithic 3D titania with ultrathin nanoshellstructures for enhanced photocatalytic activity and recyclability, *Nanoscale*, **2013**, 5, 10384–10389.
132. C. Haw, W. Chiu, S. A. Rahman, P. Khiew, S. Radiman, R. A. Shukor, M. A. A. Hamid, N. Ghazali, The design of new magnetic-photocatalystnanocomposites (CoFe₂O₄-TiO₂) as smart nanomaterials for recyclable-photocatalysis applications, *New J. Chem.*, **2016**, 40, 1124–1136.
133. D. H. Quiñones, A. Rey, P. M. Álvarez, F. J. Beltrán, P.K. Plucinski, Enhanced activity and reusability of TiO₂ loaded magnetic activated carbon for solar photocatalytic ozonation, *Appl. Catal. B: Environ.*, **2014**, 144, 96–106.
134. N. Kaur, S. K. Shahi, V. Singh, Synthesis, characterization and photocatalytic activity of magnetically separable γ -Fe₂O₃/N, Fe codoped TiO₂ heterojunction for degradation of Reactive Blue 4 dye, *RSC Adv.*, **2015**, 5, 61623–61630.
135. S. Linley, T. Leshuk, F. X. Gu, Synthesis of magnetic rattle-type nanostructures for use in water treatment, *ACS Appl. Mater. Interfaces*, **2013**, 5, 2540–2548.
136. B. Barrocas, O. C. Monteiro, M. E. Melo Jorge, S. Sérgio, Photocatalytic activity and reusability study of nanocrystalline TiO₂ films prepared by sputtering technique, *Appl. Surf. Sci.*, **2013**, 264, 111–116.
137. K. P. O. Mahesh, D.-H. Kuo, B.-R. Huang, M. Ujihara, T. Imae, Chemically modified polyurethane-SiO₂/TiO₂ hybrid composite film and its reusability for photocatalytic degradation of Acid Black 1 (AB 1) under UV light, *Appl. Catal. A: General*, **2014**, 475, 235–241.
138. P. M. Martins, V. Gomez, A. C. Lopes, C. J. Tavares, G. Botelho, S. Irusta, S. Lanceros-Mendez, Improving photocatalytic performance and recyclability by development of Er-doped and Er/Pr-codoped TiO₂/poly(vinylidene difluoride)-trifluoroethylene composite membranes, *J. Phys. Chem. C*, **2014**, 118, 27944–27953.
139. P. T. N. Nguyen, C. Salim, W. Kurniawan, H. Hinode, A non-hydrolytic sol-gel synthesis of reduced graphene oxide/TiO₂ microsphere photocatalysts, *Catal. Today*, **2014**, 230, 166–173.

-
140. L. Dou, L. Gao, X. Yang, X. Song, Hierarchical architectures TiO₂: Pollen-induced synthesis remarkable crystalline-phase stability, tunable size, and reused photocatalysis, *J. Hazard. Mater.*, **2012**, 203–204, 363–369.
 141. S. Ullah, E. P. Ferreira-Neto, A. A. Pasa, C. C. J. Alcantara, J. J. S. Acuña, S.A. Bilmes, M. L. M. Riccio, R. Landers, T. Z. Fermino, U. P. Rodrigues-Filho, Enhanced photocatalytic properties of core@shell SiO₂@TiO₂ nanoparticles, *Appl. Catal. B: Environ.*, **2015**, 179, 333–343.
 142. Semiconductor Photocatalysis. Principles and Applications, H. Kisch, Wiley-VCH, **2015**.
 143. F. Goettmann, A. Fischer, M. Antonietti, A. Thomas, Metal-free catalysis of sustainable Friedel-Crafts reactions: direct activation of benzene by carbon nitrides to avoid the use of metal chlorides and halogenated compounds, *Chem. Commun.*, **2006**, 4530–4532.
 144. X. Wang, K. Maeda, A. Thomas, K. Takanebe, G. Xin, J. M. Carlsson, K. Domen, M. Antonietti, A metal-free polymeric photocatalyst for hydrogen production from water under visible light, *Nature Mater.*, **2009**, 8, 76–80.
 145. D. M. Teter, R. J. Hemley, Low-compressibility carbon nitrides, *Science*, **1996**, 271, 53–55.
 146. Y. Zheng, L. Lin, B. Wang, X. Wang, Graphitic carbon nitride polymers toward sustainable photoredox catalysis, *Angew. Chem., Int. Ed.*, **2015**, 54, 12868–12884.
 147. J. Liu, H. Wang, M. Antonietti, Graphitic carbon nitride “reloaded”: Emerging applications beyond (photo)catalysis, *Chem. Soc. Rev.*, **2016**, 45, 2308–2326.
 148. S. Yin, J. Han, T. Zhou, R. Xu, Recent progress in g-C₃N₄ based low cost photocatalytic system: activity enhancement and emerging applications, *Catal. Sci. Technol.*, **2015**, 5, 5048–5061.
 149. S. Ye, R. Wang, M.-Z. Wu, Y.-P. Yuan, A Review on g-C₃N₄ for photocatalytic water splitting and CO₂ reduction, *Appl. Surf. Sci.*, **2015**, 358, 15–27.
 150. G. Dong, Y. Zhang, Q. Pan, J. Qiu, A fantastic graphitic carbon nitride (g-C₃N₄) material: electronic structure, photocatalytic and photoelectronic properties, *J. Photochem. Photobiol. C*, **2014**, 33–50.

REFERENCES

151. Y. Zheng, L. Lin, B. Wang, X. Wang, Graphitic carbon nitride polymers toward sustainable photoredox catalysis, *Angew. Chem., Int. Ed.*, **2015**, 54, 12868–12884.
152. Q. Zheng, H. Shen, D. Shuai, Emerging investigators series: advances and challenges of graphitic carbon nitride as a visible-light-responsive photocatalyst for sustainable water purification, *Environ. Sci.: Water Res. Technol.*, **2017**, 3, 982–1001.
153. H. Hao, L. Zhang, W. Wang, S. Zeng, Modification of heterogeneous photocatalysts for selective organic synthesis, *Catal. Sci. Technol.*, **2018**, 8, 1229–1250.
154. F. Z. Su, S. C. Mathey, G. Lipner, X. Z. Fu, M. Antonietti, S. Blechert, X. C. Wang, mpg-C₃N₄-catalyzed selective oxidation of alcohols using O₂ and visible light, *J. Am. Chem. Soc.*, **2010**, 132, 16299–16301.
155. Comprehensive Organic Transformations: A Guide to Functional Group Preparations, Ed.: R. C. Larock, Wiley-VCH, **1999**.
156. L. Kesevan, R. Tiruvalam, M. H. Ab Rahim, M. I. bin Saiman, D. I. Enache, R. L. Jenkins, N. Dimitratos, J. A. López-Sánchez, S. H. Taylor, D. W. Knight, C. K. Kiely, G. J. Hutchings, Solvent-free oxidation of primary carbon-hydrogen bonds in toluene using Au-Pd alloy nanoparticles, *Science*, **2011**, 331, 195–199.
157. W. Partenheimer, Methodology and scope of metal/bromide autoxidation of hydrocarbons, *Catal. Today*, **1995**, 23, 69–158.
158. R.L. Brutchey, I.J. Drake, A.T. Bell, T.D. Tilley, Liquid-phase oxidation of alkylaromatics by a H-atom transfer mechanism with a new heterogeneous CoSBA-15 catalyst, *Chem. Commun.*, **2005**, 29, 3736–3738.
159. Y. Wang, H. Li, J. Yao, X. Wang, M. Antonietti, Synthesis of boron doped polymeric carbon nitride solids and their use as metal-free catalysts for aliphatic C–H bond oxidation, *Chem. Sci.*, **2011**, 2, 446–450.
160. M. Ghaffarzadeh, M. Bolourtchian, M. Gholamhosseni, F. Mohsenzadeh, Synthesis of arylaldehydes: Br₂/DMSO catalytic system for the chemoselective oxidation of methylarenes, *Appl. Catal., A*, **2007**, 333, 131–135.
161. N. Tada, K. Hattori, T. Nobuta, T. Miura, A. Itoh, Facile aerobic photooxidation of methyl group in the aromatic nucleus in the presence of an organocatalyst under VIS irradiation, *Green Chem.*, **2011**, 13, 1669–1671.

-
162. S.-I. Hirashima, A. Itoh, Aerobic visible light-oxidation of aromatic methyl groups to carboxylic acids, *Photochem. Photobiol. Sci.*, **2007**, 6, 521–524.
163. G. Pandey, R. Laha, D. Singh, Benzylic C(sp³)–H functionalization for C–N and C–O bond formation via visible light photoredox catalysis, *J. Org. Chem.*, **2016**, 81, 7161–7171.
164. A. Tanaka, K. Hashimoto, H. Kominami, Preparation of Au/CeO₂ exhibiting strong surface plasmon resonance effective for selective or chemoselective oxidation of alcohols to aldehydes or ketones in aqueous suspensions under irradiation by green light, *J. Am. Chem. Soc.*, **2012**, 134, 14526–14533.
165. E. Fritz-Langhals, B. Kunath, Synthesis of aromatic aldehydes by laccase-mediator assisted oxidation, *Tetrahedron Lett.*, **1998**, 39, 5955–5956.
166. A. Potthast, T. Rosenaq, C.-L. Chen, J.S. Gratzl, Selective enzymic oxidation of aromatic methyl groups to aldehydes, *J. Org. Chem.*, **1995**, 60, 4320–4321.
167. Y. Zhu, Y. Zhu, H. Zeng, Z. Chen, R.D. Little, C. Ma, A promising electro-oxidation of methyl-substituted aromatic compounds to aldehydes in aqueous imidazole ionic liquid solutions, *J. Electroanal. Chem.*, **2015**, 751, 105–110.
168. Y. Wang, X. Wang, M. Antonietti, Polymeric graphitic carbon nitride as a heterogeneous organocatalyst: from photochemistry to multipurpose catalysis to sustainable chemistry, *Angew. Chem., Int. Ed.*, **2012**, 51, 68–89.
169. V. Augugliaro, M. Bellardita, V. Loddo, G. Palmisano, L. Palmisano, S. Yurdakal, Overview on oxidation mechanisms of organic compounds by TiO₂ in heterogeneous photocatalysis, *J. Photochem. Photobiol., C*, **2012**, 13, 224–245.
170. S. Yurdakal, G. Palmisano, V. Loddo, V. Augugliaro, L. Palmisano, Nanostructured rutile TiO₂ for selective photocatalytic oxidation of aromatic alcohols to aldehydes in water, *J. Am. Chem. Soc.*, **2008**, 130, 1568–1569.
171. P. Zhang, Y. Wang, H. Li, M. Antonietti, Metal-free oxidation of sulphides by carbon nitride with visible light illumination at room temperature, *Green Chem.*, **2012**, 14, 1904–1908.
172. F. Su, S.C. Mathew, L. Möhlmann, M. Antonietti, X. Wang, S. Blechert, Aerobic oxidative coupling of amines by carbon nitride photocatalysis with visible light, *Angew. Chem. Int. Ed.*, **2011**, 50, 657–660.

REFERENCES

173. J.-J. Zhang, J.-M. Ge, H.-H. Wang, X. Wei, X.-H. Li, J.-S. Chen, Activating oxygen molecules over carbonyl-modified graphitic carbon nitride: Merging supramolecular oxidation with photocatalysis in a metal-free catalyst for oxidative coupling of amines into imines, *ChemCatChem*, **2016**, 8, 3441–3445.
174. S. Verma, R.B.N. Baig, M.N. Nadagouda, R.S. Varma, Photocatalytic C–H activation of hydrocarbons over VO@g-C₃N₄, *ACS Sustainable Chem. Eng.*, **2016**, 4, 2333–2336.
175. Z. Ding, X. Chen, M. Antonietti, X. Wang, Synthesis of transition metal-modified carbon nitride polymers for selective hydrocarbon oxidation, *ChemSusChem*, **2011**, 4, 274–281.
176. P. Zhang, Y. Gong, H. Li, Z. Chen, Y. Wang, Selective oxidation of benzene to phenol by FeCl₃/mpg-C₃N₄ hybrids, *RSC Adv.*, **2013**, 3, 5121–5126.
177. S. Sukanuma, K. Nakajima, M. Kitano, D. Yamaguchi, Hydrolysis of cellulose by amorphous carbon bearing SO₃H, COOH, and OH groups, *J. Am. Chem. Soc.*, **2008**, 130, 12787–12793.
178. J. N. Chheda, Y. Roman-Leshkov, J. A. Dumesic, Production of 5-hydroxymethylfurfural and furfural by dehydration of biomass-derived mono- and poly-saccharides, *Green Chem.*, **2007**, 9, 342–350.
179. G. Z. Papageorgiou, D. G. Papageorgiou, Z. Terzopoulou, D. N. Bikiaris, Production of bio-based 2, 5-furan dicarboxylate polyesters: Recent progress and critical aspects in their synthesis and thermal properties, *Eur. Polym. J.*, **2016**, 83, 202–229.
180. A.F. Sousa, C. Vilela, A. C. Fonseca, M. Matos, C.S.R. Freire, G.-J.M. Gruter, J.F.J. Coelho, A.J.D. Silvestre, Biobased polyesters and other polymers from 2,5-furandicarboxylic acid: a tribute to furan excellency, *Polym. Chem.*, **2015**, 6, 5961–5983.
181. I. Delidovich, P. J. C. Hausoul, L. Deng, R. Pfützenreuter, M. Rose, R. Palkovits, Alternative Monomers Based on Lignocellulose and Their Use for Polymer Production, *Chem. Rev.*, **2016**, 116, 1540–1599.
182. A. S. Amarasekara, D. Green, L. D. Williams, Renewable resources based polymers: Synthesis and characterization of 2,5-diformylfuran–urea resin, *Eur. Polym. J.*, **2009**, 45, 595–598.

REFERENCES

183. T. Xiang, X. Liu, P. Yi, M. Guo, Y. Chen, C. Wesdemiotis, Y. Pang, Schiff base polymers derived from 2,5-diformylfuran, *Polym. Int.*, **2013**, 62, 1517–1523.
184. J.M.R. Gallo, D.M. Alonso, M.A. Mellmer, J.A. Dumesic, Production and upgrading of 5-hydroxymethylfurfural using heterogeneous catalysts and biomass-derived solvents, *Green Chem.*, **2013**, 15, 85–90.
185. X. Tong, Y. Ma, Y. Li, Biomass into chemicals: Conversion of sugars to furan derivatives by catalytic processes, *Appl. Catal. A: Gen.*, **2010**, 385, 1–13.
186. I. Sadaba, Y.Y. Gorbanev, S. Kegnæs, S. Reddy, Catalytic Performance of Zeolite-Supported Vanadia in the Aerobic Oxidation of 5-hydroxymethylfurfural to 2,5-diformylfuran, *ChemCatChem.*, **2013**, 5, 284–293.
187. C. Carlini, P. Patrono, A. Maria, R. Galletti, Selective oxidation of 5-hydroxymethyl-2-furaldehyde to furan-2,5-dicarboxaldehyde by catalytic systems based on vanadyl phosphate, *Appl. Catal. A: Gen.*, **2005**, 289, 197–204.
188. J. Nie, J. Xie, H. Liu, Efficient aerobic oxidation of 5-hydroxymethylfurfural to 2,5-diformylfuran on supported Ru catalysts, *J. Catal.*, **2013**, 30, 83–91.
189. F. Neat, N. Petrea, R. Petre, V. Somoghi, M. Florea, V.I. Parvulescu, Oxidation of 5-hydroxymethyl furfural to 2,5-diformylfuran in aqueous media over heterogeneous manganese based catalysts, *Catal. Today.*, **2016**, 278, 66–73.
190. M. Chatterjee, T. Ishizaka, A. Chatterjee, H. Kawanami, Dehydrogenation of 5-hydroxymethylfurfural to diformylfuran in compressed carbon dioxide: an oxidant free approach, *Green Chem.*, **2017**, 19, 1315–1326.
191. D.W. Wakerley, M.F. Kuehnel, K.L. Orchard, K.H. Ly, T.E. Rosser, E. Reisner, Solar-driven reforming of lignocellulose to H₂ with a CdS/CdO_x photocatalyst, *Nature Energ.*, **2017**, 2, 17021.
192. S.-H. Li, S. Liu, J.C. Colmenares, Y.-J. Xu, A sustainable approach for lignin valorization by heterogeneous photocatalysis, *Green Chem.*, **2016**, 18, 594–607.
193. L. Ozcan, P. Yalcin, O. Alagoz, S. Yurdakal, Selective photoelectrocatalytic oxidation of 5-(hydroxymethyl)-2-furaldehyde in water by using Pt loaded nanotube structure of TiO₂ on Ti photoanodes, *Catal. Today*, **2017**, 281, 205–213.
194. S. Yurdakal, B.S. Tek, O. Alagoz, V. Augugliaro, V. Loddo, G. Palmisano, L. Palmisano, Photocatalytic selective oxidation of 5-(hydroxymethyl)-2-furaldehyde to

- 2,5-furandicarbaldehyde in water by using anatase, rutile, and brookite TiO₂ nanoparticles, *ACS Sust. Chem. Eng.*, **2013**, 1, 456–461.
195. X. Dai, M. Xie, S. Meng, X. Fu, S. Chen, Coupled systems for selective oxidation of aromatic alcohols to aldehydes and reduction of nitrobenzene into aniline using CdS/g-C₃N₄ photocatalyst under visible light irradiation, *Appl. Catal. B: Environ.*, **2014**, 158–159, 382–390.
196. J. Xu, L. Luo, G. Xiao, Z. Zhang, H. Lin, X. Wang, J. Long, Layered C₃N₃S₃ polymer/graphene hybrids as metal-free catalysts for selective photocatalytic oxidation of benzylic alcohols under visible light, *ACS Catal.*, **2014**, 4, 3302–3306.
197. X. Chen, J. Zhang, X. Fu, M. Antonietti, X. Wang, Fe-g-C₃N₄-Catalyzed oxidation of benzene to phenol using hydrogen peroxide and visible light, *J. Am. Chem. Soc.*, **2009**, 131, 11658–11659.
198. X.-H. Li, X. Wang, M. Antonietti, Solvent-free and metal-free oxidation of toluene using O₂ and g-C₃N₄ with nanopores: Nanostructure boosts the catalytic selectivity, *ACS Catal.*, **2012**, 2, 2082–2086.
199. X.-H. Li, J.-S. Chen, X. Wang, J. Sun, M. Antonietti, Metal-free activation of dioxygen by graphene/g-C₃N₄ nanocomposites: Functional dyads for selective oxidation of saturated hydrocarbons, *J. Am. Chem. Soc.*, **2011**, 133, 8074–8077.
200. Q. Wu, Y. He, H. Zhang, Z. Feng, Y. Wu, T. Wu, Photocatalytic selective oxidation of biomass-derived 5-hydroxymethylfurfural to 2,5-diformylfuran on metal-free g-C₃N₄ under visible light irradiation, *Molecular Catalysis*, **2017**, 436, 10–18.
201. B. Long, Z. Ding, X. Wang, Carbon nitride for the selective oxidation of aromatic alcohols in water under visible light, *ChemSusChem.*, **2013**, 6, 2074–2078.
202. J. Liu, T. An, Z. Chen, Z. Wang, H. Zhou, T. Fan, D. Zhang, M. Antonietti, Carbon nitride nanosheets as visible light photocatalytic initiators and crosslinkers for hydrogels with thermoresponsive turbidity, *J. Mater. Chem. A.*, **2017**, 5, 8933–8938.
203. Q. Liu, X. Wang, Q. Yang, Z. Zhang, X. Fang, A novel route combined precursor-hydrothermal pretreatment with microwave heating for preparing holey g-C₃N₄ nanosheets with high crystalline quality and extended visible light absorption, *Appl. Catal. B: Environ.*, **2018**, 225, 22–29.

REFERENCES

204. Y.-P. Yuan, L.-S. Yin, S.-W. Cao, L.-N. Gu, G.-S. Xu, P. Du, H. Chai, Y.-S. Liao, C. Xue, Microwave-assisted heating synthesis: a general and rapid strategy for large-scale production of highly crystalline g-C₃N₄ with enhanced photocatalytic H₂ production, *Green Chem.*, **2014**, 16, 4663–4668.
205. C. Hu, Y.-C. Chu, M.-S. Wang, X.-H. Wu, Rapid synthesis of g-C₃N₄ spheres using microwave-assisted solvothermal method for enhanced photocatalytic activity, *J. Photochem. Photobiol. A*, **2017**, 348, 8–17.
206. Y.-S. Jun, J. Park, S. U. Lee, A. Thomas, W. H. Hong, G. D. Stucky, Three-dimensional macroscopic assemblies of low-dimensional carbon nitrides for enhanced hydrogen evolution, *Angew. Chem., Int. Ed.*, **2013**, 52, 11083–11087.
207. M. Shalom, S. Inal, C. Fettkenhauer, D. Neher, M. Antonietti, Improving carbon nitride photocatalysis by supramolecular preorganization of monomers, *J. Am. Chem. Soc.*, **2013**, 135, 7118–7121.
208. M. J. Bojdys, J.-O. Muller, M. Antonietti, A. Thomas, Ionothermal synthesis of crystalline, condensed, graphitic carbon nitride, *Chem. Eur. J.* **2008**, 14, 8177–8182.
209. X. Liu, N. Fechler, M. Antonietti, Salt melt synthesis of ceramics, semiconductors and carbon nanostructures, *Chem. Soc. Rev.*, **2013**, 42, 8237–8265.
210. J. Wang, D. Hao, J. Ye, N. Umezawa, Determination of crystal structure of graphitic carbon nitride: Ab initio evolutionary search and experimental validation, *Chem. Mater.*, **2017**, 29, 2694–2707.
211. H. Grüger, D. Selbmann, E. Wolf, A. Leonhardt, B. Arnold, CN_x-layers prepared by plasma assisted chemical vapour deposition, *Surf. Coat. Technol.*, **1996**, 86–87, 409–414.
212. L. Guan, N. Xu, X. Liu, Y. Zhao, H. Li, J. Sun, J. Wu, Z. Ying, Controlled growth of crystalline g-C₃N₄ nanocone arrays by plasma sputtering reaction deposition, *Carbon*, **2014**, 79, 578–589.
213. A. Y. Liu, M. L. Cohen, Prediction of new low compressibility solids, *Science*, **1989**, 245, 841–842.
214. A. Y. Liu, M. L. Cohen, Structural properties and electronic structure of low-compressibility materials: β-Si₃N₄ and hypothetical β-C₃N₄, *Phys. Rev. B*, **1990**, 41, 10727–10734.

-
215. D. J. Johnson, Y. Chen, Y. He, R.H. Prince, Deposition of carbon nitride via hot filament assisted CVD and pulsed laser deposition, *Diam. Relat. Mater.*, **1997**, 6, 1799–1805.
216. Z. Zhang, H. Guo, Y. Xu, W. Zhang, X. Fan, Corrosion Resistance Studies on α -C₃N₄ Thin films deposited on pure iron by plasma-enhanced chemical vapor deposition, *J. Mater. Sci. Lett.*, **1999**, 18, 685–687.
217. E. G. Wang, Carbon nitride-related nanomaterials from chemical vapor deposition: Structure and properties, *J. Am. Ceram. Soc.*, **2002**, 85, 105–108.
218. M. L. Chen, D. Li, X. Lin, V. P. Dravid, Y. W. Chung, M. S. Wong, W. D. Sproul, Analytical electron microscopy and Raman spectroscopy studies of carbon nitride thin films, *J. Vac. Sci. Technol.*, **1993**, 11, 521.
219. D. Marton, K. J. Boyd, A.H. Al-Bayati, S. S. Todorov, J. W. Rabalais, Carbon nitride deposited using energetic species: A two-phase system, *Phys. Rev. Lett.*, **1994**, 73, 118–121.
220. S. Kumar, T. L. Tansley, Growth and structure of CN thin films prepared by radio frequency reactive sputtering, *Solid State Comm.*, **1993**, 88, 803–806.
221. K. M. Yu, M. L. Cohen, E. E. Haller, W. L. Hanser, A. Y. Liu, I. C. Wu, Observation of crystalline C₃N₄, *Phys. Rev. B*, **1994**, 49, 5034–5037.
222. C. Niu, Y. Z. Lu, C. M. Lieber, Experimental realization of the covalent solid carbon nitride, *Science*, **1993**, 261, 334–337.
223. X. A. Zhao, C. W. Ong, Y. C. Tsang, Y. W. Wong, P. W. Chan, L. Choy, Reactive pulsed laser deposition of CN_x films, *Appl. Phys. Lett.*, **1995**, 66, 2652.
224. Y. Zheng, L. Lin, B. Wang, X. Wang, Graphitic carbon nitride polymers toward sustainable photoredox catalysis, *Angew. Chem.*, **2015**, 54, 12868–12884.
225. B.V. Lotsch, W. Schnick, New light on an old story: Formation of melam during thermal condensation of melamine, *Chem. Eur. J.*, **2007**, 13, 4956–4968.
226. A. Sattler, S. Pagano, M. Zeuner, A. Zurawski, D. Gunzelmann, J. Senker, K. Müller-Buschbaum, W. Schnick, Melamine–melem adduct phases: Investigating the thermal condensation of melamine, *Chem. Eur. J.*, **2007**, 7, 13161–13170.
227. Liebig, J. V. Ueber Mellon und Mellonverbindungen [German]. *Justus Liebigs Ann. Chem.*, **1844**, 50, 337–363.

-
228. F. K. Kessler, Y. Zheng, D. Schwarz, C. Merschjann, W. Schnick, X. Wang, M. J. Bojdys, Functional carbon nitride materials — design strategies for electrochemical devices, *Nat. Mater.*, **2017**, 17030.
229. C.T. Seto, G. M. Whitesides, Molecular self-assembly through hydrogen bonding: supramolecular aggregates based on the cyanuric acid-melamine lattice, *J. Am. Chem. Soc.*, **1993**, 115, 905–916.
230. C. T. Seto, J. P. Mathias, G. M. Whitesides, Molecular self-assembly through hydrogen bonding: aggregation of five molecules to form a discrete supramolecular structure, *J. Am. Chem. Soc.*, **1993**, 115, 1321–1329.
231. C. T. Seto, G. M. Whitesides, Synthesis, characterization, and thermodynamic analysis of a 1 + 1 self-assembling structure based on the cyanuric acid.cntdot.melamine lattice, *J. Am. Chem. Soc.*, **1993**, 115, 1330–1340.
232. Y.-S. Jun, J. Park, S. U. Lee, A. Thomas, H. Hong, G. D. Stucky, Three-dimensional Macroscopic assemblies of low-Dimensional carbon nitrides for enhanced hydrogen evolution, *Angew. Chem.*, **2013**, 52, 11083–11087.
233. M. Shalom, M. Guttentag, C. Fettkenhauer, S. Inal, D. Neher, A. Llobet, M. Antonietti, In situ formation of heterojunctions in modified graphitic carbon nitride: Synthesis and noble metal free photocatalysis, *Chem. Mater.*, **2014**, 26, 5812–5818.
234. E. Wirnhier, M. Döblinger, D. Gunzelmann, J. Senker, B.V. Lotsch, W. Schnick, Poly(triazine imide) with intercalation of lithium and chloride ions $[(C_3N_3)_2(NH_xLi_{1-x})_3 \cdot LiCl]$: A crystalline 2D carbon nitride network, *Chem. Eur. J.*, **2011**, 17, 3213–3221.
235. C. Fettkenhauer, J. Weber, M. Antonietti, D. Dontsova, Novel carbon nitride composites with improved visible light absorption synthesized in $ZnCl_2$ -based salt melts, *RSC Adv.*, **2014**, 4, 40803–40811.
236. C. Fettkenhauer, G. Clavel, K. Kailasam, M. Antonietti, D. Dontsova, Facile synthesis of new, highly efficient SnO_2 /carbon nitride composite photocatalysts for the hydrogen evolution reaction, *Green Chem.*, **2015**, 17, 3350–3361.
237. C. Fettkenhauer, X.C. Wang, K. Kailasam, M. Antonietti, D. Dontsova, Synthesis of efficient photocatalysts for water oxidation and dye degradation reactions using $CoCl_2$ eutectics, *J. Mater. Chem. A*, **2015**, 3, 21227–21232.

-
238. Y. J. Cui, Z. X. Ding, X. Z. Fu, X. C. Wang, Construction of conjugated carbon nitride nanoarchitectures in solution at low temperatures for photoredox catalysis, *Angew. Chem. Int. Ed.*, **2012**, 51, 11814–11818.
239. P. Niu, L. Zhang, G. Liu, H.M. Cheng, Graphene-like carbon nitride nanosheets for improved photocatalytic activities, *Adv. Funct. Mater.*, **2012**, 22, 4763–4770.
240. X. Li, G. Hartley, A. J. Ward, P.A. Young, A. F. Masters, T. Maschmeyer, Hydrogenated defects in graphitic carbon nitride nanosheets for improved photocatalytic hydrogen evolution, *J. Phys. Chem. C*, **2015**, 119, 14938–14946.
241. P. Qiu, H. Chen, C. Xu, N. Zhou, F. Jiang, X. Wang, Y. Fu, Fabrication of an exfoliated graphitic carbon nitride as a highly active visible light photocatalyst, *J. Mater. Chem. A*, **2015**, 3, 24237–24244.
242. S. Yang, Y. Gong, J. Zhang, L. Zhan, L. Ma, Z. Fang, R. Vajtai, X. Wang, P.M. Ajayan, Exfoliated graphitic carbon nitride nanosheets as efficient catalysts for hydrogen evolution under visible light, *Adv. Mater.*, **2013**, 7, 2452–2456.
243. X. She, H. Xu, Y. Xu, J. Yan, J. Xia, L. Xu, Y. Song, Y. Jiang, Q. Zhang, H. Li, Exfoliated graphene-like carbon nitride in organic solvents: enhanced photocatalytic activity and highly selective and sensitive sensor for the detection of trace amounts of Cu^{2+} , *J. Mater. Chem. A*, **2014**, 2, 2563–2570.
244. H. Wang, Y. Su, H. Zhao, H. Yu, S. Chen, Y. Zhang, X. Quan, Photocatalytic oxidation of aqueous ammonia using atomic single layer graphitic- C_3N_4 , *Environ. Sci. Technol.*, 2014, 48, 11984–11990.
245. X. Zhang, X. Xie, H. Wang, J. Zhang, B. Pan, Y. Xie, Enhanced photoresponsive ultrathin graphitic-phase C_3N_4 nanosheets for bioimaging, *J. Am. Chem. Soc.*, **2012**, 135, 18–21.
246. Q. Lin, L. Li, S. Liang, M. Liu, J. Bi, L. Wu, Efficient synthesis of monolayer carbon nitride 2D nanosheet with tunable concentration and enhanced visible-light photocatalytic activities, *Appl. Catal. B: Environ.*, **2015**, 163, 135–142.
247. Q. Han, B. Wang, J. Gao, Z. Cheng, Y. Zhao, Z. Zhang, L. Qu, Atomically thin mesoporous nanomesh of graphitic C_3N_4 for high-efficiency photocatalytic hydrogen evolution, *ACS Nano*, **2016**, 10, 2745–2751.

-
248. J. Duan, S. Chen, M. Jaroniec, S.Z. Qiao, Porous C₃N₄ Nanolayers@N-Graphene Films as Catalyst Electrodes for Highly Efficient Hydrogen Evolution, *ACS Nano*, **2015**, 9, 931–940.
249. T. Sano, S. Tsutsui, K. Koike, T. Hirakawa, Y. Teramoto, N. Negishia, K. Takeuchi, Activation of graphitic carbon nitride (g-C₃N₄) by alkaline hydrothermal treatment for photocatalytic NO oxidation in gas phase, *J. Mater. Chem. A*, **2013**, 1, 6489–6496.
250. J. Tong, L. Zhang, F. Li, M. Li, S. Cao, An efficient top-down approach for the fabrication of large-aspect-ratio g-C₃N₄ nanosheets with enhanced photocatalytic activities, *Phys. Chem. Chem. Phys.*, **2015**, 17, 23532–23537.
251. J. Tong, L. Zhang, F. Li, K. Wang, L. Hana, S. Cao, Rapid and high-yield production of g-C₃N₄ nanosheets via chemical exfoliation for photocatalytic H₂ evolution, *RSC Adv.*, **2015**, 5, 88149–88153.
252. L.-S. Lin, Z.-X. Cong, J. Li, K.-M. Ke, S.-S. Guo, H.-H. Yang, G.-N. Chen, Graphitic-phase C₃N₄ nanosheets as efficient photosensitizers and pH-responsive drug nanocarriers for cancer imaging and therapy, *J. Mater. Chem. B*, **2014**, 2, 1031–1037.
253. Y. Zhang, A. Thomas, M. Antonietti, X. Wang, Activation of carbon nitride solids by protonation: Morphology changes, enhanced ionic conductivity, and photoconduction experiments, *J. Am. Chem. Soc.*, **2009**, 131, 50–51.
254. Y. Xu, H. Xu, L. Wang, J. Yan, H. Li, Y. Song, L. Huang, G. Cai, The CNT modified white C₃N₄ composite photocatalyst with enhanced visible-light response photoactivity, *Dalton Trans.*, **2013**, 42, 7604–7613.
255. A. Akhundi, E. I. García-López, G. Marci, A. Habibi-Yangjeh, L. Palmisano, Comparison between preparative methodologies of nanostructured carbon nitride and their use as selective photocatalysts in water suspension, *Res. Chem. Intermed.*, **2017**, 43, 5153–5168.
256. M. Groenewolt, M. Antonietti, Synthesis of g-C₃N₄ nanoparticles in mesoporous silica host matrices, *Adv. Mater.*, **2005**, 17, 1789–1792.
257. X.C. Wang, K. Maeda, X.F. Chen, K. Takanahe, K. Domen, Y.D. Hou, X.Z. Fu, M. Antonietti, Polymer semiconductors for artificial photosynthesis: Hydrogen evolution by mesoporous graphitic carbon nitride with visible light, *J. Am. Chem. Soc.*, **2009**, 131, 1680–1681.

-
258. M.S. Sam, P. Tiong, H.O. Lintang, S.L. Lee, L. Yulianti, Mesoporous carbon nitride as a metal-free catalyst for the removal of aniline, *RSC Adv.*, **2015**, 5, 44578–44586.
259. F. Goettmann, A. Fischer, M. Antonietti, A. Thomas, Chemical synthesis of mesoporous carbon nitrides using hard templates and their use as a metal-free catalyst for Friedel–Crafts reaction of benzene, *Angew. Chem.*, **2006**, 45, 4467–4471.
260. Y. Fukasawa, K. Takanabe, A. Shimojima, M. Antonietti, K. Domen, T. Okubo, Synthesis of ordered porous graphitic-C₃N₄ and regularly arranged Ta₃N₅ nanoparticles by using self-assembled silica nanospheres as a primary template, *Chem. Asian. J.*, **2011**, 6, 103–109.
261. X. Chen, Y. S. Jun, K. Takanabe, K. Maeda, K. Domen, X. Fu, M. Antonietti, X. Wang, Ordered mesoporous SBA-15 type graphitic carbon nitride: A semiconductor host structure for photocatalytic hydrogen evolution with visible light, *Chem. Mater.*, **2009**, 21, 4093–4095.
262. X. Liu, F. Pang, M. He, J. Ge, Confined reaction inside nanotubes: New approach to mesoporous g-C₃N₄ photocatalysts, *Nano Res.*, **2017**, 10, 3638–3647.
263. J. Zhang, M. Zhang, C. Yang, X. Wang, Nanospherical carbon nitride frameworks with sharp edges accelerating charge collection and separation at a soft photocatalytic interface, *Adv. Mater.*, **2014**, 26, 4121–4126.
264. W. Shen, L. Ren, H. Zhou, S. Zhang, W. Fan, Facile one-pot synthesis of bimodal mesoporous carbon nitride and its function as a lipase immobilization support, *J. Mater. Chem.*, **2011**, 21, 3890–3894.
265. M. Peer, M. Lusardi, K.F. Jensen, Facile Soft-templated synthesis of high-surface area and highly porous carbon nitrides, *Chem. Mater.*, **2017**, 29, 1496–1506.
266. Q. Fan, J. Liu, Y. Yu, S. Zuo, A template induced method to synthesize nanoporous graphitic carbon nitride with enhanced photocatalytic activity under visible light, *RSC Adv.*, **2014**, 4, 61877–61883.
267. H. Yan, Soft-templating synthesis of mesoporous graphitic carbon nitride with enhanced photocatalytic H₂ evolution under visible light, *Chem. Commun.*, **2012**, 48, 3430–3432.
268. Y. Wang, X. Wang, M. Antonietti, Y. Zhang, Facile one-pot synthesis of nanoporous carbon nitride solids by using soft templates, *ChemSusChem*, **2010**, 3, 435–439.

-
269. Y. Wang, J. Zhang, X. Wang, M. Antonietti, H. Li, Boron- and fluorine-containing mesoporous carbon nitride polymers: Metal-free catalysts for cyclohexane oxidation, *Angew. Chem.*, **2010**, 49, 3356–3359.
270. Z. Lin, X. Wang, Ionic liquid promoted synthesis of conjugated carbon nitride photocatalysts from urea, *ChemSusChem*, **2014**, 7, 1547–1550.
271. Y. Zhang, T. Mori, J. Ye, M. Antonietti, Phosphorus-doped carbon nitride solid: Enhanced electrical conductivity and photocurrent generation, *J. Am. Chem. Soc.*, **2010**, 132, 6294–6295.
272. L. Zhang, X. Chen, J. Guan, Y. Jiang, T. Hou, X. Mu, Facile synthesis of phosphorus doped graphitic carbon nitride polymers with enhanced visible-light photocatalytic activity, *Mater. Res. Bull.*, **2013**, 48, 3485–3491.
273. G. Liu, P. Niu, C. Sun, S. C. Smith, Z. Chen, G.Q. Lu, H.-M. Cheng, Unique electronic structure induced high photoreactivity of sulfur-doped graphitic C₃N₄, *J. Am. Chem. Soc.*, **2010**, 132, 11642–11648.
274. D.-H. Lan, H.-T. Wang, L. Chen, C.-T. Au, S.-F. Yin, Phosphorous-modified bulk graphitic carbon nitride: Facile preparation and application as an acid-base bifunctional and efficient catalyst for CO₂ cycloaddition with epoxides, *Carbon*, **2016**, 100, 81–89.
275. S.C. Yan, Z.S. Li, Z.G. Zou, Photodegradation of rhodamine B and methyl orange over boron-doped g-C₃N₄ under visible light irradiation, *Langmuir*, **2010**, 26, 3894–3901.
276. Y. Wang, Y. Di, M. Antonietti, H. Li, X. Chen, X. Wang, Excellent visible-light photocatalysis of fluorinated polymeric carbon nitride solids, *Chem. Mater.*, **2010**, 22, 5119–5121.
277. S. Guo, Y. Zhu, Y. Y. Yan, Y. L. Min, J. C. Fan, Q. J. Xu, Holey structured graphitic carbon nitride thin sheets with edge oxygen doping via photo-Fenton reaction with enhanced photocatalytic activity, *Appl. Catal. B: Environ.*, **2016**, 185, 315–321.
278. G. Dong, Z. Ai, L. Zhang, Efficient anoxic pollutant removal with oxygen functionalized graphitic carbon nitride under visible light, *RSC Adv.*, **2014**, 4, 5553–5560.

REFERENCES

279. X. She, L. Liu, H. Ji, Z. Mo, Y. Li, L. Huang, D. Du, H. Xu, H. Li, Template-free synthesis of 2D porous ultrathin non-metal-doped g-C₃N₄ nanosheets with highly efficient photocatalytic H₂ evolution from water under visible light, *Appl. Catal. B: Environ.*, **2016**, 287, 144–153.
280. L. Ming, H. Yue, L. Xu, F. Chen, Hydrothermal synthesis of oxidized g-C₃N₄ and its photocatalytic activity regulation, *J. Mater. Chem. A*, **2014**, 2, 19145–19149.
281. J. Li, B. Shen, Z. Hong, B. Lin, B. Gao, Y. Chen, A facile approach to synthesize novel oxygen-doped g-C₃N₄ with superior visible-light photoreactivity, *Chem. Commun.*, **2012**, 48, 12017–12019.
282. Z.-F. Huang, J. Song, L. Pan, Z. Wang, X. Zhang, J.J. Zou, W. Mi, X. Zhang, L. Wang, Carbon nitride with simultaneous porous network and O-doping for efficient solar-energy-driven hydrogen evolution, *Nano Energ.*, **2015**, 12, 646–656.
283. G. Dong, K. Zhao, L. Zhang, Carbon self-doping induced high electronic conductivity and photoreactivity of g-C₃N₄, *Chem. Commun.*, **2012**, 48, 6178–6180.
284. Z. Zhao, Y. Sun, F. Dong, Y. Zhang, H. Zhao, Template synthesis of carbon self-doped g-C₃N₄ with enhanced visible to near-infrared absorption and photocatalytic performance, *RSC Adv.*, **2015**, 5, 39549–39556.
285. Z. Pei, J. Gu, Y. Wang, Z. Tang, Z. Liu, Y. Huang, Y. Huang, J. Zhao, Z. Chen, C. Zhi, Component matters: Paving the roadmap toward enhanced electrocatalytic performance of graphitic C₃N₄-based catalysts via atomic tuning, *ACS Nano*, **2017**, 11, 6004–6014.
286. X. Wang, X. Chen, A. Thomas, X. Fu, M. Antonietti, Metal-containing carbon nitride compounds: A new functional organic–metal hybrid material, *Adv. Mater.*, **2009**, 21, 1609–1612.
287. S. Hua, L. Ma, J. You, F. Li, Z. Fan, G. Lu, D. Liu, J. Gu, Enhanced visible light photocatalytic performance of g-C₃N₄ photocatalysts co-doped with iron and phosphorus, *App. Surf. Sci.*, **2014**, 314, 164–171.
288. S. Zhang, J. Li, M. Zeng, J. Li, J. Xu, X. Wang, Bandgap engineering and mechanism study of nonmetal and metal ion codoped carbon nitride: C+Fe as an example, *Chem. Eur. J.*, **2014**, 20, 9805–9812.

-
289. M. Zhang, X. Bai, D. Liu, J. Wang, Y. Zhu, Enhanced catalytic activity of potassium-doped graphitic carbon nitride induced by lower valence position, *Appl. Catal. B: Environ.*, **2015**, 164, 77–81.
290. J. Zhang, S. Hu, Y. Wang, A convenient method to prepare a novel alkali metal sodium doped carbon nitride photocatalyst with a tunable band structure, *RSC Adv.*, **2014**, 4, 62912–62919.
291. J. Zhang, X. Chen, K. Takanebe, K. Maeda, K. Domen, J.D. Epping, X. Fu, M. Antonietti, X. Wang, Synthesis of a carbon nitride structure for visible-light catalysis by copolymerization, *Angew. Chem. Int. Ed.*, **2010**, 49, 441–444.
292. Y. Chen, J. Zhang, M. Zhang, X. Wang, Molecular and textural engineering of conjugated carbon nitride catalysts for selective oxidation of alcohols with visible light, *Chem. Sci.*, **2013**, 4, 3244–3248.
293. J. Zhang, M. Zhang, S. Lin, X. Fu, X. Wang, Molecular doping of carbon nitride photocatalysts with tunable bandgap and enhanced activity, *J. Catal.*, **2014**, 310, 24–30.
294. M. Zhang, X. Wang, Two dimensional conjugated polymers with enhanced optical absorption and charge separation for photocatalytic hydrogen evolution, *Energy Environ. Sci.*, **2014**, 7, 1902–1906.
295. Z. Chen, P. Sun, B. Fan, Q. Liu, Z. Zhang, X. Fang, Textural and electronic structure engineering of carbon nitride via doping with deficient aromatic pyridine ring for improving photocatalytic activity, *Appl. Catal. B: Environ.*, **2015**, 170–171, 10–16.
296. W. Ho, Z. Zhang, W. Lin, S. Huang, X. Zhang, X. Wang, Y. Huang, Copolymerization with 2,4,6-Triaminopyrimidine for the rolling-up the layer structure, tunable electronic properties, and photocatalysis of g-C₃N₄, *ACS Appl. Mater. Interfaces*, **2015**, 7, 5497–5505.
297. X. Fan, L. Zhang, M. Wang, W. Huang, Y. Zhou, M. Li, R. Cheng, J. Shi, Constructing carbon-nitride-based copolymers via Schiff base chemistry for visible-light photocatalytic hydrogen evolution, *Appl. Catal. B: Environ.*, **2016**, 182, 68–73.
298. P. Mazierski, B. Bajorowicz, E. Grabowska, A. Zaleska-Medynska, Heterogeneous photocatalysis. From Fundamentals to Green Applications. Eds.: J.C. Colmenares, Y-J. Xu, Springer, **2016**.

REFERENCES

299. J. Marugán, M. J. López-Muñoz, P. Fernández-Ibáñez, S. Malato, Photocatalysis. Applications. Eds.: D. D. Dionysiou, G. Li Puma, J. Ye, J. Schneider, D. Bahnemann, RSC Energy and Environment Series, **2016**.
300. R. W. Matthews, Purification of water with near-u.v. illuminated suspensions of titanium dioxide, *Water Res.*, **1990**, 24, 653–660.
301. C. Guillard, J. Disdier, C. Monnet, J. Dussaud, S. Malato, J. Blanco, M.I. Maldonado, J.M. Herrmann, Solar efficiency of a new deposited titania photocatalyst: chlorophenol, pesticide and dye removal applications, *Appl. Catal. B: Environ.*, **2003**, 46, 319–332.
302. S. Malato, J. Blanco, D. C. Alarcón, M. I. Maldonado, P. Fernández-Ibáñez, W. Gernjak, Photocatalytic decontamination and disinfection of water with solar collectors, *Catal. Today*, **2007**, 122, 137–149.
303. K. Wang, Q. Li, B. Liu, B. Cheng, W. Ho, J. Yu, Sulfur-doped g-C₃N₄ with enhanced photocatalytic CO₂-reduction performance, *Appl. Catal. B: Environ.*, **2015**, 176–177, 44–52.
304. F. Dong, Y. Li, Z. Wang, W.K. Ho, Enhanced visible light photocatalytic activity and oxidation ability of porous graphene-like g-C₃N₄ nanosheets via thermal exfoliation, *Appl. Surf. Sci.*, **2015**, 358, 393–403.
305. Y. Li, S. Ouyang, H. Xu, X. Wang, Y. Bi, Y. Zhang, J. Ye, Constructing solid–gas–interfacial Fenton reaction over alkalinized-C₃N₄ photocatalyst to achieve apparent quantum yield of 49% at 420 nm, *J. Am. Chem. Soc.*, **2016**, 138, 13289–13297.
306. A.A. Granovsky. Firefly version 8. <http://classic.chem.msu.su/gran/firefly/index.html>
307. G.A. Andrienko, Chemcraft v.1.6, <http://www.chemcraftprog.com/index.html>
308. R.F.W. Bader, Atoms in Molecules. A Quantum Theory, Oxford University Press, **1990**.
309. E. Espinosa, E. Molins, C. Lecomte, Hydrogen bond strengths revealed by topological analyses of experimentally observed electron densities, *Chem. Phys. Lett.*, **1998**, 285, 170–173.
310. K.A. Lyssenko, A.A. Korlyukov, D.G. Golovanov, S. Yu. Ketkov, M. Yu. Antipin, Estimation of the Barrier to Rotation of Benzene in the (η⁶-C₆H₆)₂Cr Crystal via

REFERENCES

- Topological Analysis of the Electron Density Distribution Function, *J. Phys. Chem. A.*, **2006**, 110, 6545–6551.
311. Z. Shields, J.S. Murray, P. Politzer, Directional tendencies of halogen and hydrogen bonds, *Int. J. Quant. Chem.*, **2010**, 110, 2823–2832.
312. T. Lu, F. Chen, Multiwfn: a multifunctional wavefunction analyzer, *J. Comput. Chem.*, **2012**, 33, 580–592.
313. C.B. Hubschle, B. Dittrich, MoleCoolQt - a molecule viewer for charge-density research, *J. Appl. Crystallogr.*, **2011**, 44, 238–240.
314. H.S. Kibombo, R. Peng, S. Rasalingam, R.T. Koodali, Versatility of heterogeneous photocatalysis: Synthetic methodologies epitomizing the role of silica support in TiO₂ based mixed oxides, *Catal. Sci. Technol.*, **2012**, 2, 1737–1766.
315. D. Spasiano, L.P.P. Rodríguez, J.C. Olleros, S. Malato, R. Marotta, R. Andreozzi, TiO₂/Cu(II) photocatalytic production of benzaldehyde from benzyl alcohol in solar pilot plant reactor, *Appl. Catal. B: Environ.*, **2013**, 136–137, 56–63.